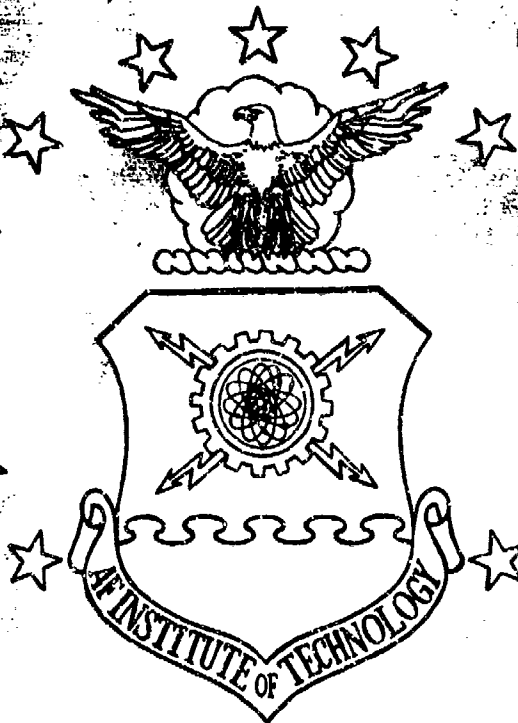


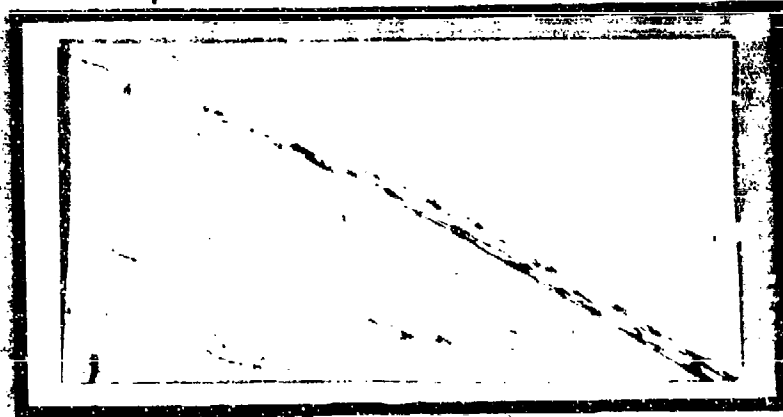
ADA083517



①
NW

LEVEL

DIIC
ELECTE
APR 28 1980
S D
E



Approved for public release,
Distribution Unlimited

UNITED STATES AIR FORCE
AIR UNIVERSITY
AIR FORCE INSTITUTE OF TECHNOLOGY
Wright-Patterson Air Force Base, Ohio

DDC FILE COPY

80 4 25 048

Accession For	
NTIS Avail	<input checked="" type="checkbox"/>
DOC TAB	<input type="checkbox"/>
Unprocessed	<input type="checkbox"/>
Justification	
By _____	
Distribution/_____	
Special Codes	
Dist	Avail and/or special
A	

6. A METHOD OF CHARACTERIZING AIR-TO-AIR
MISSILE ENDGAME MODELS.

9. *Misc* THESIS

14. AFIT/GST/MA/80M-2 | Gregory A. Keethler
Captain | USAF

10

11/10/80

12 227

Approved for public release; distribution unlimited.

0133-55

AFIT/GST/MA/80M-2

A METHOD OF CHARACTERIZING AIR-TO-AIR
MISSILE ENDGAME MODELS

THESIS

Presented to the Faculty of the School of Engineering
of the Air Force Institute of Technology
Air University
In Partial Fulfillment of the
Requirements for the Degree of
Master of Science

by

Gregory A. Keethler
Captain USAF

Graduate Strategic and Tactical Sciences

March 1980

Approved for public release; distribution unlimited.

Preface

The idea for this research project was spawned during my tenure as a missile effectiveness analyst at the Air Force Armament Laboratory (AFATL). Mr. Craig Olson of the Aircraft Systems Division, Analysis Directorate, Air Force Test and Evaluation Center (AFTEC/OAW) provided the necessary impetus by conveying to me his concern (which I share) over the historically inordinate cost of air-to-air missile endgame analyses, both in terms of funds and computer time.

I wish to gratefully acknowledge the generous assistance given by Mr. Patrick Coffield, the author of SHAZAM, and Mr. Carson Sasser, the air-to-air analysis program manager at AFATL, without which this project could not have succeeded nor even been attempted.

I wish to also thank Capt. Brian W. Woodruff, my faculty advisor, for his ongoing assistance during the project, but most of all for his patience, sound advice, and unfailing support.

Finally, I wish to thank Mrs. Suzanne Weber for her tireless efforts and professional work in typing this thesis, Major Thomas P. Flanagan for his help in drawing some of the figures, and my wife, Gloria, for her patience and understanding of the long hours spent on this project.

Gregory A. Keethler

Contents

	<u>Page</u>
Preface	ii
List of Figures	v
List of Tables.	xi
Abstract.	xii
I. Introduction.	1
Background.	1
Analysis Methodology.	2
Problem Statement	4
Scope	6
Objectives.	6
Utility of Results.	8
Approach.	9
Overview.	10
II. Available Methodologies	11
III. Analysis.	14
Factor Selection.	14
The Empirical Approach.	21
A Semi-Empirical Approach	28
Assessment of the Fit	45
IV. Suggested Method of Characterizing Endgame Models (MOCEM).	49
V. Summary, Conclusions, and Recommendations . . .	54
Bibliography.	58
Appendix A: Relationship Between Selected Factors and SHAZAM Inputs.	59
Appendix B: Results of the Empirical Approach. . . .	61
Appendix C: Approximation of the Warhead Pattern With a Cone.	95

	<u>Page</u>
Appendix D: Simultaneous Solution of the Cone/Line Intersection	104
Appendix E: Determination of "a" and "b"	111
Appendix F: The First Characterization Applied to the Basic Data	116
Appendix G: "109 Cell Model" of the Circular Normal Distribution	165
Appendix H: The First Characterization With Random Miss Distance.	167
Appendix I: Improved Characterization With Random Miss Distance.	181
Appendix J: Selected Plots of the Improved Characterization Applied to the Basic Data	195
Appendix K: Comparison of the Final Characterization to the 10 Selected Random Trajectories .	206
Vita.	218

List of Figures

<u>Figure</u>		<u>Page</u>
1	An Endgame "Black Box"	5
2	Kinematic Geometry.	16
3	Spatial Geometry.	18
4	Comparison Between Data With And Without Random Alpha.	34
5	109 Cell Model Versus 1000 Random Samples . . .	43
A-1	Factor Relationships.	60
B-1	Location Function, $\text{PSI} = 0$	63
B-2	Location Function, $\text{PSI} = 45$	64
B-3	Location Function, $\text{PSI} = 90$	65
B-4	Location Function, $\text{PSI} = 135$	66
B-5	Location Function, $\text{PSI} = 180$	67
B-6	Half Width Function, $\text{PSI} = 0$	68
B-7	Half Width Function, $\text{PSI} = 45$	69
B-8	Half Width Function, $\text{PSI} = 90$	70
B-9	Half Width Function, $\text{PSI} = 135$	71
B-10	Half Width Function, $\text{PSI} = 180$	72
B-11	Location Function, Constant Term.	73
B-12	Location Function, Amplitude Term	74
B-13	Location Function, Phase Term	75
B-14	Half Width Function, Constant Term.	76
B-15	Half Width Function, Amplitude Term	77
B-16	Half Width Function, Phase Term	78

"Empirical Characterization Versus Stage 1 Data"

	<u>PSI</u>	<u>THETA</u>	<u>VR</u>	<u>RM</u>	<u>BETA</u>	
B-17	0	135	2000	15	0.	79
B-18	0	225	2000	15	0.	80
B-19	45	45	2000	15	15.	81
B-20	45	135	2000	15	15.	82
B-21	45	225	2000	15	15.	83
B-22	45	315	2000	15	15.	84
B-23	90	45	2000	15	15.	85
B-24	90	135	2000	15	15.	86
B-25	90	225	2000	15	15.	87
B-26	90	315	2000	15	15.	88
B-27	135	45	2000	15	15.	89
B-28	135	135	2000	15	15.	90
B-29	135	225	2000	15	15.	91
B-30	135	315	2000	15	15.	92
B-31	180	135	2000	15	15.	93
B-32	180	225	2000	15	15.	94

C-1	Vector Geometry.	97
C-2	Vector Addition of \bar{V}_R and \bar{V}_F	98
C-3	Warhead Cone Orientation	98

"Cone Approximation Versus True Warhead Pattern"

	<u>VR</u>	<u>PSI</u>	<u>BETA</u>	<u>DP</u>	
C-4	2000	45	15	30.	99
C-5	3000	45	15	30.	100
C-6	2000	10	15	30.	101
C-7	2000	70	15	30.	102
C-8	3000	45	40	30.	103

D-1	Geometry of the Cone/Line Intersection Problem .	110
-----	--	-----

E-1	The Vulnerable Length.	114
-----	--------------------------------	-----

<u>Figure</u>		<u>Page</u>
E-2	Illustration of X_{M_R} and X_{M_F}	114
E-3	The Drop-Out Situation.	115
E-4	Illustration of Drop-Out Bias	115

"First Characterization Versus Basic Data"

	<u>PSI</u>	<u>THETA</u>	<u>VR</u>	<u>RM</u>	<u>BETA</u>	
F-1	0	225	2000	15	0	117
F-2	0	225	2000	27.5	0	118
F-3	0	225	2000	40	0	119
F-4	0	225	3000	15	0	120
F-5	0	135	2000	15	0	121
F-6	0	135	3000	15	0	122
F-7	45	45	2000	15	15	123
F-8	45	45	2000	27.5	15	124
F-9	45	45	2000	40	15	125
F-10	45	135	2000	15	15	126
F-11	45	135	3000	15	15	127
F-12	45	225	2000	15	15	128
F-13	45	315	2000	15	15	129
F-14	45	315	3000	15	15	130
F-15	90	45	2000	15	15	131
F-16	90	135	2000	15	15	132
F-17	90	135	3000	15	15	133
F-18	90	225	2000	15	15	134
F-19	90	225	2000	27.5	15	135
F-20	90	225	2000	40	15	136
F-21	90	315	2000	15	15	137
F-22	135	45	1000	15	15	138
F-23	135	45	2000	15	15	139
F-24	135	135	2000	15	15	140
F-25	135	135	2000	27.5	15	141
F-26	135	135	2000	40	15	142
F-27	135	225	1000	15	15	143
F-28	135	225	2000	15	15	144

<u>Figure</u>	<u>PSI</u>	<u>THETA</u>	<u>VR</u>	<u>RM</u>	<u>BETA</u>	<u>Page</u>
F-29	135	315	2000	15	15.	145
F-30	180	135	1000	15	15.	146
F-31	180	135	1000	27.5	0.	147
F-32	180	135	1000	40	0.	148
F-33	180	135	2000	15	0.	149
F-34	180	135	2000	27.5	0.	150
F-35	180	135	2000	40	0.	151
F-36	180	135	3000	15	0.	152
F-37	180	135	3000	27.5	0.	153
F-38	180	135	3000	40	0.	154
F-39	180	225	1000	15	0.	155
F-40	180	225	1000	27.5	0.	156
F-41	180	225	1000	40	0.	157
F-42	180	225	2000	15	0.	158
F-43	180	225	2000	27.5	0.	159
F-44	180	225	2000	40	0.	160
F-45	180	225	3000	15	0.	161
F-46	180	225	3000	27.5	0.	162
F-47	180	225	3000	40	0.	163
F-48	180	225	2000	52.5	0.	164
G-1	The 109 Cell Model					166

"First Characterization with Random Miss
Distance"

	<u>PSI</u>	<u>VR</u>	<u>BETA</u>	<u>SIGMA</u>	
H-1	0	2000	0	10.	168
H-2	45	2000	15	10.	169
H-3	90	2000	15	10.	170
H-4	135	1000	15	10.	171
H-5	135	2000	15	10.	172
H-6	135	2000	15	15.	173
H-7	135	2000	15	20.	174
H-8	180	1000	1	10.	175

<u>Figure</u>	<u>PSI</u>	<u>VR</u>	<u>BETA</u>	<u>SIGMA</u>	<u>Page</u>
H-9	180	2000	0	10.	176
H-10	180	2000	0	15.	177
H-11	180	2000	0	20.	178
H-12	180	2000	0	25.	179
H-13	180	3000	0	10.	180

"Improved Characterization with Random Miss Distance"

	<u>PSI</u>	<u>VR</u>	<u>BETA</u>	<u>SIGMA</u>	
I-1	0	2000	0	10.	182
I-2	45	2000	15	10.	183
I-3	90	2000	15	10.	184
I-4	135	1000	15	10.	185
I-5	135	2000	15	10.	186
I-6	135	2000	15	15.	187
I-7	135	2000	15	20.	188
I-8	180	1000	0	10.	189
I-9	180	2000	0	10.	190
I-10	180	2000	0	15.	191
I-11	180	2000	0	20.	192
I-12	180	2000	0	25.	193
I-13	180	3000	0	10.	194

"Improved Characterization Versus Basic Data"

	<u>PSI</u>	<u>THETA</u>	<u>VR</u>	<u>RM</u>	<u>BETA</u>	
J-1	0	225	2000	27.5	0.	196
J-2	0	225	3000	15	0.	197
J-3	45	45	2000	27.5	15.	198
J-4	45	135	3000	15	15.	199
J-5	90	135	3000	15	15.	200
J-6	90	315	2000	15	15.	201
J-7	135	135	2000	40	15.	202
J-8	135	315	2000	15	15.	203
J-9	180	225	2000	27.5	0.	204
J-10	180	225	3000	40	0.	205

Figure

Page

"Final Characterization Versus Random Trajectories"

	<u>PSI</u>	<u>VR</u>	<u>BETA</u>	<u>SIGMA</u>	
K-1	9	2480	4	8.5	207
K-2	30	2604	14	7.6	208
K-3	55	2447	24	16.1	209
K-4	64	2105	17	24.8	210
K-5	89	1152	41	16.8	211
K-6	105	1799	21	13.5	212
K-7	122	1068	30	9.0	213
K-8	128	1171	20	15.9	
	(109 Cell Model)				214
K-9	128	1171	20	15.9	
	(1000 Samples)				215
K-10	146	1467	11	29.7	216
K-11	168	1646	5	15.2	217

List of Tables

<u>Table</u>	<u>Page</u>
I. Definitions Related to the Kinematic Geometry .	17
II. Definitions Related to the Spatial Geometry . .	19
III. Region of Experimentation	23
IV. Staged Experimental Design.	24
V. Combinations of Factor Values Examined in Basic Data.	32
VI. Ten Selected Random Trajectories.	47

Abstract

Air-to-air missile endgame programs typically require tens of seconds of computer time to calculate a single estimate of probability of kill (P_K). Thousands of these estimates may be required in any given endgame analysis. The main objective of this research was to develop a method for characterizing an endgame model using only a fraction of the amount of data generated by such analyses. In pursuit of this objective, a second objective of actually accomplishing a characterization of an existing endgame program was established.

The endgame program SHAZAM was used to generate data upon which to base a characterization. A purely empirical approach was first attempted wherein all main and interactive effects of the critical factors were to be assessed strictly by experimentation with and observation of the behavior of SHAZAM. The high order of interactions between the factors precluded completion of this approach.

A semi-empirical approach was then pursued whereby the interactions between the endgame geometry and warhead characteristics were accounted for geometrically. A two-parameter exponential function was used to describe the behavior of P_K as a function of the warhead burst point. Values of the two parameters were calculated based upon the settings of the remaining factors. A "vulnerable length" was used to account

for the target's vulnerability. After several iterations of refinement, the characterization was compared to SHAZAM for ten randomly selected trajectories. The characterization's P_K estimates were within 0.1 of SHAZAM's estimates for 97 percent of these random data. A simple computer program implementing the mathematics of the characterization required a maximum of 0.2 seconds of computer time per P_K estimate. Approximately two hours of computer time were consumed by SHAZAM in generating the necessary data. Thus, with a relatively modest investment of computer time, two orders of magnitude improvement in time required per P_K estimate was achieved.

The suggested method for characterizing air-to-air missile endgame programs is based on the semi-empirical approach and its application to SHAZAM. The method is heuristic, rather than algorithmic, due to the subjective nature of the characterization process.

A METHOD OF CHARACTERIZING AIR-TO-AIR
MISSILE ENDGAME MODELS

I. Introduction

Background

The last 100 milliseconds or so of an air-to-air missile's encounter with a target are critical to its eventual success or failure. The guidance system has already done what it is capable of doing and can no longer change the outcome of the encounter. If it has done its job well, the missile will hit the target and will be considered successful. More likely, at least for most missiles, is that the missile itself will not make physical contact with the target. In this case, it is up to the fuze and warhead system to destroy, or "kill," the target.

The warhead is a combination of high explosive and metal and can kill the target with one of two mechanisms. The first is with the air blast accompanying warhead detonation. If detonation occurs sufficiently close to the target, the resulting overpressure will cause structural failure and subsequent destruction. Otherwise, destruction can only result from fragmentation, the second kill mechanism. Upon detonation, the metal in the warhead is fragmented and ejected at very high velocities. If one of these fragments strikes a vulnerable component of the target, there is a finite

probability that the entire target will be destroyed.

The purpose of the fuze is to detonate the warhead at a time which allows at least one of the warhead kill mechanisms to destroy the target.

Analysis Methodology

Over the years, much analysis of the terminal encounter, or "endgame,"¹ situation has been done. Numerous computer programs have been written which predict missile kill probabilities--ENDGAME, AMEGS, SCAN, SHAZAM, and SESTEM II, just to name a few (Ref 1: Sec 5-40 to 5-55). Not all of the programs deal with the endgame problem at the same level of detail, and some of them perform other functions as well.

There are numerous purposes for which endgame analyses are undertaken. One might be trying to select the best warhead out of a number of candidates, or he might be trying to find ways to improve the effectiveness of an existing one. Other objectives might be estimation of an existing fuze/warhead system's effectiveness, generation of effectiveness tables, or selection of a fuze time delay.

Regardless of the objective, the underlying question being asked in any such analysis is this: given a specific terminal encounter situation, what is the probability that the target is killed by the missile? This question may be

¹Henceforth, the term "endgame" is used to mean that part of the missile's trajectory during which the closest approach to the target occurs and all velocity vectors can be considered constant.

asked thousands of times during a given analysis. Before the question can be answered, a more fundamental question must be answered: what are the vulnerabilities of the target? For any given target, the answer to this question is very difficult to obtain. Usually, teams of vulnerability analysts combine test data with their knowledge of physics, mechanics, material properties, and hydrodynamics to create what is known as a "vulnerability model." These "models" come in a variety of forms, and generally an endgame program is structured to accept only a limited number of these forms.

The purpose of an endgame program, then, is to account for the interaction between the warhead, the dynamics of the terminal encounter, and the vulnerability model to yield an estimate of the probability of kill (P_K).

The most common approach to modeling the endgame situation is to describe the physical process of fragment ejection mathematically. Two binary criteria are examined first: whether or not the encounter was a direct hit, or whether or not detonation occurred within the blast envelope. If neither criterion is met, then the dynamics of the encounter are combined with the motion of the fragments to determine where and how often the fragments strike the target. Frequently, there are stochastic elements in the mathematical description of fragment ejection and motion. Also, fragmentation may be modeled as a "beam" with a certain density of fragments. In this case, the area of the intersection of the beam with the

target is calculated. In either case, the frequency, location, and characteristics of the fragments striking the target are compared to or combined with the vulnerability model to yield an estimate of P_K .

Frequently, endgame programs are operated in a "Monte Carlo" fashion in which variables such as miss distance are treated as random variables and sampled from distributions. Each iteration results in a kill probability. The average of these individual probabilities is the overall probability of kill for the encounter. The sampling variance of the mean P_K is reduced by increasing the number of iterations.

One way of viewing an endgame program is that it is just a "black box" (see Figure 1). Certain inputs are required, the program processes the information, and a P_K comes out. Most endgame "black boxes" have two characteristics in common: they are "large" in terms of computer memory required, and they are slow (and consequently expensive to operate). Ten seconds of central processor time per P_K estimation is considered "fast" in the endgame business.

Problem Statement

Given that an endgame program is run thousands of times per analysis, is it possible to characterize the behavior of the output, P_K , with respect to changes in the inputs so that this characterization can be used for subsequent P_K estimations? If so, how does one develop such a characterization? It is the purpose of this thesis to investigate these questions.

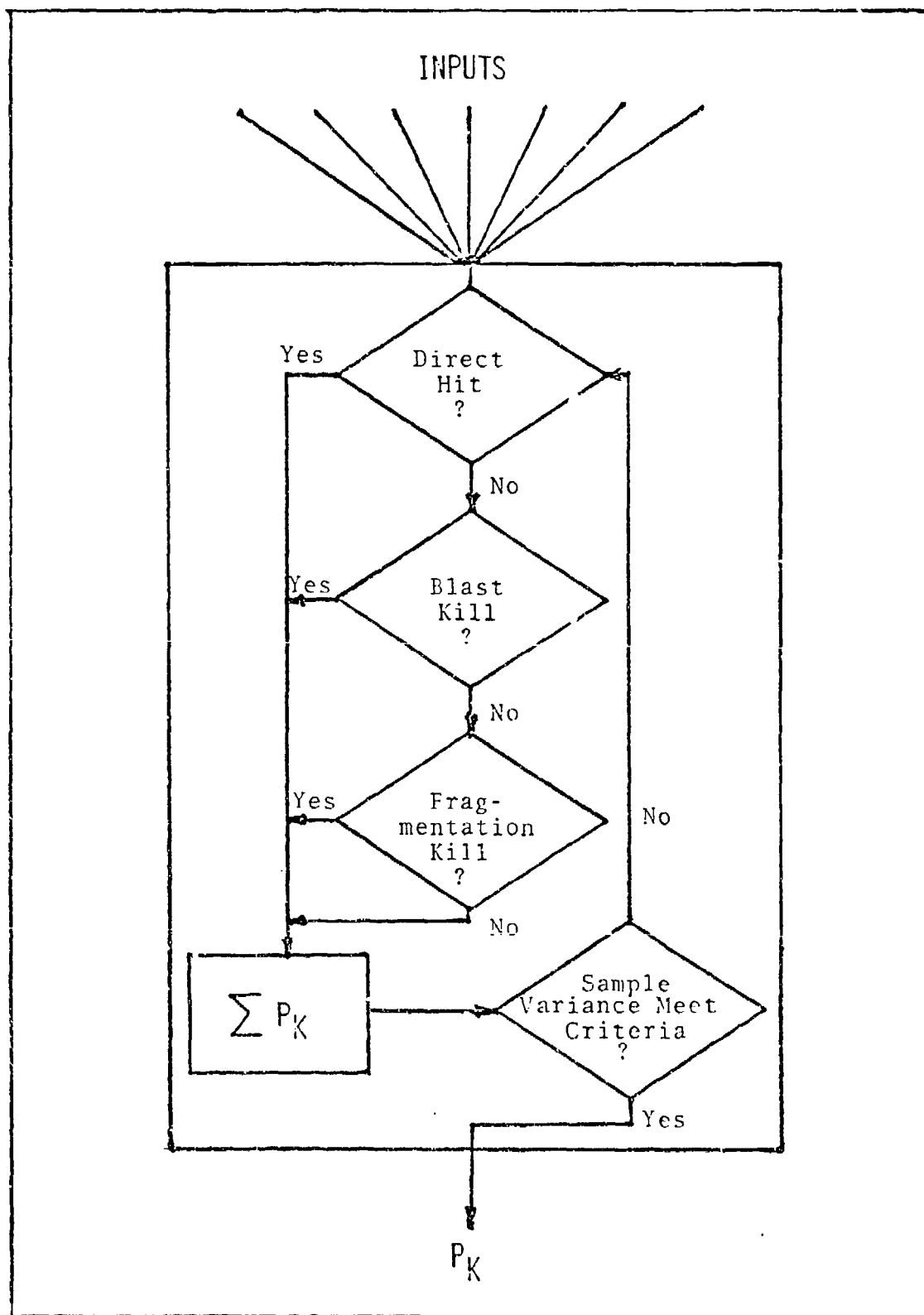


Fig 1. An Endgame "Black Box"

Scope

To answer the above questions for the general case is a large and, perhaps, impossible task. This thesis investigates the question for the case of a single endgame program with a single vulnerability model and a single warhead description. The role of the fuze is not considered in the investigation. A characterization accomplished under these circumstances would indicate that it is possible the same method can be applied to different programs, vulnerability models and warhead descriptions.

Objectives

Given the nature and scope of the problem, two specific objectives must be accomplished. One is to obtain a "characterization" of an endgame program's behavior. The other is to define a method for arriving at this characterization.

By characterization is meant an entity which mimics the behavior of the endgame program. There are many forms that such an entity can have: equations, statistical relationships, algorithms, and tables, just to mention a few. For purposes of this thesis, the tabular form--i.e., tables of outputs versus inputs--is unacceptable because it would not be an improvement over existing methodology. Most any other form should be acceptable, as long as it is not more cumbersome, expensive or time-consuming than the "black box" it replaces.

By mimic is meant that given the same inputs, the

characterization should yield the same output as the endgame program would have. Exact duplication of results, however, is a rather heroic objective. A more realistic goal is to yield an output which is within an acceptable tolerance of the real output. As mentioned previously, the output of many endgame programs has a statistical uncertainty associated with it which is dependent upon the number of iterations run. This is not an uncertainty about the real value of P_K , but is an uncertainty about the F_K the program would predict with a very large number of iterations. This uncertainty is usually expressed in the form of a confidence interval about the P_K estimate. A commonly accepted level of uncertainty is to achieve a 90% confidence interval with a halfwidth of 0.1 centered on the P_K estimate. It follows then that an error of this magnitude resulting from the use of a characterization is also acceptable.

In terms of useful results, the actual characterization arrived at in this thesis only serves to demonstrate the feasibility of the method. The behavior of any particular endgame program is dependent upon the warhead description and vulnerability model used as well as the algorithm employed in the program itself. What should be of interest to the reader is the method of arriving at this characterization. In that endgame programs are all models of the same basic process, this method should be applicable to any of them. Hence, development of the method of obtaining an endgame program characterization is the most important objective of this thesis.

Utility of Results

No characterization can predict as well as the endgame program itself. One might then logically question the wisdom of pursuing such an endeavor. The fact is that a characterization which meets the stated tolerance criteria for a particular endgame program would have several potential benefits.

Once established and verified, the characterization could be used in place of the endgame program/vulnerability model/warhead description combination on which it is based. It should be able to estimate an individual P_K in a fraction of a central processor second. In addition, the characterization should contribute to better understanding of the processes and interrelationships which affect the endgame situation.

There are several applications of endgame analysis which would also benefit from a characterization. One of these is real time missile simulation such as that used on the Air Combat Maneuvering Instrumentation/Range (ACMI/R) at Nellis Air Force Base, Nevada. Currently, the results of the missile simulation are used to enter a table from which a P_K value is obtained. The increments on the table parameters are relatively large and, hence, in general yield a crude estimate of P_K . Since endgame programs are used to generate these tables, a characterization based on the same amount (or less) of data as is in the tables would be a more accurate representation of the program's behavior, would use less computer memory than large look-up tables, and could conceivably be a

faster way to get a P_K estimate.

A related application is in the area of missile launch envelopes. These envelopes are used by pilots to help them fire their missiles under conditions which supposedly will result in a "kill." Currently, these envelopes are based on miss distance or some other criteria. The concept of using a P_K criterion has long been proposed, but not pursued due to the inordinate cost of the endgame analysis required. With a characterization of the endgame program's behavior, such P_K envelopes would be much easier and cheaper to produce and could conceivably even be implemented in aircraft fire control computers.

A final application of endgame analysis which could benefit from characterization is the area of fuzing analysis. Of primary importance to the fuze is the question of how long the time delay between target detection and warhead detonation should be. Since a characterization could very quickly yield the location of maximum P_K for any given trajectory, one need only relate this location to the fuze detection location for the same trajectory. Currently, most endgame programs must "search" for the point of maximum P_K . With "searching" being expensive and time-consuming, such analysis has been limited in the past.

Approach

The approach to the problem taken herein is a heuristic one. Of utmost importance is the availability of an endgame

program which is typical of those in use. The Missiles and Guns Analysis Branch of the Air Force Armament Laboratory has provided a version of its primary endgame program known as SHAZAM. The warhead description and vulnerability model included in this version are representative of the type encountered in modern endgame analyses. Hence, the program should provide a realistic challenge in terms of behavior characterization.

Given the endgame program, the approach is to use any available methodology to establish and characterize its behavior. To the extent that available methodology is inadequate, it is supplemented with appropriate "ad hoc" methods to accomplish the same end.

Overview

The remainder of this thesis is devoted to the pursuit of the objectives. The second chapter contains a discussion of available methodologies which are of potential usefulness in this problem. Chapter III contains a description of the characterization effort, while Chapter IV delineates the resulting suggested procedure for obtaining a characterization. The final chapter contains a summary, conclusions, and recommendations for further research.

II. Available Methodologies

The basic problem addressed in this thesis bears resemblance to several which have been treated in the literature. In fact, there are three somewhat overlapping "disciplines" which are concerned with the general problem of describing the relationship between several independent variables and a dependent variable when the true relationship is either not known, not understood, or not practically useful.

The first and, perhaps, oldest of these disciplines is numerical analysis. A fundamental concept in numerical analysis is the collocation polynomial. It can be mathematically shown that for any collection of observations taken at different values of the independent variables, there exists a unique polynomial which takes on the corresponding values of (i.e., collocates with) the value of the dependent variable (Ref 2:10). Much of numerical analysis is devoted to methods for finding or approximating the collocation polynomial.

The main disadvantage of collocation polynomials is that there is no assurance regarding the behavior (or misbehavior) of the function between the observed points. Furthermore, because each set of data has a unique polynomial which collocates with it, it is indeed unlikely that two independent sets of observations of the same process will yield the same collocation polynomial. Finally, the order of the

collocation polynomial increases with the number of observations, making it unwieldy for large data sets.

Another method of numerical analysis which remedies some of these problems is the so-called "spline fit." This involves "piecing" together a set of cubic polynomials, each of which fits the data in some sub-interval. At the points where the curves join, their first and second derivatives are forced to be equal. This method is most useful for interpolation and for calculating integrals and derivatives. It is, however, somewhat cumbersome, particularly for large volumes of data where more than one independent variable is involved (Ref 3:474-488).

Linear regression analysis is an approach more suited to large volumes of data. Rather than requiring collocation, regression analysis seeks to minimize the error between the regression function and the observed data. The regression function is a linear combination of different functions and must be linear in all coefficients. Transformations can often be performed on both the data and the proposed function in order to meet these requirements. Given the data and the proposed function, linear regression analysis yields values for the coefficients which minimize the sum of the squared differences between the observed values of the dependent variable and the corresponding values of the regression function. The resulting equation is guaranteed to give the best fit (in the least squares sense) of all possible equations with the form of the regression function. There is no guarantee, however, that

this form is the best from which to choose (Ref 4; 5; and 6).

The newest discipline which deals with the problem is Response Surface Methodology (RSM). On the surface, at least, it appears to be a panacea for just the type of problem represented by this thesis. In the context of RSM, one has a process with a single measurable output (response) and perhaps several (say m) inputs (factors). For any combination of values of the factors, there is but a single response. Though the measurement of the response may be subject to error, the underlying process can be viewed as a surface in $m + 1$ space. RSM seeks to explore this surface in such a way as to accomplish some goal. There are two goals with which RSM is concerned: the attainment of optimum conditions and the characterization of the surface itself. Unfortunately, the overwhelming majority of the literature is devoted to the former goal, while the treatment of the latter is largely lip-service.

A large part of the methodology of RSM is actually numerical analysis and regression analysis. However, a significant portion of the discipline is also devoted to experimental design--i.e., how best to "examine" the surface to accomplish the goal with a minimum of experimentation. This portion of the discipline is of particular interest to anyone faced with the basic RSM problem (Ref 7; 8; and 9).

The purpose of this rather cursory discussion of available methods has been to acquaint the reader with them and to acknowledge their existence. They are kept in the "characterization tool box" for use as needed.

III. Analysis

Factor Selection

In any endeavor in which one is exploring the relationship between an output and numerous inputs, the selection of the set of inputs to be studied is of utmost importance. Most processes can be described by several different sets of factors (or inputs). These sets are generally related to each other somehow and might be overlapping, but they do not necessarily contain the same number of factors. The goal is to select that set of factors which is most suitable for use in predicting the response (or output). In general, the factors in this set have the most direct impact upon the response and the least amount of interaction between them. If the researcher is completely ignorant of the process under study, a large amount of experimentation may be required to find the most appropriate factor set. On the other hand, he may have sufficient knowledge of the process to choose the factor set without any experimentation.

In the case of the endgame situation, there are several sets of variables which can precisely define it. There are fundamentally only two factors involved: spatial relationship and motion. In three dimensions, three is the minimum number of parameters required to describe translational motion. The position of one point with respect to another point in three

dimensions also requires a minimum of three descriptive parameters. Additional parameters are required to describe the angular orientation and motion of any rigid bodies involved.

Figure 2 depicts that part of the geometry which results from the motion of the target and the missile. The coordinate system is the target coordinate system with the X-axis coincident with the target centerline, the Y-axis directed out the port side of the target, and the Z-axis directed out of the top of the target perpendicular to the wing plane. The origin of the system is the target centroid--i.e. the geometric center of the target. For purposes of this study, it is assumed that the target centerline is aligned with the target velocity vector and that the target is not rolled out of the horizontal plane. In the definitions presented in Table 1, azimuth refers to the angle as measured in the horizontal (X-Y) plane and elevation refers to the angle as measured from the horizontal plane. Also, to maintain mathematical correctness, the angles in these definitions must be described with respect to the negative of both the missile and relative velocity vectors. This can be reconciled with Figure 2 by remembering that all vectors, by necessity, are defined with respect to the origin of the coordinate system. In Figure 2, vectors have been moved from the origin in order to more clearly illustrate the geometry. The reader should refer to Figure 2 when reading the definitions.

Figure 3 depicts that part of the geometry resulting from the spatial relationships between the missile and the target. The definitions in Table II apply to this figure.

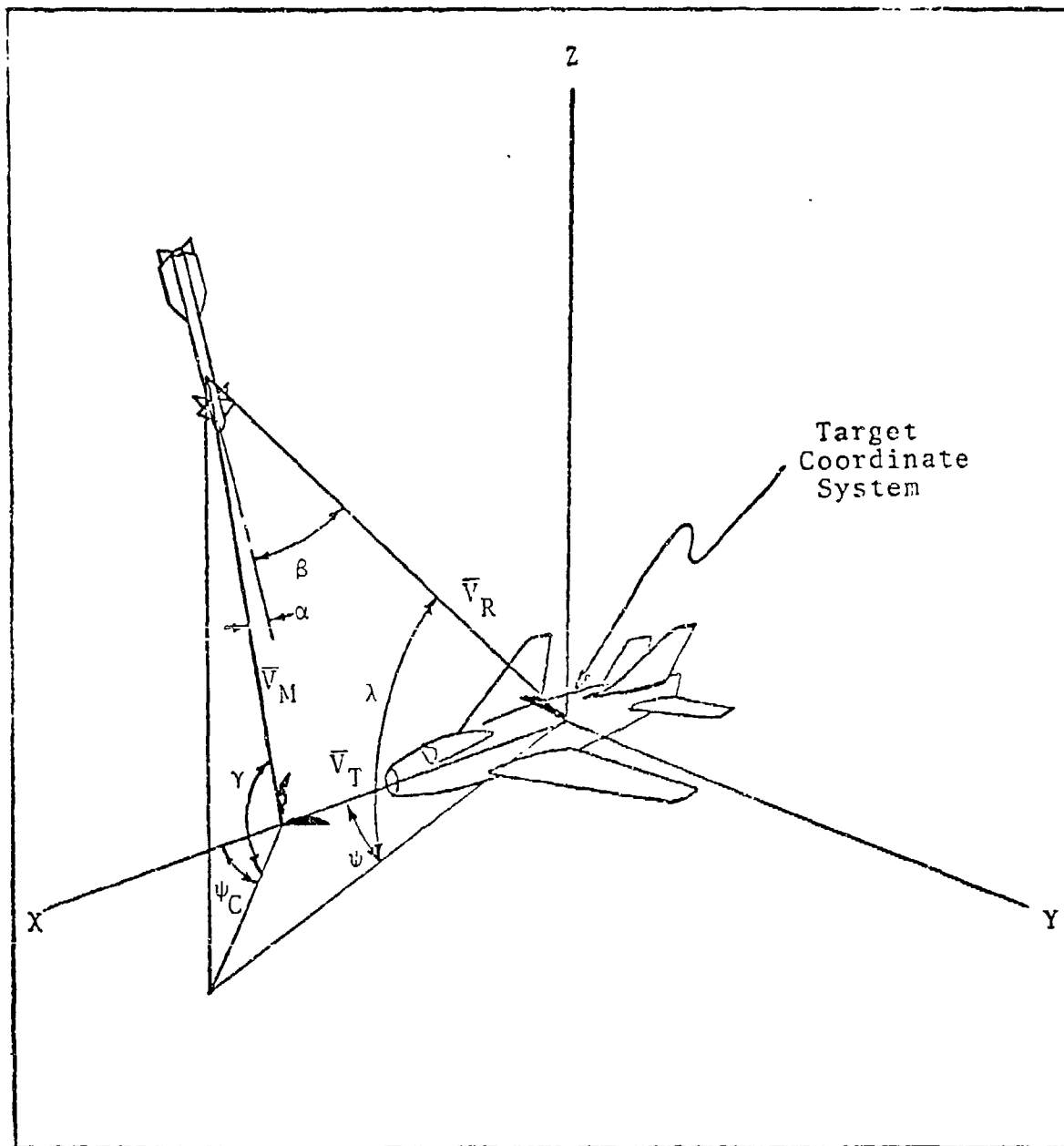


Fig 2. Kinematic Geometry

TABLE I
 Definitions Related to the
 Kinematic Geometry

Term	Definition
\bar{V}_T	the target velocity vector
\bar{V}_M	the missile velocity vector
\bar{V}_R	the relative velocity vector defined by the vector difference between \bar{V}_M and \bar{V}_T i.e. $\bar{V}_R = \bar{V}_M - \bar{V}_T$
V_T	magnitude of \bar{V}_T
V_M	magnitude of \bar{V}_M
V_R	magnitude of \bar{V}_R
ψ_C	azimuth angle of $-\bar{V}_M$ with respect to \bar{V}_T
γ	elevation angle of $-\bar{V}_M$ with respect to \bar{V}_T
ψ	azimuth angle of $-\bar{V}_R$ with respect to \bar{V}_T
λ	elevation angle of $-\bar{V}_R$ with respect to \bar{V}_T
α	angle between \bar{V}_M and the missile centerline
β	angle between \bar{V}_R and the missile centerline

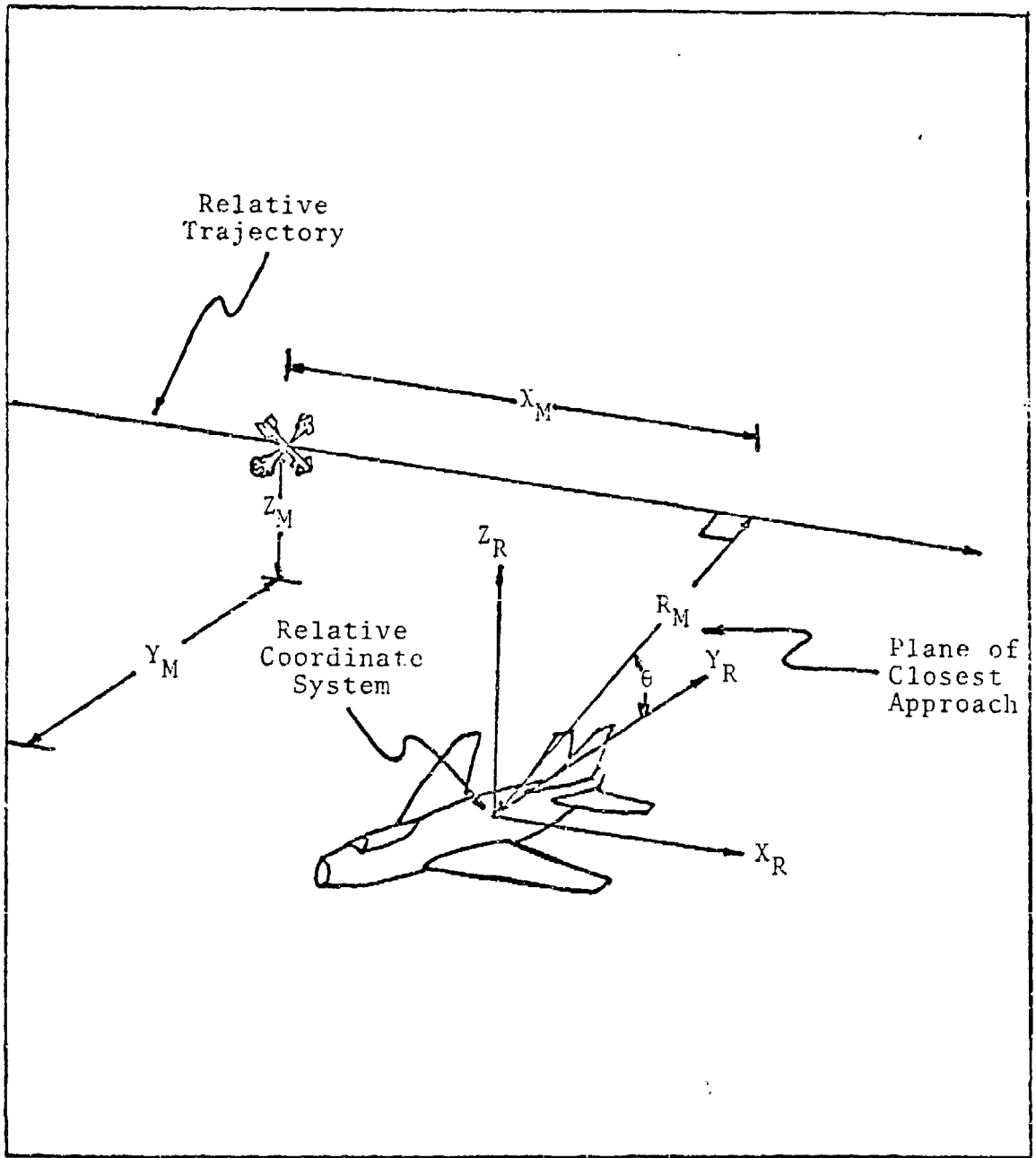


Fig 3. Spatial Geometry

TABLE II
 Definitions Related to the
 Spatial Geometry

Term	Definition
Relative Trajectory	path of the missile with respect to the target. Direction corresponds to the direction of \bar{V}_R .
Point of Closest Approach	Point on the relative trajectory at which the line-of-sight to the target centroid is perpendicular to \bar{V}_R
Plane of Closest Approach	Plane which contains the target centroid and is perpendicular to \bar{V}_R
Relative Coordinate System	Coordinate system obtained by rotating the target coordinate system first through the supplement of ψ and then through $-\lambda$ such that the X-axis is aligned with \bar{V}_R . Note that the Y-Z plane is the plane of closest approach.
X_M (Burst point)	X coordinate in the relative coordinate system of the point at which the warhead is detonated
Y_M	Y coordinate in the relative coordinate system of the point of closest approach
Z_M	Z coordinate in the relative coordinate system of the point of closest approach
R_M (miss distance)	distance between point of closest approach and target centroid
θ	Angle whose tangent is $\frac{Z_M}{Y_M}$

Note that in the plane of closest approach, Y_M and Z_M are the rectangular coordinates of the point of closest approach, while R_M and θ are its polar coordinates.

Thus, to define a particular endgame situation, one can specify the values of V_M , V_T , ψ_C , γ , α , X_M , Y_M , and Z_M , or one can specify the values of V_R , ψ , λ , β , X_M , R_M , and θ , or one can specify some other set of parameters which contains the essential information. To limit the scope of this project, the value of γ (and hence, also λ) is assumed to be zero. Therefore, all endgame encounters considered herein can be completely described without consideration of any elevation angles. For purposes of methodology demonstration, this limitation has negligible impact because the means of accounting for λ should be essentially the same as that for ψ . The assumption is made merely to limit the size of the project.

The set of factors containing V_R , ψ , β , X_M , R_M , and θ is deemed the most appropriate set of inputs for purposes of studying the input/output relationships of SHAZAM for several reasons. First, it combines the information provided by V_T , V_M , ψ_C , and α into just three factors: V_R , ψ , and β . Secondly, the individual effect of V_M on P_K depends not only on the value of V_T , but on the value of ψ_C as well. The relationship of P_K to both V_R and ψ , however, is more direct and less dependent on interaction. Finally, the effects of Y_M and Z_M are also highly interdependent, while the use of R_M and θ separates the effects of distance and orientation.

Unfortunately, SHAZAM is designed to accept only V_M ,

V_T , ψ_C , α , X_M , Y_M , and Z_M as inputs to describe the geometry. The relationship between these inputs and those mentioned above is given in Appendix A.

The Empirical Approach

In a purely empirical approach, it is necessary to design an experiment which exposes the effects of the factors on P_K . There are both individual effects and combined effects which must be accounted for. Classical designs such as those utilized in RSM generally require a large number of data points. For example, a full factorial experiment with six factors at four levels each requires 4096 data points. The amount of computer time required by SHAZAM to compute a single P_K is dependent upon the number of iterations required to achieve the specified variance. The smallest acceptable number of iterations is 30, while no more than 70 iterations are required to attain a 90 percent confidence interval about the P_K estimate with a halfwidth of 0.1. Under these conditions, SHAZAM requires an average of about 10 CP seconds (on a CYBER 175) to compute a single P_K . Hence, a full factorial experiment would require 40,960 seconds (or more than 11 hours) of CP time!

A second problem with classical designs is that in the case of the endgame situation, not all combinations of factor levels would yield a viable endgame encounter. For example, if $\psi = 180^\circ$, β must be very small in order for the geometry to resemble reality. However, for $\psi = 90^\circ$, β cannot be very small

at all. Hence, many data points would have to be omitted from even a partial factorial experiment. The result would be the loss of most of the advantages that these designs are supposed to provide.

Finally, X_M exhibits properties of both a factor and a response. For any combination of the other five factors, changing X_M (the burst point) can cause P_K to change from 0 to 1.0 or vice versa. Furthermore, the values of X_M which yield non-zero values of P_K are highly dependent upon the settings of the other factors.

In view of these difficulties, it is necessary to custom design an experiment to yield the necessary information with a reasonable amount of computer time. The selected region of experimentation is presented in Table III. The range of values for V_R is based on values which are typically encountered in most missile systems. Because the target is symmetric and $\lambda = 0^\circ$, ψ need only be examined from 0° (head-on) to 180° (tail-on). The value of β can range from 0 to an upper limit which is determined by the maximum look-angle of the missile's seeker. The value of 45° is fairly typical of this limit for many missiles. The range selected for R_M encompasses all values of conceivable interest since the P_K at 100 feet is generally very close to zero under any conditions. Of course, θ can have any value from 0° to 360° , and the value of X_M is dependent upon the other factors as previously mentioned.

TABLE III
Region of Experimentation

Factor	Minimum	Maximum
V_R	1000 ft/sec	3000 ft/sec
ψ	0°	180°
β	0°	45°
R_M	0 ft	100 ft
θ	0°	360°
X_M	as needed	as needed

Table IV is a staged experimental design over this region. The underlying premise is that the highest order of significant factor interaction is three. The first stage is designed to yield information about the individual and combined effects of ψ , θ , and X_M . The second stage is designed to expose any change in these effects if only one of the remaining three factors is changed. Stage three examines the effect of simultaneously changing any two of the factors V_R , R_M , and β . Note that in stage three, only one combination of ψ and θ is called for. The assumption is that the effects discovered in this stage are the same for all combinations of ψ and θ . In stage four, the effect of simultaneously varying all three of V_R , R_M , and β is examined. Again, this effect is assumed to be independent of ψ and θ . Stage five is simply a means for verifying that the assumptions hold.

For reasons which are explained later, only the first

TABLE IV
Staged Experimental Design

	ψ°	θ°	$Z_M(\text{ft})$	$V_R(\text{fps})$	$R_M(\text{ft})$	β°
<u>Stage 1:</u>						
	0	45				
	45	135				
	90	225	5	2000	15	15
	135	315	NZYV*			
	180					
<u>Stage 2:</u>						
	45	45	5	1000	15	15
	180	225	NZYV	3000		
	45	45	5	2000	27.5	15
	180	225	NZYV		40	
	45	45	5	2000	15	7.5
	180	225	NZYV			22.5
<u>Stage 3:</u>						
	135	225	5	1000	27.5	15
			NZYV	3000	40	
	135	225	5	1000	15	7.5
			NZYV	3000		22.5
	135	225	5	2000	27.5	7.5
			NZYV		40	22.5
<u>Stage 4:</u>						
	135	225	5	1000	27.5	7.5
			NZYV	3000	40	22.5
<u>Stage 5:</u>						
Experiment as needed.						
*NZYV = Non-zero yielding values						

stage of this experiment was completed. The following is a discussion of the analysis of the data generated by this first stage.

For each combination of ψ and θ , the data were plotted with P_K as the ordinate and χ_M as the abscissa. All of these plots displayed a common characteristic: in each case, P_K was zero until a very steep rise to one, where it stayed for some distance and then rapidly dropped to zero again. The width and location of this "pulse" varied with ψ and θ .

All attempts to fit polynomial functions to these pulses using either numerical analysis or linear regression were fruitless. No polynomial of reasonably low order could be found to fit all of the pulses. In fact, to fit any single pulse, it was necessary to "clip" every polynomial that was examined to prevent it from either exceeding one or going below zero. It became apparent that some other means of fitting these pulses was needed.

After numerous candidate functions were examined, it was found that the function:

$$P_K = e^{-\left(\frac{\chi_M + a}{b}\right)^g}$$

could be made to fit each plot reasonably well just by changing a and b . In addition, no clipping was necessary since the function can never exceed one nor be less than zero. Unfortunately, the non-linear nature of this function virtually eliminates RSM as a useful tool.

The problem then became one of accounting for the changes in a and b due to changes in ψ and θ . The value of a corresponds to the negative of the value of X_M at the center of the pulse while b is the halfwidth of the pulse as measured between the points $P_K = 1/e$ on the up and down side.

For each data plot, the values of a and b were visually estimated. These estimates were plotted versus θ , holding ψ constant. In each case, it was found that a function of the form

$$C_1 + C_2 \sin^2 \left(\frac{1}{2}\theta + C_3 \right)$$

could be used to reasonably fit each of these plots (see Appendix B, Figures 1 through 5 for a and Figures 6 through 10 for b). It then remained to describe the changes in C_1 , C_2 , and C_3 with changes in ψ for the "location" (a) function and the "halfwidth" (b) function (see Appendix B, Figures 11 through 13 for location and Figures 14 through 16 for halfwidth). The resulting functions were as follows:

$$a = 5.5 + 5 \sin \psi - 10 \sqrt{\sin^2 \left(\frac{\psi}{180} \right) \sin^2 \left(\frac{\theta}{2} \right)}$$

$$b = 10 - 3 \sin \left(\frac{\psi}{90} \right) - 5e^{-\left(\frac{\psi - 100}{84} \right)^8} [H]$$

where

$$H = \sin^2 \left[\frac{1}{2}\theta + 90 \cos^2 \left(\frac{1.33(\psi - 45)}{4} \right) \cos^3 (1.33[\psi - 45]) \right]$$

Thus, the function arrived at to predict P_K , given ψ , θ , and X_M was:

$$P_K = f(\psi, \theta, X_M) = e^{-\left(\frac{X_M + a}{b}\right)^\beta}$$

with a and b as described above. For each of the 16 combinations of ψ and θ generated in stage one, this function was plotted along with the data points to visually examine the fit (see Appendix B, Figures 17 through 32).

Examination of these plots led to several conclusions. First, although the basic behavior of SHAZAM was captured by the function, there was substantial error on some of the plots. This error was partially due to the fact that in some cases, the rise was either too steep or too shallow. A second contributor to the error was the generally poor fits to the functions for C_1 , C_2 , C_3 , a , and b . Obviously a second iteration was required using linear regression to fit these functions rather than rough calculation.

The second conclusion was that while the functions for a and b only accounted for two of the factors ψ , θ , V_R , R_M , and β , they had already become immensely cumbersome and almost intractable. How much more so would they become for all five factors?

In contemplation of this question, the conclusion was reached that the original assumption concerning the insignificance of higher than third order interactions was incorrect. Clearly, since ψ , θ , V_R , R_M , and β are all essential in describing the endgame geometry, then the effect of any one of these factors on the width and location of the pulse is dependent on the settings of all four of the remaining factors.

To discover the functional relationship which accounts for this fifth order interaction would require an excessive amount of experimentation. Whether such a function could be found is questionable, and even if it could, it would probably be so unmanageable and error prone that it would be of limited usefulness. Furthermore, in terms of a general methodology, it must be remembered that an additional factor, elevation angle, must eventually be included. Therefore, it was decided to abandon the purely empirical approach in favor of a method utilizing the geometry itself to account for the interactive effects of the factors on a and b.

A Semi-Empirical Approach

The idea in this approach is to explain as much as possible of the variation in a and b caused by the factors ψ , V_R , R_M , θ , and β with the geometry itself. The remaining variation is then explained on the basis of empirical observation. Hence, this semi-empirical approach is a combination of analytical and empirical methods.

Recall that the purpose of an endgame program is to account for the interaction between the warhead characteristics, the geometry, and the vulnerability model. This interaction can be viewed as consisting of two processes: the interactive effect of the warhead characteristics and the geometry on the motion of the warhead fragments, and the interaction between the fragments and the vulnerability model. Note that blast effects have been excluded in this discussion and will be

addressed later.

The interaction between the fragments and the vulnerability model is determined by the nature of the fragments themselves as well as by the direction and magnitude of their velocity vectors. None of the parameters which describe the geometry have any effect upon such things as fragment mass and size. However, the geometry does have a profound effect on the speed and direction of travel of the fragments.

The interaction between the warhead characteristics and the geometry can be analytically calculated given enough information about the warhead model. The information needed concerns the direction and speed with which fragments are ejected from the warhead under static conditions. For the warhead model in the version of SHAZAM used in this study, the fragment velocity, V_F , is 5500 feet per second. There are two directions between which fragments are ejected: 84° and 91° as measured from the missile centerline.

An accurate way to describe fragment motion is to consider each fragment individually. In this method, the fragment velocity vector is added to the relative velocity vector to determine the path of the fragment relative to the target.

Another way of accounting for fragment motion is to consider the static fragment pattern as a cone emanating from the warhead. In the dynamic situation, the orientation of the cone with respect to the missile centerline as well as the half-angle of the cone are changed according to the magnitude and direction of the relative velocity vector. This

process is an approximation to the true dynamic warhead pattern described in the preceding paragraph. The approximation is generally very good, but some error is introduced in the case when β is large and the conic section described by the intersection of the X-Z plane (in the target coordinate system) and the cone is an ellipse or a circle. The method of calculating the cone and some illustrations of the approximation are given in Appendix C.

The advantage of a cone description of the warhead pattern is that the intersection between the cone and the infinite line containing the target centerline can be obtained analytically. There are two ways to solve for this intersection: 1) given a specific point on the line, determine the value of X_M at which the point lies on the cone; or, 2) given X_M , find the point or points on the line, if any, which are also on the cone. The mathematical solutions to these two problems are given in Appendix D.

For each data point generated in stage one of the experiment described in the preceding section, the points on the target centerline lying on the cone were obtained using the second method of solution mentioned above. There seemed to be a relationship between where the pulse "jumped" and where the cone hit on the target centerline. In fact, it seemed that whenever at least one of the two fragment cones (one cone representing the leading edge and one the trailing edge of the warhead pattern) was hitting the target centerline between about seven feet behind the centroid and about five feet in front of the centroid, the

P_K was near its highest value.

To further test this relationship, more data were generated using differing values of V_R and R_M . In all, a total of 48 P_K versus X_M data plots were produced. The combinations of factor values examined are given in Table V. Examination of these plots revealed that the relationship was fairly good except for situations when R_M was large. In such cases, the maximum value of P_K seemed to decrease, while the "vulnerable length" along the target centerline seemed to shrink considerably. While the decrease in P_K can be rationalized, the shrinkage in the vulnerable length seemed excessive. The pulse became exceedingly narrow for only moderately high values of R_M .

A possible reason for this apparent shrinkage in the vulnerable length was the use of the random angle-of-attack (α) option in SHAZAM in the generation of the data. This option was intentionally exercised for the original experiment in hopes of making the rise from $P_K = 0$ to maximum P_K more shallow and, hence, possibly easier to fit. In fact, for larger miss distances, it had the opposite effect.

To understand the reason for this, one must understand the way that SHAZAM treats α as a random variable when that option is exercised. A mean value and standard deviation for α must be specified. Then, for each iteration, SHAZAM selects a random sample from a normally distributed population with mean and standard deviation as specified. This value is then used as the value for α for that single iteration. For the

TABLE V

Combination of Factor Values Examined in Basic Data

$\psi(^{\circ})$	$\theta(^{\circ})$	V_R (fps)	R_M (ft)	$\beta(^{\circ})$	$\psi(^{\circ})$	$\theta(^{\circ})$	V_R (fps)	R_M (ft)	$\beta(^{\circ})$
0	225	2000	15	0	135	135	2000	27.5	15
0	225	2000	27.5	0	135	135	2000	40	15
0	225	2000	40	0	135	225	1000	15	15
0	225	3000	15	0	135	225	2000	15	15
0	135	2000	15	0	135	315	2000	15	15
0	135	3000	15	0	180	135	1000	15	0
45	45	2000	15	15	180	135	1000	27.5	0
45	45	2000	27.5	15	180	135	1000	40	0
45	45	2000	40	15	180	135	2000	15	0
45	135	2000	15	15	180	135	2000	27.5	0
45	135	3000	15	15	180	135	2000	40	0
45	225	2000	15	15	180	135	3000	15	0
45	315	2000	15	15	180	135	3000	27.5	0
45	315	3000	15	15	180	135	3000	40	0
90	45	2000	15	15	180	225	1000	15	0
90	135	2000	15	15	180	225	1000	27.5	0
90	135	3000	15	15	180	225	1000	40	0
90	225	2000	15	15	180	225	2000	15	0
90	225	2000	27.5	15	180	225	2000	27.5	0
90	225	2000	40	15	180	225	2000	40	0
90	315	2000	15	15	180	225	2000	52.5	0
135	45	1000	15	15	180	225	3000	15	0
135	45	2000	15	15	180	225	3000	27.5	0
135	135	2000	15	15	180	225	3000	40	0

next iteration, a new value of α is chosen. The effect is that for each burst point, the missile centerline "oscillates" back and forth, changing from iteration to iteration.

For all of the data points thus far generated, the mean value of α was set at 3° while the standard deviation was set at 1° . This had little effect at small values of R_M since $3'$ results in a deflection of only 52 feet per 1000 feet of distance. Hence, for $R_M = 15$ feet, the fragment cone moved less than a foot along the target centerline. However, at $R_M = 50$ feet, the fragment cone moved up to 2.6 feet! This distance was sufficient to pull the fragment cone out of the vulnerable length completely. The result was that, for a burst point at which a constant $\alpha = 0^\circ$ would have yielded a high P_K due to the leading fragment cone intersecting the vulnerable length, the oscillations of α moved the cone away from the vulnerable length a sufficient number of times to lower the P_K . A comparison between data points generated for the same trajectory both with and without α as a random variable is shown in Figure 4. Note that, as expected, setting $\alpha = 0^\circ$ made the pulse wider.

In view of this effect, all of the data were re-generated with α set to zero. Some shrinkage was still observed in the vulnerable length as R_M became large. This can be explained by noting that since the fragment pattern expands with time, the fragment density grows smaller and, consequently, the pattern is less lethal. This explanation can also be applied to the decrease in maximum P_K with increasing values of R_M . At very

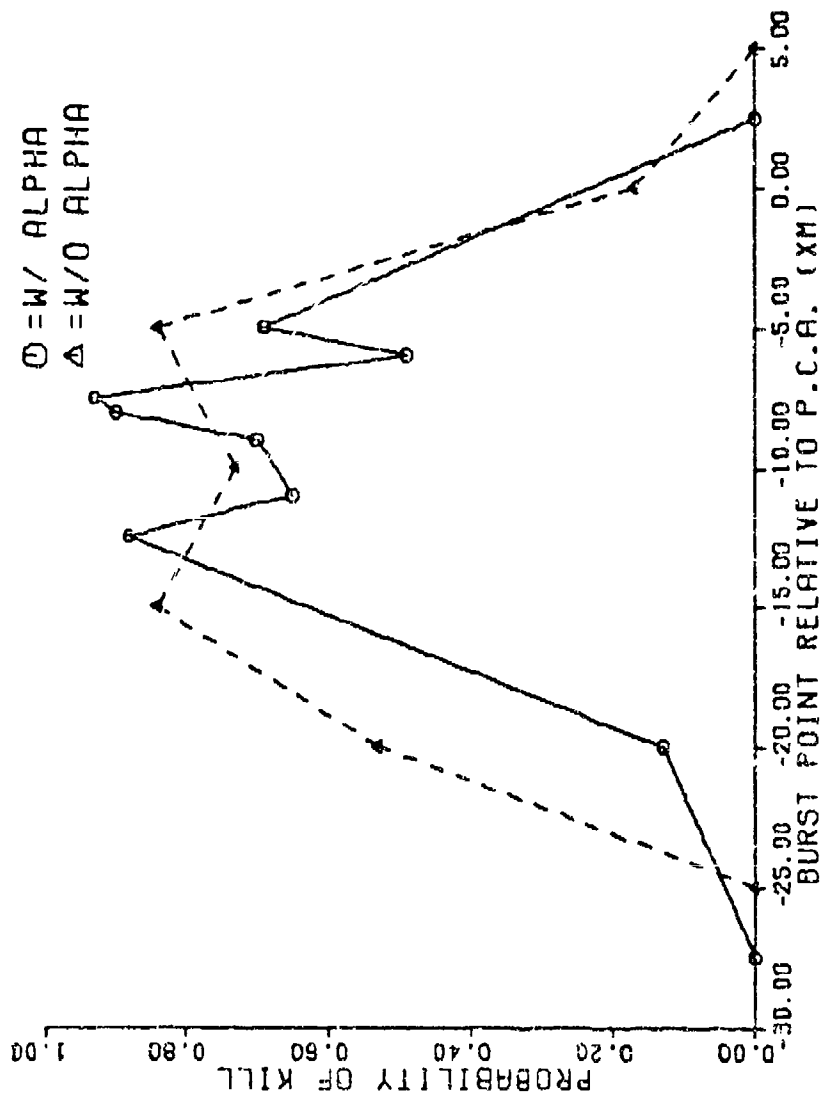


FIG 4 : PSI=180. THETA=225. VR=2000. RM=27.5 BETA=0.

Comparison Between Data With and Without Random Alpha

large miss distances (> 75 feet), the vulnerable length appeared to grow again. Since miss distances of these magnitudes have low P_K 's and are generally rare, this discrepancy has little impact on the characterization.

In examining the newly generated data, it was observed that the vulnerable length appeared longer when θ was between 0° and 180° than it did when θ was between 180° and 360° . The only possible explanation for this is that the target is apparently more vulnerable from the top than it is from the bottom. This also manifests itself in the fact that maximum P_K tends to decrease more slowly with increasing R_M for trajectories above the target as opposed to those below.

The importance of finding this "vulnerable length" relationship is profound. It allows a and b to be determined strictly from the geometry. One need only determine what proportion of maximum P_K is achieved when the vulnerable length is first contacted by a fragment cone. Because of the symmetry of the function, the same proportion of maximum P_K will be achieved when the vulnerable length is last contacted by a fragment cone. The determination of a and b , given this information, is illustrated in Appendix E.

Unfortunately, the endpoints of the vulnerable length and the proportion (P) of maximum P_K achieved at these points cannot be arrived at independently. The selection of each has its own effect on the resultant pulse. Therefore, the selection process is an iterative one--different combinations of endpoints and proportions must be tried and compared to the

data. The final selection of these values is strictly a matter of the experimenter's judgment as to which combination seems to result in the best fit.

In pursuit of this "final selection," it was found that a fixed vulnerable length would not suffice. As previously mentioned, the vulnerable length tended to shrink as R_M increased and this shrinkage occurred at different rates, depending on the value of θ . Furthermore, the endpoints of the vulnerable length seemed to move as ψ moved from 0° to 180° . In fact, for a given value of P , the vulnerable length which yielded the best fit was different for each of the 48 data plots. The problem, then, became one of accounting for the effects of the five factors on the endpoints of the vulnerable length.

The reason for the changes in the endpoints of the vulnerable length with changes in the factors is due to the structure of the vulnerability model. Typically, these models are very detailed descriptions of the vulnerable components of the target. Fragment damage to these components is limited in the model by such things as shielding, angle of incidence, velocity, mass, and fragment density. Obviously, the best way to capture the effects of all of these parameters is with the vulnerability model itself. This, however, is what an endgame program does and is obviously the cause of the excessive computer time requirement.

For the approach taken herein, the vulnerable length is used as a surrogate for the vulnerability model. The ultimate question is: how much of the behavior of the

vulnerability model must be accounted for with changes in the vulnerable length? The answer to this question is again a matter of the experimenter's subjective judgment as to what constitutes an adequate fit. Thus, the experimenter must observe as much of the behavior as possible in the data and then attempt to account for that which he or she thinks is important. If the results are then unsatisfactory, another iteration of the process is required to account for more of the vulnerability model's behavior.

For the data generated in this project, three iterations were performed. The first iteration has essentially already been discussed--that is, the discovery of a vulnerable length with endpoints seven feet before and five feet after the target centroid that seemed to provide a "rough" correlation with the data. In the second iteration, the exponent in the function was changed from eight to six. The result of this was to make the pulse rise and fall more slowly, which seemed to be a more accurate representation of the data. In addition, a linear function was used to describe the decrease in maximum P_K . Also, the rear endpoint of the vulnerable length was moved toward the forward endpoint as a linear function of R_M . The details of these adjustments as well as plots of the resultant characterization for all 48 factor combinations are presented in Appendix F. The plots show that while in many circumstances the fit is very good, there are some situations where the detail in the vulnerability model was not captured very well

at all. The latter is especially true for the larger values of R_M .

The impact of these errors can only be assessed when the results are compared to results produced by SHAZAM in its normal mode of operation. Normally, SHAZAM (as well as other endgame programs) treats R_M and θ as random variables. The reason is that, in reality, the miss distance achievable by a particular missile under a given set of launch conditions is uncertain. Flight tests over the years have shown that although other parameters of the endgame geometry can be fairly well duplicated from firing to firing, the values of R_M and θ cannot be duplicated with any certainty, even though the firing conditions are as closely duplicated as possible. The reasons for this phenomenon are too numerous and complex to discuss here, but the important point is that in actual missile endgame analyses, R_M and θ (and, consequently, Y_M and Z_M) are most often treated as random variables. The most common probability distribution used to describe the distribution of miss distance is the bivariate normal (or Gaussian) distribution, wherein Y_M and Z_M are each assumed to be normally distributed but independently of each other. The mean of each is usually taken to be zero, while the standard deviations are usually made equal and denoted by σ . The result is what is sometimes referred to as the "Circular Normal Distribution." In terms of R_M and θ , the equivalent distribution is the Rayleigh distribution. An important point about this distribution is that only about 39 percent of the possible values of R_M lie

within one standard deviation from the mean, whereas roughly 68 percent lie within one standard deviation from the mean in the univariate normal distribution.

When SHAZAM treats miss distance as a random variable, values for Y_M and Z_M are selected from a normal distribution in a psuedo-random fashion. A new selection of values for Y_M and Z_M , as well as all of the other random variables in the model, is made for each iteration. As previously mentioned, the total number of samples required for each specification of ψ , V_R , β , and σ is between 30 and 70 to achieve a 90 percent confidence interval about the P_K estimate with a half-width of 0.1. The interpretation of this confidence interval is that there is a .9 probability that the estimate is within 0.1 of the "true" estimate. By "true" estimate is meant the estimate that would result if the number of samples approached infinity.

To compare the results of the characterization to those of SHAZAM under these circumstances, it is necessary to account for the randomness in R_M and θ . What is actually called for is the following integration:

$$P_{K_{TOT}} = \int_0^\infty \int_0^{2\pi} P_K(R_M, \theta) P_r(R_M, \theta) d\theta dR_M \quad (3.1)$$

where

$P_K(R_M, \theta)$ is the value of P_K at R_M and θ and

$P_r(R_M, \theta)$ is the joint probability of occurrence of R_M and θ

With the characterization, $P_K(R_M, \theta)$ can easily be found, while

$P_T(R_M, \theta)$ results from the Rayleigh distribution. This integration can be performed numerically with what is known as a "109 Cell Model" of the Rayleigh Distribution. What this model does is to break up the plane of closest approach into 109 cells. For 97 of the cells, the probability that R_M and θ lie within each cell is .01. For the remaining 12 cells, this probability is .0025. The model is illustrated in Appendix G.

One way of estimating Eq (3.1) using the characterization is to find values of a and b for each of the 109 relative trajectories which penetrate the probabilistic "centers" of each of the cells. Then

$$P_{K_{TOT}}(X_M) \approx \sum_{i=1}^{97} (.01) f_i(X_M, a_i, b_i) + \sum_{i=98}^{109} (.0025) f_i(X_M, a_i, b_i) \quad (3.2)$$

where $f_i(X_M, a_i, b_i)$ is the characterization function for the combination of factors ψ , V_R , β , R_{M_i} , and θ_i . R_{M_i} and θ_i represent the probabilistic "center" of the i^{th} cell.

There are two reasons for approaching the miss distance distribution problem in this way. First, there is no variance in the result. The procedure will produce the same answer every time. The error introduced by using Eq (3.2) to estimate Eq (3.1) results from the sum of the weighted differences between the P_K at the probabilistic "center" of each cell and the true average P_K for that cell as predicted by the

characterization. The weight for the difference is just the probability associated with that cell. For example, if the average within-cell error is 0.1, then the total error induced by the 109 Cell Model (E_M) is

$$E_M = \sum_{i=1}^{97} (.01)(0.1) + \sum_{i=98}^{109} (.0025)(0.1) = 0.1 \quad (3.3)$$

Since most of the cells are small, one would expect a much smaller average within-cell error. Note that E_M is just the error caused by using Eq (3.2) to estimate Eq (3.1). The error in using the characterization instead of SHAZAM to estimate P_K can be estimated by

$$E_C = \sum_{i=1}^{97} (.01)(P_{K_{C_i}} - P_{K_{SH_i}}) + \sum_{i=98}^{109} (.0025)(P_{K_{C_i}} - P_{K_{SH_i}}) \quad (3.4)$$

where $P_{K_{C_i}}$ is the average P_K given by the characterization for each cell and $P_{K_{SH_i}}$ is the previously mentioned "true" SHAZAM estimate of the average cell P_K .

The second reason to use the "109 Cell Model" is that for a given combination of ψ , V_R , β , and σ , one need only calculate 109 pairs of values for a and b. Thereafter, an infinite number of values of X_M can be examined.

Actual calculation of E_C using Eq (3.4) is impractical. A total of 109 values of $P_{K_{SH}}$ would have to be calculated. Since $P_{K_{SH}}$ can only be estimated by SHAZAM, the error in the estimate would confound the true value of each of the $(P_{K_{C_i}} - P_{K_{SH_i}})$ terms. Furthermore, a minimum of $30 \times 109 = 3270$

iterations (1/2 hour of CP time) of SHAZAM would be required just to get a single estimate of E_C for a given combination of factor values.

Eq (3.4) does, however, give some indication of the sensitivity of E_C to the kinds of errors observable in the plots in Appendix F. The maximum possible error in any cell is 1.0. The plots show that, in general, the difference between the SHAZAM P_K and the characterization's P_K is much closer to (and quite often less than) 0.1. Furthermore, since some of the P_{K_C} 's are less than the corresponding estimates of the $P_{K_{SH}}$'s while others are larger, there is a tendency to cancel. Therefore, it seems a reasonable expectation that the E_C of the characterization is on the order of 0.1 or less. If E_M is negligible, then a total error of 0.1 or less also seems a reasonable expectation. Figure 5 is an overlay of an evaluation of Eq (3.2) (for a candidate characterization) superimposed on an estimate of Eq (3.1) based on 1000 samples using the same characterization. It appears that E_M (the difference between the two curves) is indeed very small. (The "109 Cell" curve is the lower one.)

The only practical way to estimate E_C is to execute both SHAZAM and the characterization for identical settings of R_M , V_R , β , and σ , and then compare the results. This was done for 13 such combinations using the characterization shown in Appendix F. The resulting data plots are shown in Appendix H.

It is appropriate at this point to discuss the manner in which SHAZAM deals with the problem of direct hit. When

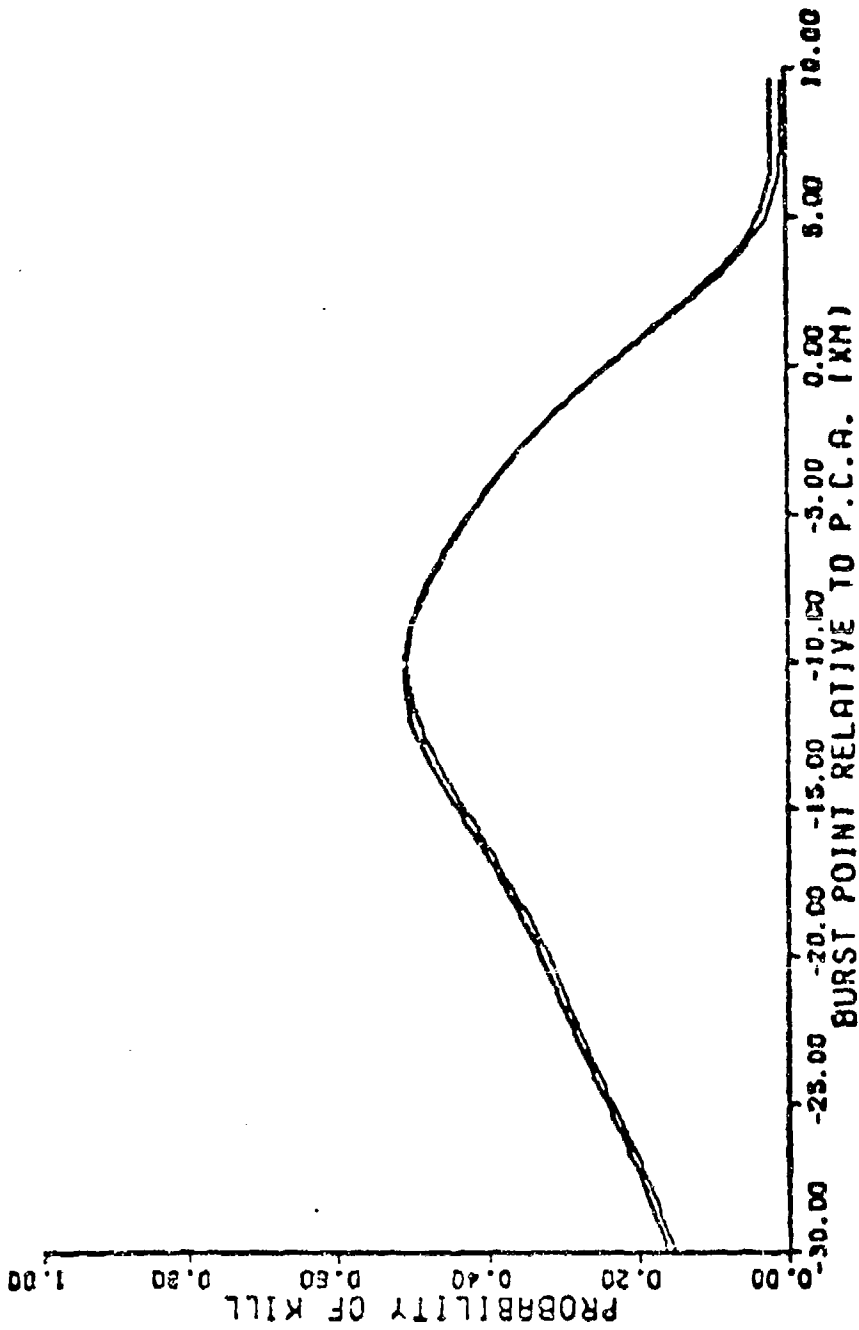


FIG 5 : PSI=145. VR=2200. BETA=15. SIGMA=30.0

109 Cell Model Versus 1000 Random Samples

sampling from a circular normal distribution, there is a certain probability of selecting values of Y_M and Z_M such that the relative trajectory penetrates the target fuselage. The version of SHAZAM used in this study assigns the value of one to the P_K for all such trajectories regardless of burst point. In order to match the SHAZAM results, it is necessary to check for this condition before evaluating the characterization function. Without knowing any of the physical attributes of the target, it was necessary to experimentally determine the target's length and width. A width of about 5 feet and a length of about 30 feet seemed to match the SHAZAM direct hit calculations reasonably well. Hence, in using the 109 Cell Model, the trajectory represented by each cell must first be checked to see if $|Z_M|$ is less than 2.5 feet and $|D_{\text{OFFSET}}|$ (as described in Appendix D) is less than 15 feet. If these conditions are met, the value of P_K for that cell must be set to one for all values of X_M .

The third iteration consisted of making further adjustments to the function in an attempt to correct some of its deficiencies as observed in the plots in Appendix H. The result of this iteration was the following final form of the characterization:

$$P_K = F \cdot e^{-\left(\frac{X_M + a}{b}\right)^6} \quad (3.5)$$

where

$$F = \text{the lesser of } \begin{cases} 1.0 \\ 1.22 - .014R_M \end{cases}$$

and

a and b are determined as described in Appendices D and E with $P = .90$.

The vulnerable length is between BTP and ATP, where

$$ATP = 5$$

$$BTP = [-9.5 + 2.5(\sin[\frac{\psi}{2}]) + 2CH]$$

and

CH is the greater of $\{ (R_M - 15) / 12.5 \}$

and the dropout bias (see Appendix E) is 1 foot.

The 13 plots of this final characterization corresponding to those in Appendix H are shown in Appendix I. Also, some selected plots of this final characterization versus the original data are contained in Appendix J. The reader may wish to compare these to the corresponding plots in Appendix F.

Assessment of the Fit

The 13 combinations of ψ , V_R , β , and σ represented by the plots in Appendix I all have values of ψ , V_R , and β which were used to generate the original data. The ultimate test of this entire method is to compare the final characterization to SHAZAM at points in the region of experimentation which were not used to generate the function. The purpose of the test is to estimate the total error caused by the use of the characterization in lieu of SHAZAM.

As previously mentioned, there is no practical way to precisely calculate this error. It is, therefore, difficult

to construct a test to measure its value. The procedure finally arrived at was to "randomly" select ten combinations of ψ , V_R , and β from the region of experimentation shown on Table III (page 23). The value of σ was selected randomly from the interval (5,30). For each of the ten combinations of ψ , V_R , β , and σ , six equi-spaced values of X_M were examined using SHAZAM. The minimum number of iterations was increased from 30 to 150 and the maximum number from 70 to 385 in order to reduce the halfwidth of the 90 percent confidence intervals to approximately .04.

The ten selected combinations are shown in Table VI. The reader should bear in mind that a truly random combination of ψ , V_R , and β has a low probability of representing a trajectory which is achievable in reality. For example, V_R tends to be higher for low values of ψ than for high values of ψ . Therefore, some selectivity was necessary in choosing the combinations. The most important feature of the selections is that they represent a cross-section of the achievable trajectories within the region of experimentation.

Trajectory number 8 was chosen for use in an additional experiment. In this experiment, SHAZAM was run with angle of attack (α) treated as a normally distributed random variable with a mean of 5° and standard deviation of 1° . The characterization was then exercised also treating α as a random variable with the same distribution. In one case, a single selection of α was made for each cell. In the second case, the "109 Cell Model" was replaced by a random sample of 1000 trajectories

TABLE VI

Ten Selected Random Trajectories

Traj No.	ψ°	V_R (fps)	β°	σ (ft)	ψ_C°	V_M (fps)	V_T (fps)
1	9	2480	4	8.5	13	1724	769
2	30	2604	14	7.6	44	1874	907
3	55	2447	24	16.1	79	2042	1014
4	64	2105	17	24.8	81	1916	623
5	89	1152	41	16.8	130	1504	987
6	105	1799	21	13.5	126	2148	797
7	122	1068	30	9.0	152	1929	1137
8	128	1171	20	15.9	148	1741	756
9	146	1467	11	29.7	157	2099	716
10	168	1646	5	15.2	173	2808	1177

with R_M , θ , and α treated as random variables with distributions as previously described.

The results for the ten combinations are displayed in the form of plots in Appendix K. For the nine combinations with $\alpha = 0^\circ$, approximately 75 percent of the characterization's estimates are within .05 of SHAZAM's estimates at those points where SHAZAM was exercised. At only two (4%) of the SHAZAM estimates is the characterization's estimate farther away than 0.1. The larger errors seem to be a reflection of the tendency of the characterization to drop from its maximum earlier than the SHAZAM estimates.

For the combination with α treated as a random variable,

all estimates are within .05 of SHAZAM's estimates for both the "109 Cell Model" and the random sample of 1000 trajectories. The only detectable difference between these two methods is in the region between $X_M = -15$ and $X_M = -5$. The maximum discrepancy is about .02. Hence, it appears that no significant error is introduced by the use of the "109 Cell Model" with a single random selection of α for each cell.

Thus, the semi-empirical approach resulted in a characterization which met the previously stated tolerance criteria. It remains to develop a general procedure for characterization based on this experience.

IV. Suggested Method of Characterizing Endgame Models (MOCEM)

Recall that the objectives of this thesis are twofold. Eq (3.5) and its associated parameters represents the accomplishment of the first objective of achieving a characterization. The second objective, that of defining a procedure for arriving at a characterization, is discussed in this chapter.

The most desirable form of such a procedure would be that of an "algorithm" so that an endgame model could be inserted in one side and its characterization would then emerge from the other side. Unfortunately, the procedure used to arrive at the final characterization in Chapter III does not easily lend itself to mechanization. The degree of subjectivity used in each iteration was so large that it defies rigorous definition.

Consequently, based on the experience represented by Chapter III, only a heuristic procedure can be suggested. The following steps are recommended to the reader who wishes to perform his or her own characterization of an endgame model:

- 1) Disable the blast kill calculation portion of the endgame program.
- 2) Select the set of factors which seems to have the most direct impact on the P_K predictions of the

endgame program under consideration.

- 3) Select a range for each parameter to define a region of experimentation. Beware that the larger the region of experimentation, the more the probable effort required to arrive at a characterization.
- 4) Perform a small preliminary experiment over the region of experimentation to determine the general nature of the function required. Select discrete values of miss distance--i.e., do not treat it as a random variable in this step.
- 5) Search for a function which exhibits the appropriate behavior. Hopefully, a function of the form:

$$f = e^{-\left(\frac{X+a}{b}\right)^{2n}}, \text{ n an integer}$$

is satisfactory. (The remainder of this procedure assumes that this is the case.)

- 6) Adjust the cone approximation of Appendix C to fit the behavior of the warhead model.
- 7) Generate a data base with the endgame program. Select factor combinations from all parts of the region of experimentation. It is not necessary to perform a full factorial experiment. Simply select enough factor combinations to create what seems to be a representative sample of the region of experimentation. Again, do not treat miss distance as a random variable--i.e., select discrete relative trajectories.

- 8) Use the cone solutions of Appendix D (suitably generalized to account for elevation angle if needed) to establish a vulnerable length for each factor combination. Depending on the nature of the warhead model and the vulnerability model, it may be necessary to define more than one vulnerable length along the target.
- 9) Observe the effects of factor changes on the endpoints of the vulnerable length(s). Use any available means to describe these relationships analytically. When it is felt that a sufficient amount of the behavior of the vulnerability model has been captured in this way, plot the function versus the data and note any deficiencies. Attempt to correct these deficiencies before proceeding to step 10.
- 10) Select a "comfortable" number of factor combinations from those used to generate the data. Using these combinations, exercise the endgame program, treating miss distance as a random variable. Be sure that the method of dealing with direct hit is the same for the characterization as it is for the endgame model. If the distribution of miss distance is circular normal, use the "109 Cell Model" in Appendix G. Otherwise, draw a sample of about size 300 from the appropriate distribution for each combination of factors. In either case, compare the results and attempt to correct any unacceptable deficiencies.

If the deficiencies cannot be corrected, go back to step 9; otherwise proceed to step 11.

- 11) Select a number of "random" combinations of factors from the region of experimentation. Be sure to include the parameter(s) which describe the miss distance distribution in the random selection process. The number of samples selected depends on the subjective "confidence" desired. Exercise both the endgame program and the characterization, treating miss distance as a random variable. Again, compare results. If unsatisfactory, go back to step 9. Otherwise, it is now acceptable to use the characterization arrived at for whatever purpose it was intended. (Note: Any subsequent arrival at step 11 will require generation of a new "random" sample of factor combinations. It is improper to use the same sample to test for the same deficiencies which were discovered in prior accomplishments of step 11. It is, however, acceptable to use the previous "random" sample(s) from step 11 in subsequent accomplishments of step 10.)
- 12) Be wary of using the characterization outside of the region of experimentation. Larger than acceptable errors may be encountered. It is also prudent to question any unusual behavior of the characterization within the region of experimentation. Such behavior should be verified with the endgame program

upon which the characterization is based.

There are two special considerations to be reckoned with in this procedure. The first concerns the blast kill mechanism. If the experimenter feels that there are a significant number of factor combinations which would result in blast kills but would not otherwise result in fragmentation kills in the endgame program, a blast envelope calculation should be performed in the characterization immediately following the direct hit calculation and the blast kill calculation in the endgame program should not be disabled. This may pose some difficulty if the actual physics of the blast is modeled in the endgame program. There should, however, be no difficulty with the standard "envelope" type of calculation.

The second consideration concerns the fuze. If a fuze model is included in the endgame program, it must be detached and dealt with separately. Otherwise, X_M cannot be treated as a factor (as this method requires) since the value is determined by the fuze model. Upon completion of the characterization, the fuze model can then be linked to the characterization in the same manner that it was originally linked to the endgame program.

V. Summary, Conclusions,
and Recommendations

The objectives of this research have been to: 1) characterize an endgame model, and 2) develop a method for accomplishing such a characterization.

In accomplishing the first objective, a version of the endgame program known as SHAZAM was taken to be representative of such programs in terms of difficulty in characterization. The factors studied were selected based on the geometric fundamentals of the endgame problem. No experimentation was performed for the purpose of factor selection.

A purely empirical approach was pursued in the first attempt to characterize SHAZAM. A mathematical function was found which demonstrated the same basic behavior as the data generated with SHAZAM. The high order of interaction between the factors prevented the accomplishment of a complete characterization with this approach.

A semi-empirical approach was then pursued. This approach attempted to account for the factor interactions caused by the combined effects of the geometry and the war-head characteristics. It was found that a "vulnerable length" along the target centerline could be used as a surrogate for the vulnerability model. Adjustments to this vulnerable length due to factor changes were arrived at empirically.

The resulting information was used to adjust the basic function discovered in the empirical approach. The final characterization resulting from the semi-empirical approach was compared to a "random" selection of data generated by SHAZAM. The characterization's estimates were within 0.1 of SHAZAM's estimates for 97 percent of these cases.

The second objective of developing a characterization method was accomplished based on the semi-empirical approach. The resulting method was a heuristic one due to the subjective nature of the characterization process.

The amount of computer time consumed by the semi-empirical approach in arriving at the final characterization was approximately one hour (on a CYBER 175). Another hour was consumed in generating the 60 data points used to verify the performance of the characterization. A computer program implementing the mathematics of Appendices C, D, E, and G consisted of less than 150 FORTRAN statements and could generate a single P_K prediction in approximately 0.2 CP seconds. Since no attempt was made to make the program efficient, it follows that even less time is actually required. Using the "109 Cell Model" of Appendix G, any number of burst points can be evaluated with very little additional expenditure of computer time. For example, each curve representing the characterization in the plots in Appendices H, I, and K consists of 100 burst points. The total CP time expended to calculate each curve was 0.6 seconds, including the time required to generate the plot. Thus, the time expended per

P_K estimation has an upper bound of 0.2 CP seconds, but can be lower depending on the efficiency of the program and the number of points calculated.

Although it is difficult to calculate the exact error which results from the use of the characterization in lieu of SHAZAM, the results indicate that the error is of approximately the same magnitude as the uncertainty in the SHAZAM results when 30 to 70 iterations are used. Since SHAZAM requires from 10 to 20 CP seconds for each such P_K estimate, the time savings resulting from the substitution of the characterization for SHAZAM is approximately two orders of magnitude and possibly more.

Not a great deal of time was spent in attempting to capture the details of the vulnerability model's behavior. It is conceivable that if one was willing to spend the time, sufficient refinements could be made to the characterization to virtually duplicate the SHAZAM results with no detectable error.

Hence, what has been shown is that an endgame model can be sufficiently characterized under somewhat limited conditions. Whether every endgame model can be characterized in this way is another question. Differences in warhead characteristics, target characteristics, and endgame program methodology may have a critical impact upon the ability of the method to accomplish an adequate characterization. However, the suggested procedure, having worked in this case, should be the first approach taken in any future efforts of this

nature.

There are several potential areas of future research which would provide more generality to the results presented herein. The inclusion of elevation angle is certainly the area which demands first attention. In addition, application of the method to different combinations of endgame models, warhead models, and vulnerability models would illuminate the question of general applicability of the approach. Also, a method for mechanizing the suggested characterization procedure is highly desirable. Accomplishment of such an algorithm depends highly on the development of a "measure-of-merit" of fit which can suitably replace the subjective judgment as used herein. Finally, expansion of the method of characterization to include the fuze model should be investigated.

Bibliography

1. Military Handbook-XXX-1. Survivability/Vulnerability, Aircraft-Nonnuclear, General, Vol. 1. Washington, DC: Department of Defense, 30 April 1979.
2. Scheid, Francis. Theory and Problems of Numerical Analysis. Schaum's Outline Series. New York: McGraw-Hill, 1968.
3. Gerald, Curtis F. Applied Numerical Analysis. 2d Ed. Reading, Mass.: Addison-Wesley, 1978.
4. Draper, N.R., and H. Smith. Applied Regression Analysis. New York: John Wiley & Sons, 1966.
5. Mendenhall, William, and Richard S. Schaefer. Mathematical Statistics With Applications. North Scituate, Mass.: Duxbury Press, 1975.
6. Graybill, Franklin A. Linear Statistical Models. New York: McGraw-Hill, 1961.
7. Box, G.E.P. "The Exploration and Exploitation of Response Surfaces: Some General Considerations and Examples," Biometrics, X (1954), 16-60.
8. _____ and N.R. Draper. "A Basis for the Selection of a Response Surface Design," Journal of the American Statistical Association, LIV (1959), 622-654.
9. Davies, O.L. (Ed.). Design and Analysis of Industrial Experiments. New York: Hafner Publishing Company, 1963.

APPENDIX A

Relationship Between Selected Factors
and SHAZAM Inputs

This appendix contains a description of the relationship between the selected factors V_R , β , and ψ to the SHAZAM inputs V_M , V_T , ψ_C when $\lambda = 0$.

From Figure A-1, and if $\alpha = 0$, we have:

$$\psi_C = \psi + \beta$$

Given V_R , β , and ψ , by the Law of Sines,

$$\frac{V_M}{\sin \psi} = \frac{V_R}{\sin(180 - \psi_C)}$$
$$\Rightarrow V_M = \frac{V_R \sin \psi}{\sin \psi_C}$$

Similarly,

$$V_T = \frac{V_R \sin \beta}{\sin \psi_C}$$

Given V_T , V_M , and ψ_C , by the Law of Cosines,

$$V_R^2 = V_M^2 + V_T^2 - 2V_M V_T \cos(180 - \psi_C)$$

$$\psi = \sin^{-1} [(V_M/V_R) \sin \psi_C]$$

$$\beta = \psi_C - \psi$$

If $\alpha \neq 0$, $\beta - \alpha$ should be substituted for β in the above expressions. The values of X_M , Y_M , and Z_M are the same for the

selected factors as for SHAZAM. R_M and θ are defined in Chapter III.

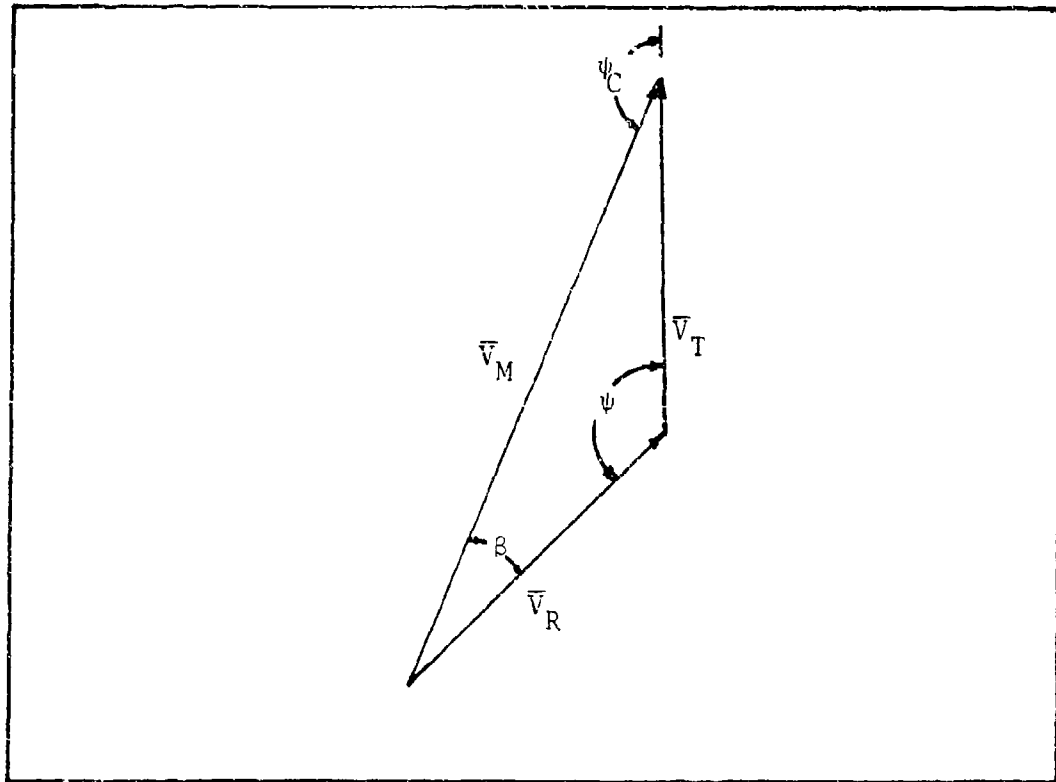


Fig A-1: Factor Relationships

APPENDIX B

Results of the Empirical Approach

This appendix contains plots which depict the results of the empirical approach discussed in Chapter III.

Figures B-1 through B-5 represent the plots of "a" versus θ (location function) for the five values of ψ in the first stage of the experiment. Figures B-6 through B-10 are the plots of "b" versus θ (halfwidth function) for the five values of ψ . The curves are the "fits" whose equations are shown on the individual plots.

The fit equations in Figures B-1 through B-10 are all of the form:

$$C_1 + C_2 \sin^2\left(\frac{1}{2}\theta + C_3\right)$$

The data points in Figures B-11 through B-16 represent the values of C_1 , C_2 and C_3 as a function of ψ for both the location function and the halfwidth function. C_1 is the constant term, C_2 is the amplitude term, and C_3 is the phase term. The curves represent the fitted equation which is shown on each plot.

Figures B-17 through B-32 are plots of the characterization (from the empirical approach) versus the data generated by SHAZAM for stage 1 of the experiment. The values of the factors are shown on each plot. The "error bars" on the data

points represent the 90 percent confidence interval about the mean P_K --i.e., $\pm .10$.

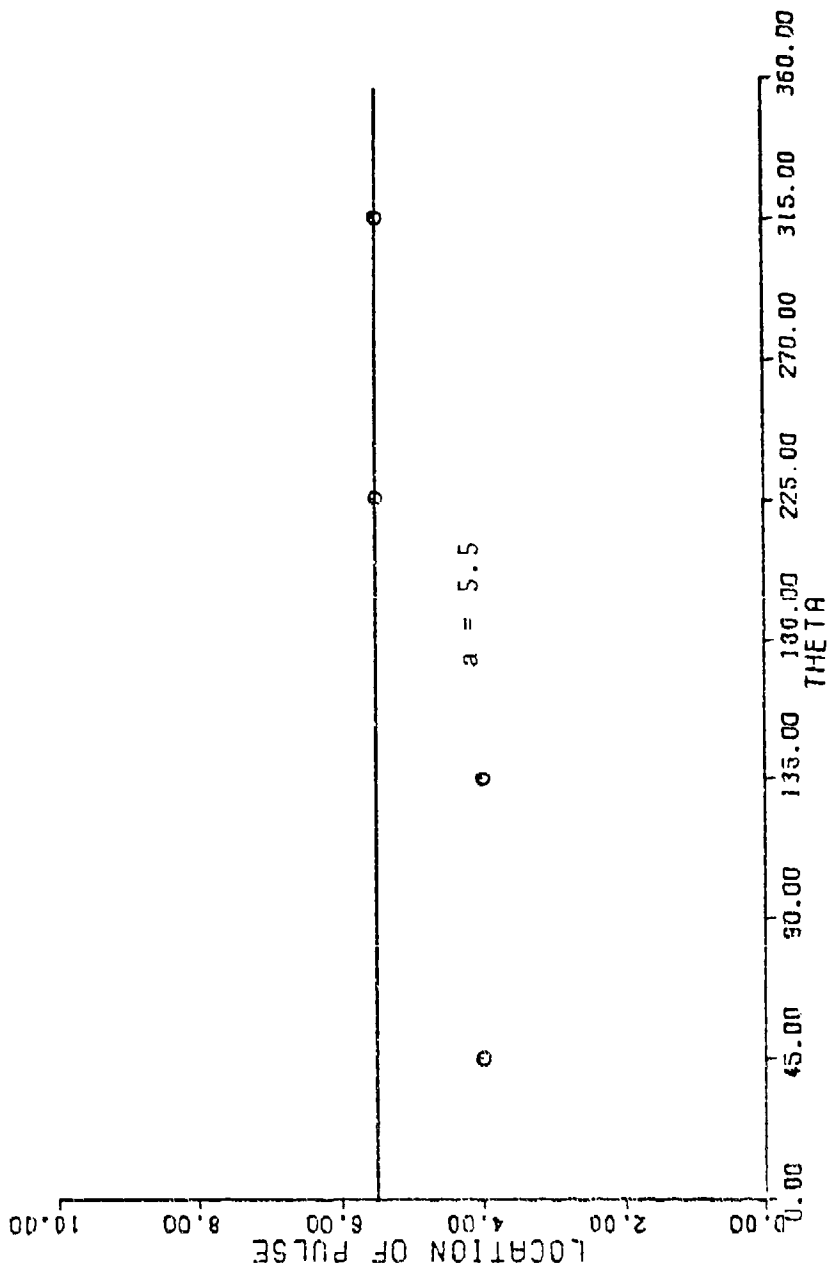


FIG B-1: LOCATION FUNCTION, PSI = 0.

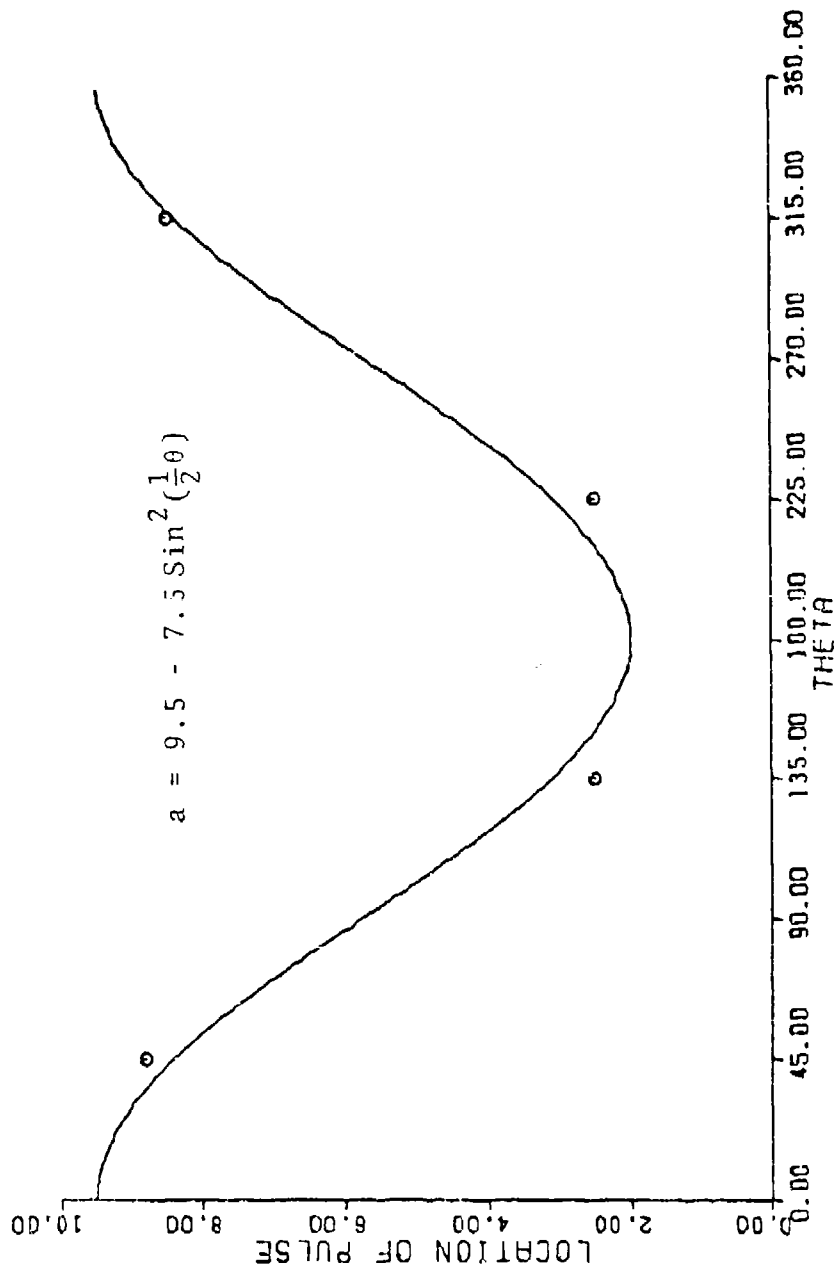


FIG B-2 : LOCATION FUNCTION, PSI= 45.

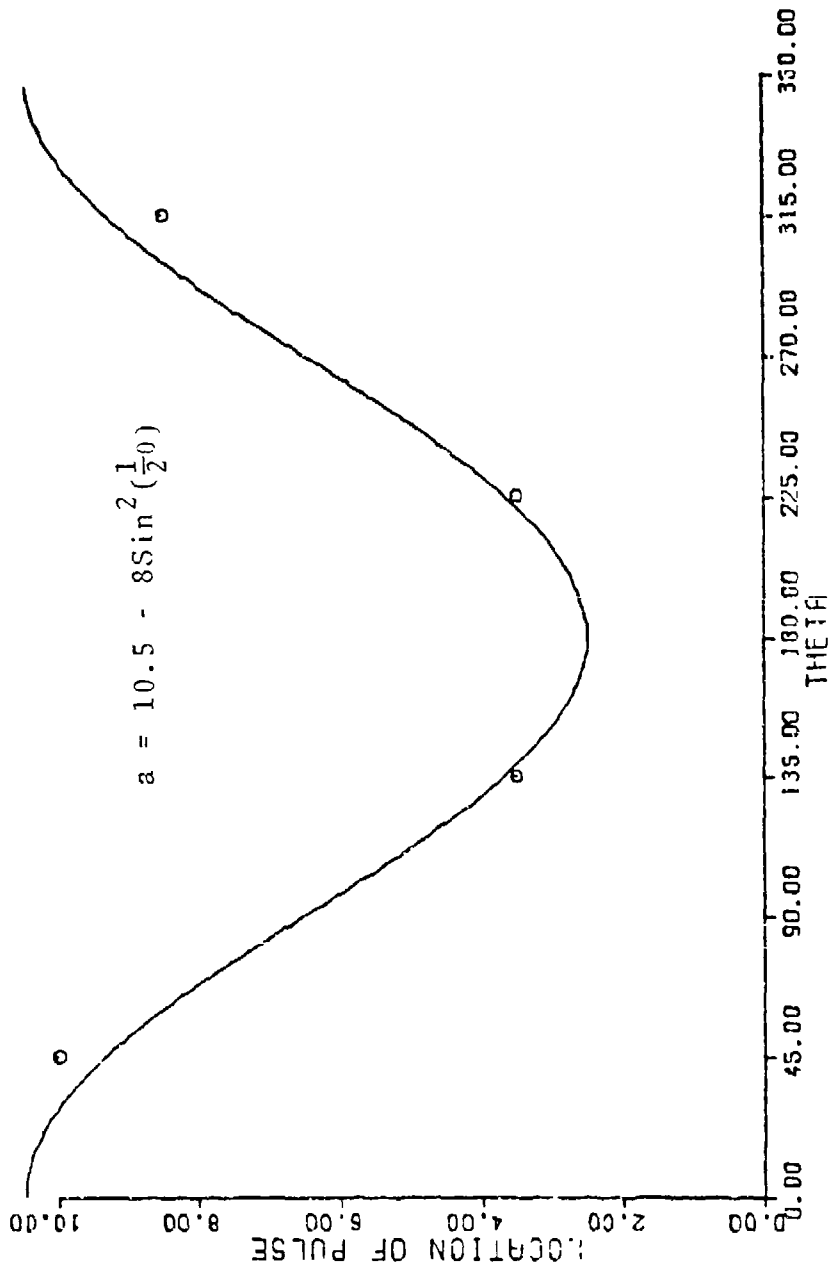


FIG B-3: LOCATION FUNCTION, PSI= 90.

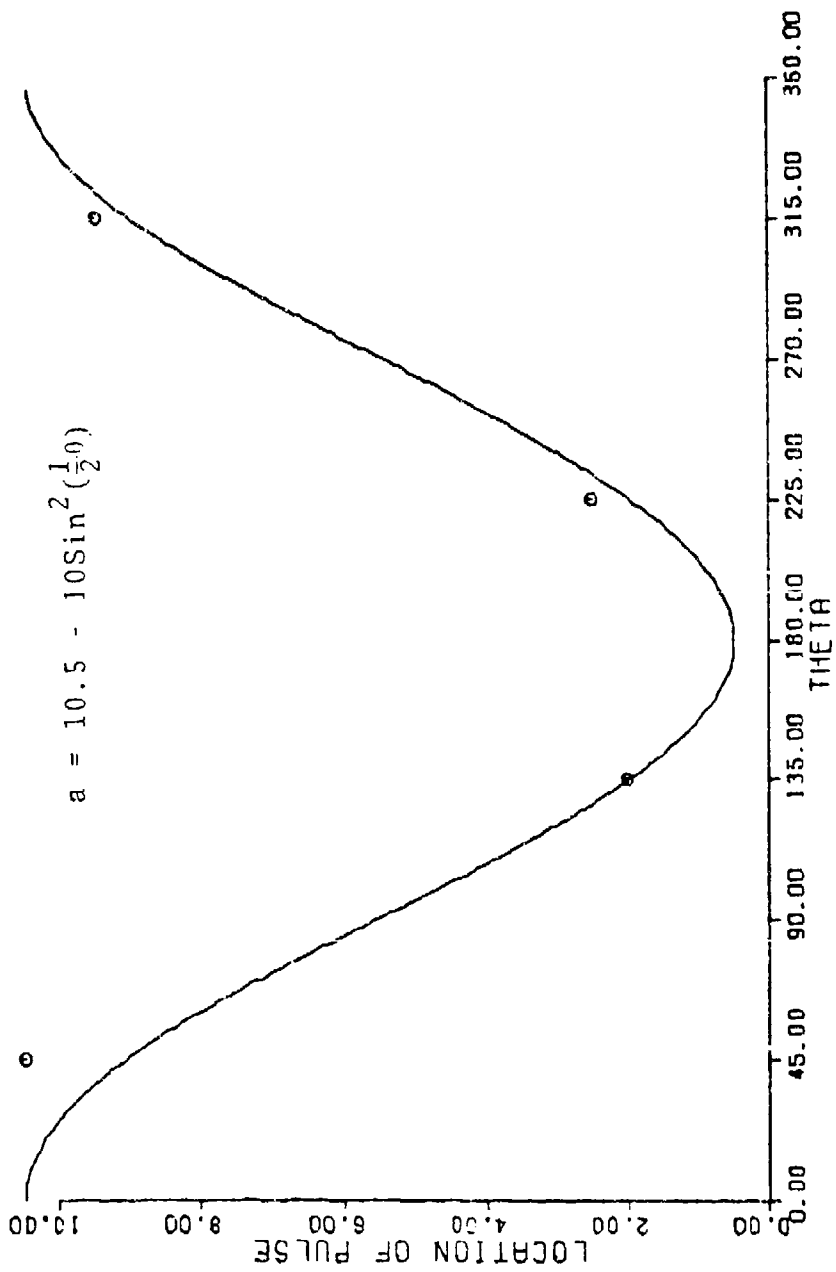


FIG B-4: LOCATION FUNCTION, PSI = 135.

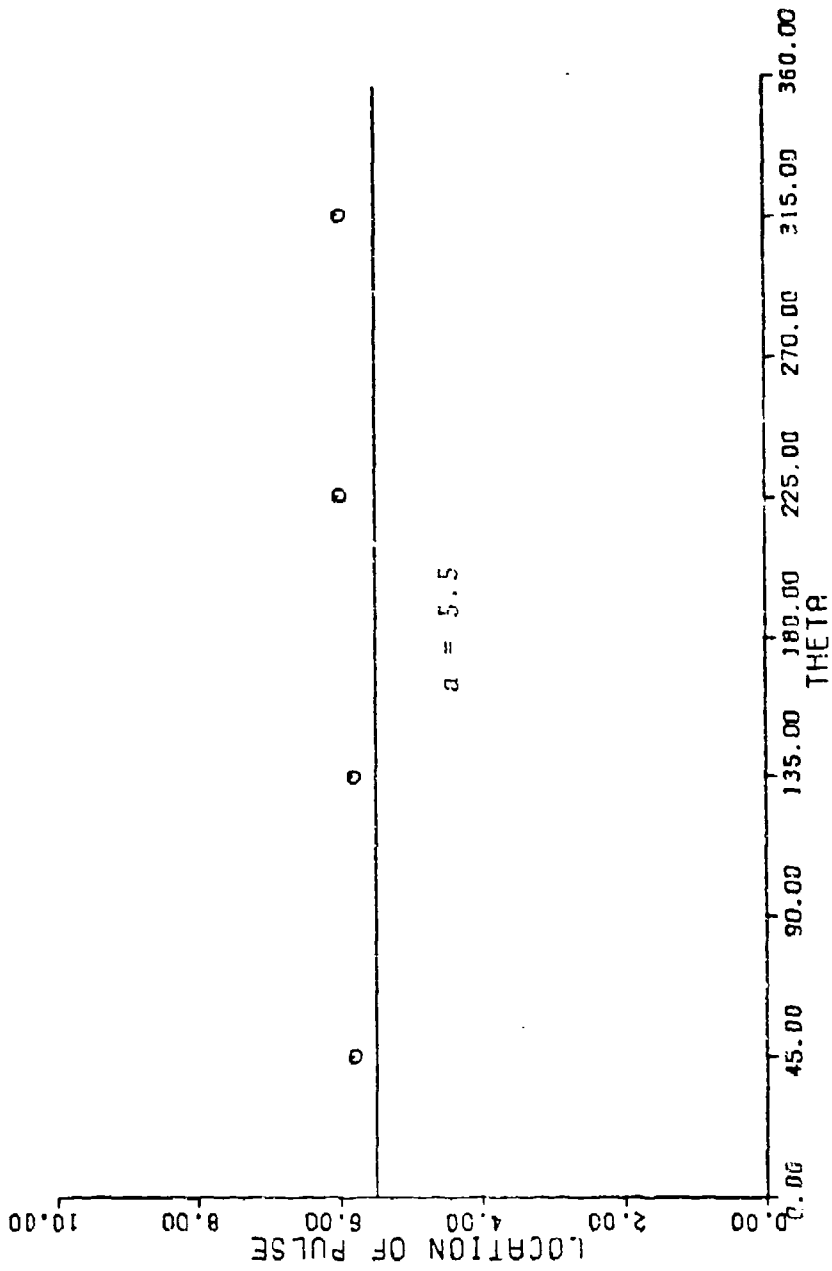


FIG B-5: LOCATION FUNCTION. PSI = 180.

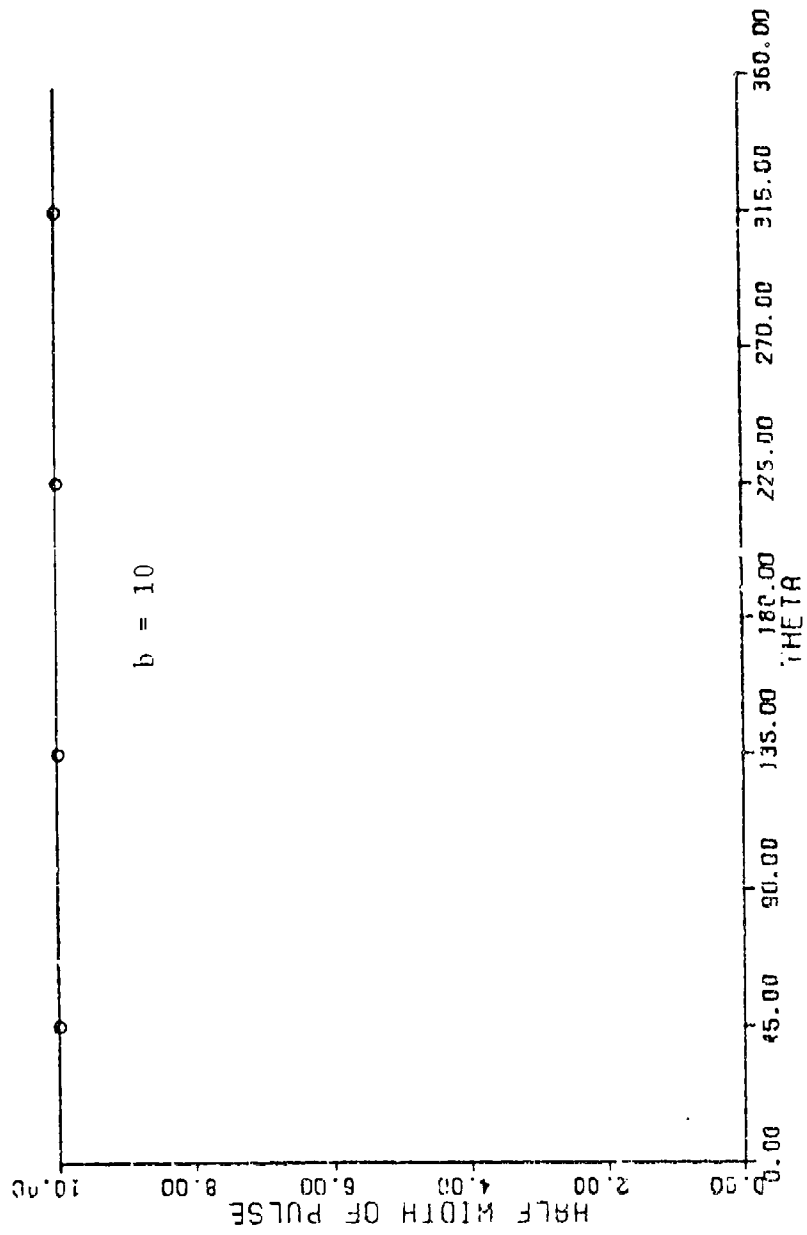


FIG B-6: HALF WIDTH FUNCTION, PSI = 0.

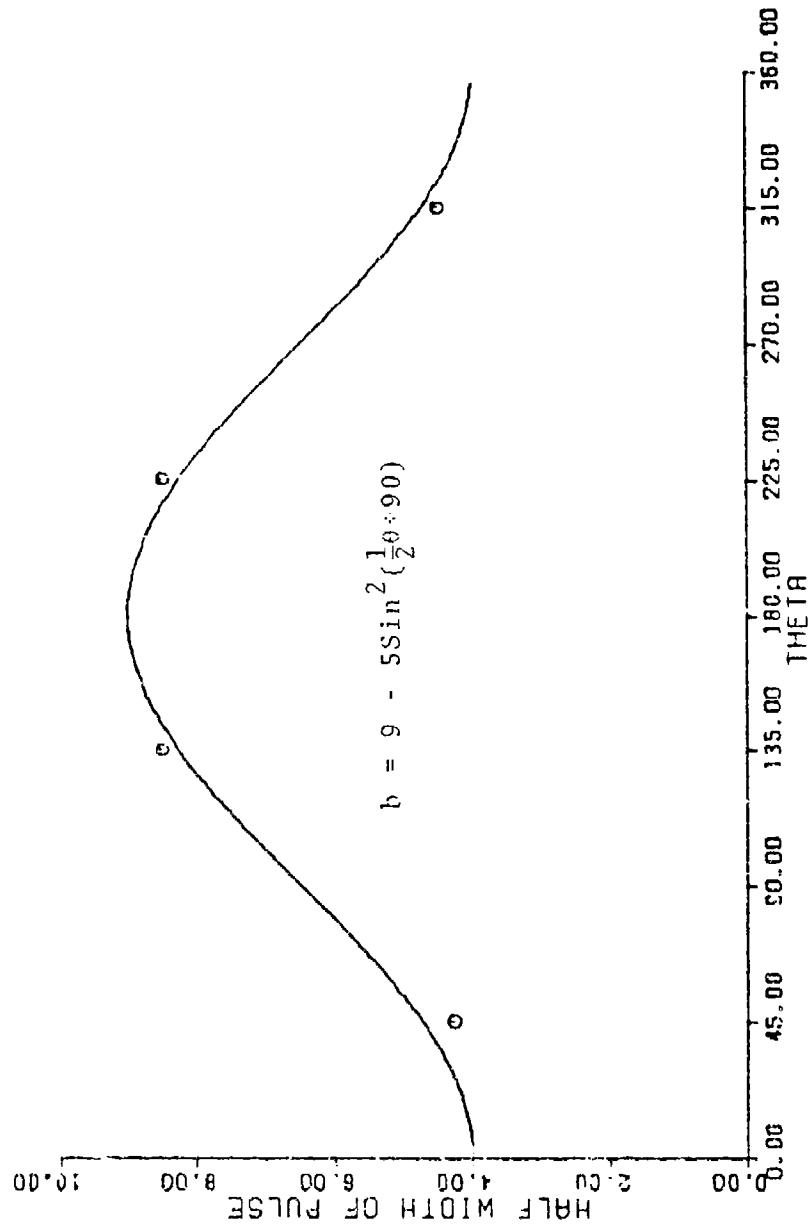


FIG B-7: HALF WIDTH FUNCTION, PSI= 45.

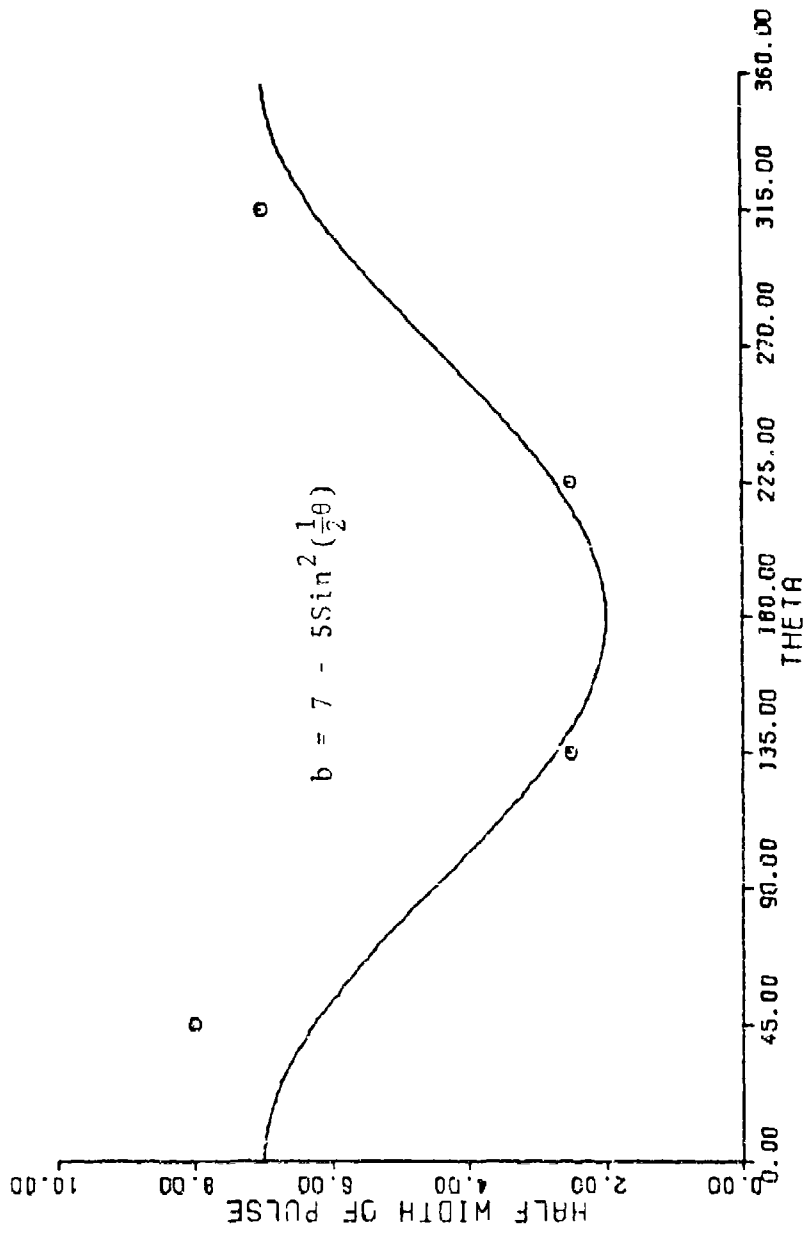


FIG B-8: HALF WIDTH FUNCTION. PSI= 90.

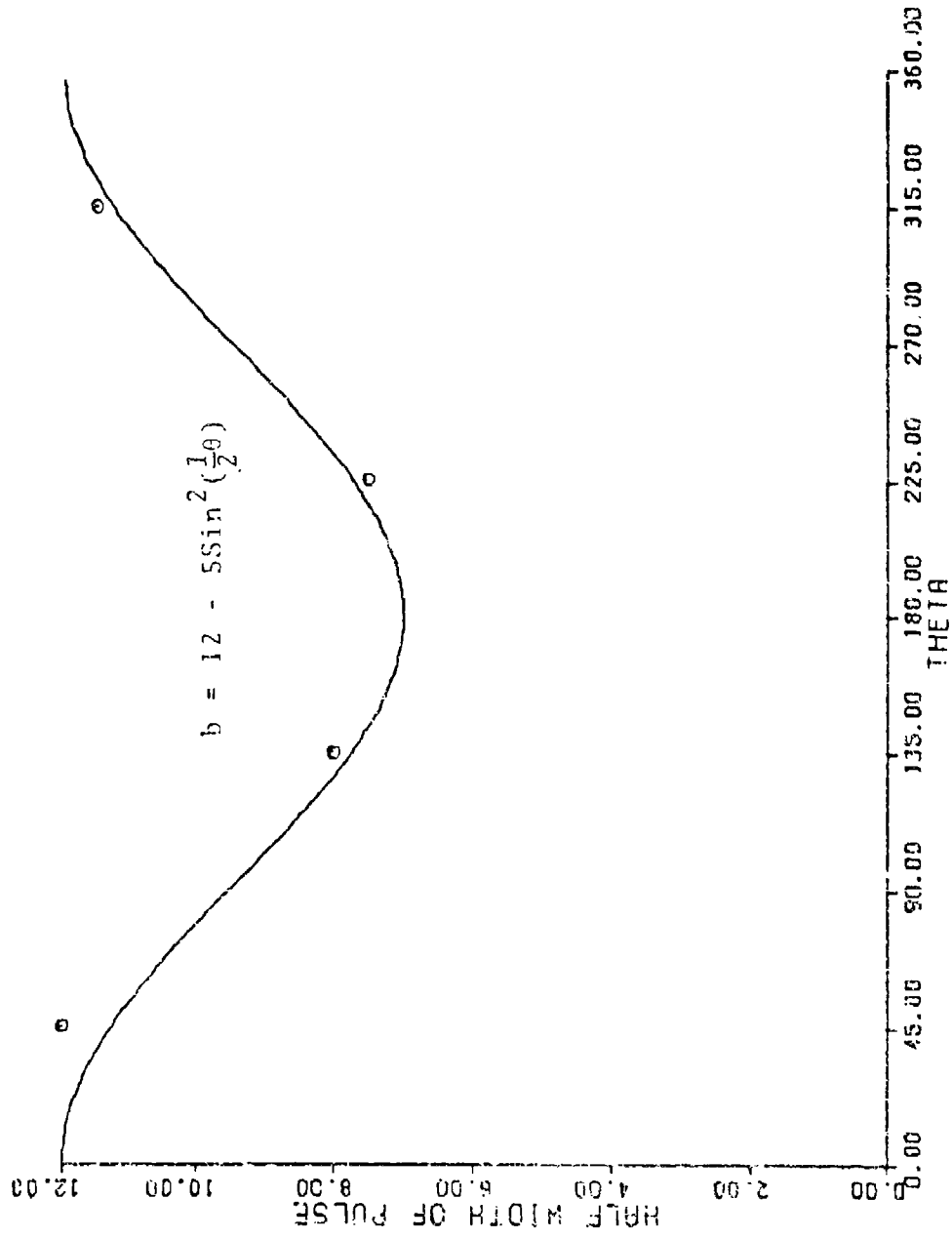


FIG B-9: HALF WIDTH FUNCTION, PSI = 135.

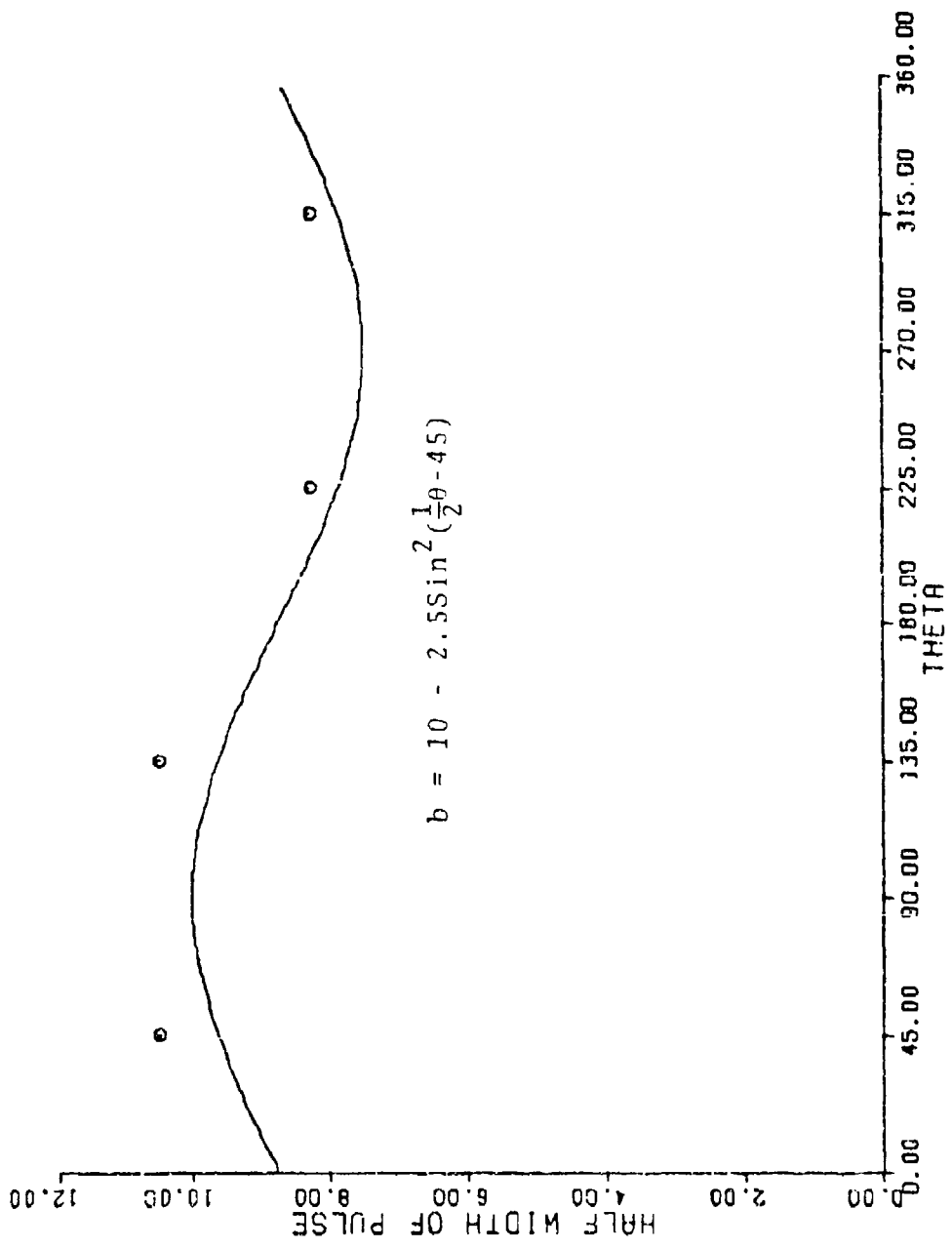


FIG B-10: HALF WIDTH FUNCTION, PSI = 180.

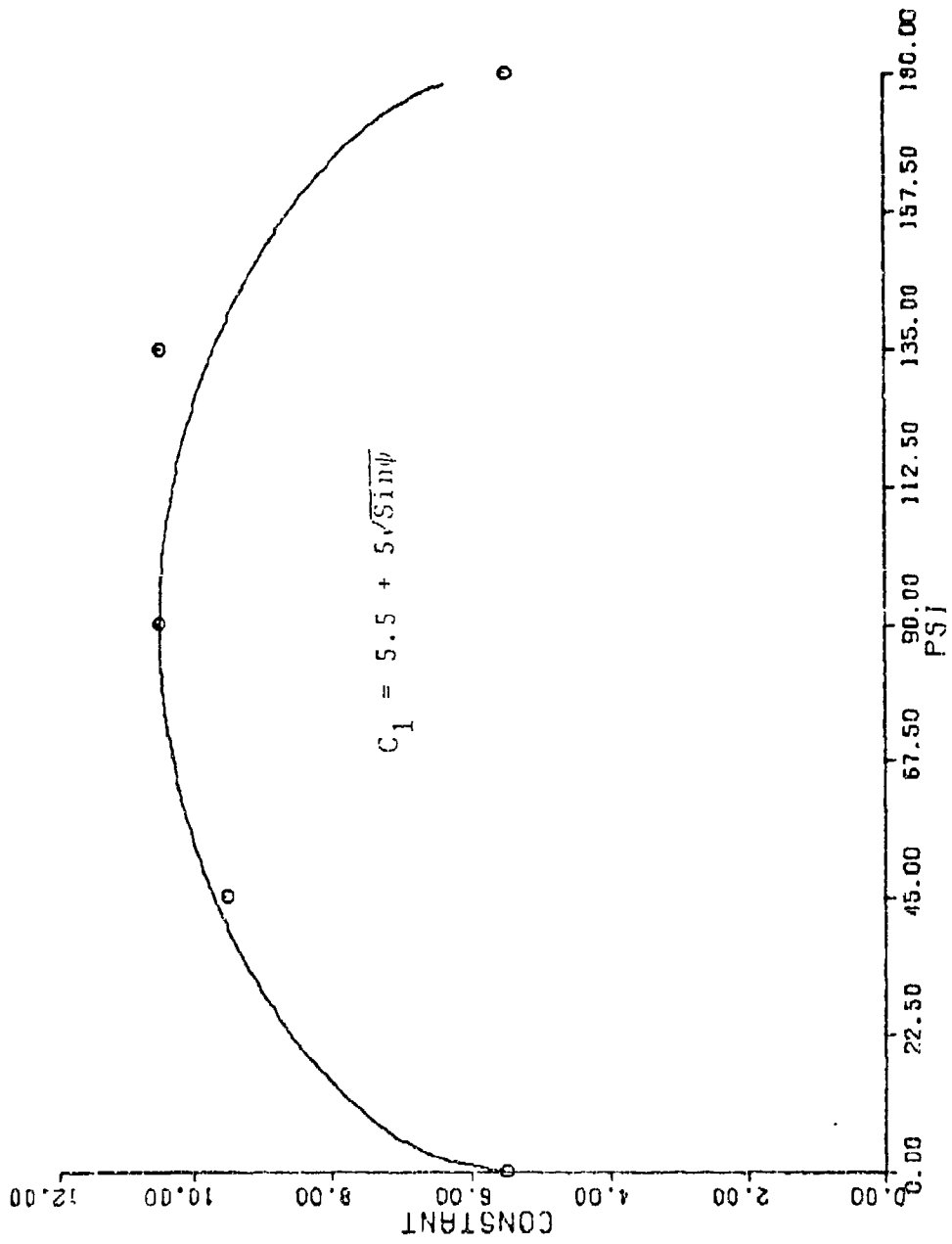


FIG B-11: LOCATION FUNCTION. CONSTANT TERM

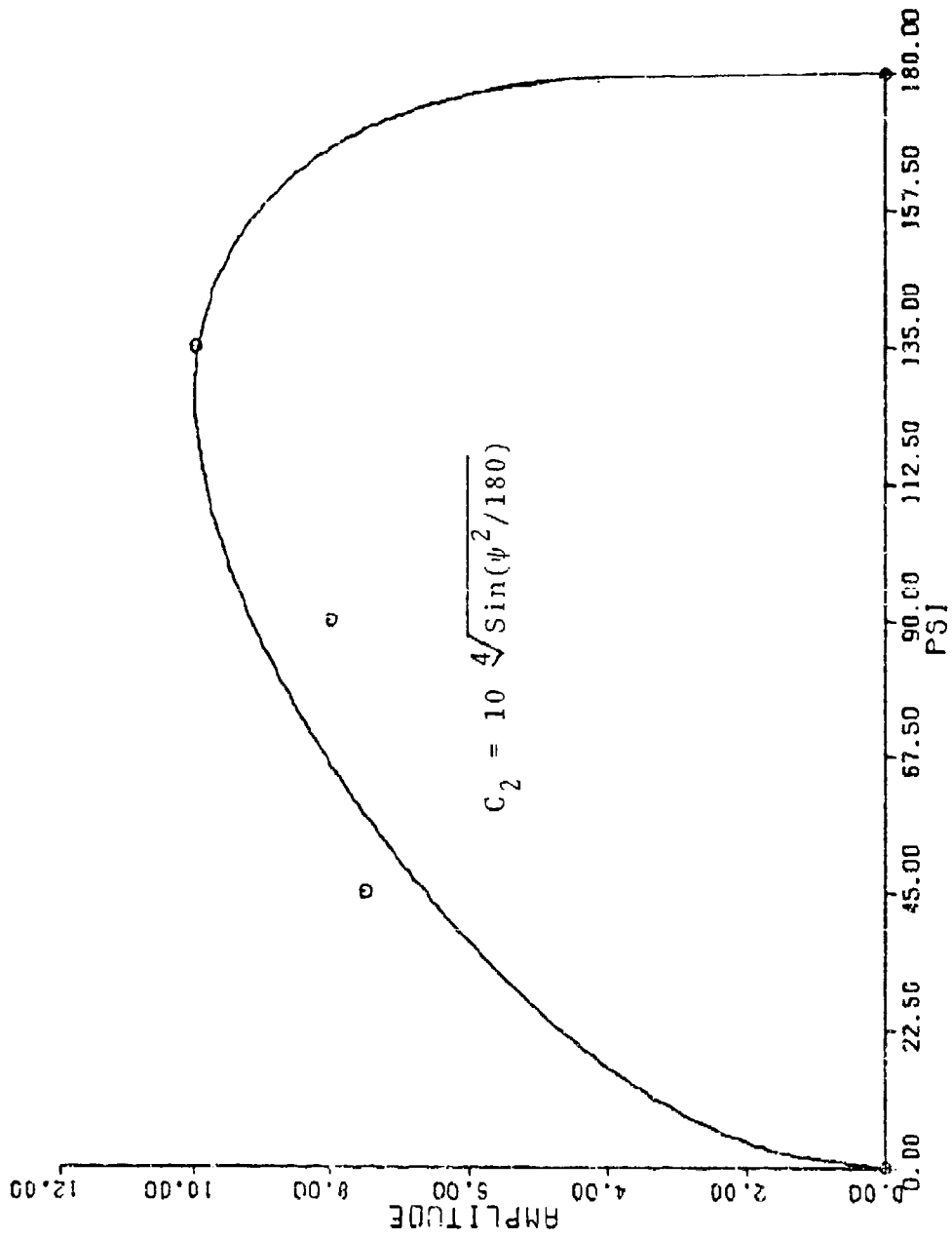


FIG D-12: LOCATION FUNCTION, AMPLITUDE TERM

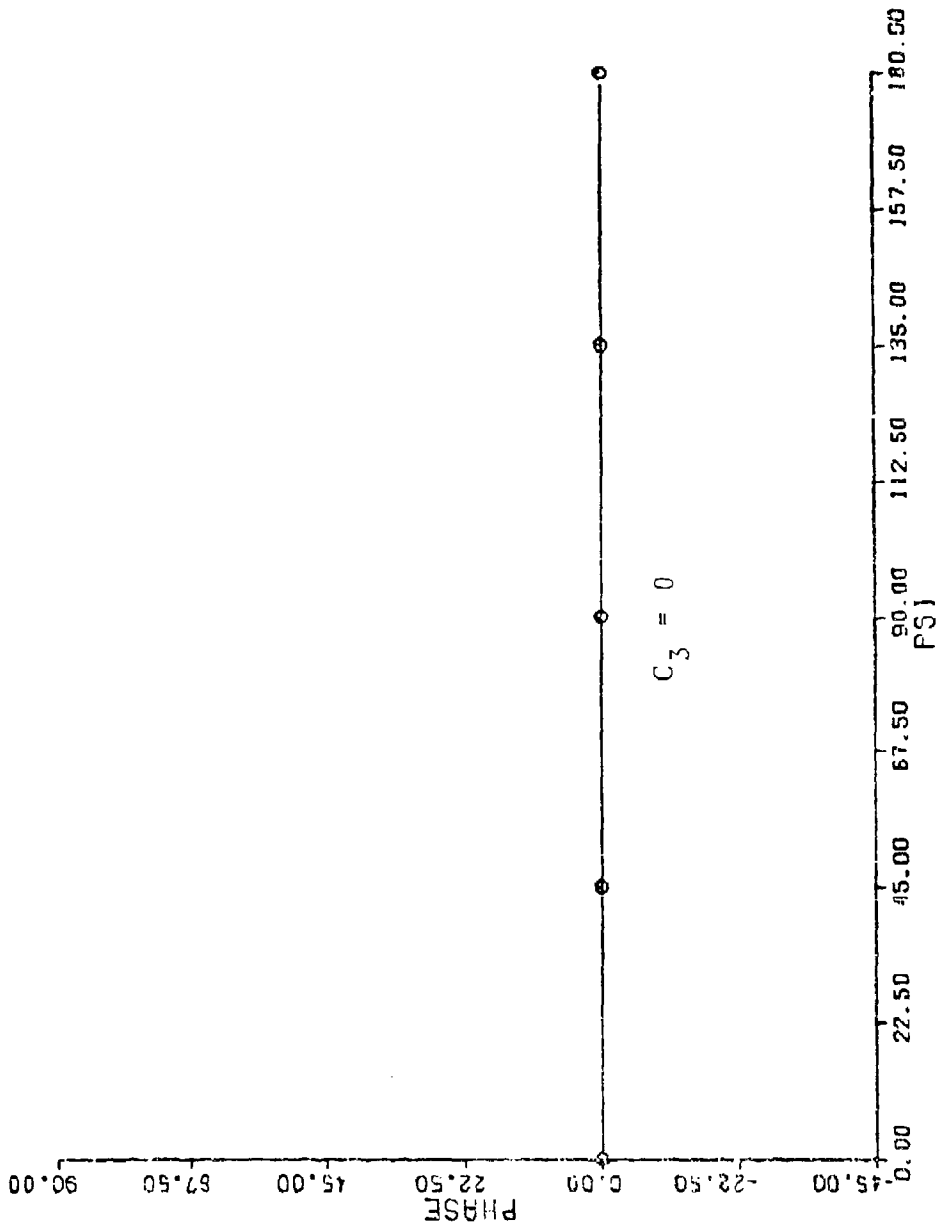
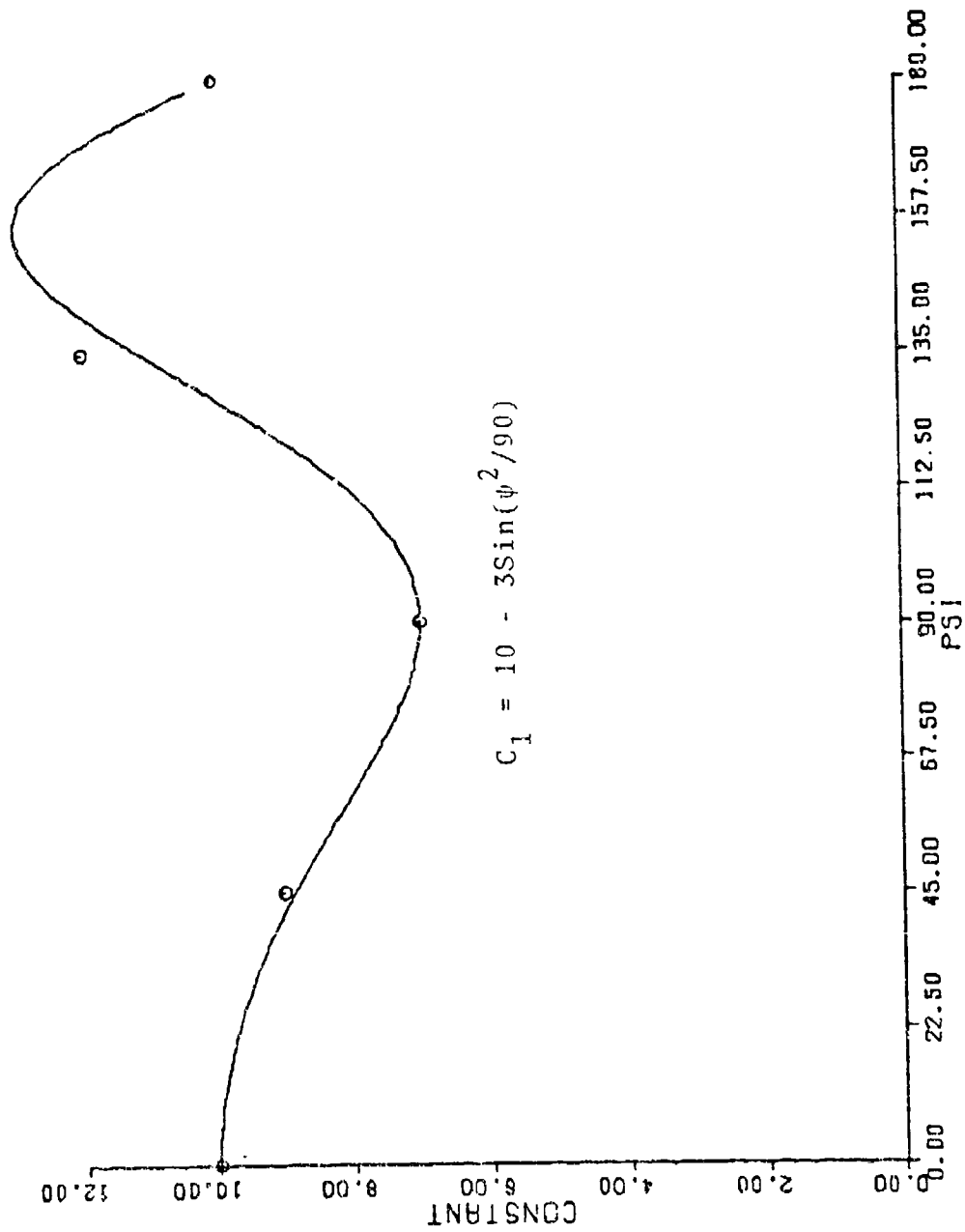


FIG B-13: LOCATION FUNCTION, PHASE TERM



FIGB-14: HALF WIDTH FUNCTION, CONSTANT TERM

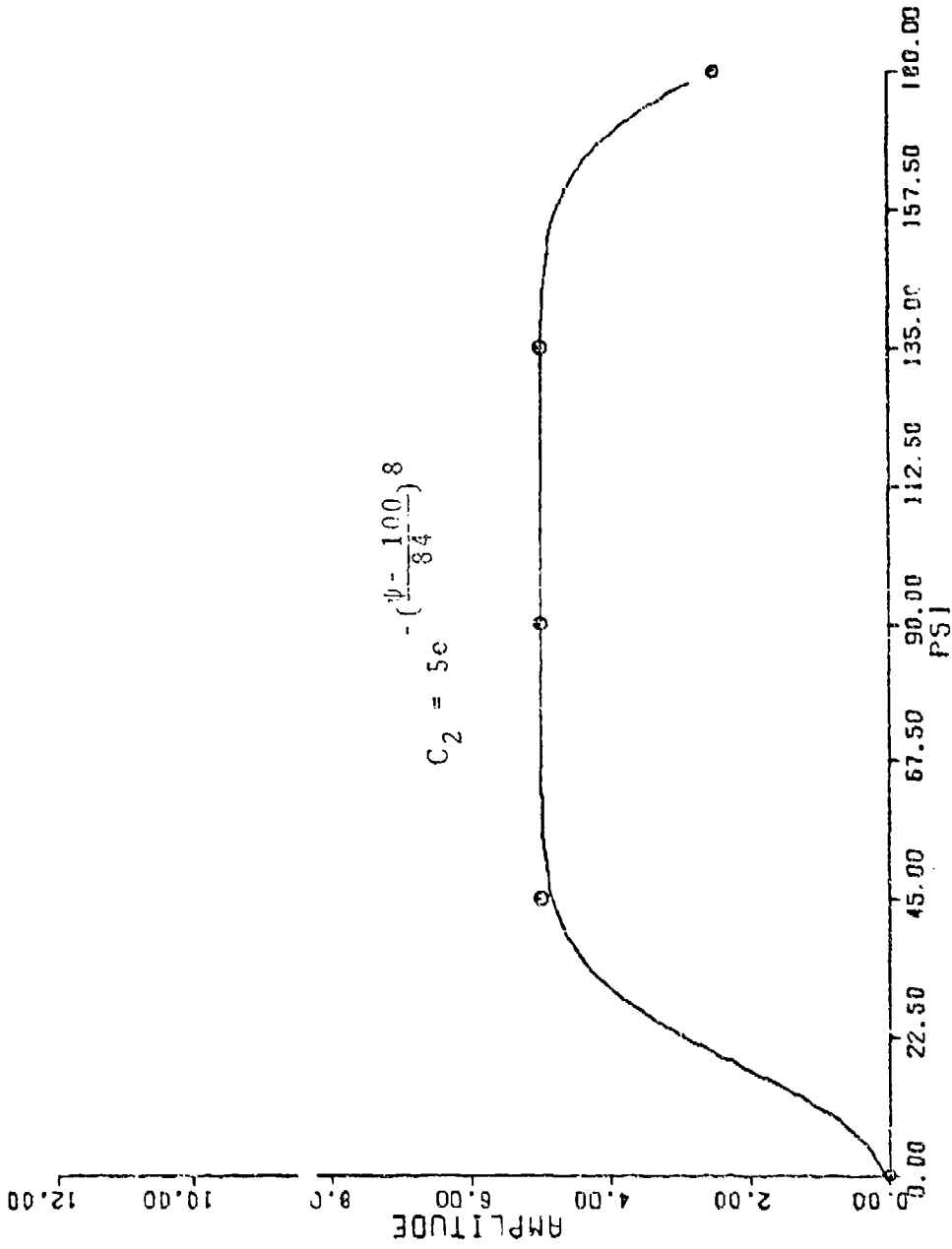


FIG B-15: HALF WIDTH FUNCTION. AMPLITUDE TERM

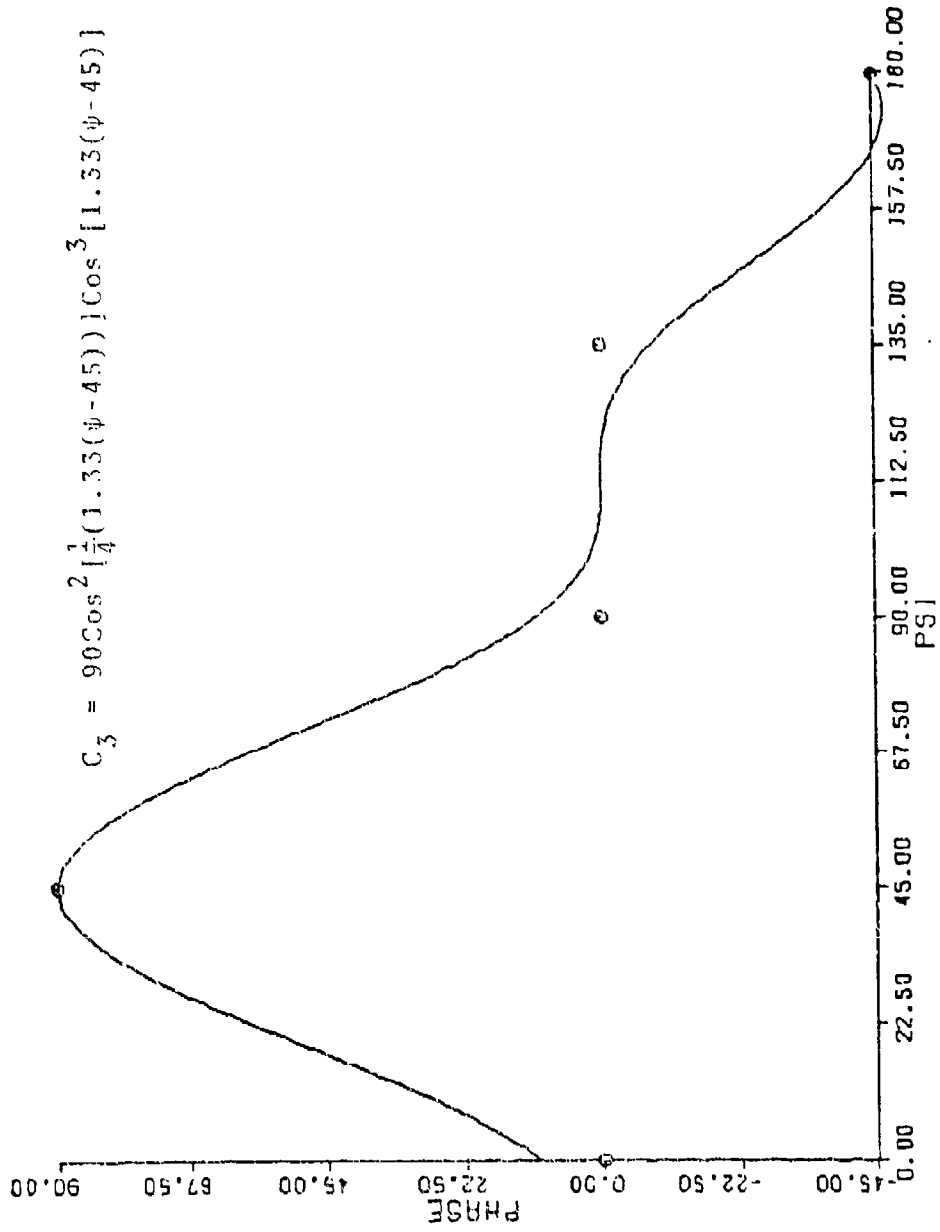


FIG B-16: HALF WIDTH FUNCTION. PHASE TERM

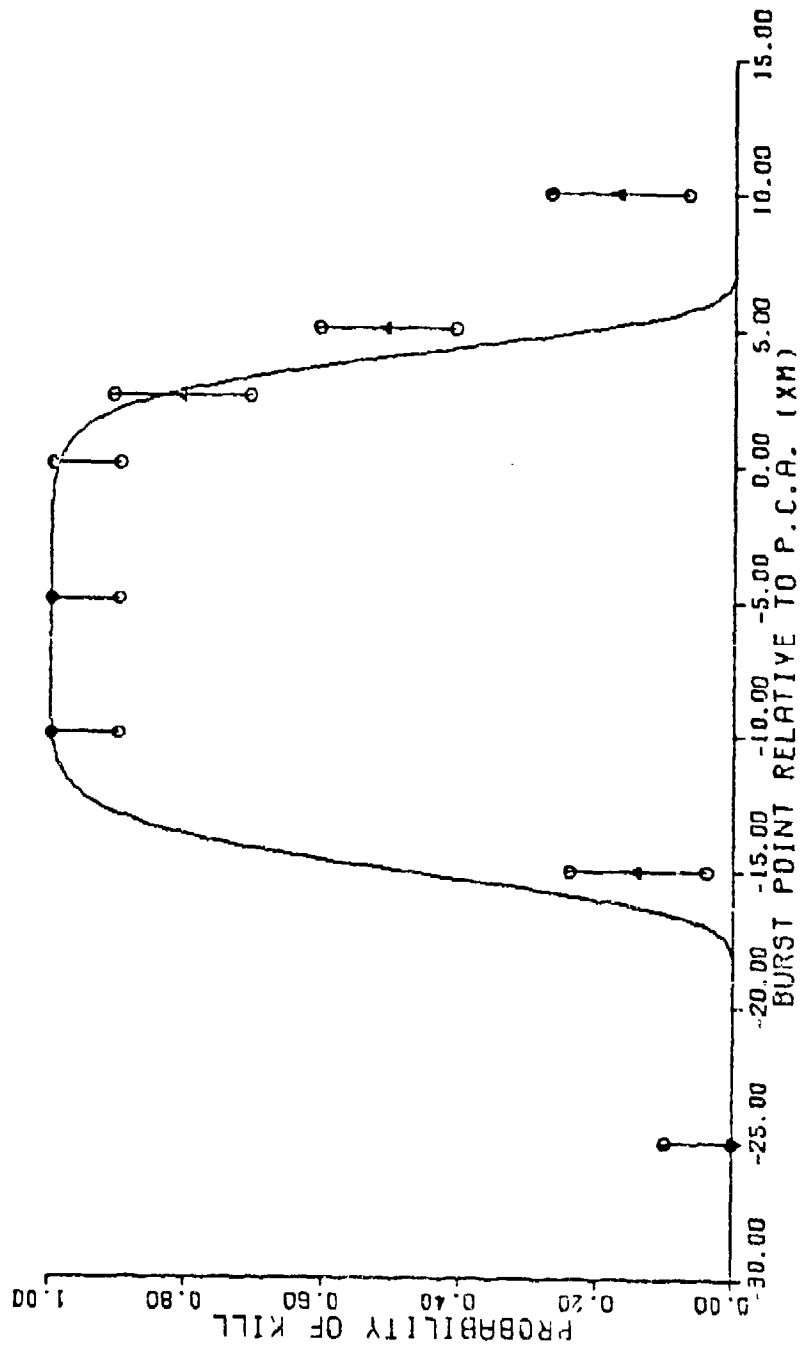


FIG B-17 : PSI=0. THETA=135. VR=2000. RM=15.0 BETA=0.

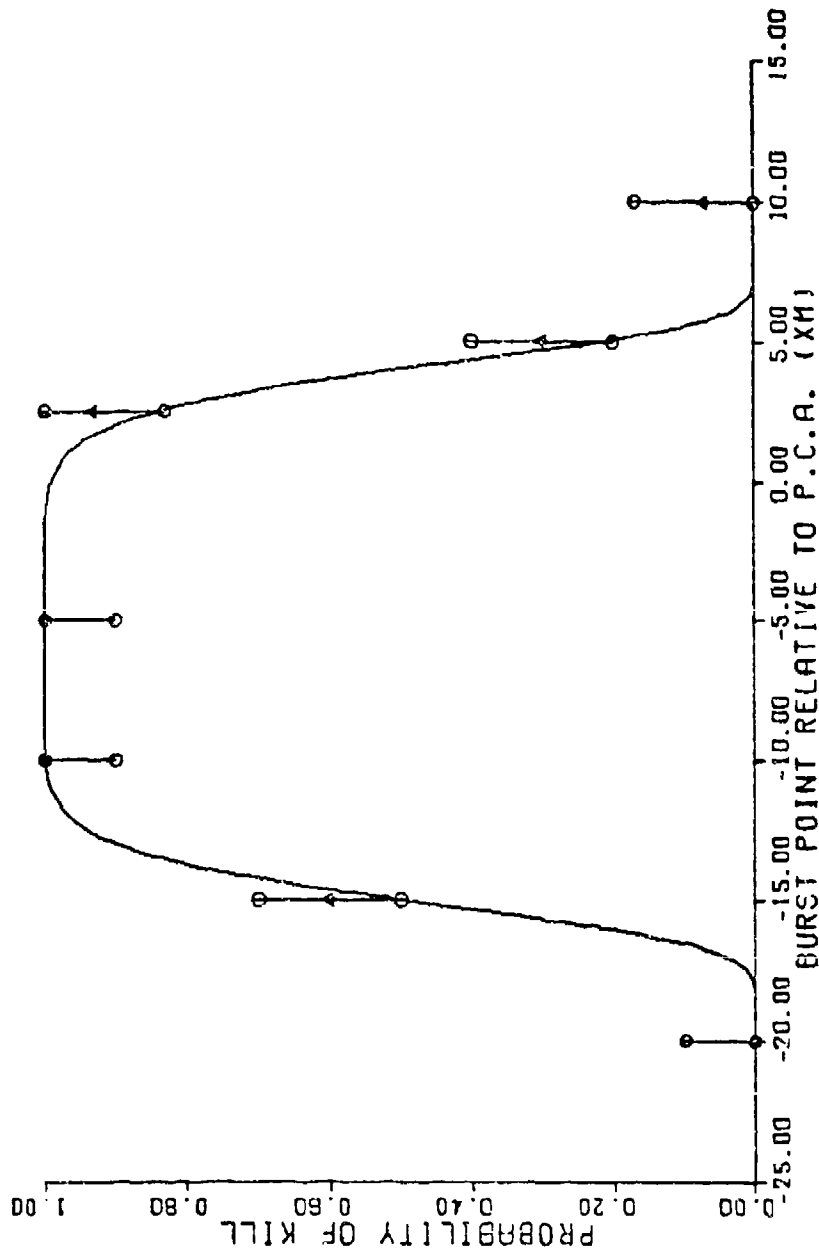


FIG B-18 : PSI=0. THETA=225. VR=2000. RM=15.9 BETA=0.

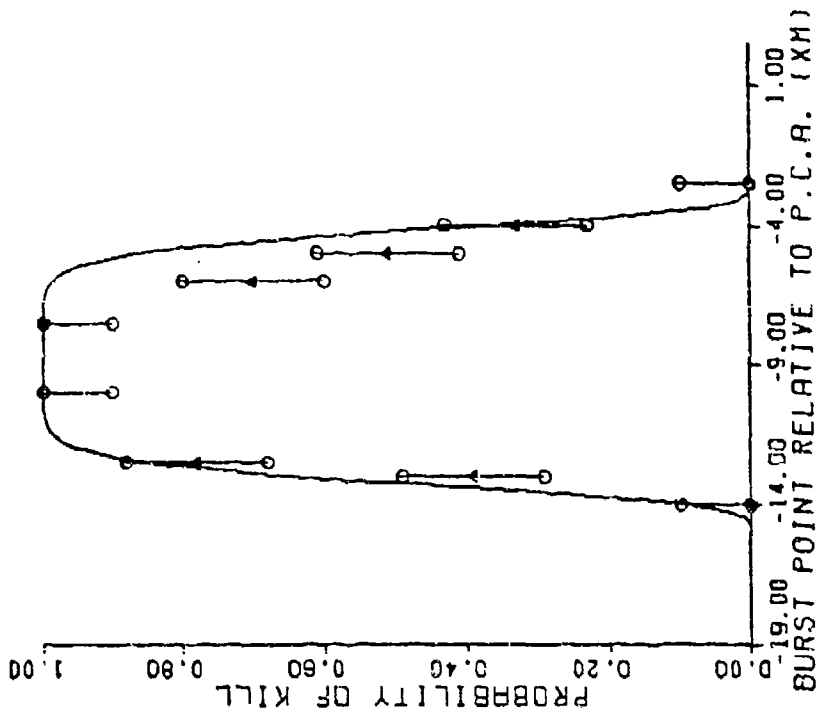


FIG B-19: PSI=45. THETA=45. VR=2000. RM=15.0 BETA=15.

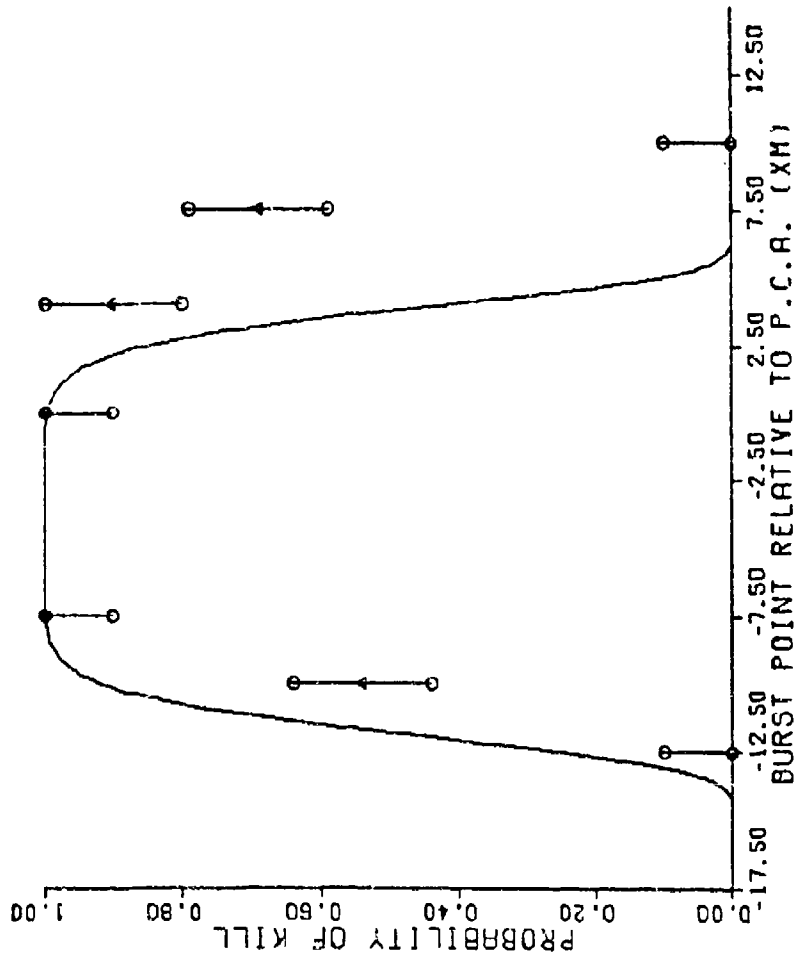


FIG B-20 : PSI=45. THETA=135. VR=2000. RM=15.0 BETA=15.

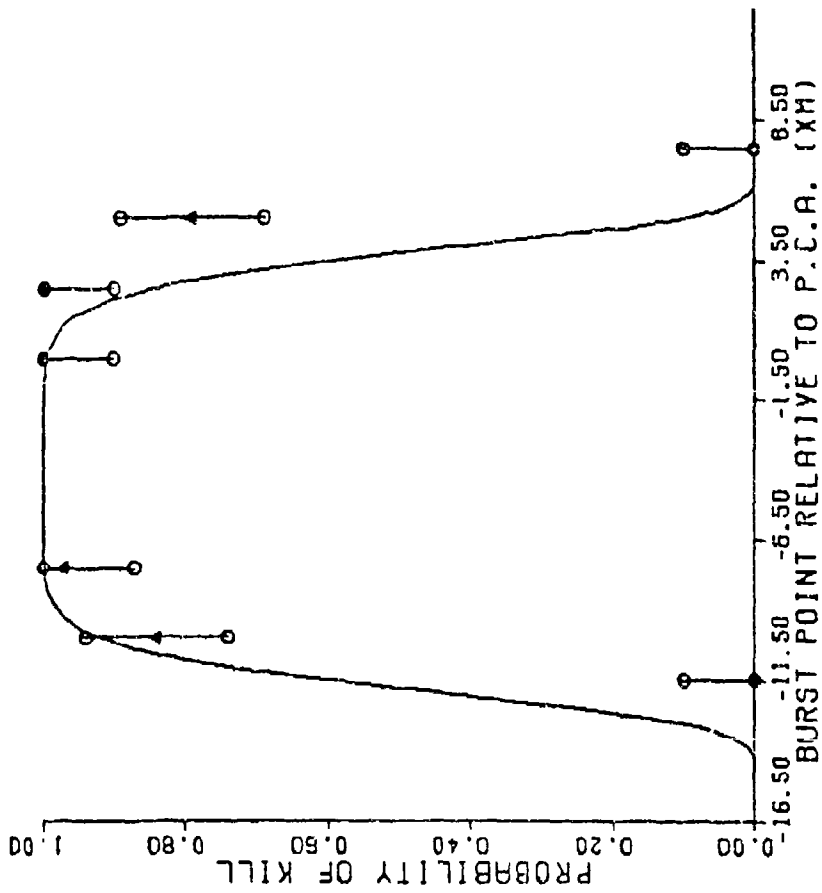


FIG B-21 : PSI=45. THETA=225. VR=2000. RM=15.0 BETA=15.

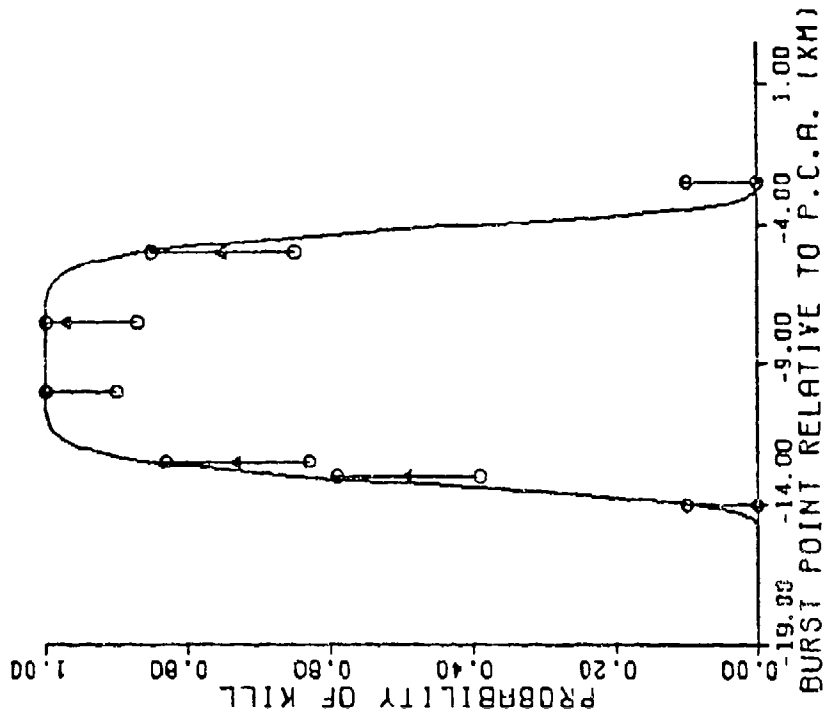


FIG B-22 : PSI=45. THETA=315. VR=2000. RM=15.0 BETA=15.

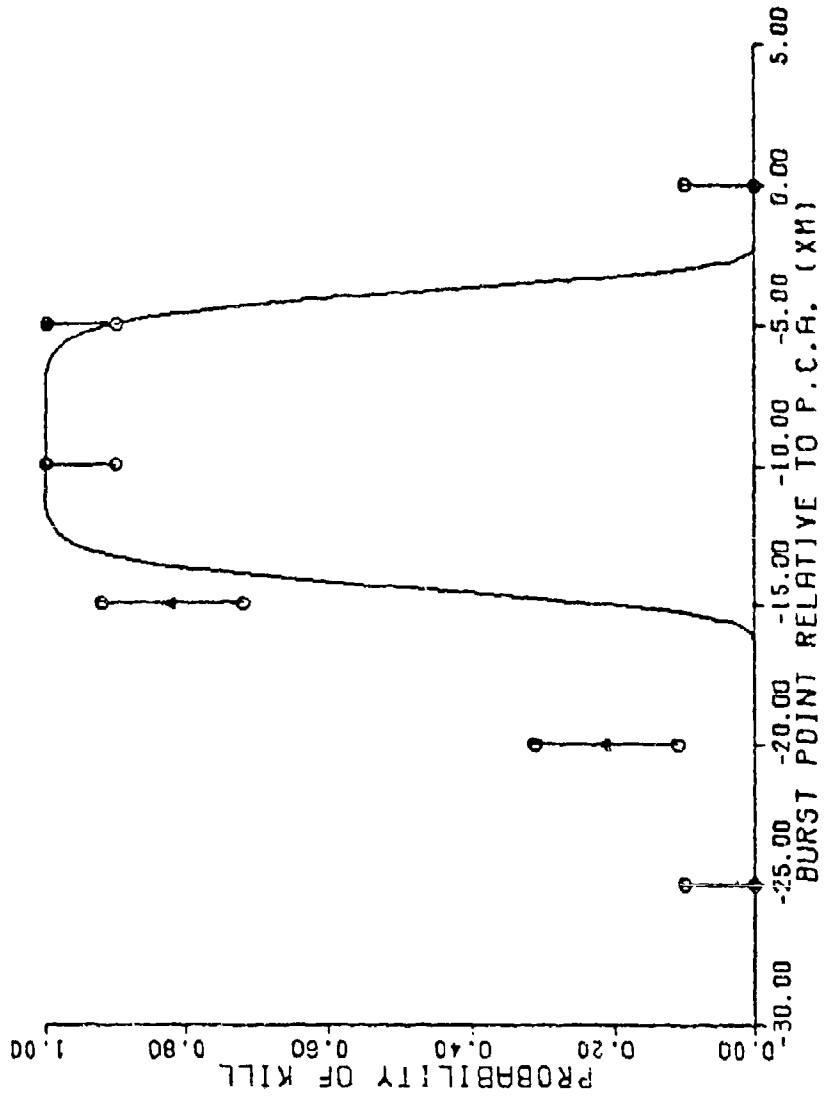


FIG B-23 : PSI=90. THETA=45. VR=2000. RM=15.0 BETA=15.

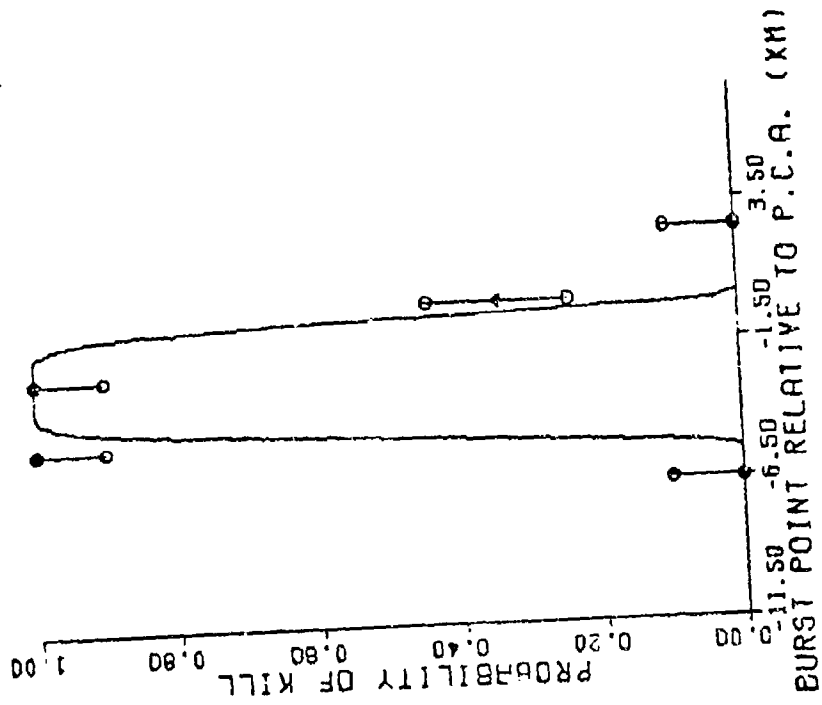


FIG B-24 : PSI=90. THETA=135. VR=2000. RM=15.0 BETA=15

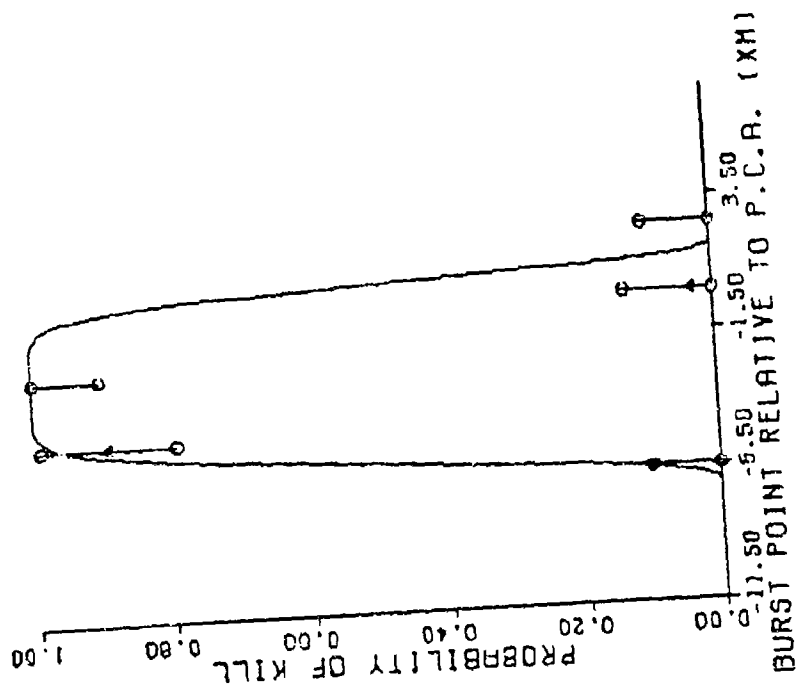


FIG B-25: PSI=90. THETA=225. VR=2000. RM=15.0 BETA=15.

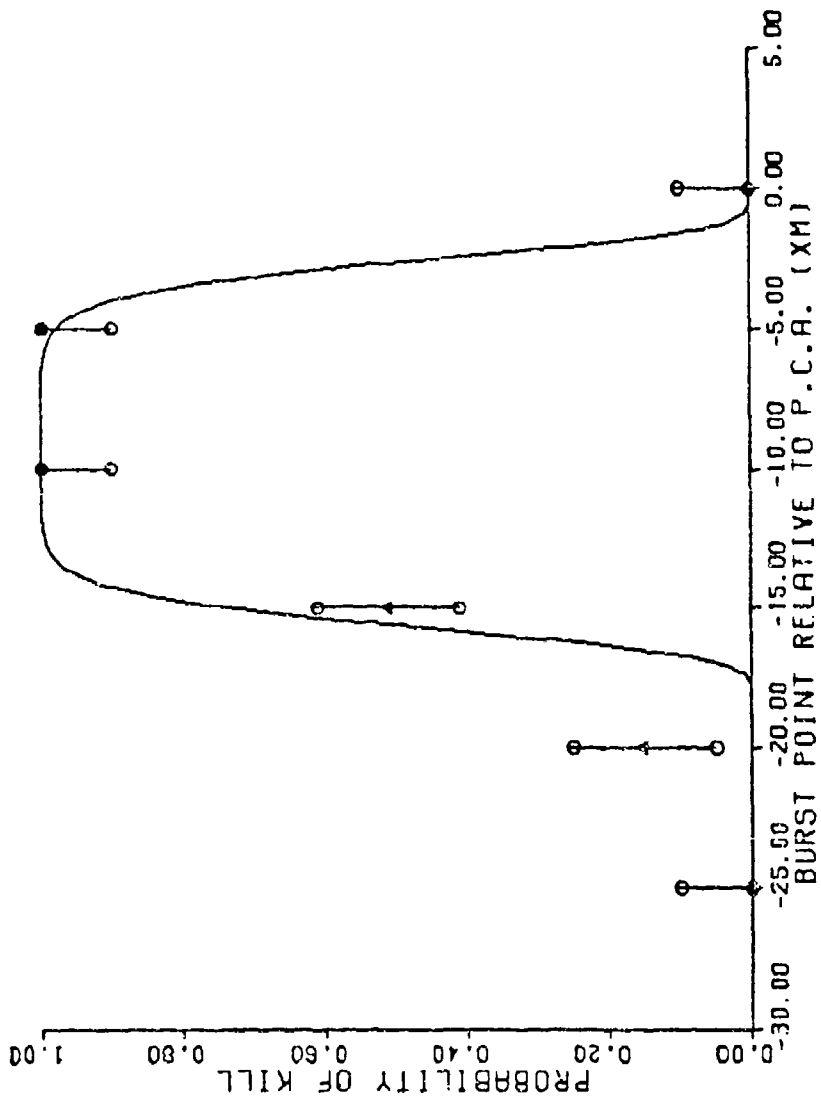


FIG B-26: PSI=90. THETA=315. VR=2000. RM=15.0 BETA=15

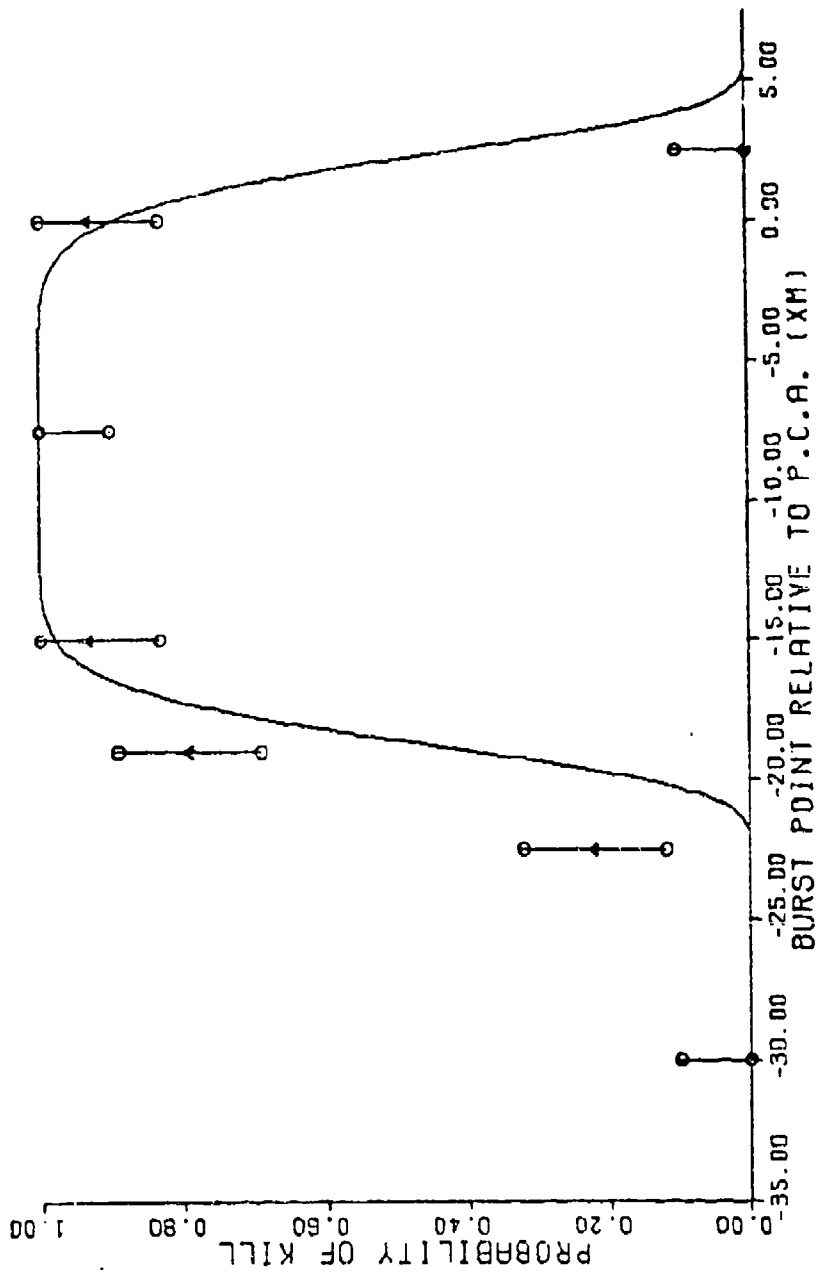


FIG B-27 : PSI=135. THETA=45. VR=2000. RM=15.0 BETA=15.

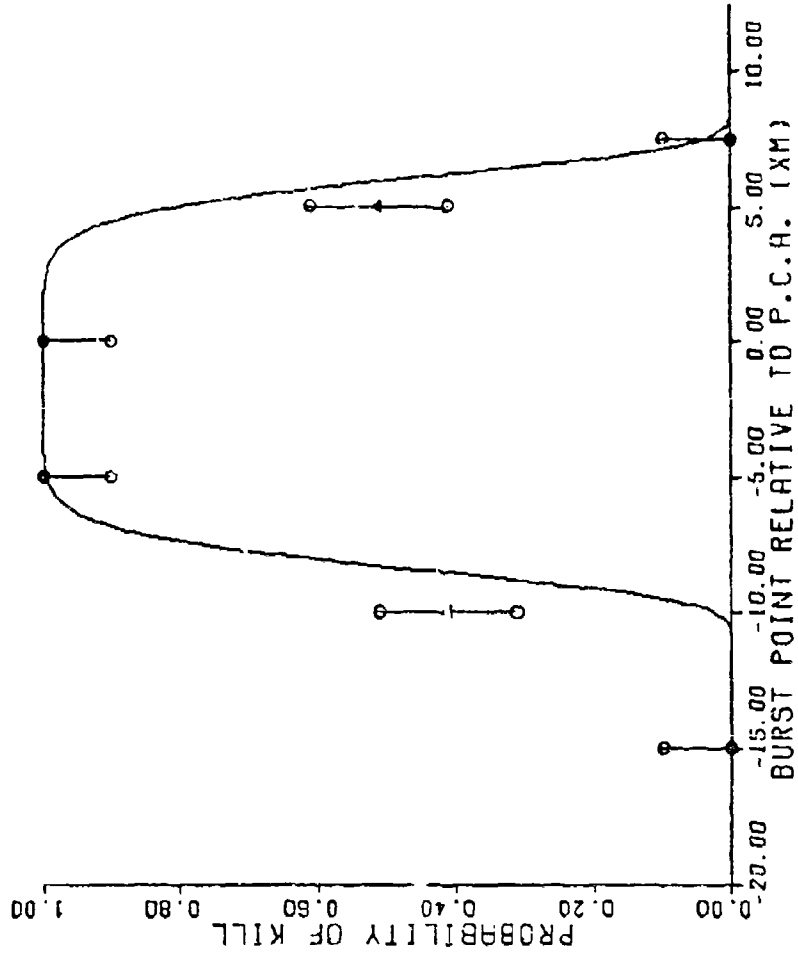


FIG B-28 : PSI=135. THETA=135. VR=2000. RM=15.0 BETA=15.

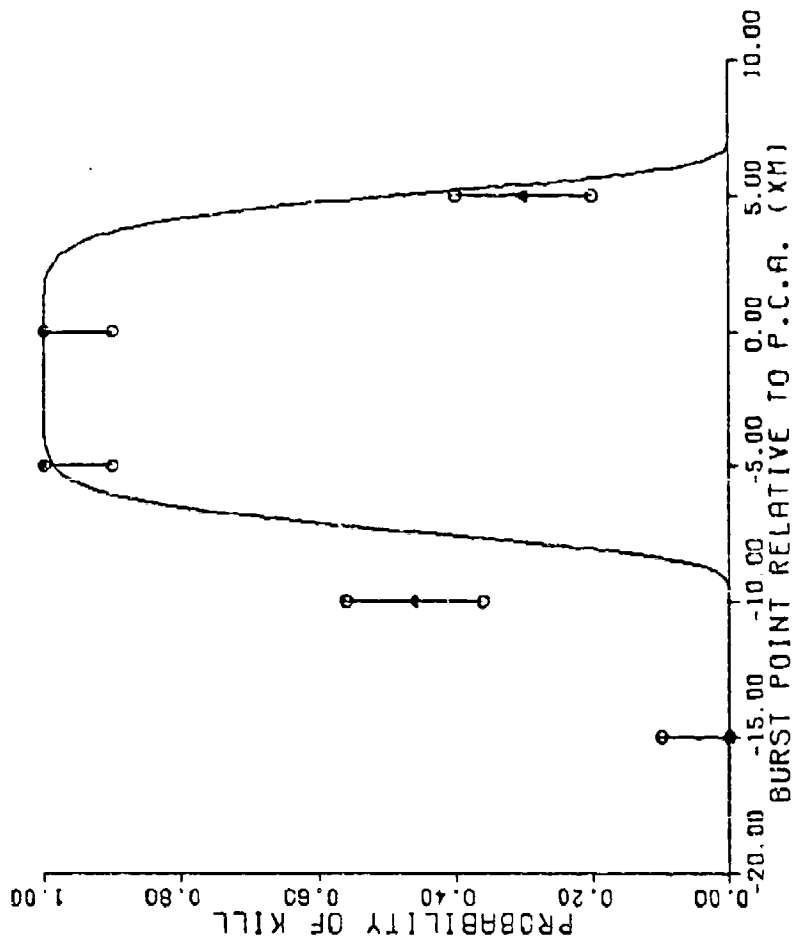


FIG B-29: PSI=135. THETA=225. VR=2000. RM=15.0 BETA=15.

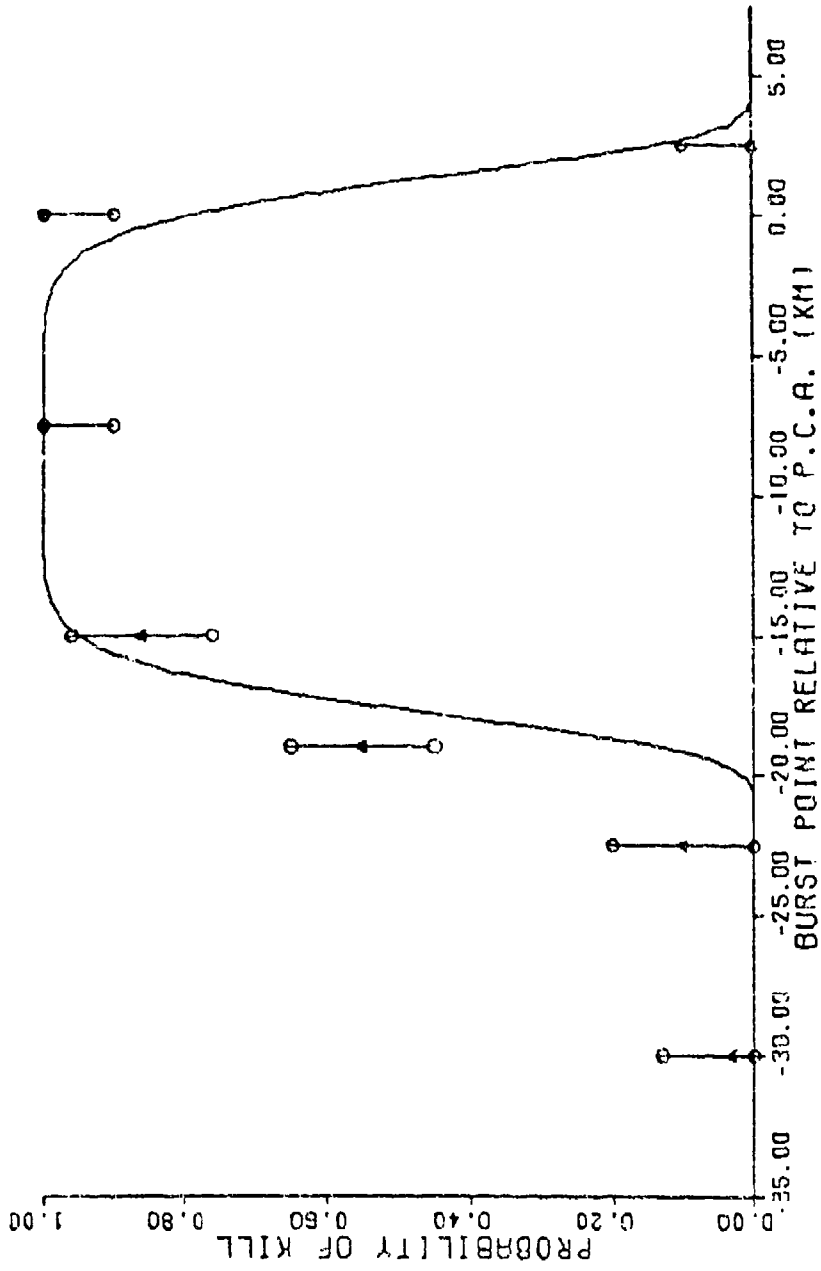


FIG B-30: PSI=135. THETA=315. VR=2000. RM=15.0 BETA=15

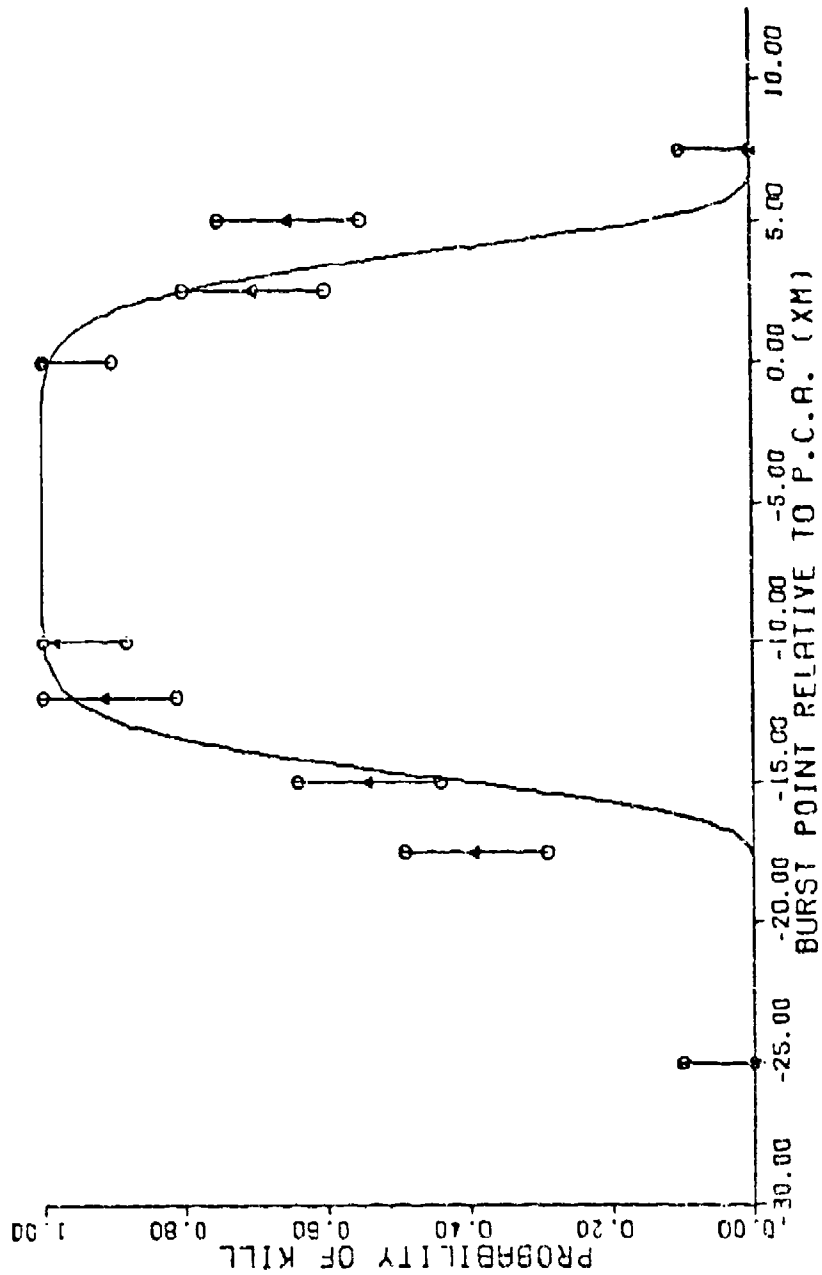


FIG B-31 : PSI=180. THETA=135. VR=2000. RM=15.0 BETA=0.

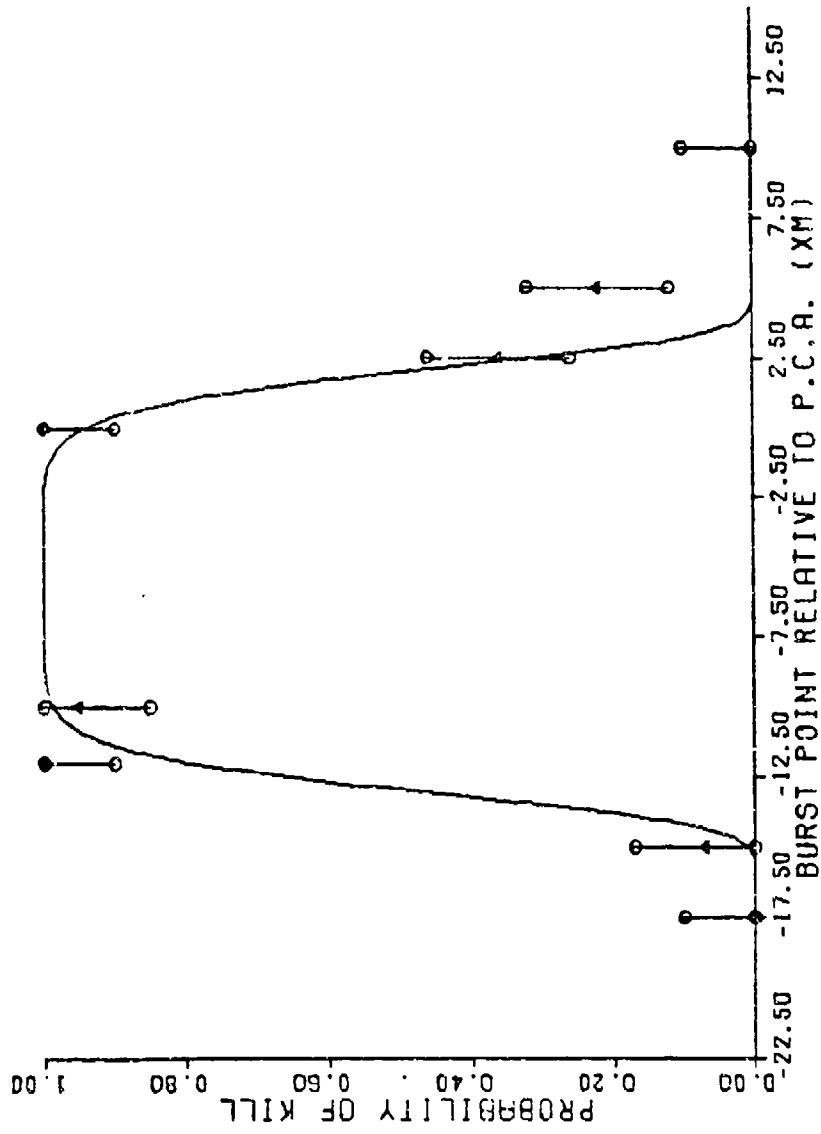


FIG B-32: PSI=180. THETA=225. VR=2000. RM=15.0 BETA=0.

APPENDIX C

Approximation of the Warhead Pattern

With a Cone

This appendix describes the cone approximation of the warhead pattern discussed in Chapter III.

Let V_F be the fragment velocity and ϕ be the angle of fragment ejection as measured from the missile centerline under static conditions. Assume that $\lambda = 0$ and $\alpha = 0$. Then in the relative reference frame, the situation shown in Figure C-1 represents the vector geometry in a plane which is parallel to the X-Y plane and contains the missile centerline. η_1 and η_2 are the angles (in this plane) between \bar{V}_R and \bar{V}_{F_1} and \bar{V}_R and \bar{V}_{F_2} , respectively, and are given by:

$$\eta_1 = \phi + \beta$$

$$\eta_2 = \phi - \beta$$

The magnitudes of \bar{V}_{F_1} and \bar{V}_{F_2} are both equal to V_F . \bar{V}_{F_1} represents the velocity vector of the fragment which is ejected to the port side of the missile parallel to the X-Y plane. \bar{V}_{F_2} represents the analogous vector on the starboard side.

As shown in Figure C-2, the vector addition of \bar{V}_R and \bar{V}_F (either \bar{V}_{F_1} or \bar{V}_{F_2}) yields a resultant \bar{V}_F' which makes an angle μ with \bar{V}_R where

$$\nu = \tan^{-1} \left(\frac{V_F \sin \eta}{V_R + V_F \cos \eta} \right)$$

Figure C-3 depicts the relationship between these resultants, V_R , and the missile centerline. The cone half-angle, δ , is given by:

$$\delta = \frac{\mu_1 + \mu_2}{2}$$

The angle ϵ between the cone axis and V_R is given by:

$$\epsilon = \delta - \mu_2$$

Therefore, the angle between the cone axis and the missile centerline is just $\beta - \epsilon$. If α is not zero, then $\beta + \alpha$ is substituted for β in all expressions.

Figures C-4 through C-8 are comparisons between this cone approximation and the true dynamic warhead pattern. The plane of the plot represents the Y - Z plane in the target coordinate system. The axes are centered on the target centroid. The squares represent the penetration points of the plane for the true dynamic warhead pattern if fragments were spaced every 10° around the warhead. The +'s are the corresponding points of intersection between the approximating cone and the Y-Z plane of the target coordinate system. The scales are in units of feet, and DP is the distance in feet, measured along the missile centerline, to the Y-Z plane. For each of these plots, $V_F = 5500$ feet per second and $\phi = 84^\circ$. The values of the other factors are shown on each plot.

The reader should remember that it is the continuous intersection with the Y-Z plane which is of interest, not the individual points of intersection. Therefore, that the approximation calculates individual fragment penetrations of the plane incorrectly is not important--it is the pattern which is of concern in the semi-empirical approach of Chapter III.

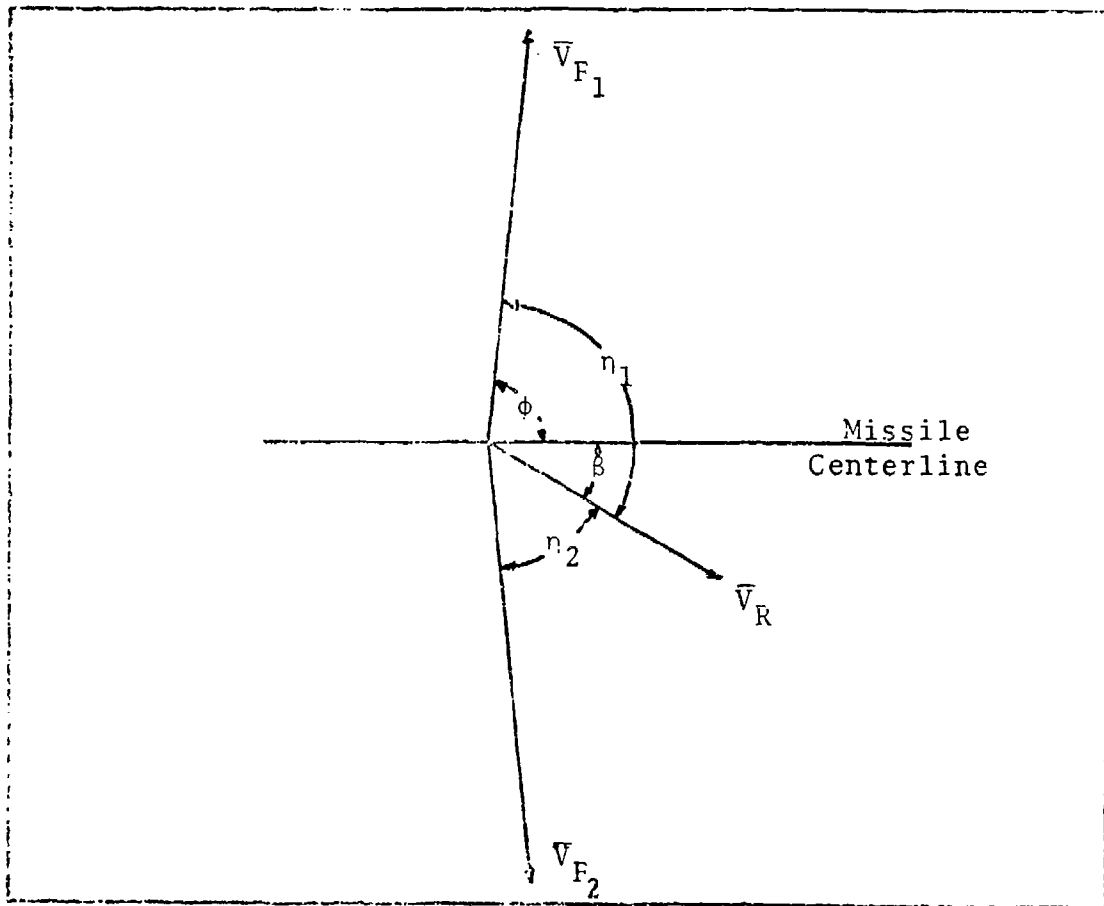


Fig C-1: Vector Geometry

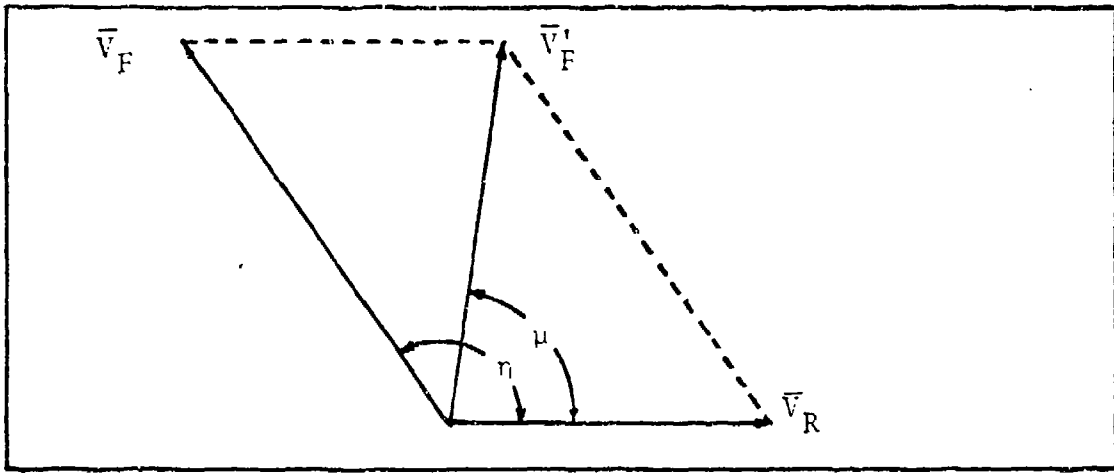


Fig C-2: Vector Addition of \bar{V}_R and \bar{V}_F

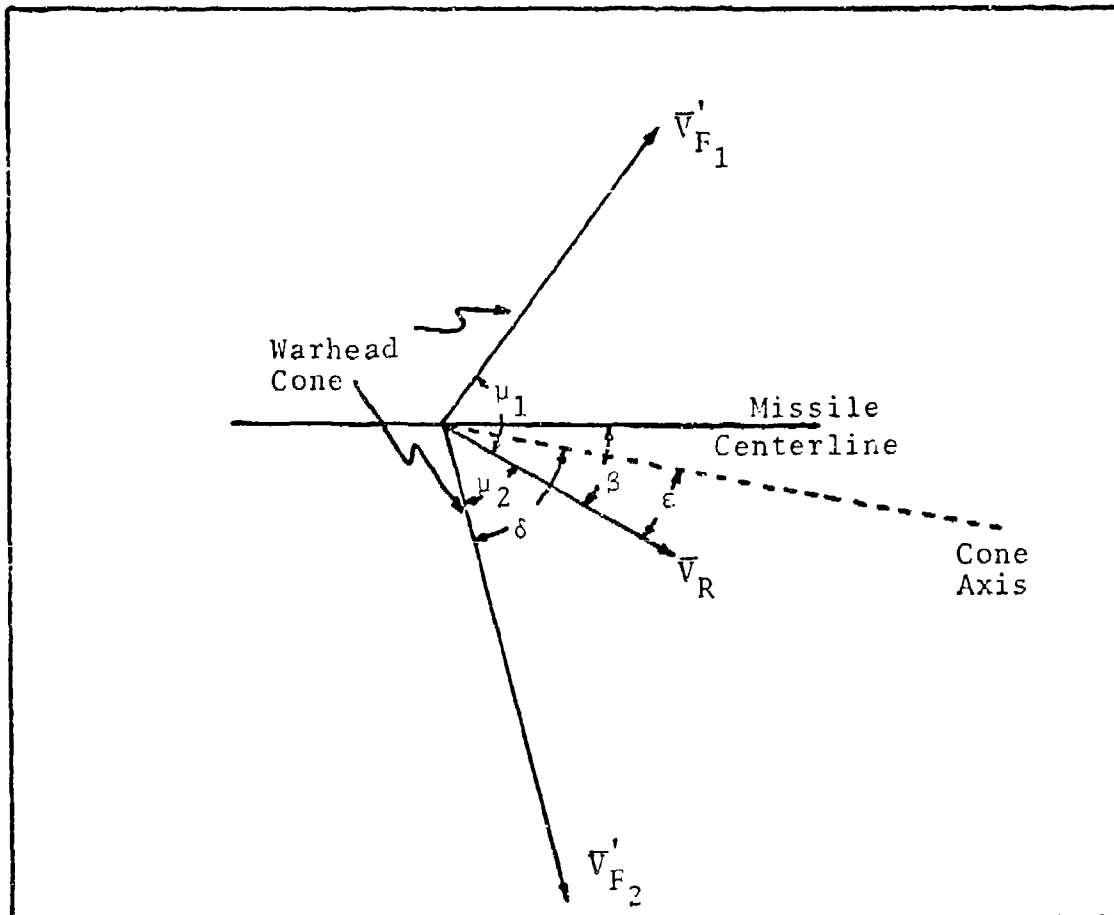


Fig C-3: Warhead Cone Orientation

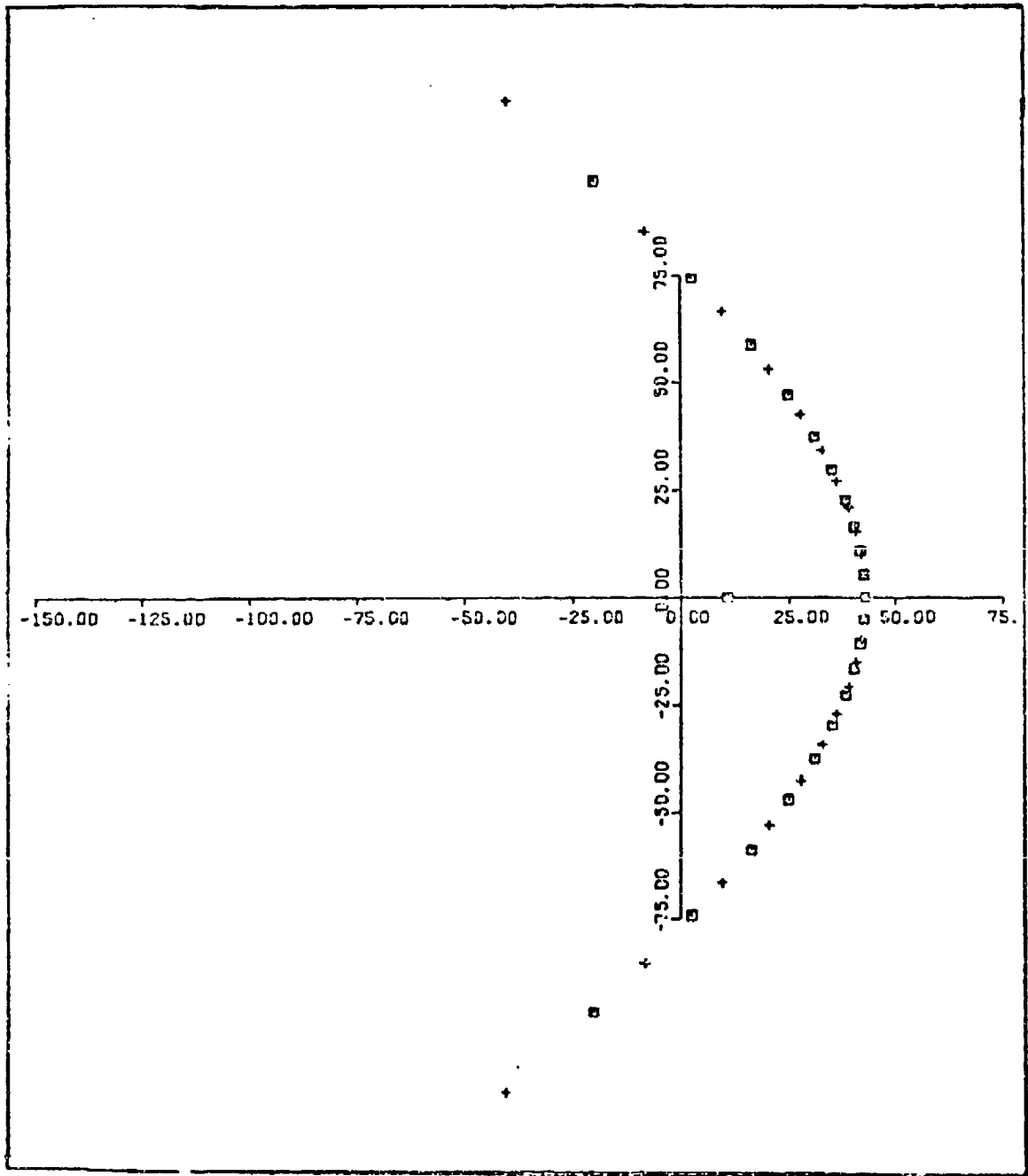


Fig C-4: VR = 2000, PSI = 45, BETA = 15, DP = 30

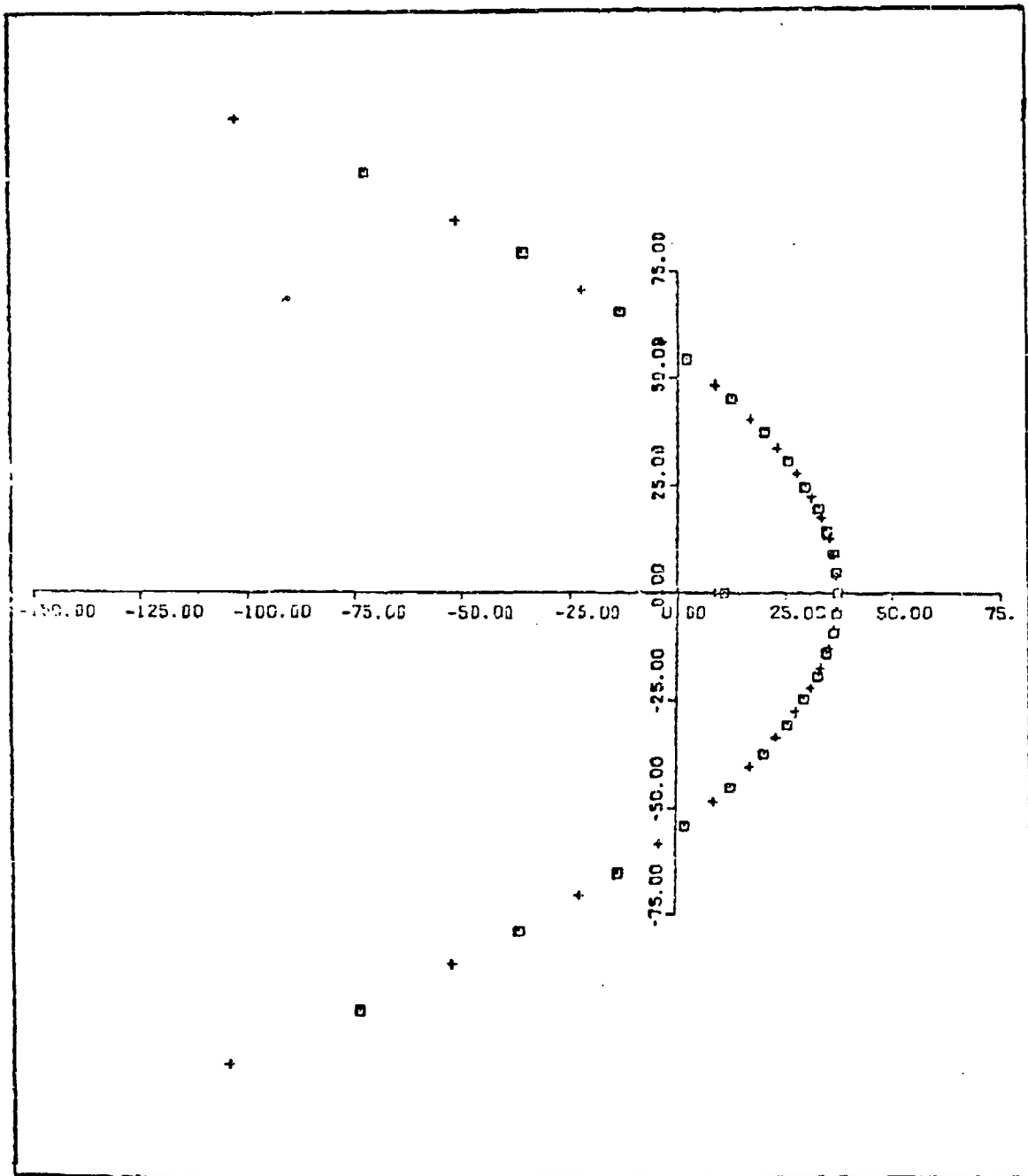


Fig C-5: VR = 3000, PSI = 45, BETA = 15, DP = 30

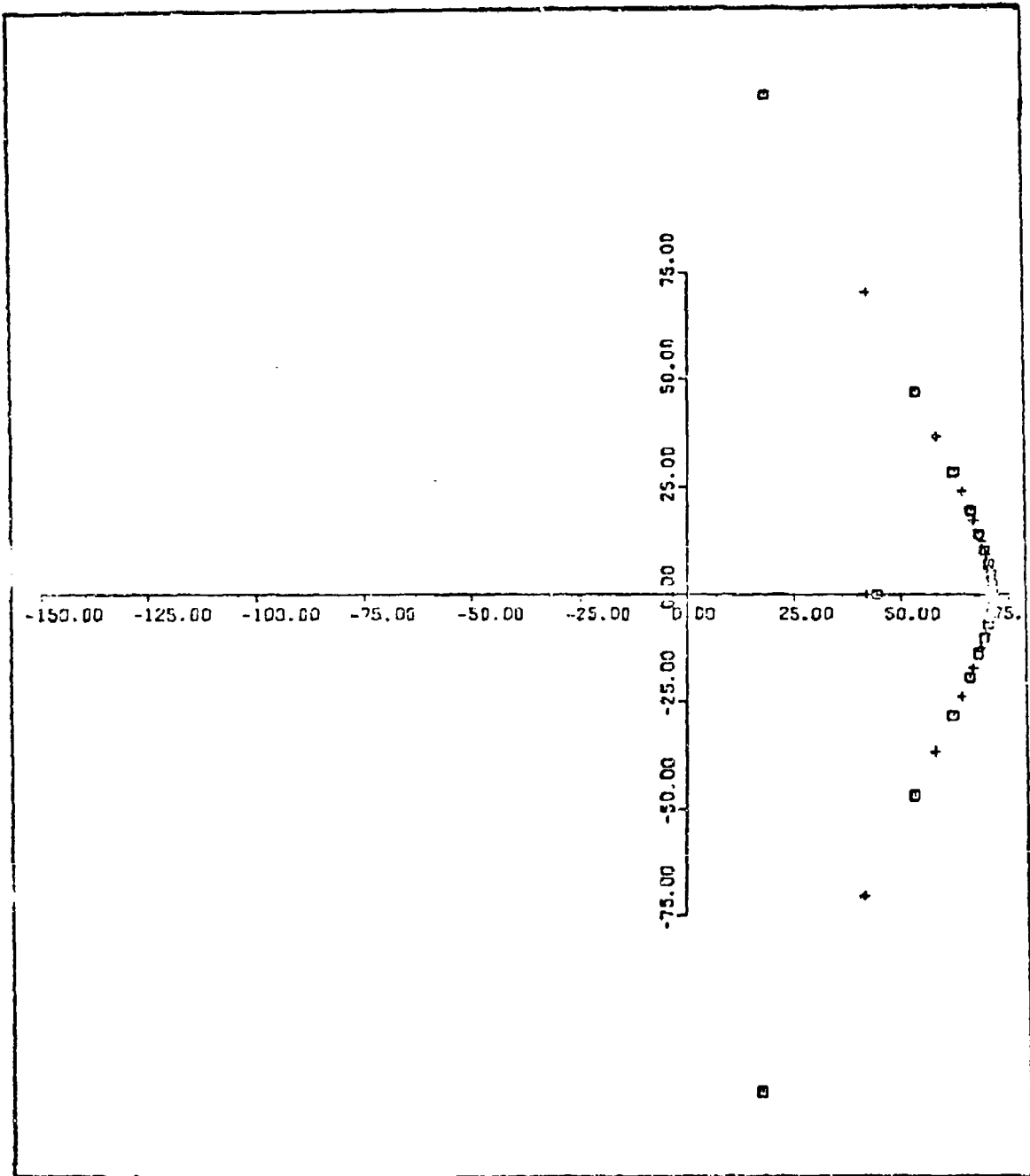


Fig C-6: VR = 2000, PSI = 10, BETA = 15, DP = 30

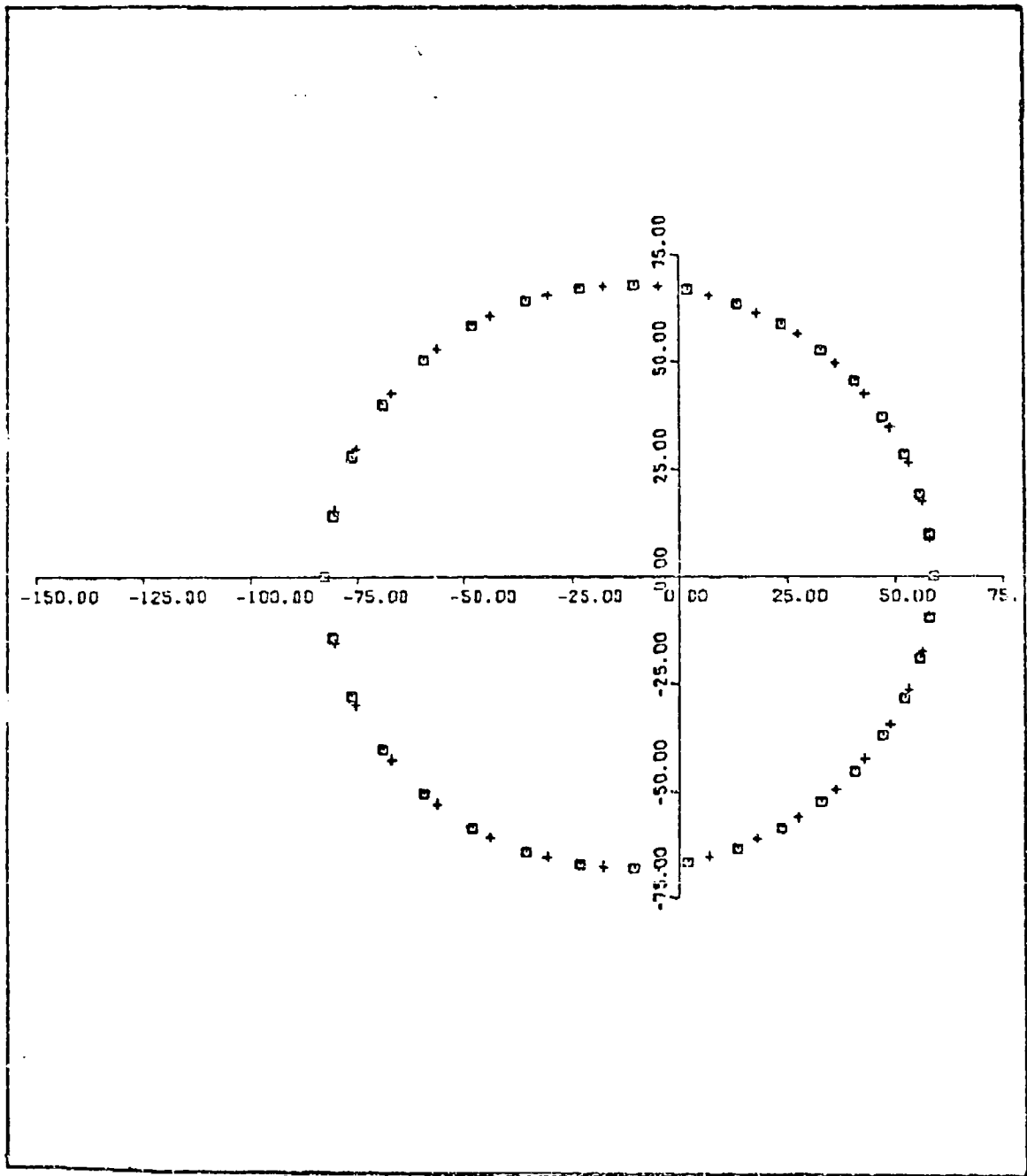


Fig C-7: VR = 2000, PSI = 70, BETA = 15, DP = 30

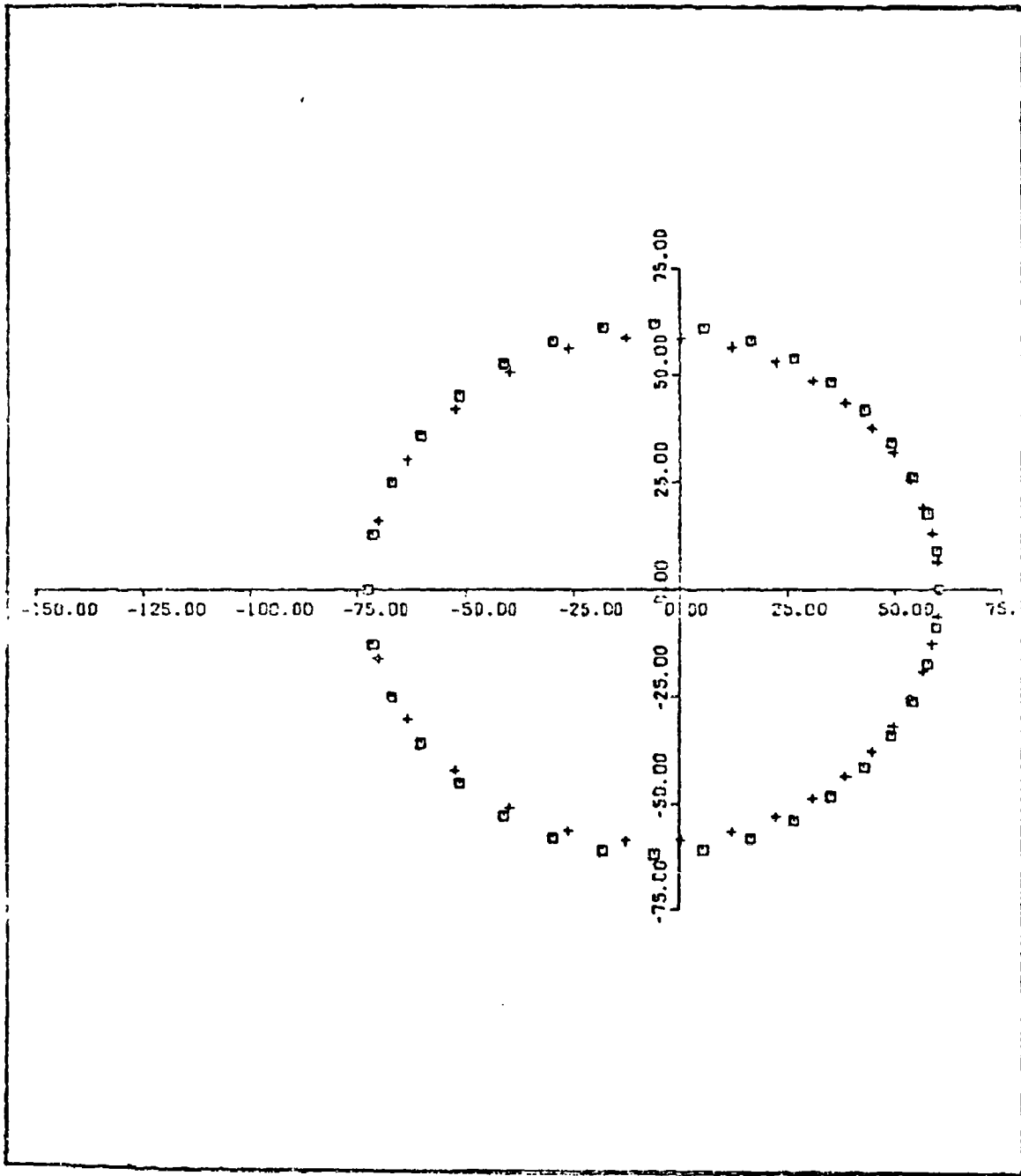


Fig C-8: VR = 3000, PSI = 45, BETA = 40, DP = 30

APPENDIX D

Simultaneous Solution of the Cone/Line Intersection

This appendix develops the mathematics required to solve for the intersection between a line and a cone. In the context of this thesis, the line represents the infinite line which is coincident with the target centerline and the cone represents the warhead pattern approximation presented in Appendix C. The value of λ is assumed to be zero for all of the derivations contained herein.

If $Z_M = 0$, Figure D-1 represents the geometry of the problem. There are two ways of solving for the intersection, depending upon the information given. If DT is known, then it is possible to solve for the distances D1 and D2. Conversely, if either D1 or D2 is known, it is possible to solve for DT. In either case, the following relationships hold:

Y_M, Z_M are as defined in Chapter III

$$X_M = -(DT + DF)$$

$$DF = Y_M / \tan \psi$$

$$\omega = -90 + (\psi + \epsilon)$$

$$DP = \frac{DT \sin \psi}{\sin(\psi + \epsilon)}$$

$$D_3 = \frac{DT \sin \epsilon}{\sin(\psi + \epsilon)}$$

$$D_{\text{OFFSET}} = \frac{Y_M}{\sin \psi}$$

Define the primed coordinate system to have its origin at the warhead centroid, its X-axis (X') coincident with the cone axis, its Z-axis (Z') in the same direction as the Z-axis of the target coordinate system, and its Y-axis (Y') defined according to the right hand rule. Then, if the coordinates of a point on the X-axis in the target coordinate system are (X, 0, 0), then its coordinates in the primed system are given by:

$$X' = (X - \Delta) \sin \omega + DP$$

$$Y' = (X - \Delta) \cos \omega$$

$$Z' = -Z_M$$

where

$$\Delta = D_3 + D_{\text{OFFSET}}$$

In the primed coordinate system, the equation of the warhead cone is

$$Y'^2 + Z'^2 = X'^2 (\tan \delta)^2$$

To solve for D1 and D2 when DT is known, let (X₁, 0, 0) and (X₂, 0, 0) be two arbitrary points on the X-axis of the target coordinate system. Let (X₁', Y₁', Z₁') and (X₂', Y₂', Z₂') be the coordinates (respectively) of these two points in the primed coordinate system. Then, if TP is any point on the X-axis of the target coordinate system, there exists a t such that the coordinates of TP in the primed coordinate system are

$$\begin{aligned} X_{TP}' &= X_1' + (X_2' - X_1')t \\ Y_{TP}' &= Y_1' + (Y_2' - Y_1')t \\ Z_{TP}' &= Z_1' + (Z_2' - Z_1')t = -Z_M \end{aligned}$$

If TP lies on the cone, then

$$\begin{aligned} Y_{TP}'^2 + Z_{TP}'^2 &= X_{TP}'^2 (\tan \delta)^2 \\ \Rightarrow (Y_1' + (Y_2' - Y_1')t)^2 + (-Z_M)^2 &= (X_1' + (X_2' - X_1')t)^2 \tan^2 \delta \\ \Rightarrow Y_1'^2 + 2Y_1'(Y_2' - Y_1')t + (Y_2' - Y_1')^2 t^2 + Z_M^2 \\ &= \tan^2 \delta (X_1'^2 + 2X_1'(X_2' - X_1')t + (X_2' - X_1')^2 t^2) \end{aligned}$$

After some rearrangement, this yields:

$$\begin{aligned} &[(Y_2' - Y_1')^2 - (X_2' - X_1')^2 \tan^2 \delta] t^2 \\ &+ 2[Y_1'(Y_2' - Y_1') - X_1'(X_2' - X_1') \tan^2 \delta] t \\ &+ [Z_M^2 + Y_1'^2 - X_1'^2 \tan^2 \delta] = 0 \end{aligned}$$

which has solutions:

$$t = \frac{-B \pm \sqrt{B^2 - 4AC}}{2A}$$

where

$$\begin{aligned} A &= (Y_2' - Y_1')^2 - (X_2' - X_1')^2 \tan^2 \delta \\ B &= 2[Y_1'(Y_2' - Y_1') - X_1' \tan^2 \delta (X_2' - X_1')] \\ C &= Z_M^2 + Y_1'^2 - X_1'^2 \tan^2 \delta \end{aligned}$$

If $B^2 < 4AC$, the cone and the X-axis of the target coordinate system do not intersect. If $B^2 = 4AC$, then the X-axis of the target coordinate system is tangent to the cone. Otherwise, $B^2 > 4AC$ and there are two solutions: t_1 and t_2 .

The value of t is just the parameter associated with the parametric description of the X -axis of the target coordinate system. If the two points defining the line are the same in absolute space, the value of t is the same in any coordinate system. Since (X_1', Y_1', Z_1') and (X_2', Y_2', Z_2') correspond to X_1 and X_2 , respectively, in the target coordinate system, then the coordinates of ATP and BTP in the target coordinate system are just

$$(X_{ATP}, 0, 0) \text{ and } (X_{BTP}, 0, 0)$$

where

$$X_{ATP} = X_1 + (X_2 - X_1)t_1 \quad \text{and} \quad X_{BTP} = X_1 + (X_2 - X_1)t_2$$

There is a pathology associated with this solution. The mathematical equation of a cone actually describes two cones in mathematical space. The warhead cone is that portion of the mathematical cone for which the X' coordinate is positive. Therefore, any of the solutions for t which result in a negative value of X' should be rejected. Note that in the situation depicted in Figure D-1, the intersection of the cone and the X - Z plane of the target coordinate system is an ellipse. If, and only if, this is the case will both ATP and BTP exist for a given value of DT .

Note that in Figure D-1, $Z_M = 0$. If $Z_M \neq 0$, then the lines connecting ATP and BTP to the origin of the primed system will not make an angle δ with the cone axis in the $X' - Y'$ plane. Rather, the total angle (in three dimensions) between the cone axis and either of the two lines is δ , since by assumption,

ATP and BTP lie on the cone.

Now, if ATP and BTP are specified, it is possible to solve for DT. For purposes of generality, assume that ATP and BTP need not lie on the cone simultaneously--i.e. for a given value of DT. The following development centers on the solution for DT if ATP is known. The development if BTP is known is completely analogous.

Let the coordinates of ATP in the target coordinate system be $(X_{ATP}, 0, 0)$, then its coordinates in the primed coordinate system are:

$$\begin{aligned} X' &= (X_{ATP} - \Delta) \sin \omega + DP \\ &= \left(X_{ATP} - \frac{DT \sin \epsilon}{\sin(\psi + \epsilon)} - \frac{Y_M}{\sin(\psi)} \right) \sin \omega + \frac{DT \sin \psi}{\sin(\psi + \epsilon)} \\ &= X_{ATP} \sin \omega - \frac{Y_M \sin \omega}{\sin \psi} + DT \left(\frac{\sin \psi - \sin \epsilon \sin \omega}{\sin(\psi + \epsilon)} \right) \end{aligned}$$

It can be shown that

$$\frac{\sin \psi - \sin \epsilon \sin \omega}{\sin(\psi + \epsilon)} = \cos \epsilon$$

Thus, the equation for X' becomes:

$$= X_{ATP} \sin \omega - \frac{Y_M \sin \omega}{\sin \psi} + DT \cos \epsilon$$

$$\begin{aligned} Y' &= (X_{ATP} - \Delta) \cos \omega \\ &= (X_{ATP} - \Delta) \sin(\psi + \epsilon) \\ &= \left(X_{ATP} - \frac{DT \sin \epsilon}{\sin(\psi + \epsilon)} - \frac{Y_M}{\sin \psi} \right) \sin(\psi + \epsilon) \\ &= X_{ATP} \sin(\psi + \epsilon) - DT \sin \epsilon - \frac{Y_M \sin(\psi + \epsilon)}{\sin \psi} \end{aligned}$$

Now, substituting these expressions into the cone equation,

$$Y'^2 + Z'^2 = X'^2 \tan^2 \delta$$

and solving for DT yields:

$$DT = - \frac{B \pm \sqrt{B^2 - 4AC}}{2A}$$

where

$$A = \sin^2 \epsilon - \tan^2 \delta \cos^2 \epsilon$$

$$B = -2(X_{ATP} - Y_M / \sin \psi) [\sin \epsilon \cos \omega + \tan^2 \delta \sin \omega \cos \epsilon]$$

$$C = Z_M^2 + (X_{ATP} - Y_M / \sin \psi)^2 [\cos^2 \omega - \tan^2 \delta \sin^2 \omega]$$

Again, there are pathologies associated with this solution when $B^2 \leq 4AC$. If $B^2 < 4AC$, there is no value of DT for which ATP lies on the cone. If $B^2 = 4AC$, there is only one value of DT for which ATP lies on the cone. Otherwise, there are two values of DT for which ATP lies on the cone. Since

$$X_M = -DT + DF$$

choose that value of DT which minimizes X_M . This assures that the forward half of the mathematical cone (i.e. the warhead cone) is the one on which ATP lies.

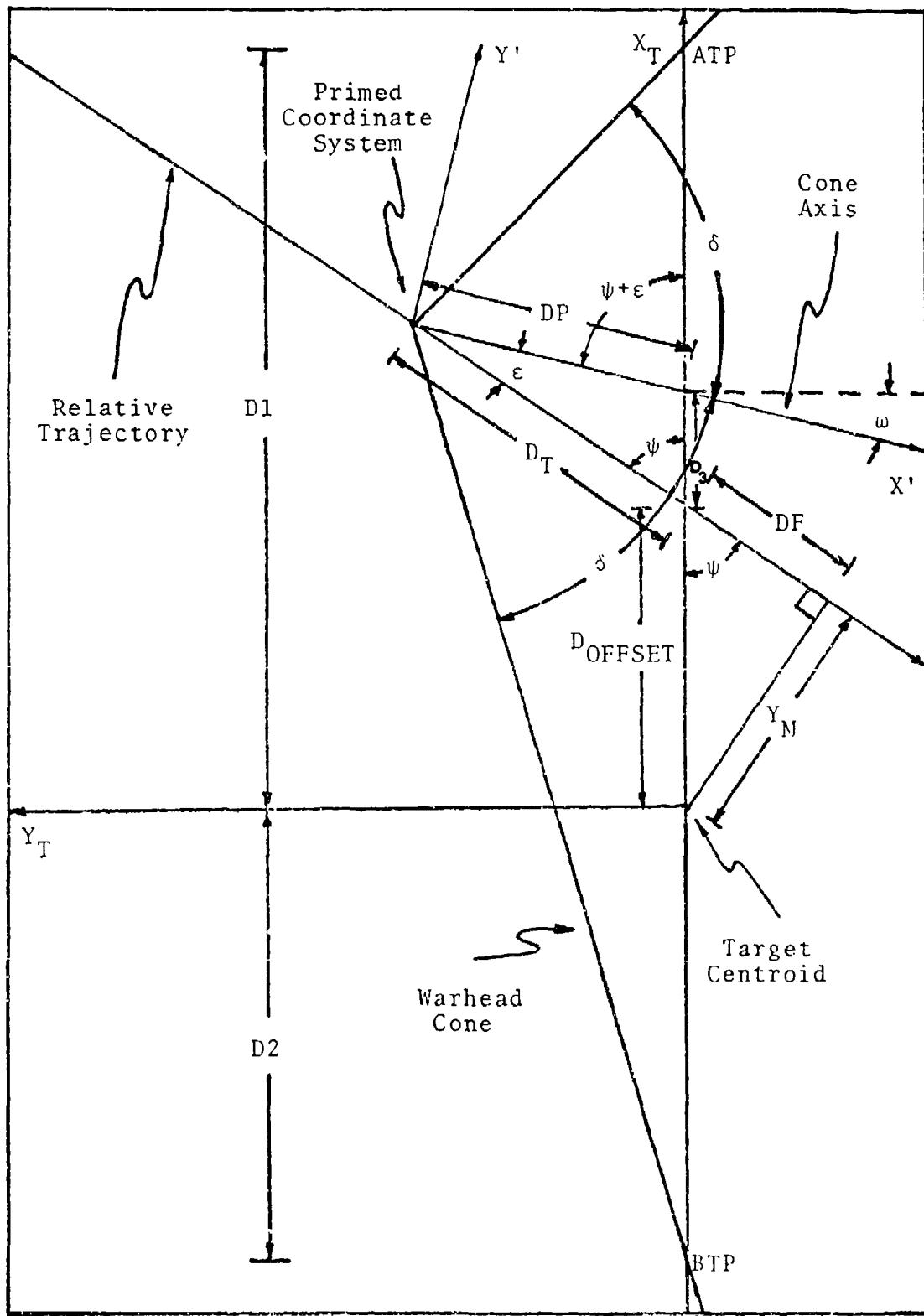


Fig D-1: Geometry of the Cone/Line Intersection Problem

APPENDIX E

Determination of "a" and "b"

This appendix describes how a and b are determined given the values of X_M at which ATP and BTP are intersected by the warhead cone.

Let X_{MF1} be the value of X_M when ATP lies on the leading warhead cone, X_{MF2} be the value of X_M when ATP lies on the trailing warhead cone, X_{MR1} be the value of X_M when BTP lies on the leading warhead cone, and X_{MR2} be the value of X_M when BTP lies on the trailing warhead cone. X_{MF1} , X_{MF2} , X_{MR1} , and X_{MR2} are determined as described in Appendix D. In this context, ATP refers to the forward limit of the vulnerable length (i.e. the end of the vulnerable length closest to the nose of the target) while BTP refers to the rearward limit (see Figure F-1). Let P denote the proportion of maximum P_K which is achieved when either ATP or BTP is first or last contacted by a warhead cone. Define X_{MF} and X_{MR} as follows:

$$\begin{aligned} \text{if } X_{MF1} > X_{MR1} \quad & X_{MF} = X_{MF2} \\ \text{and} \quad & X_{MR} = X_{MR1} \end{aligned}$$

Otherwise,

$$\begin{aligned} X_{MF} &= X_{MF1} \\ X_{MR} &= X_{MR1} \end{aligned}$$

This definition assumes that the value of P_K first reaches $P \cdot P_{K_{MAX}}$ whenever the vulnerable length is first contacted by a warhead cone, whether it be on the ATP end or the BTP end. P_K is then last equal to $P \cdot P_{K_{MAX}}$ whenever the vulnerable length is last contacted by a warhead cone, again regardless of which end (see Fig. E-2).

Let $W = |X_{M_F} - X_{M_R}|$ and $L =$ the minimum of X_{M_F} and X_{M_R} .
Then,

$$a = -(L + W/2)$$

Now,

$$e^{-\left(\frac{X_M + a}{b}\right)^6} = P \text{ whenever } X_M = X_{M_F} \text{ or } X_M = X_{M_R}$$

In particular,

$$e^{-\left(\frac{X_{M_F} + a}{b}\right)^6} = P$$

$$\Rightarrow -\ln P = \left(\frac{X_{M_F} + a}{b}\right)^6$$

$$\Rightarrow \sqrt[6]{-\ln P} = \frac{X_{M_F} + a}{b}$$

$$\Rightarrow b = \frac{X_{M_F} + a}{\sqrt[6]{-\ln P}}$$

There is a phenomenon whereby the vulnerable length is sometimes last contacted by a warhead cone after both ATP and BTP have last been contacted. This situation, depicted in Figure E-3, can occur only when the intersections of the warhead cones with the X-Z plane in the target coordinate system are ellipses. The situation is of concern whenever a point between ATP and BTP becomes a point of tangency between the line

and a warhead cone. The result is that the vulnerable length suddenly "drops-out" of the fragment pattern.

Mathematically, the necessary condition for dropout is that $B^2 = 4AC$ where A, B, and C are as defined by the first solution in Appendix D. Substitution of these expressions for A, B, and C into $B^2 = 4AC$ and subsequent algebraic manipulation reveals that an equivalent necessary condition is that

$$DT = |Z_M / \sin\psi| \sqrt{(\cos^2\omega / \tan^2\delta) - \sin^2\omega}$$

Thus, to account for drop-out, one should substitute this value of DT (say $DT_{DROPOUT}$) into the first cone/line intersection solution of Appendix D. If and only if the resulting point is between BTP and ATP does drop-out occur. If it does, then $X_{M_R} = DT_{DROPOUT}$ and X_{M_F} = the minimum of $X_{M_{F1}}$, $X_{M_{F2}}$, $X_{M_{R1}}$, and $X_{M_{R2}}$.

When the vulnerable length drops-out of the warhead cone, the fragment pattern is still intersecting the target fuselage surrounding it. Obviously, there are vulnerable components in this part of the fuselage, for otherwise the vulnerable length would be elsewhere along the target centerline. Therefore, it is necessary to "bias" X_{M_R} by some amount to account for the width of the fuselage. This is accomplished by adding a "drop-out bias" to $DP_{DROPOUT}$ in obtaining X_{M_R} (See Fig. E-4).

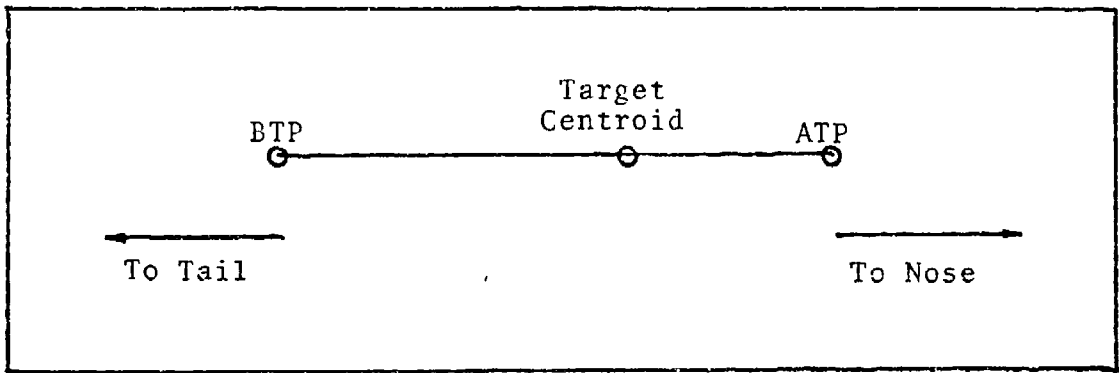


Fig E-1: The Vulnerable Length

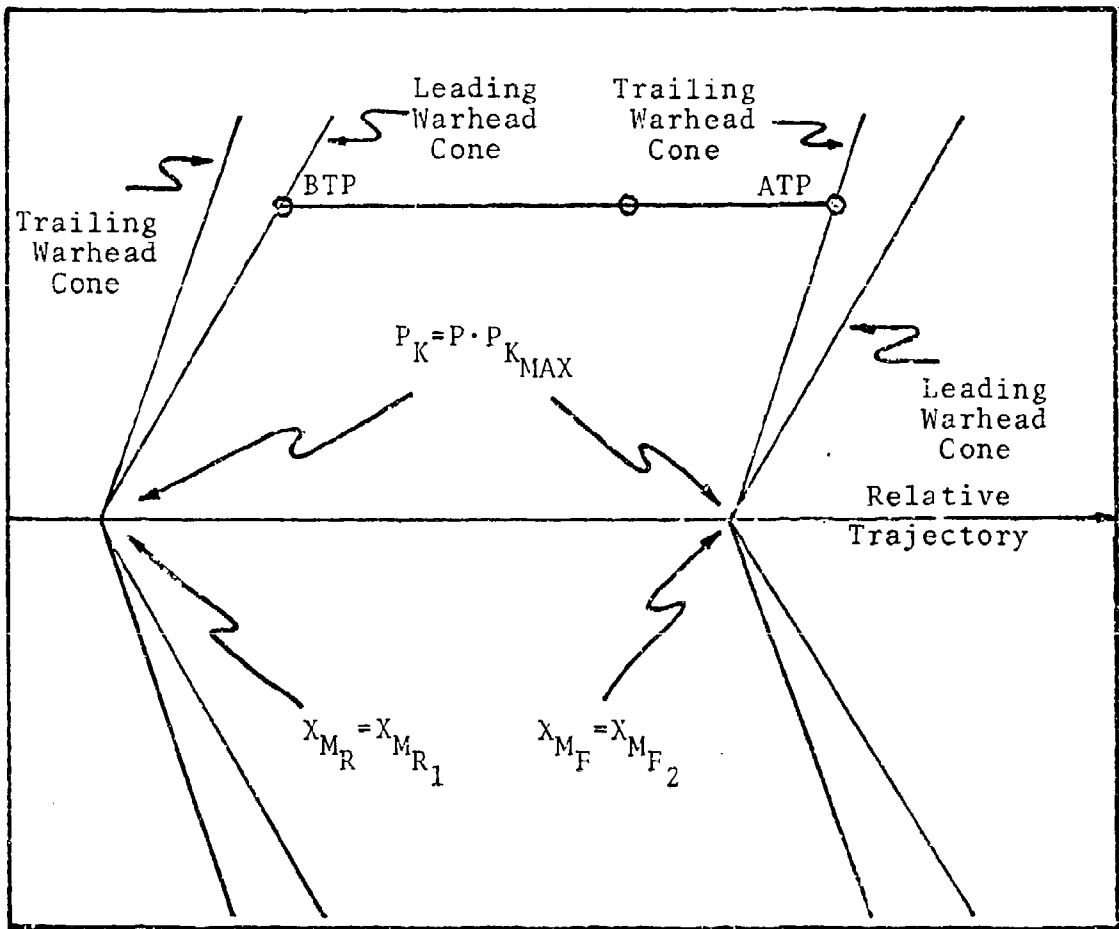


Fig E-2: Illustration of X_{M_R} and X_{M_F}

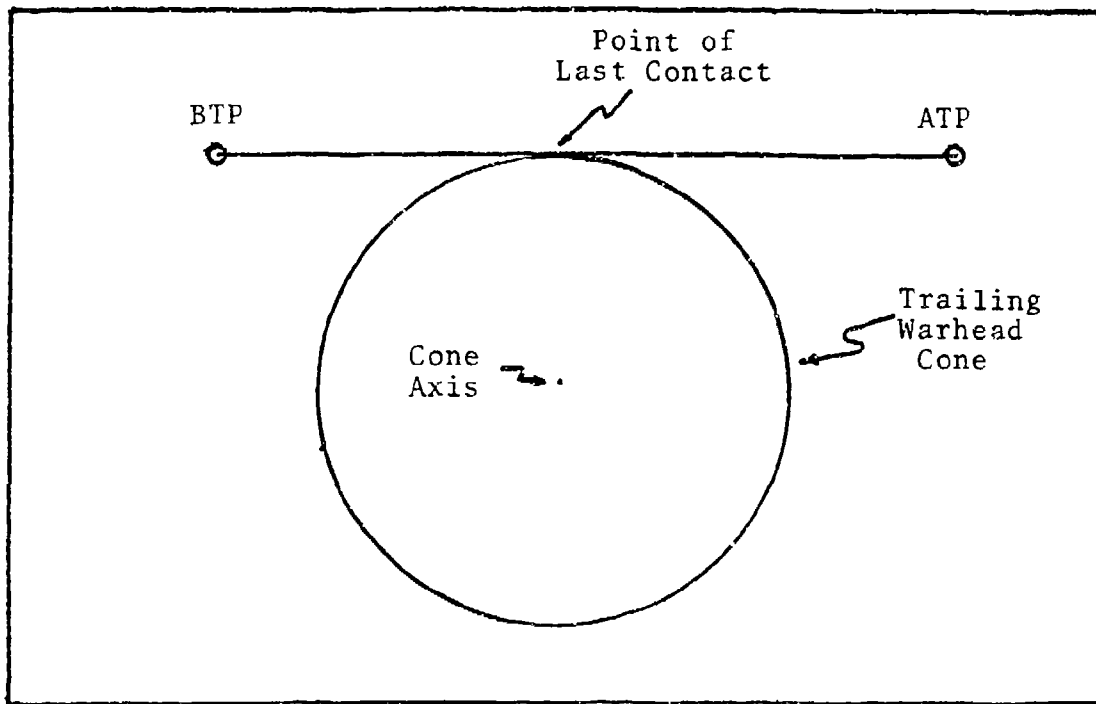


Fig E-3: The Drop-Out Situation

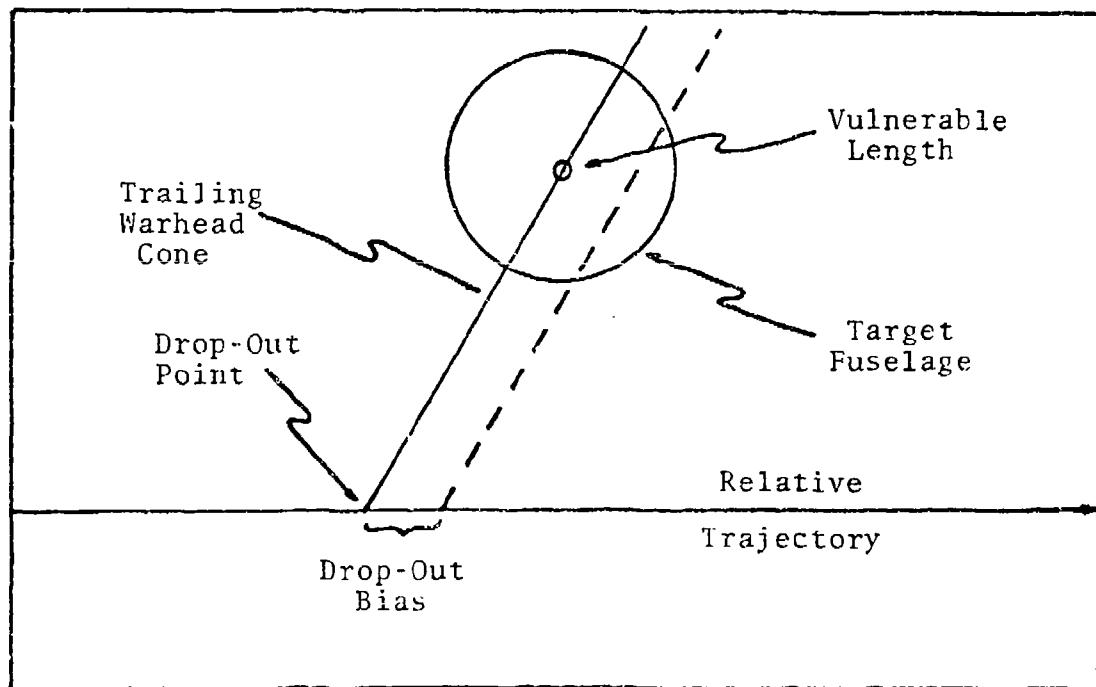


Fig E-4: Illustration of Drop-Out Bias

APPENDIX F

The First Characterization Applied
to the Basic Data

The 48 plots in this appendix represent a comparison between the first semi-empirical characterization and the basic data. The following is a description of this first characterization

$$P_K = F \cdot e^{-\left(\frac{X_M + a}{b}\right)^6}$$

where

F = the lesser of $\begin{cases} 1.0 \\ 1.22 - .14R_M \end{cases}$

and a and b are determined as described in Appendices D and E with P = 0.9 and

$$ATP = 5$$

$$BTP = -7 + 2.5 CH$$

where CH is the greater of $\begin{cases} 0 \\ (R_M - 15)/12.5 \end{cases}$

and the drop-out bias is one foot.

There is one plot for each entry in Table V. The combination of factor values is given on each plot. The error bars are $\pm .10$ 90% confidence intervals about the SHAZAM estimates.

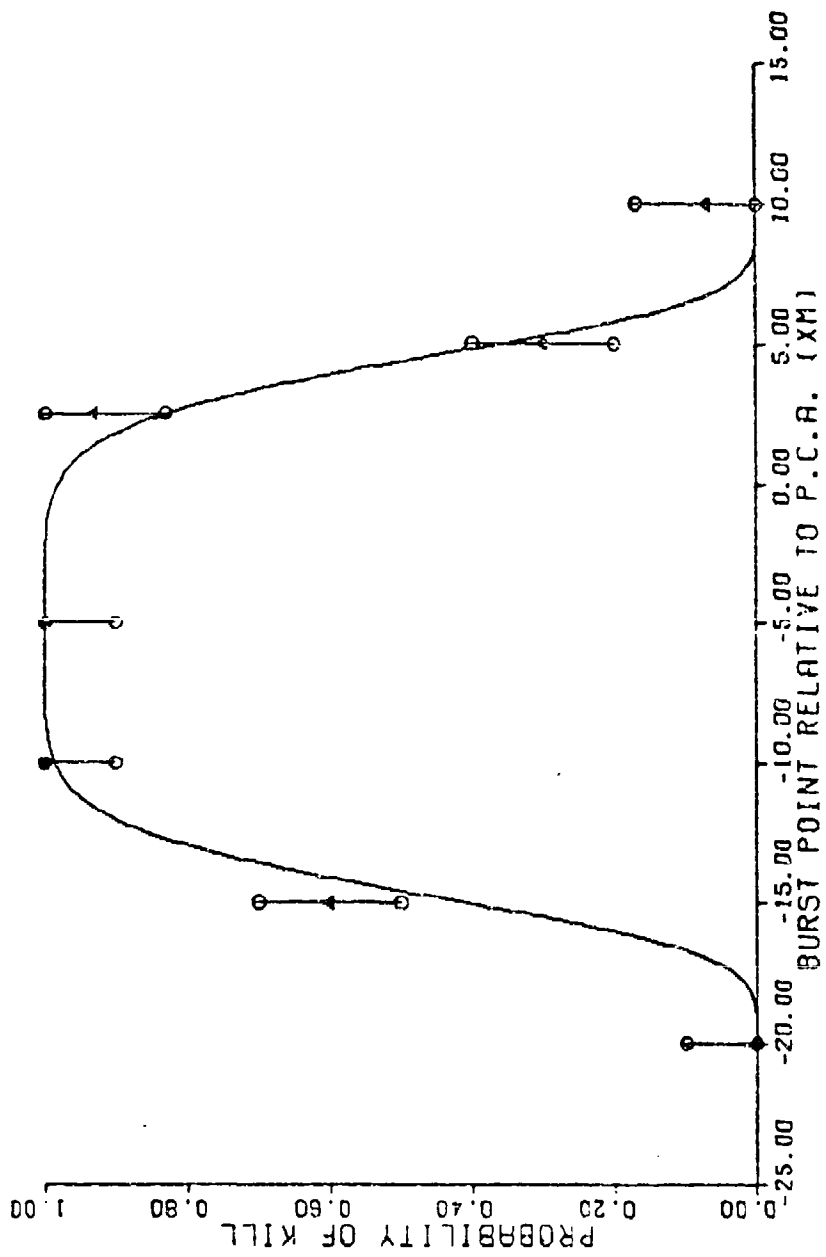


FIG F-1 : PSI=0. THETA=225. VR=2000. RM=15.0 BETA=0.

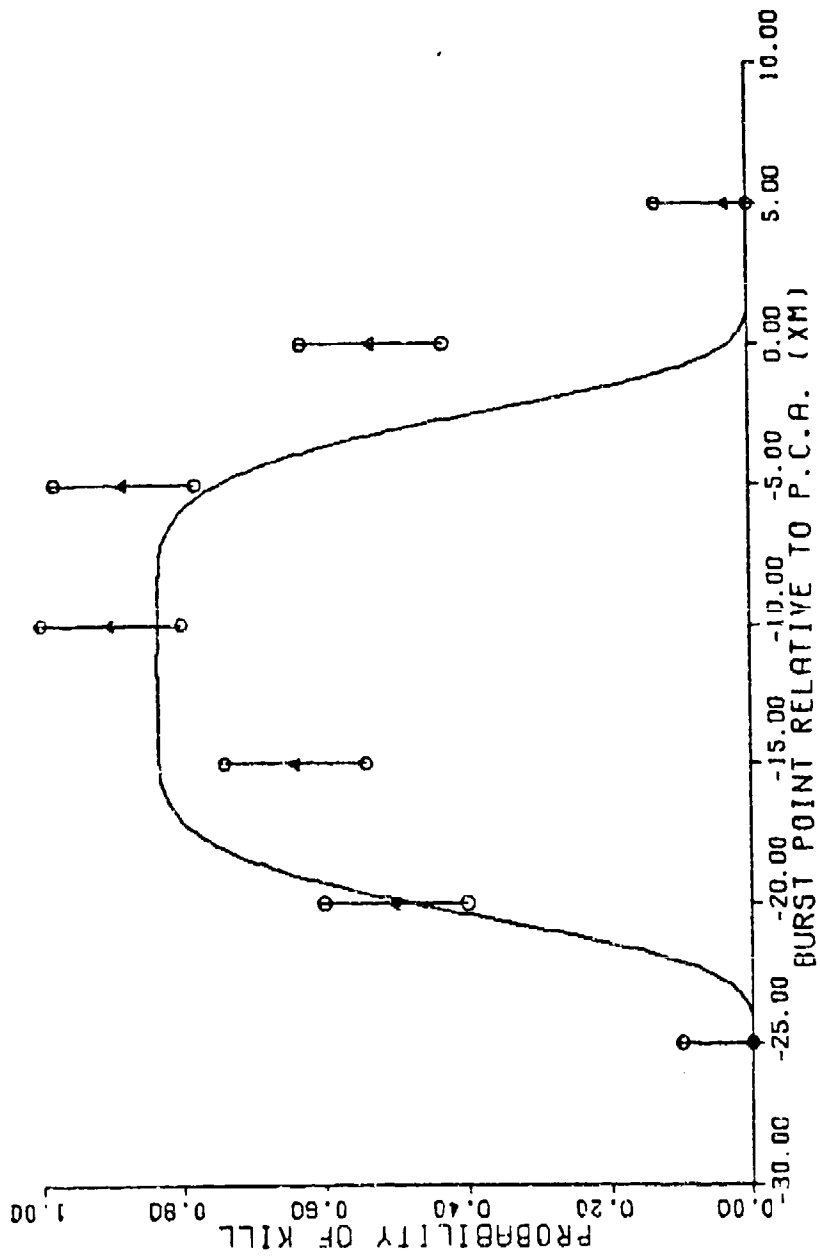


FIG F-2 : PSI=0. THETA=225. VR=2000. RM=27.5 BETA=0.

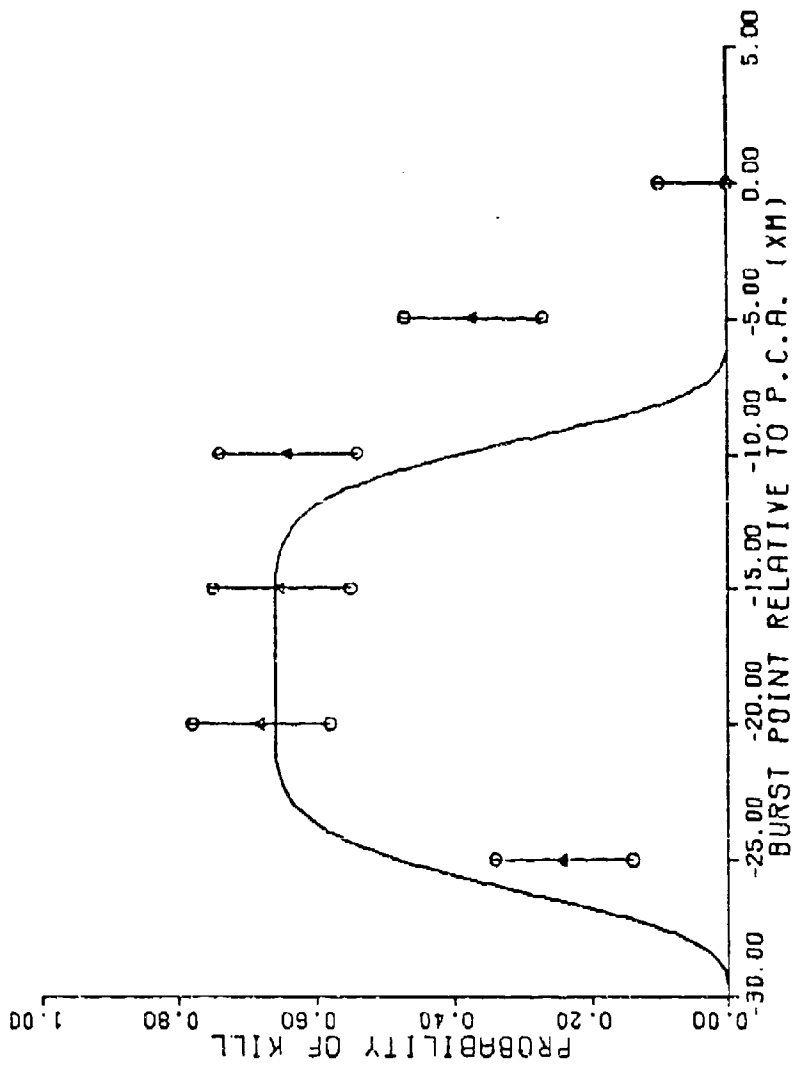


FIG F-3 : PSI=0. THETA=225. VR=2000. RM=40.0 BETA=0.

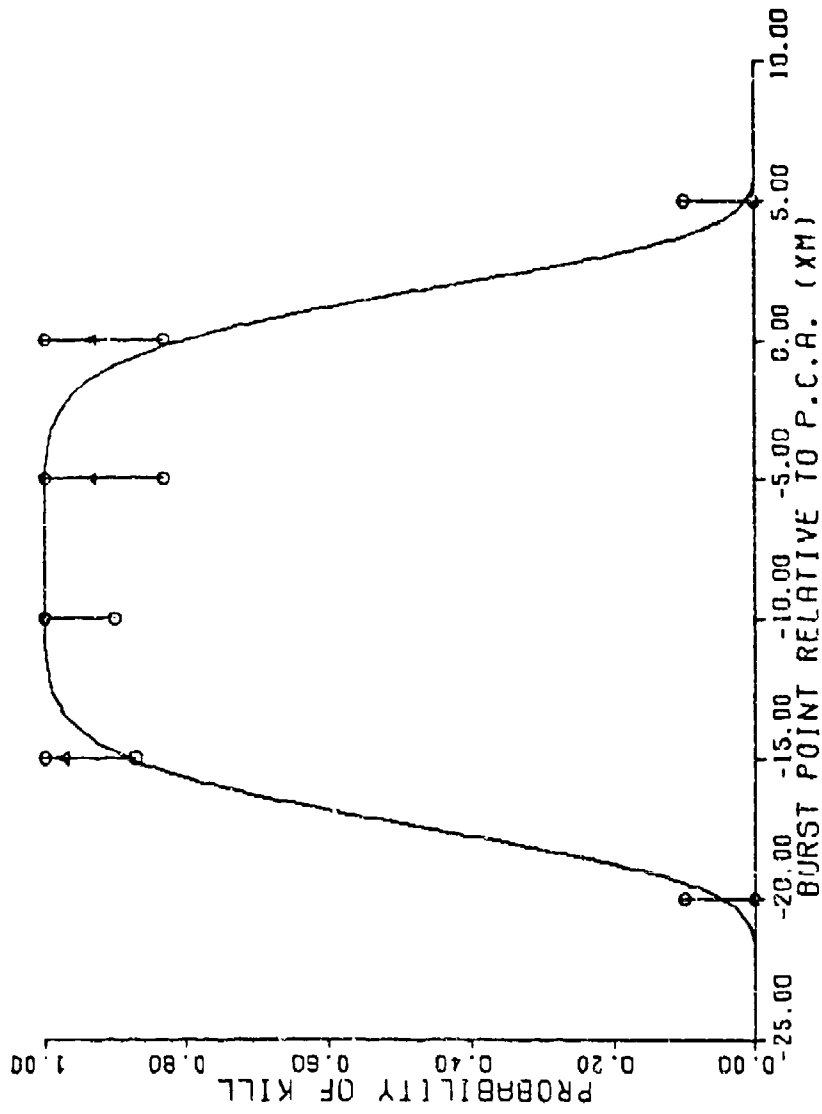


FIG. F-4 : PSI=0. THETA=225. VR=3000. RM=15.0 BETA=0.

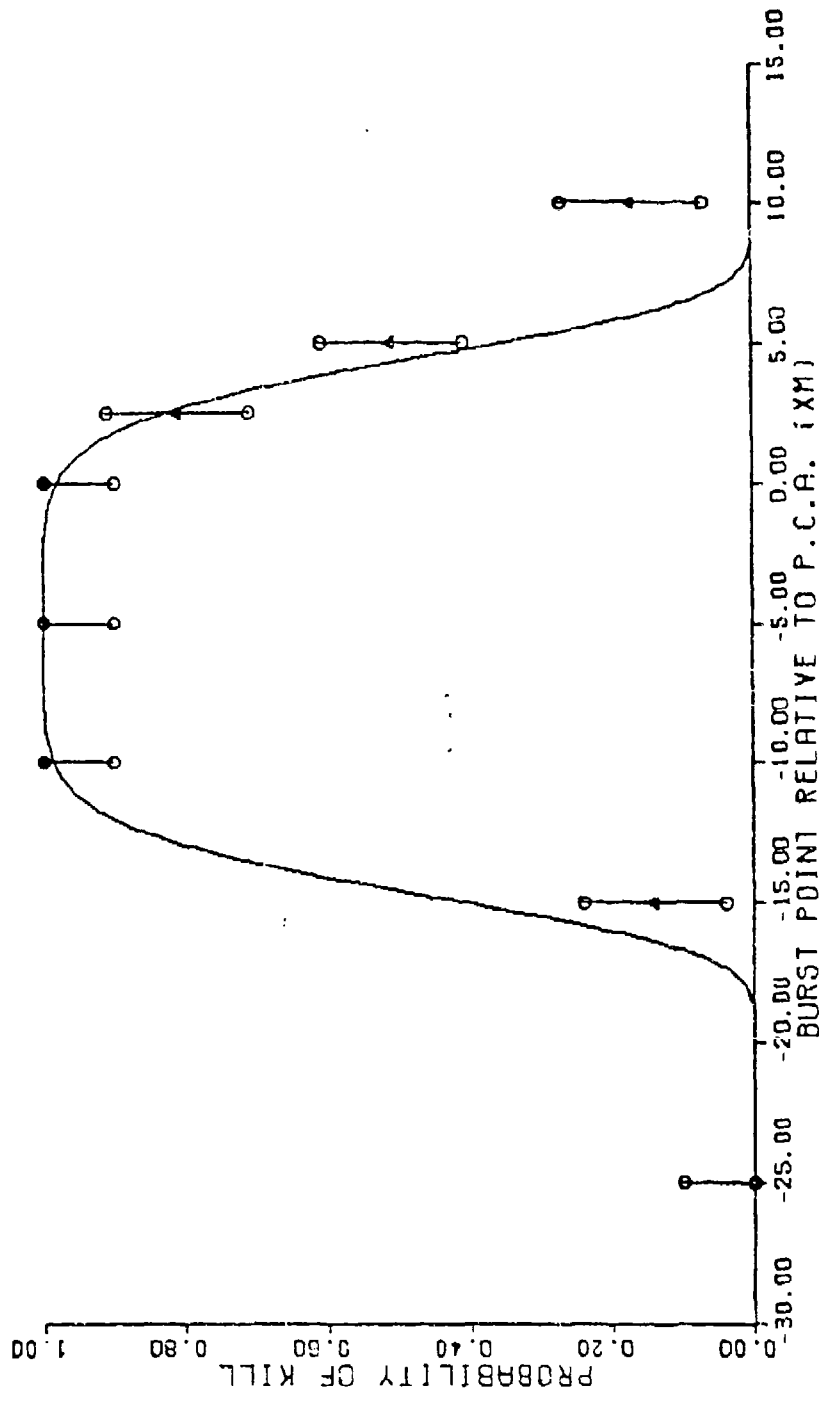


FIG F-5: PSI=0. THETA=135. VR=2000. RM=15.0 BETA=0.

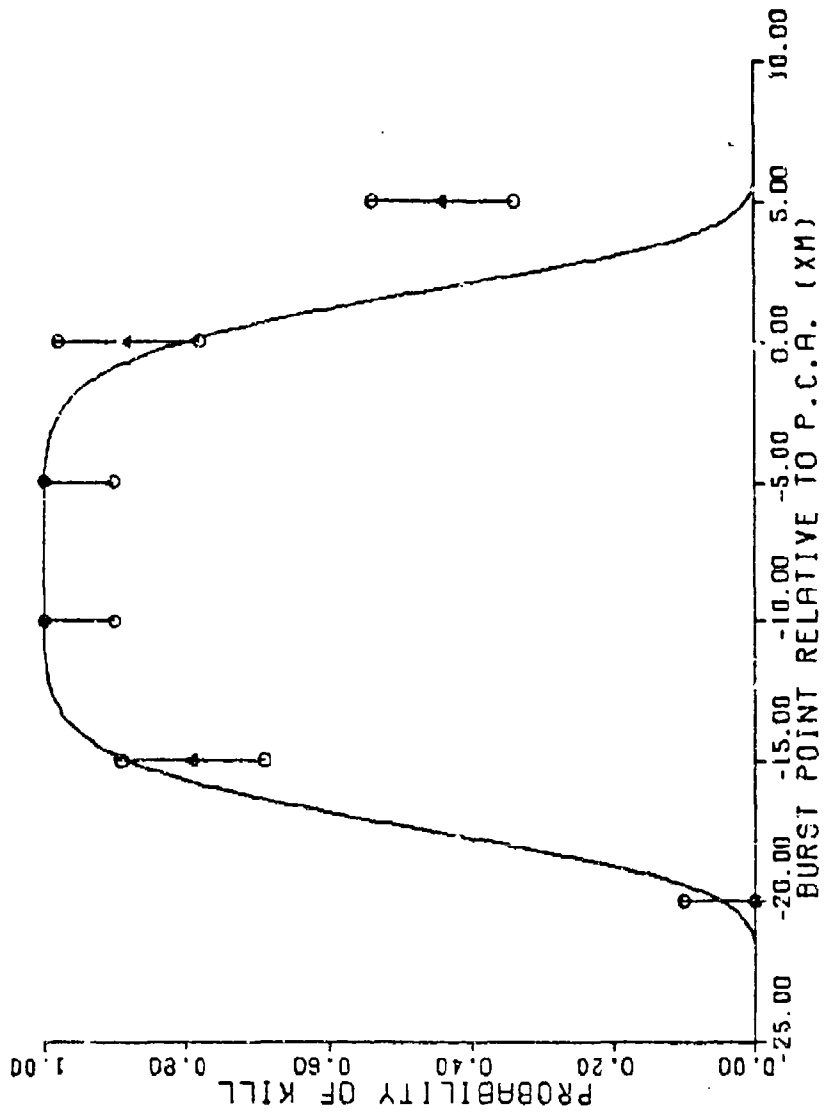


FIG F-6 : PSI=0. THETA=135. VR=3000. RM=15.0 BETA=0.

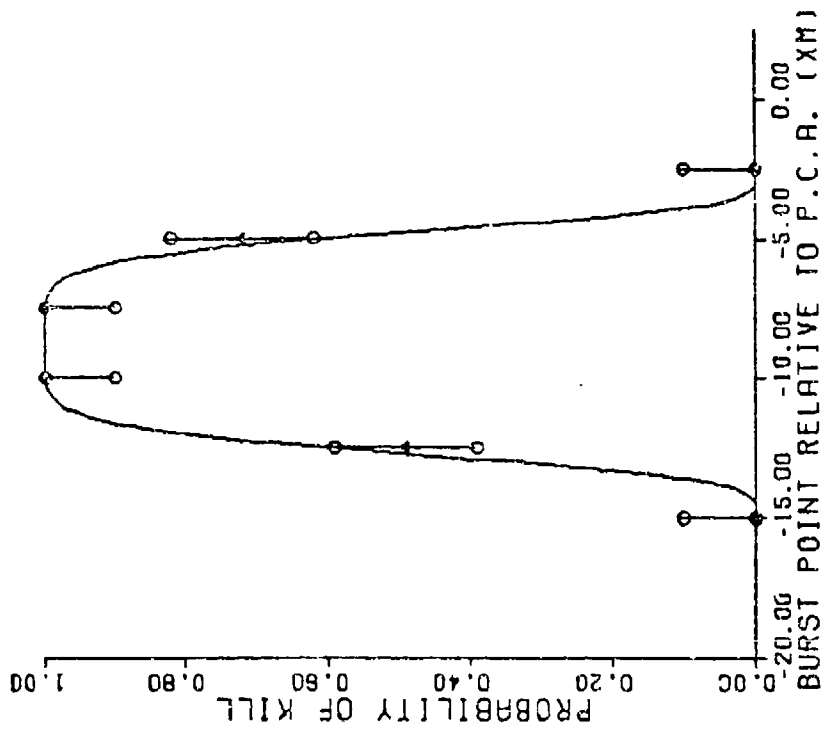


FIG F-7 : PSI=45. THETA=45. VR=2000. RM=15.0 BETA=15.

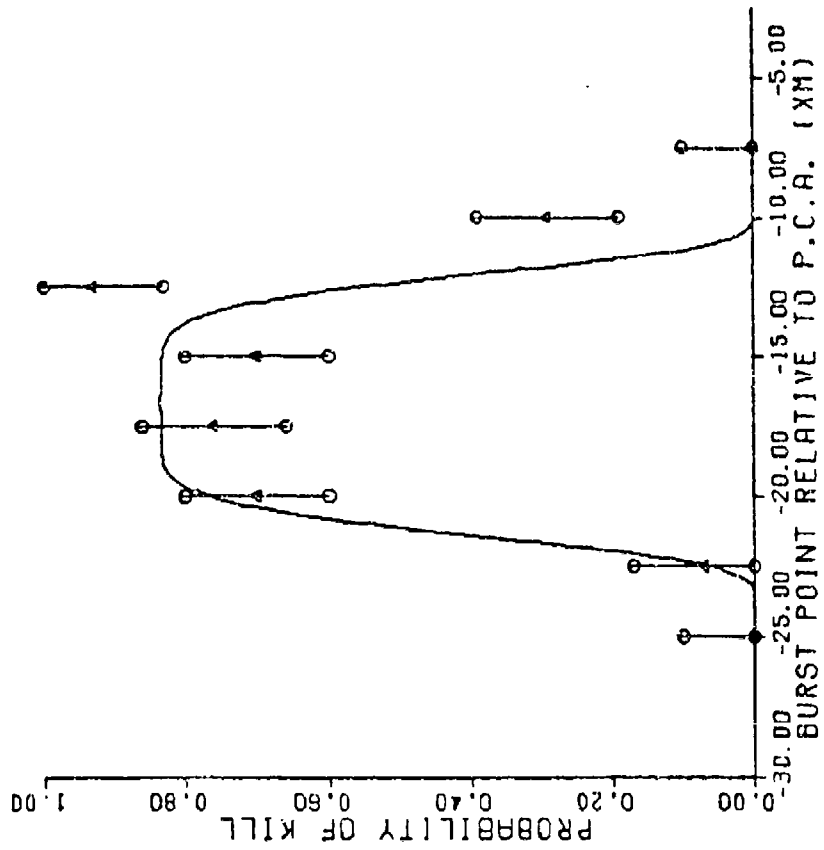


FIG F-8 : PSI=45. THETA=45. VR=2000. RM=27.5 BETA=15.

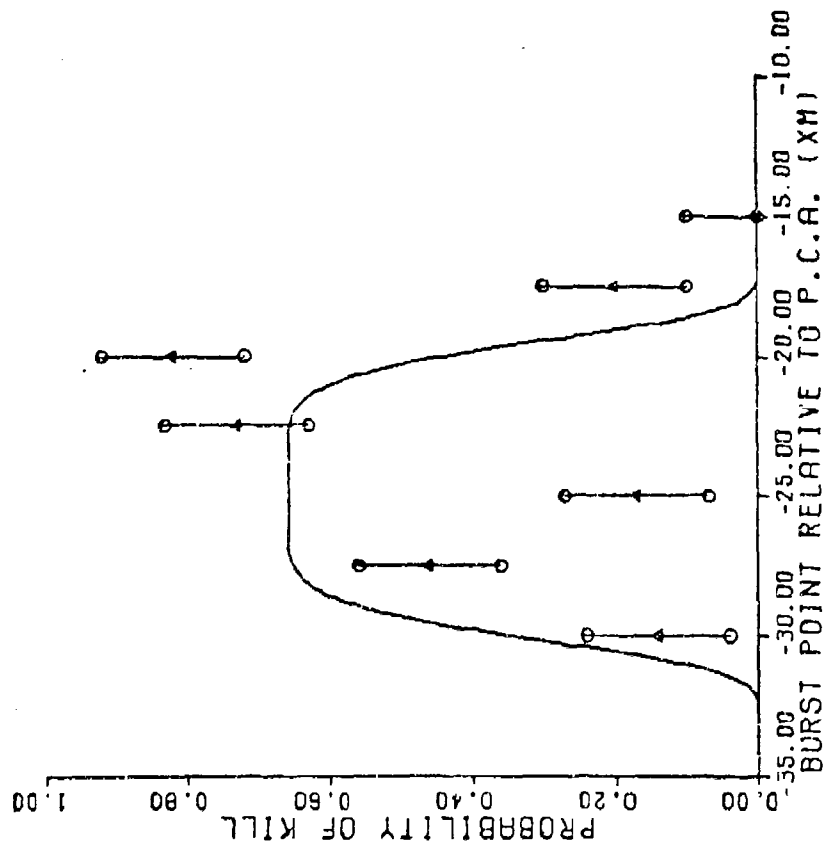


FIG F-9 : PSI=45. THETA=45. VR=2000. RM=40.0 BETA=15.

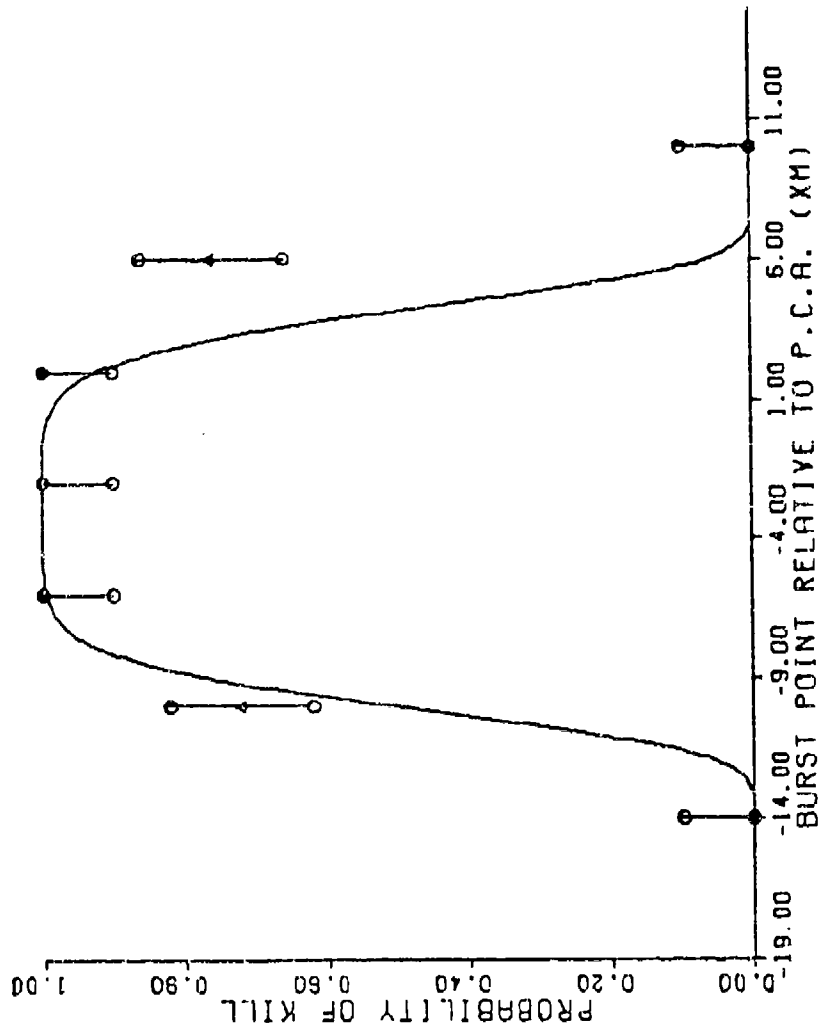


FIG F-10 : PSI=45. THETA=135. VR=2000. RM=15.0 BETA=15.

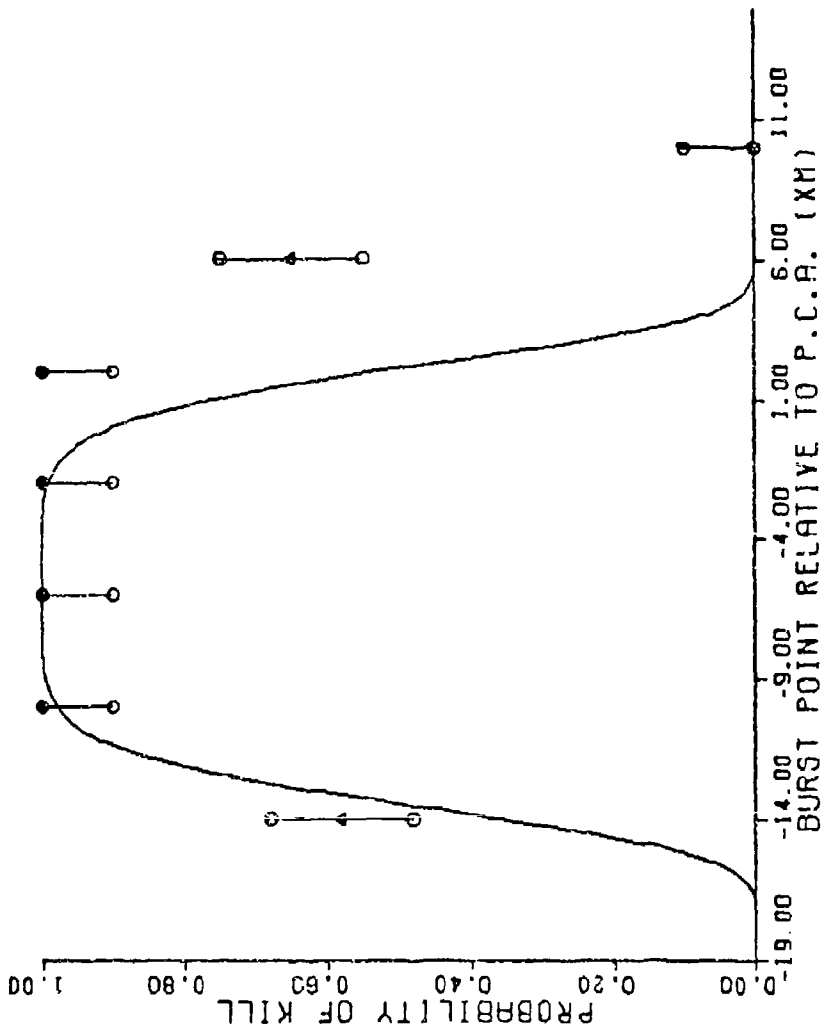


FIG F-11: PSI=45. THETA=135. VR=3000. RM=15.0 BETA=15.

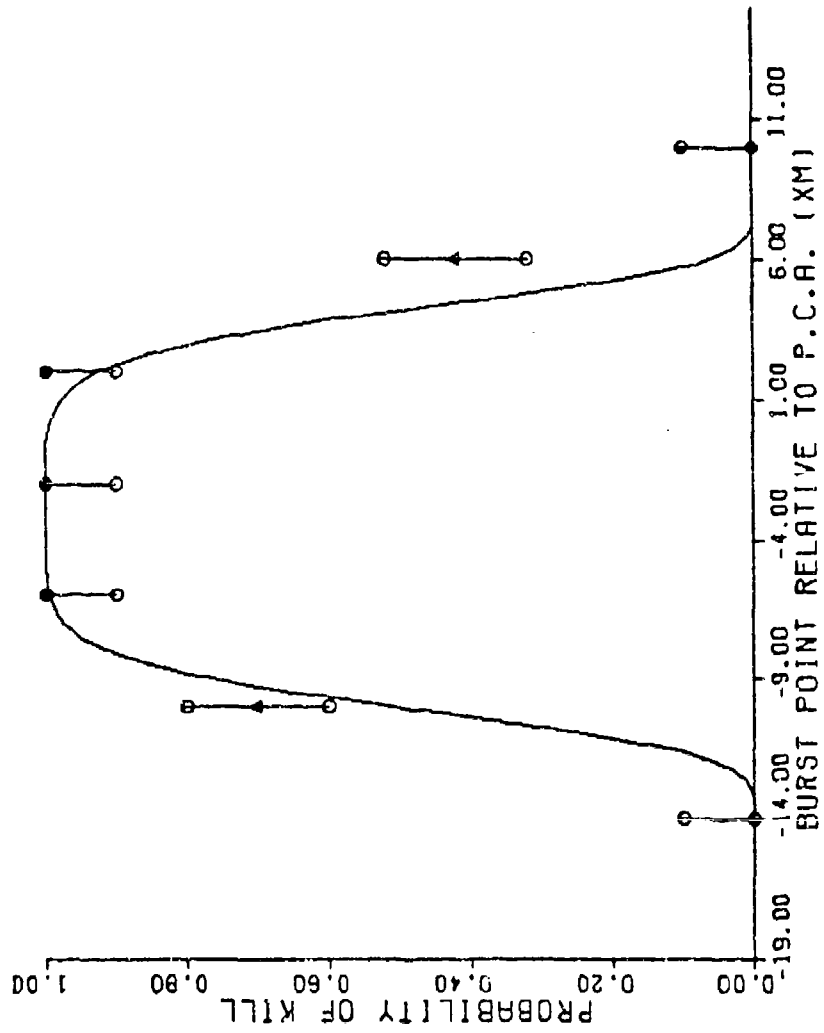


FIG F-12: PSI=45. THETA=225. VR=2000. RM=15.0 BETA=15.

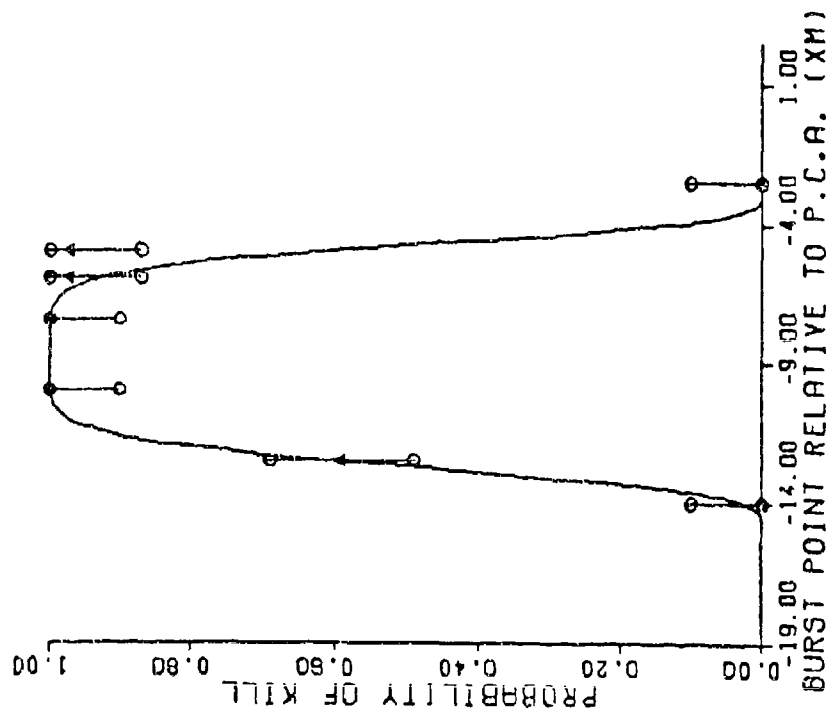


FIG F-13: PSI=45. THETA=315. VR=2000. RM=15.0 BETA=15.

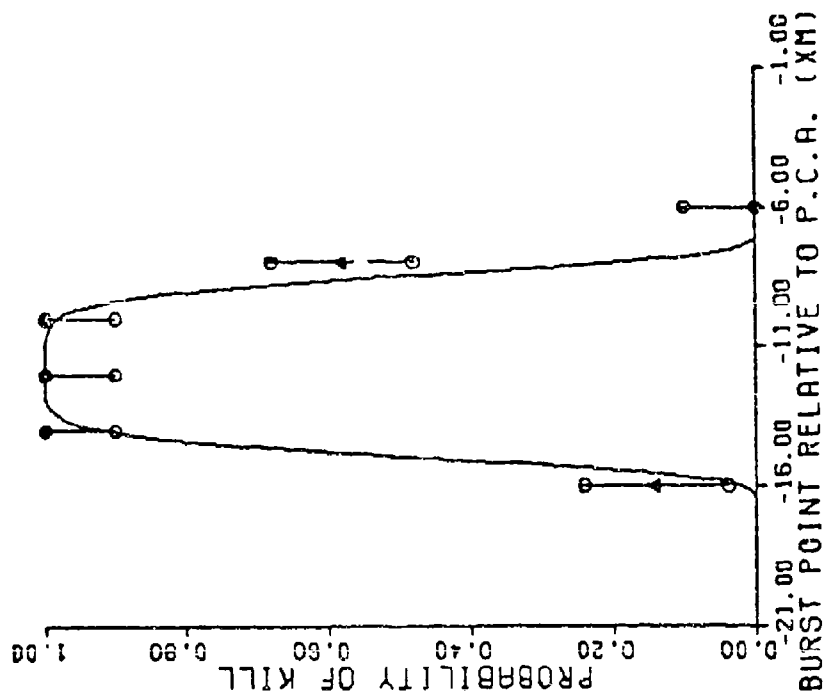


FIG F-14: PSI=45. THETA=315. VR=3000. RM=15.0 BETA=15.

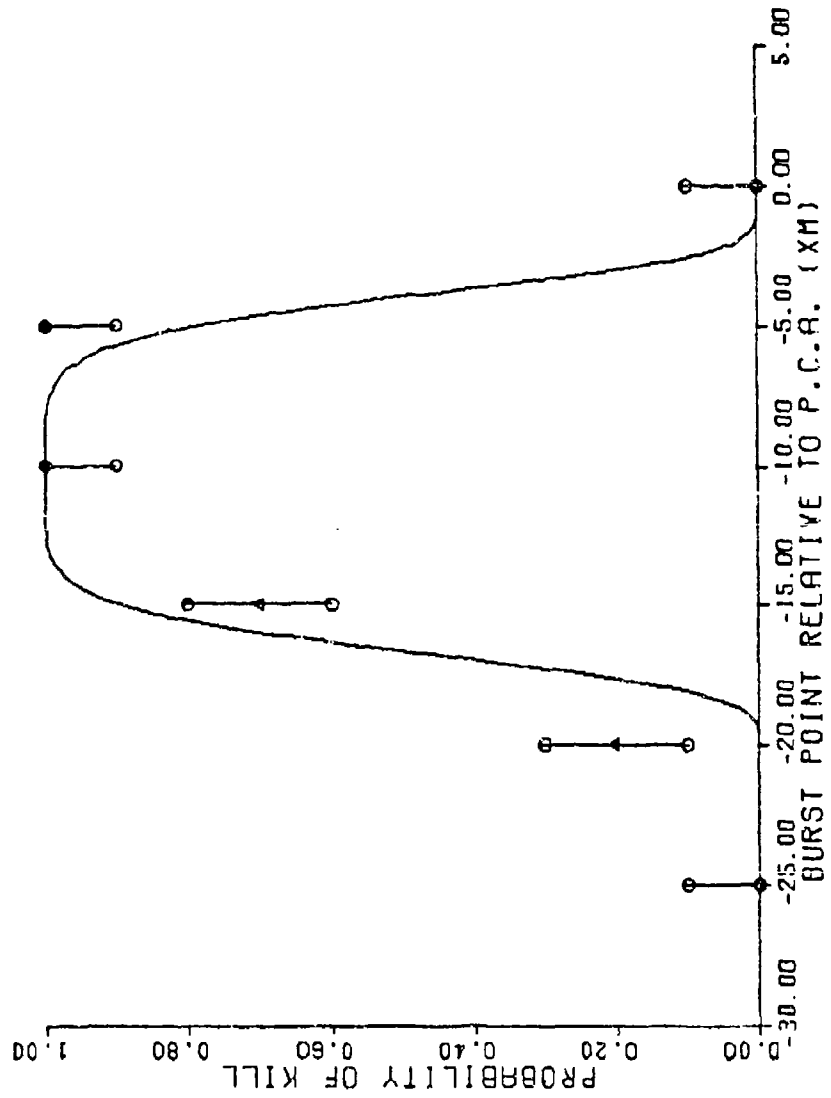


FIG F-15: PSI=90. THETA=45. VR=2000. RM=15.0 BETA=15.

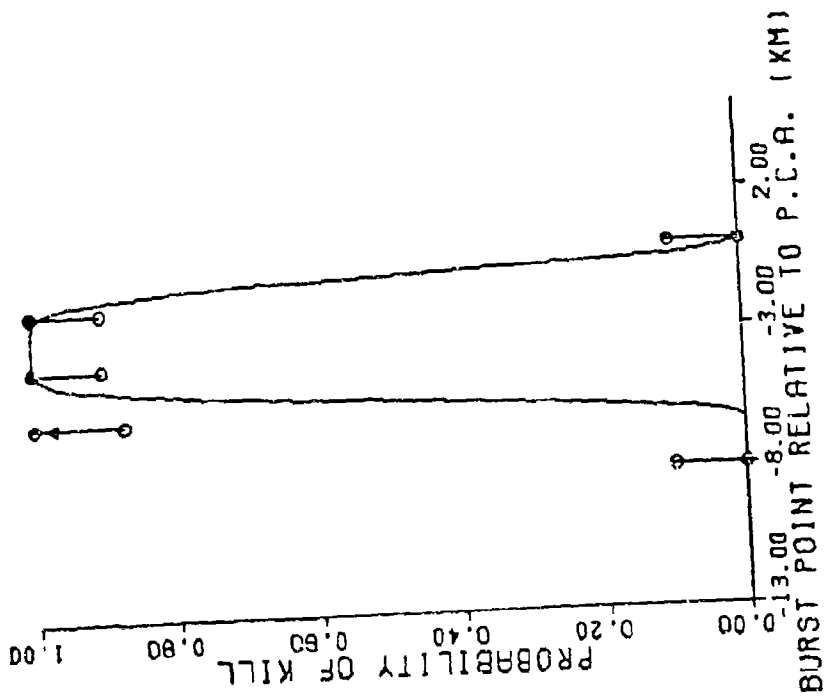


FIG F-16: PSI=90. THETA=135. VR=2000. RM=15.0 BETA=15

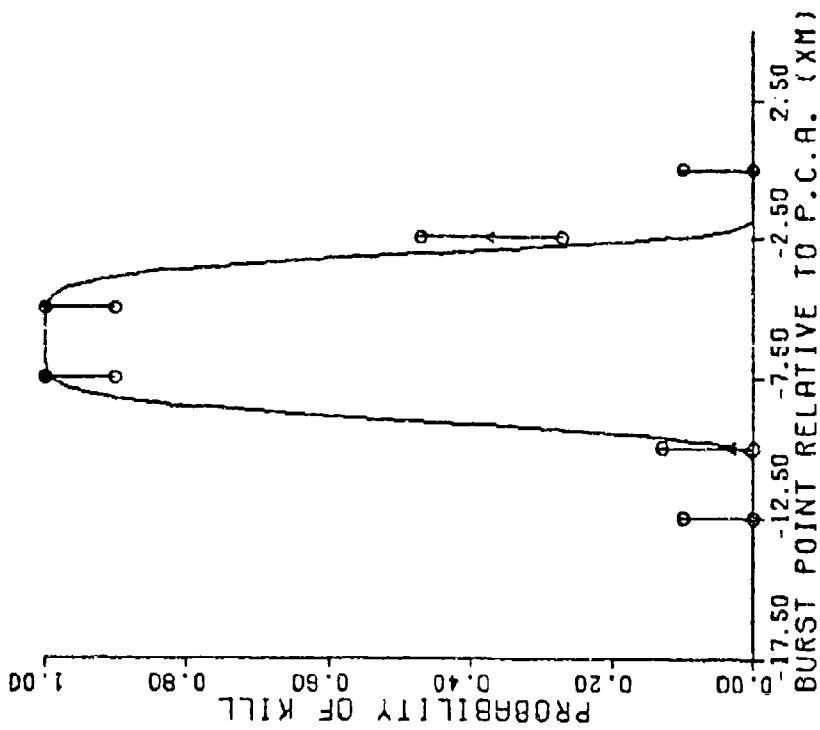


FIG F-17 : PSI=90. THETA=135. VR=3000. RM=15.0 BETA=15.

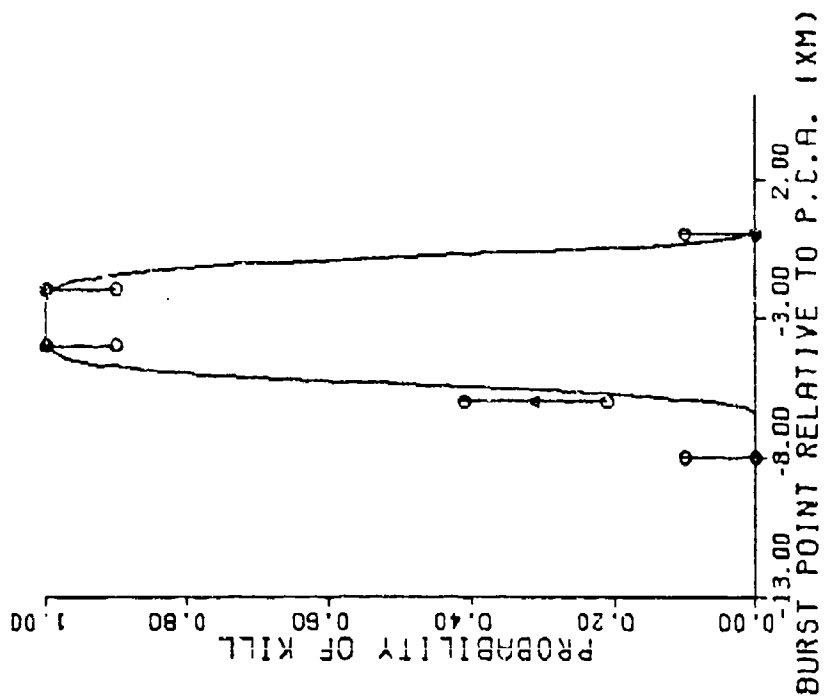


FIG F-18 : PSI=90. THETA=225. VR=2000. RM=15.0 BETA=15.

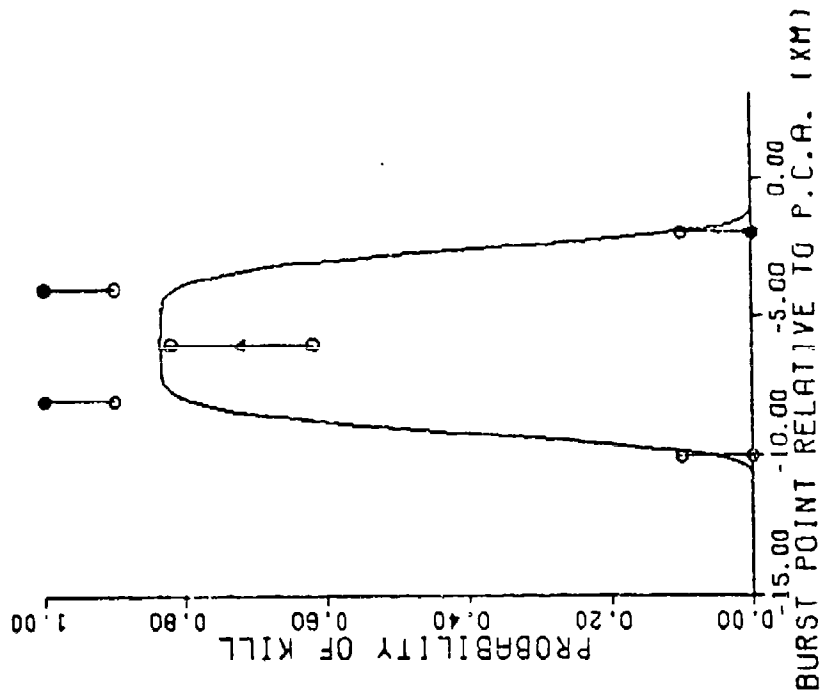


FIG F-19: PSI=90. THETA=225. VR=2000. RM=27.5 BETA=15.

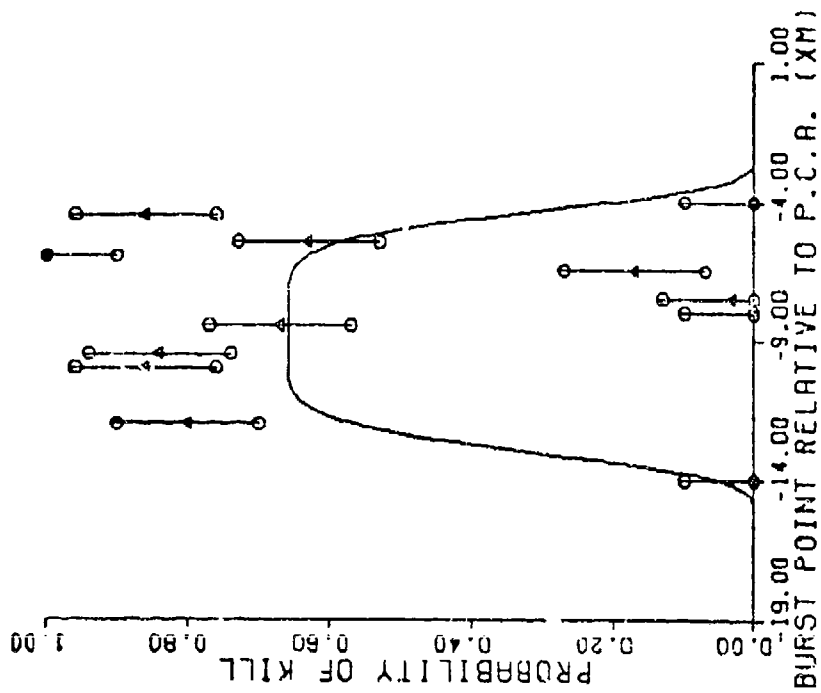


FIG F-20: PSI=90. THETA=225. VR=2000. RM=40.0 BETA=15.

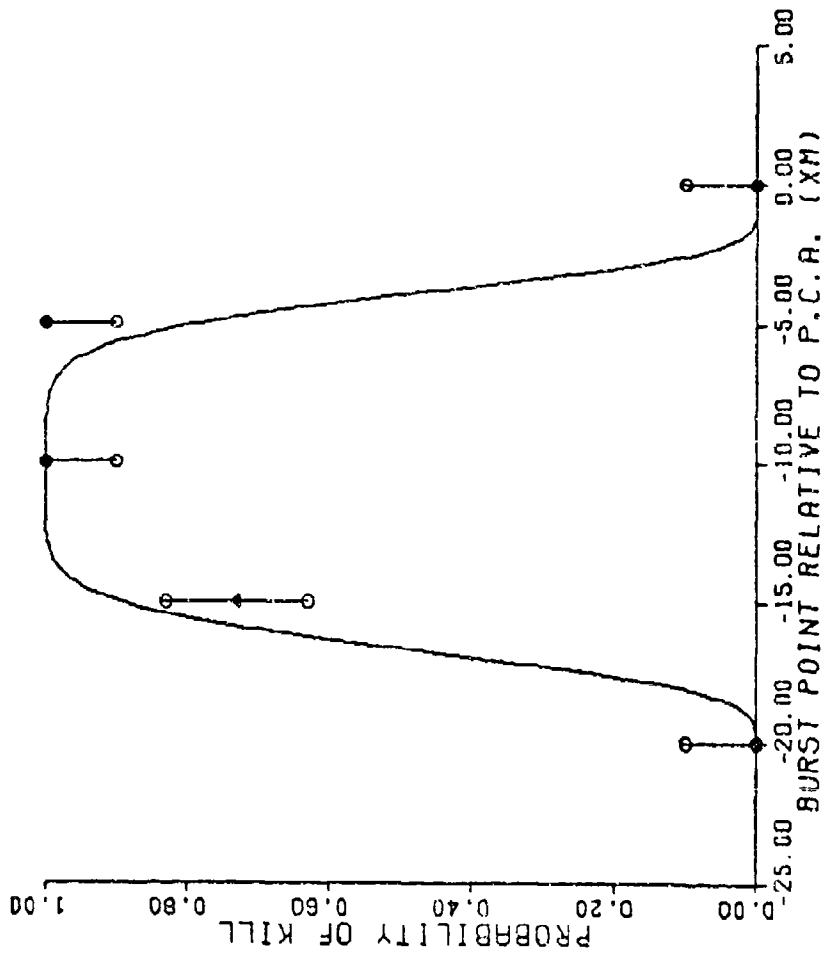


FIG F-71: PSI=90. THETA=315. VR=2000. RM=15.0 BETA=15.

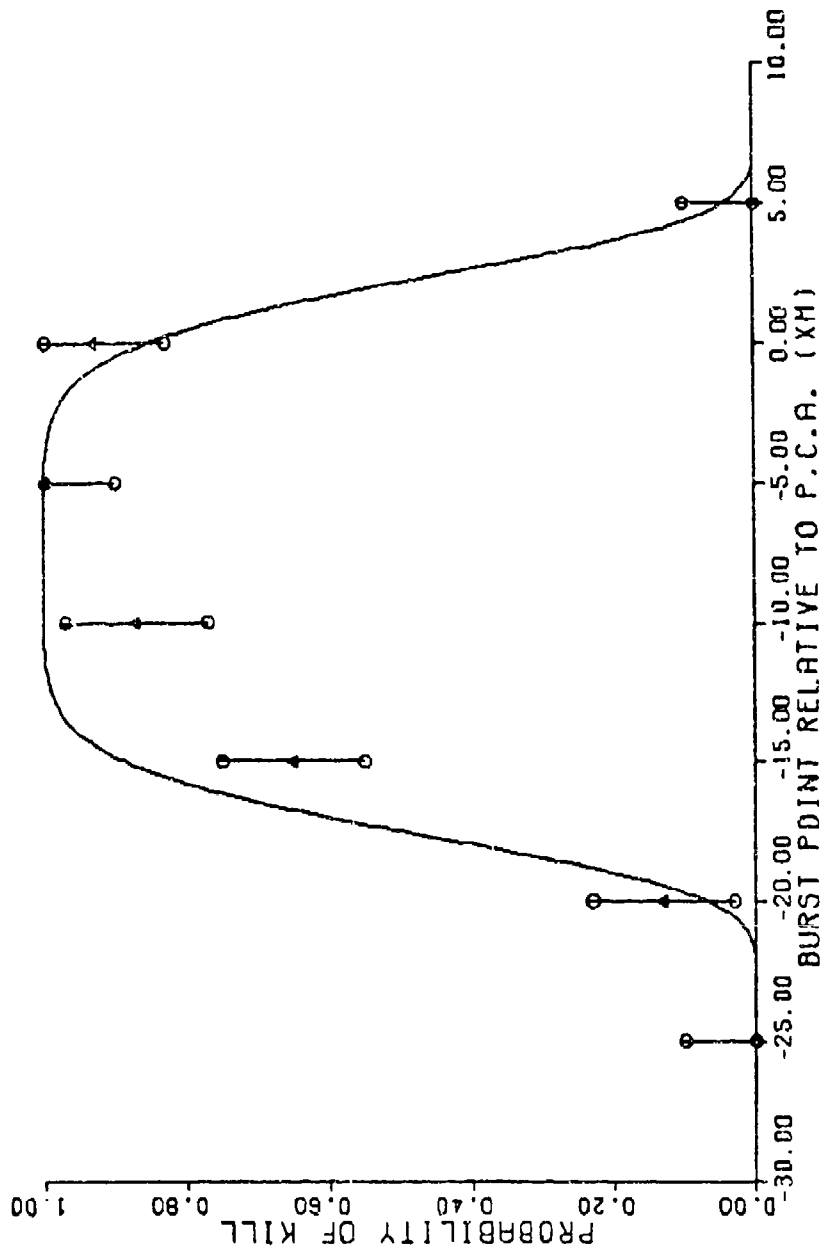


FIG F-22 : PSI=135. THETA=45. VR=1000. RM=15.0 BETA=15.

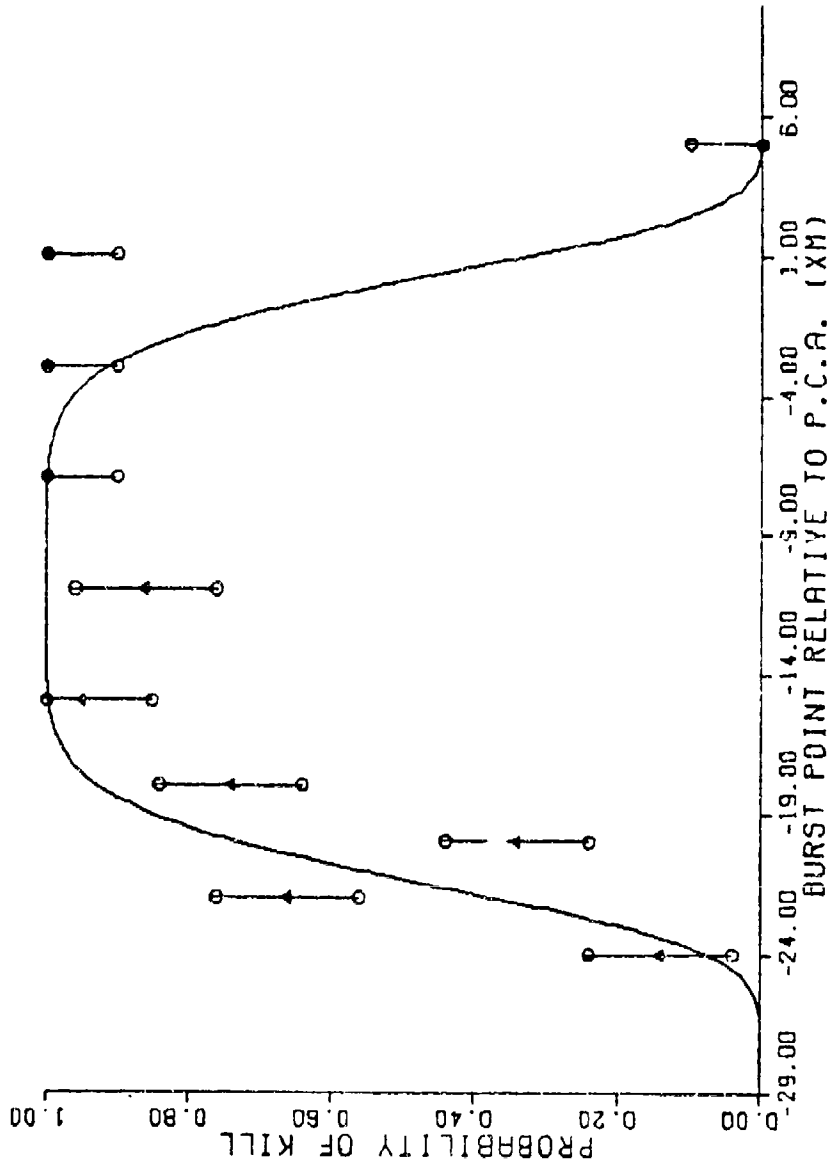


FIG F-23 : PSI=135. THETA=45. VR=2000. RM=15.0 BETA=15.

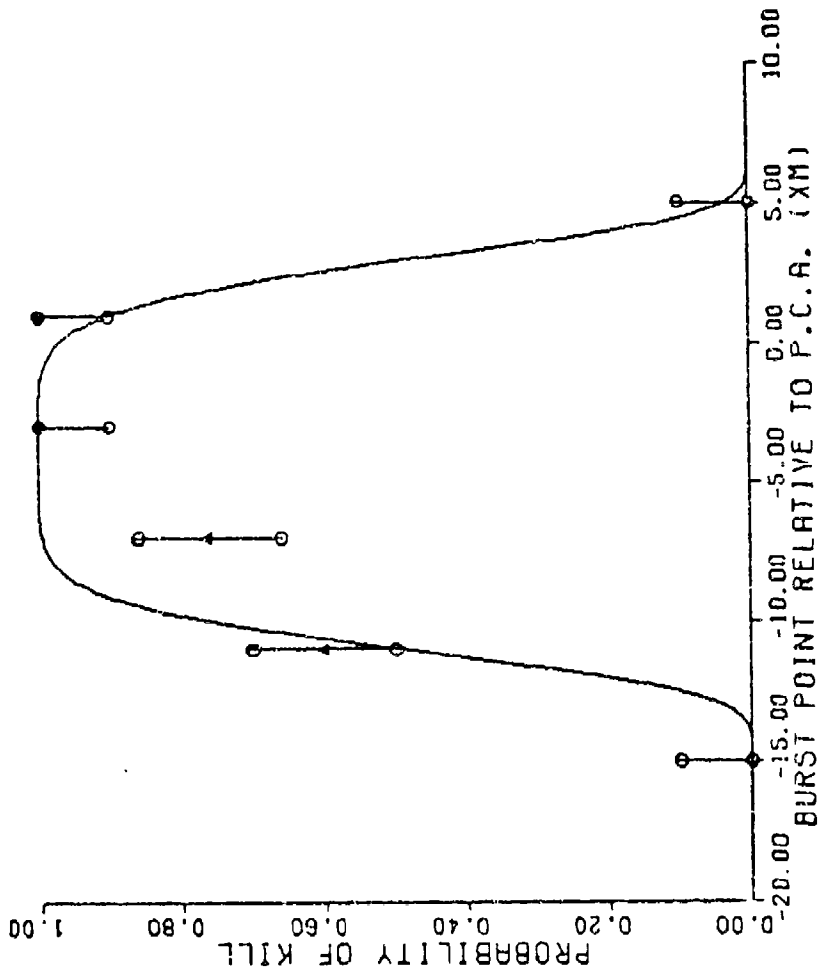


FIG F-24 : PSI=135. THETA=135. VR=2000. RM=15.0 BETA=15.

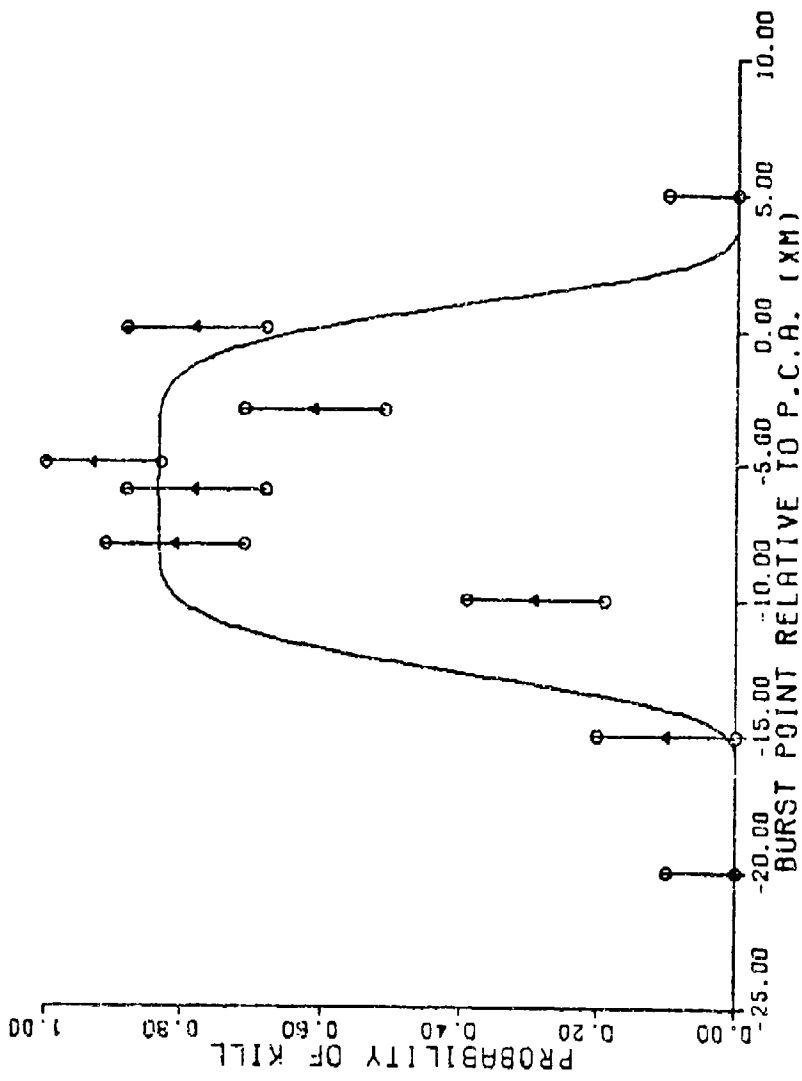


FIG F-25 : PSI=135. THETA=135. VR=2000. RM=27.5 BETA=15.

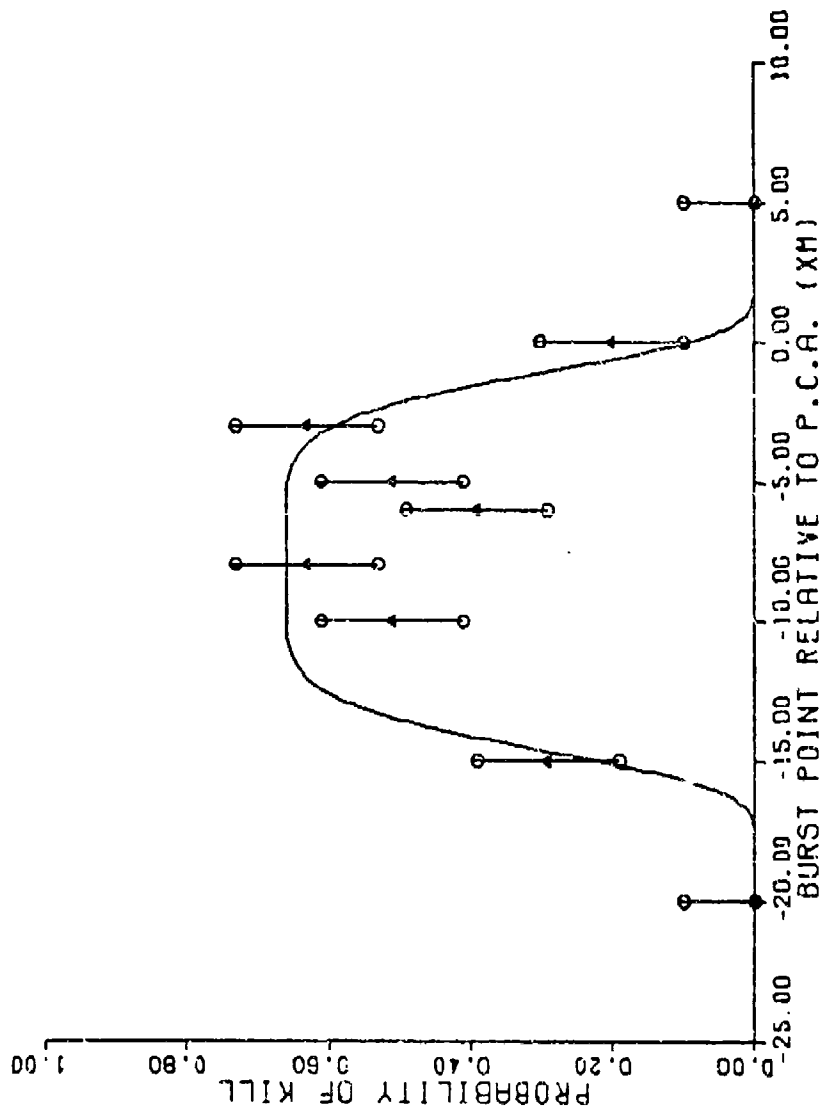


FIG F-26: PSI=135. THETA=135. VR=2000. RM=40.0 BETA=15.

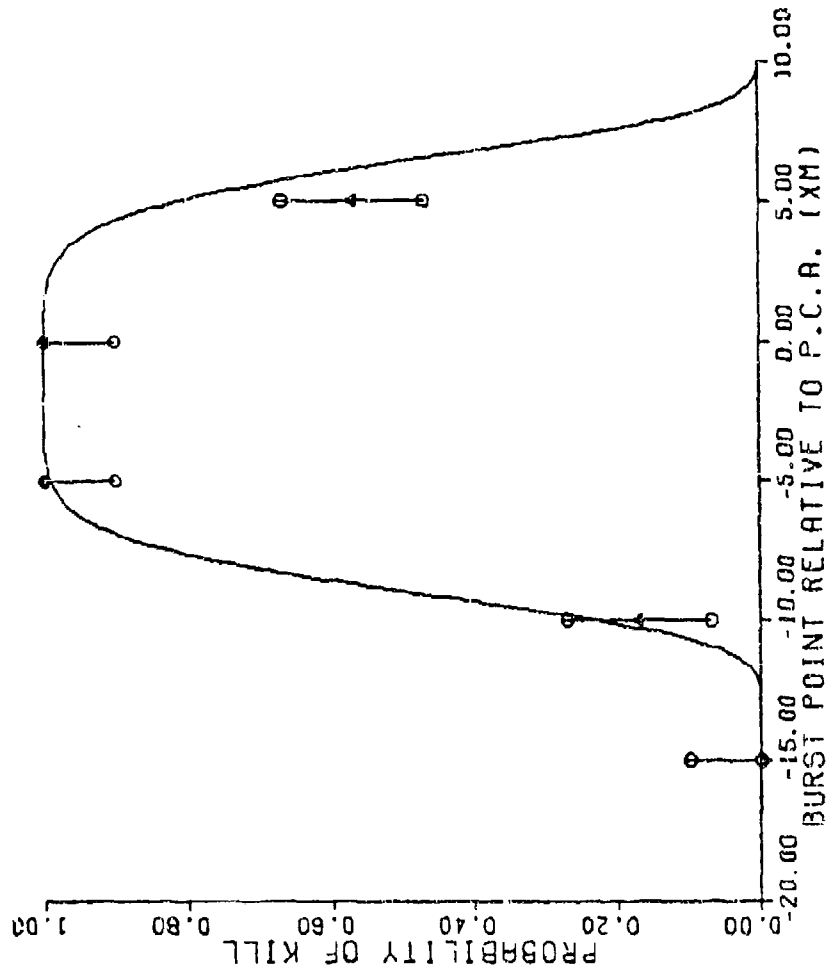


FIG F-27: PSI=135. THETA=225. VR=1000. RM=15.0 BETA=15.

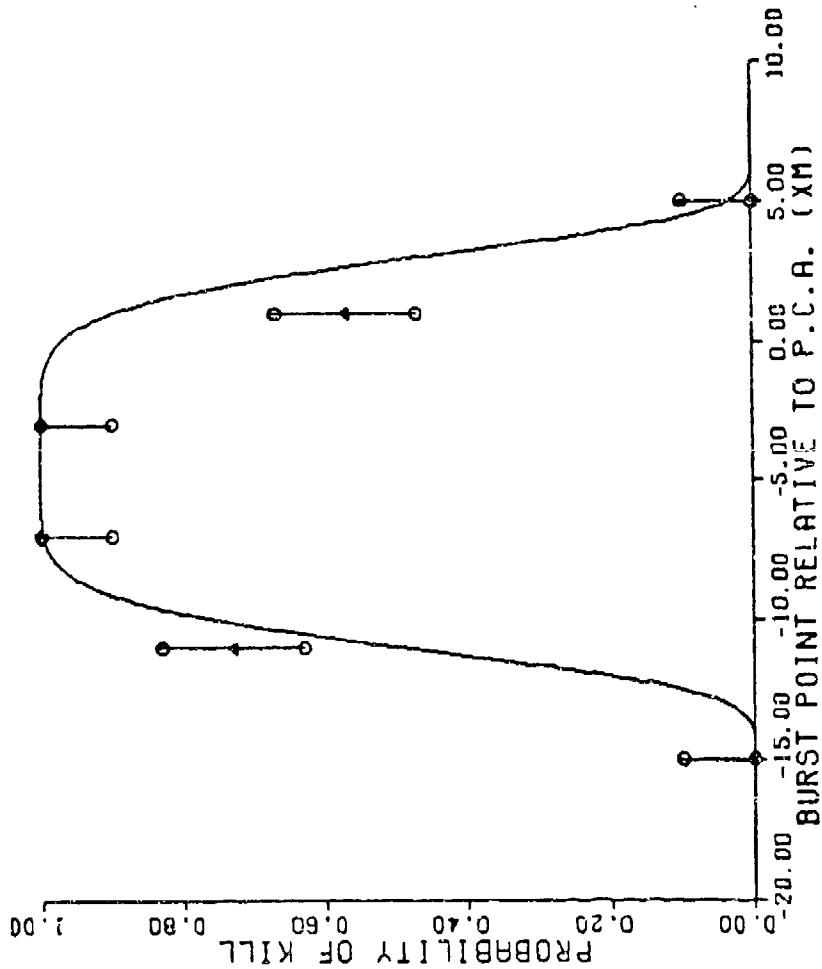


FIG. F-28: PSI=135. THETA=225. VR=2000. RM=15.0 BETA=15.

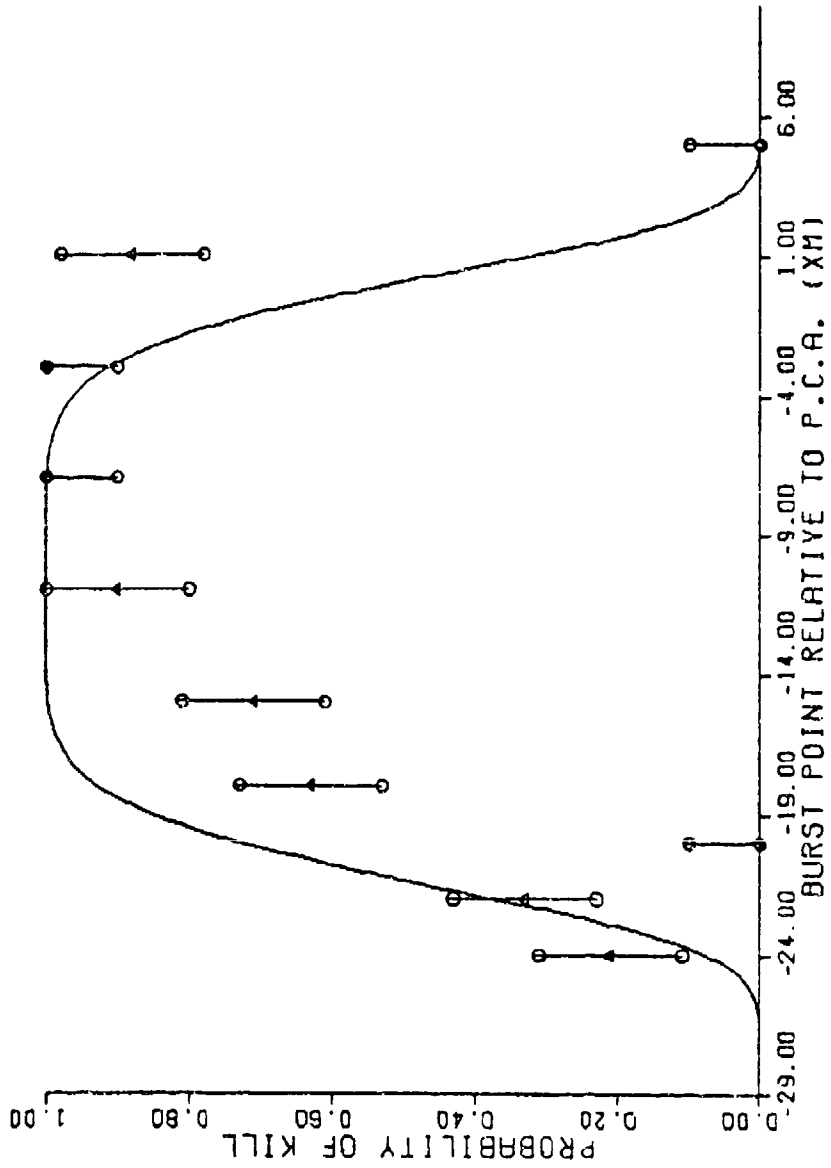


FIG F-20: PSI=135. THETA=315. VR=2000. RM=15.0 BETA=15.

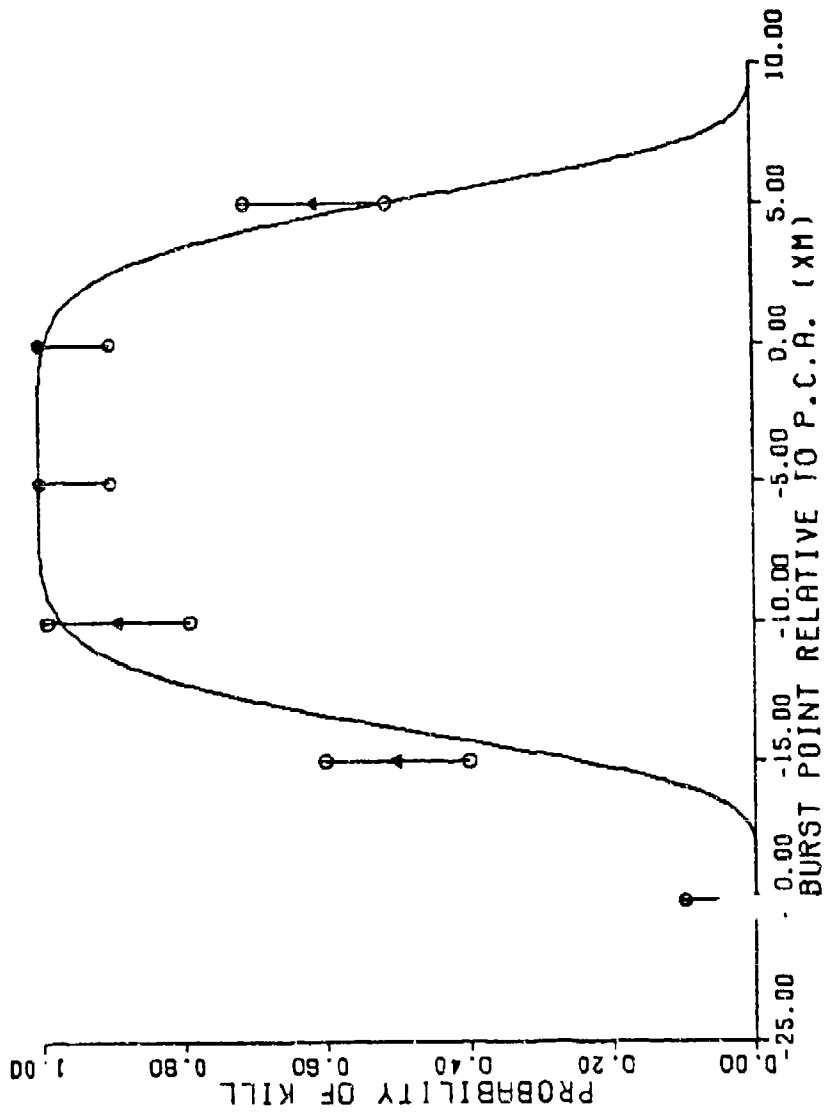


FIG F-30: PSI=180. THETA=135. VR=1000. RM=15.0 BETA=0.

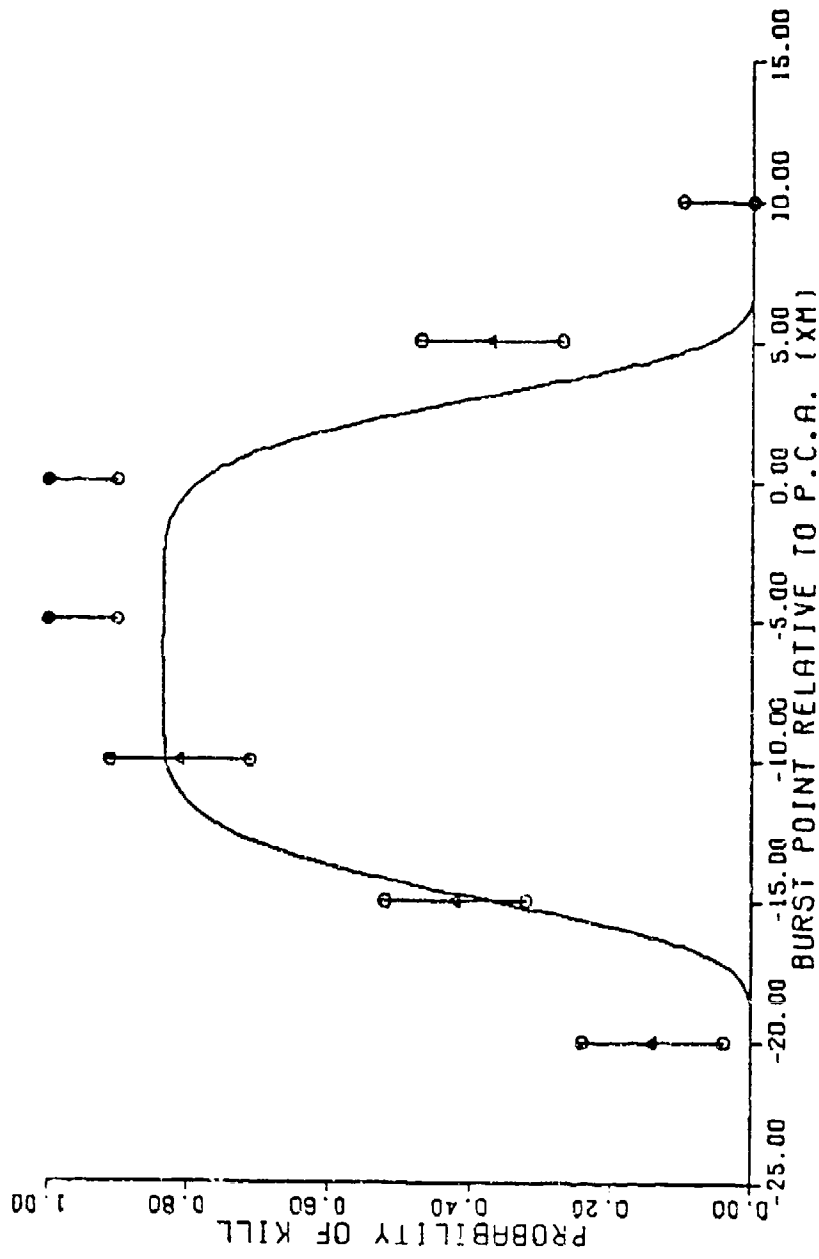


FIG F-31: PSI=180. THETA=135. VR=1000. RM=27.5 BETA=0.

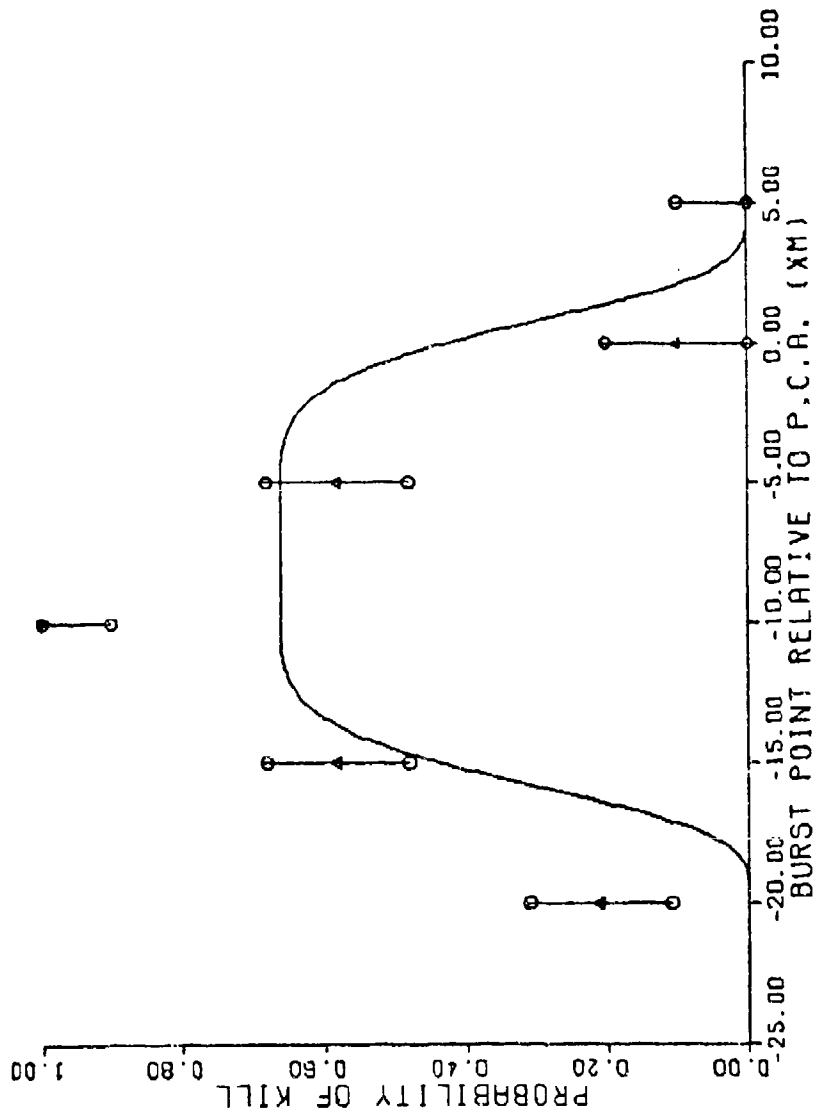


FIG F-32: PSI=180. THETA=135. VR=1000. RM=40.0 BETA=0.

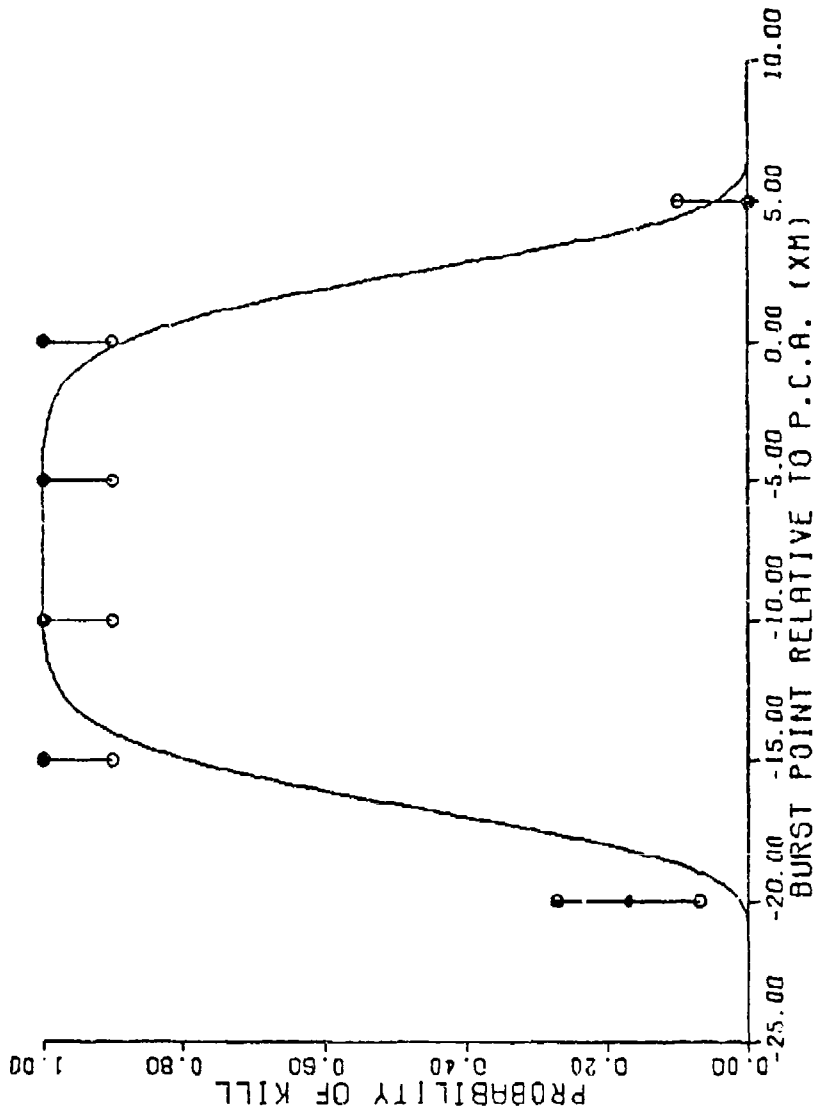


FIG F-33: PSI=180. THETA=135. VR=2000. RM=15.0 BETA=0.

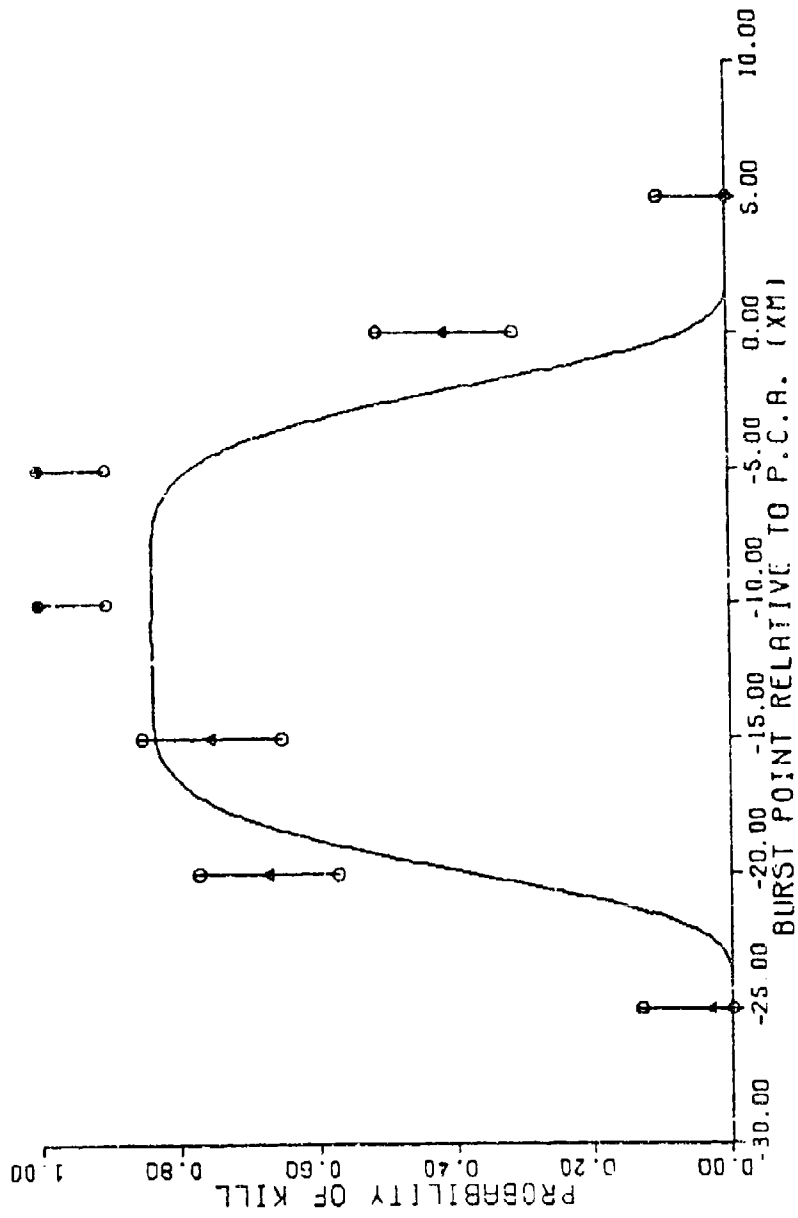


FIG F-34 : PSI=180. THETA=135. VR=2000. RM=27.5 BETA=0.

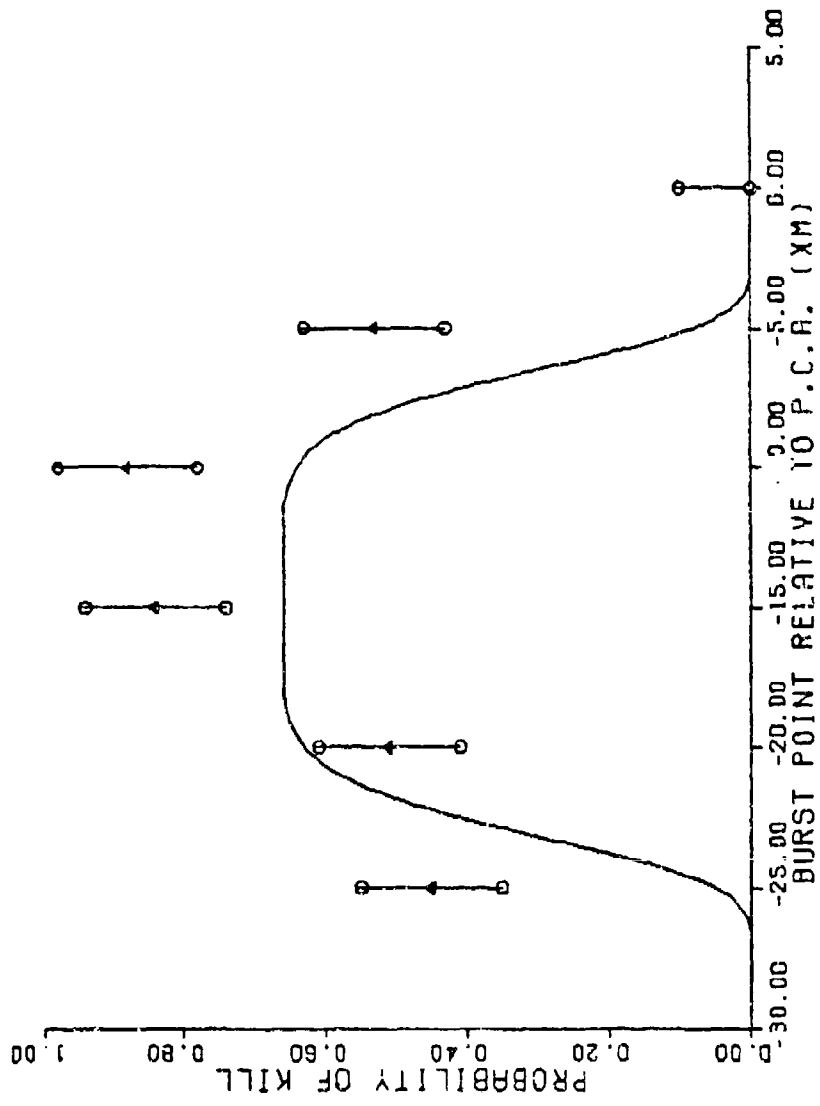


FIG F-35: PSI=180. THETA=135. VR=2000. RM=40.0 BETA=0.

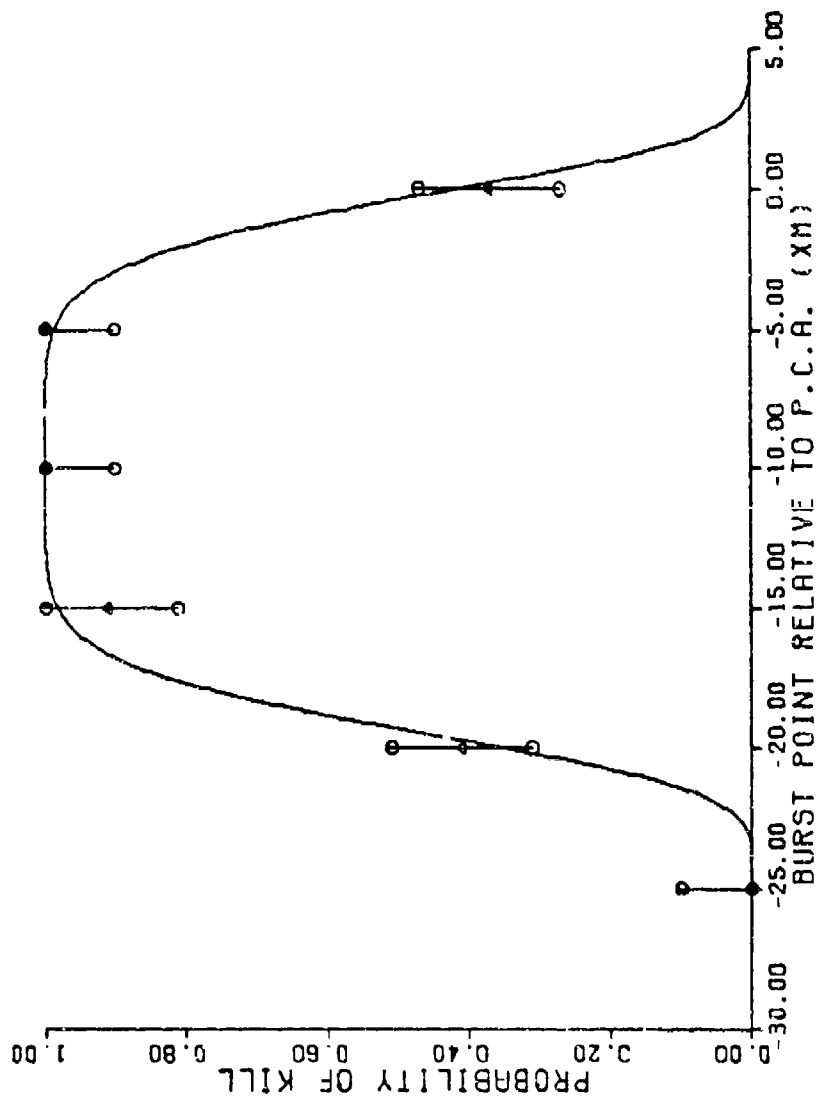


FIG F-36: PSI=180. THETA=135. VR=3000. RM=15.0 BETA=0.

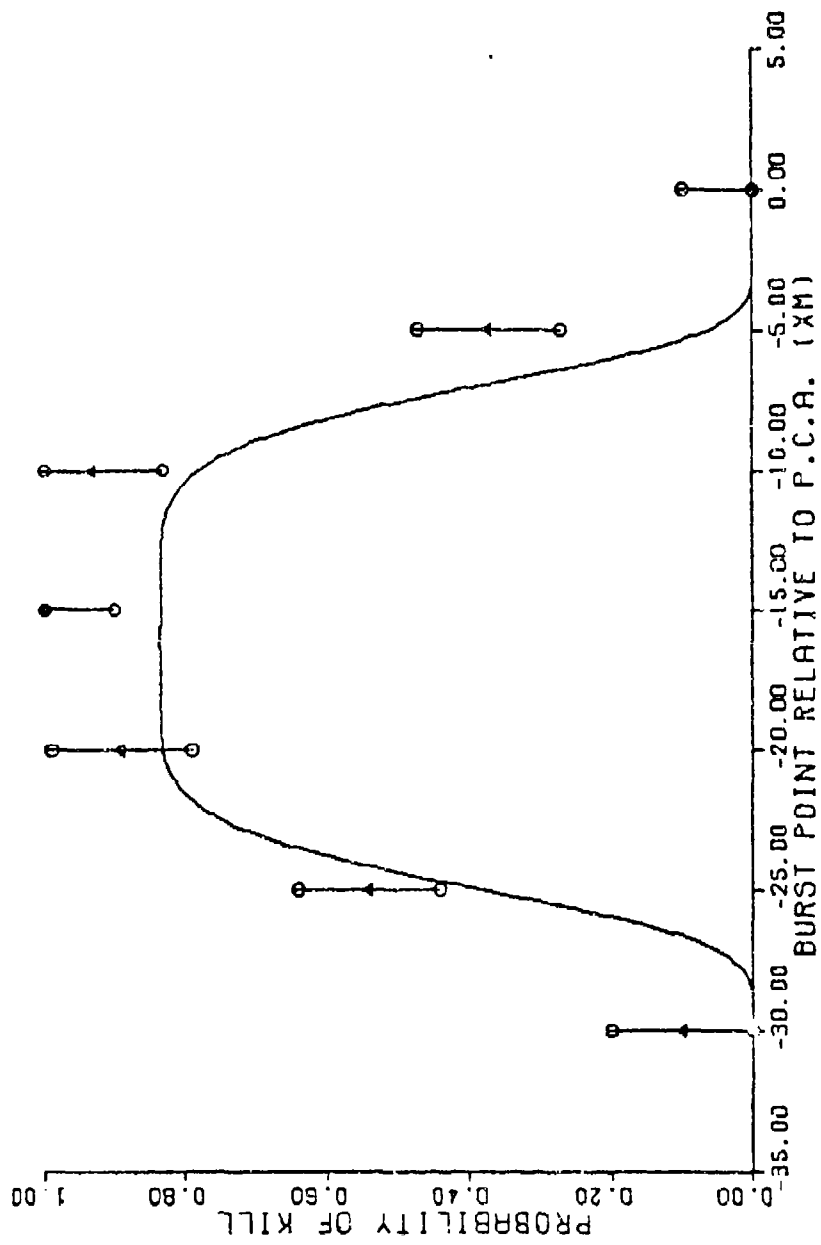


FIG F-37: PSI=180. THETA=135. VR=3000. RM=27.5 BETA=0.

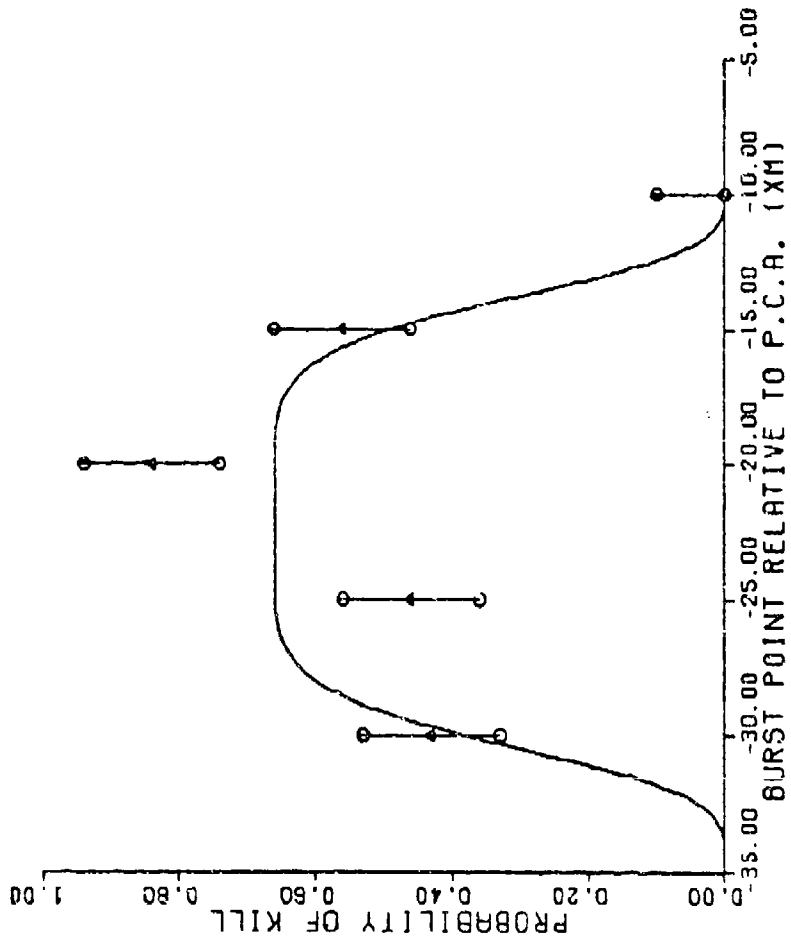


FIG F-38: PSI=180. THETA=135. VR=3000. RM=40.0 BETA=0.

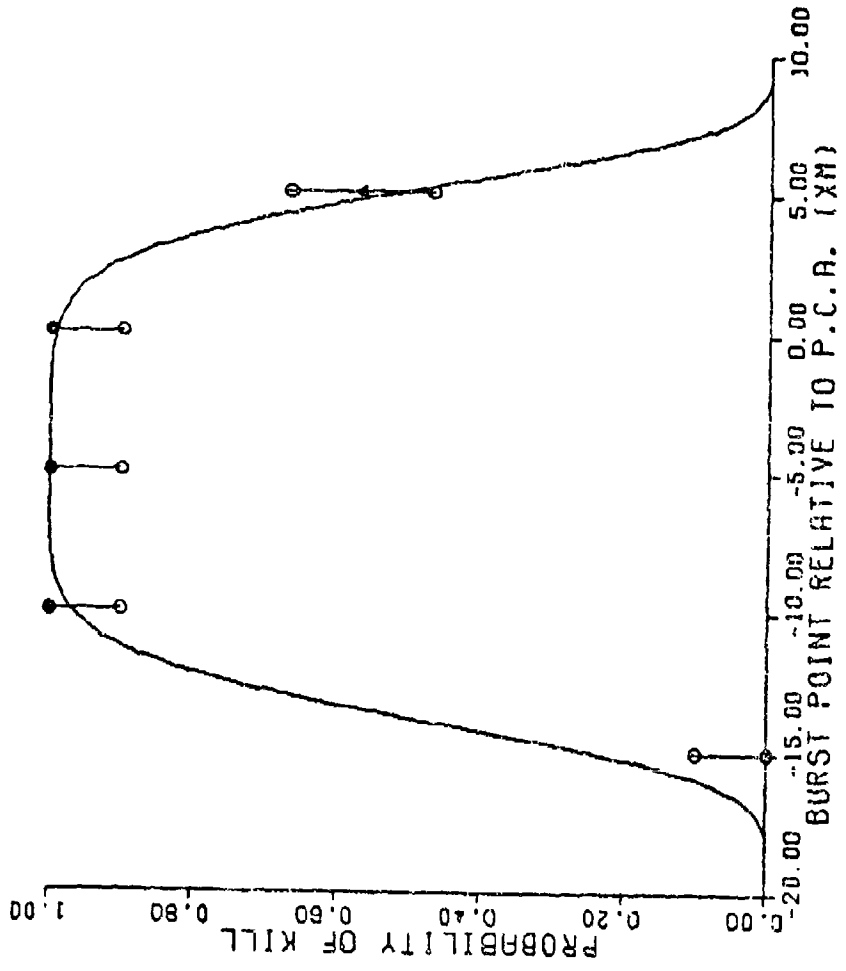


FIG F-39 : PSI=180. THETA=225. VR=1000. RM=15.0 BETA=0.

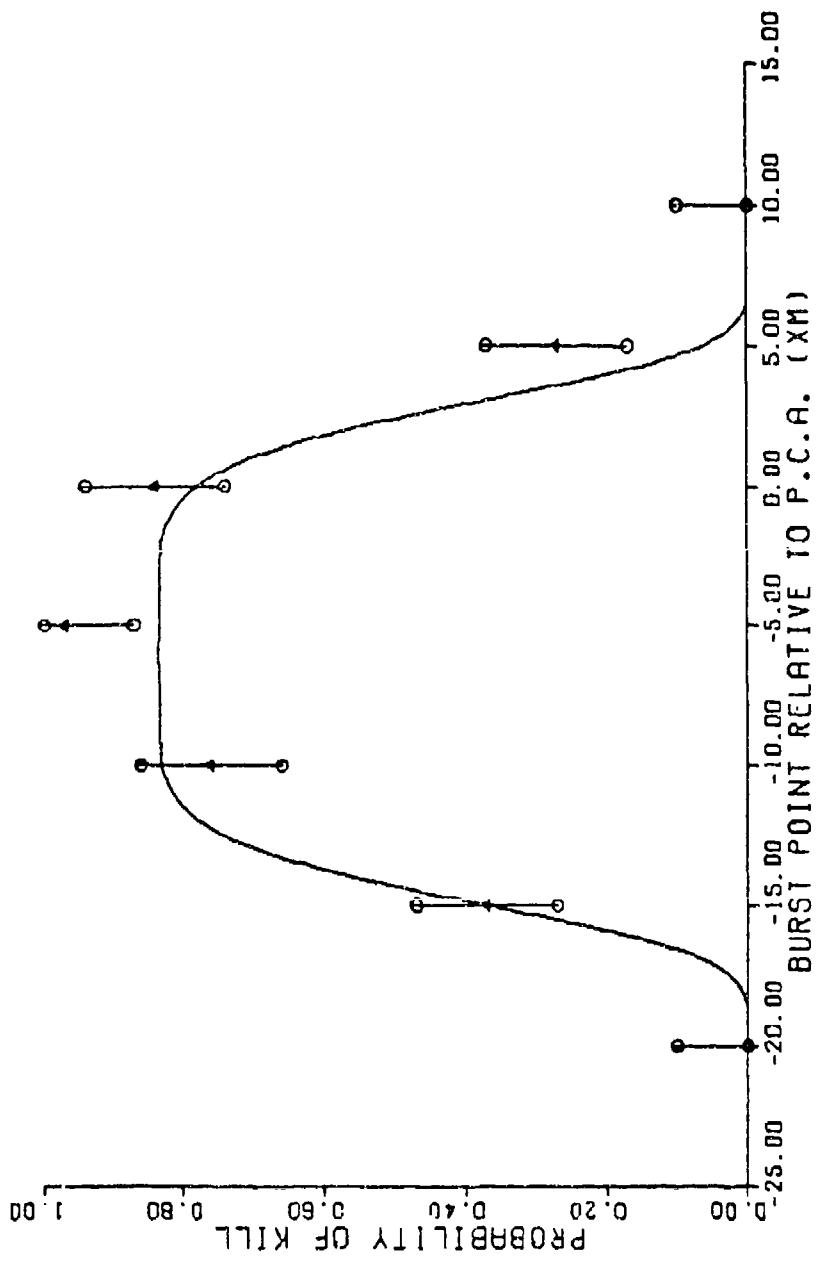


FIG F-40: PSI=180. THETA=225. VR=1000. RM=27.5 BETA=0.

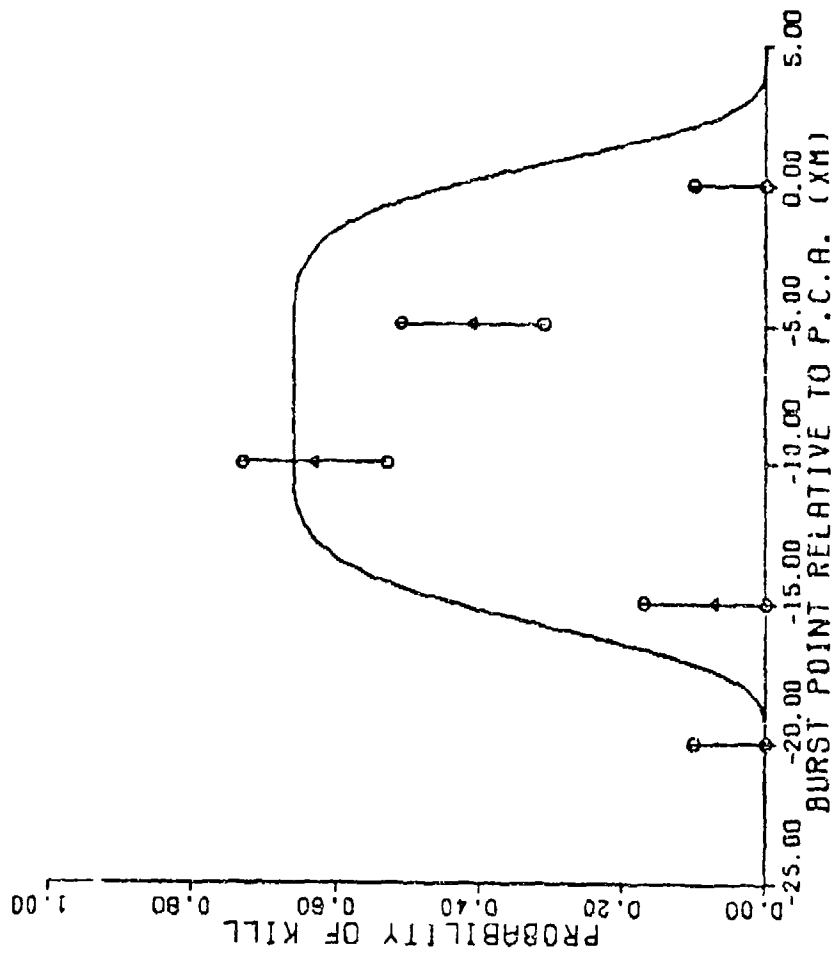


FIG F-41: PSI=180. THETA=225. VR=1000. RM=40.0 BETA=0.

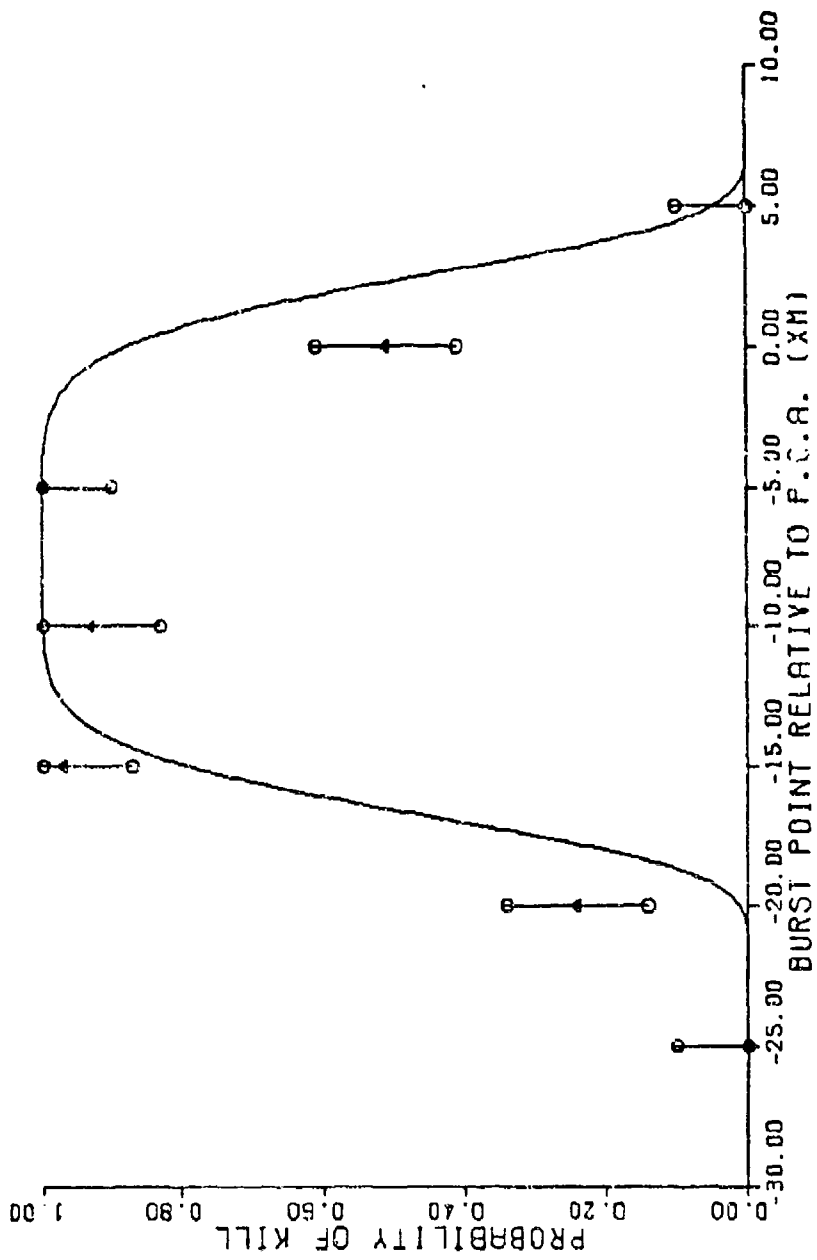


FIG F-42: PSI=180. THETA=225. VR=2000. RM=15.0 BETA=0.

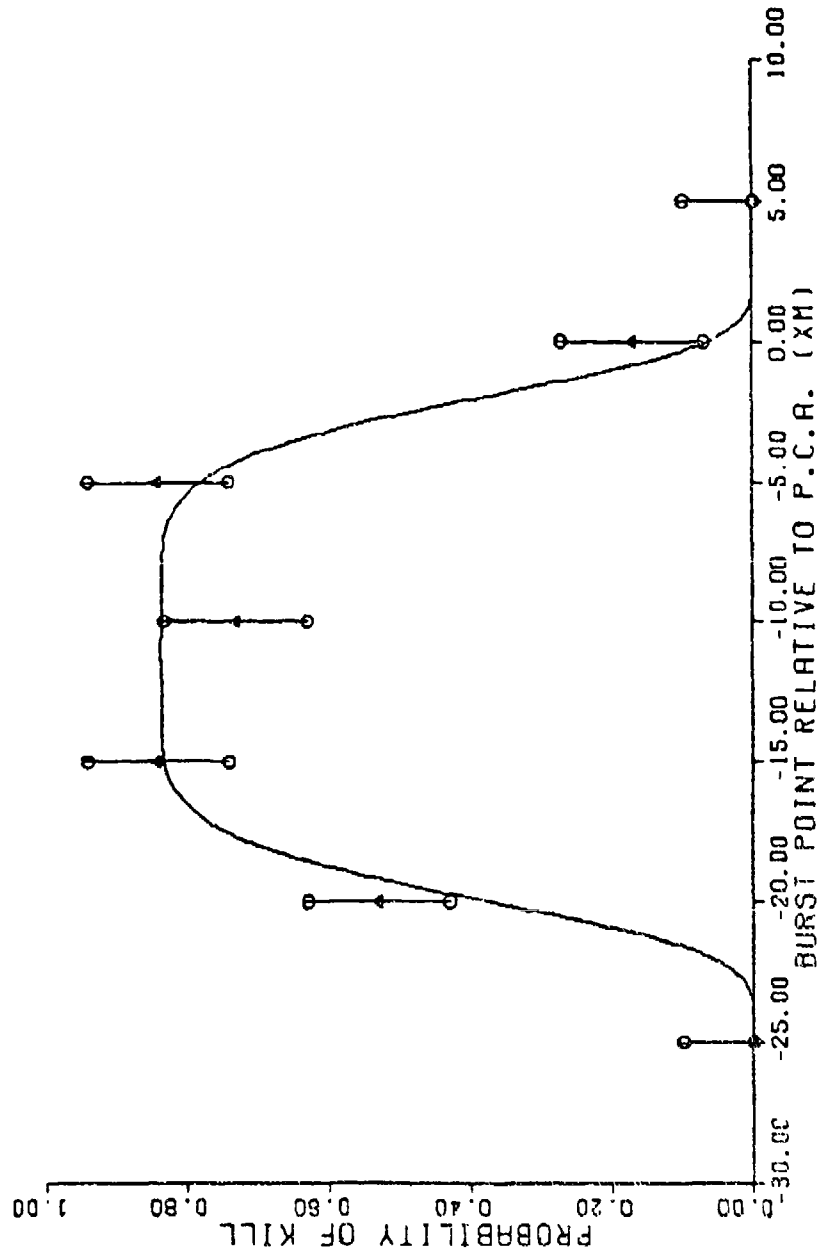


FIG F-43: PSI=180. THETA=225. VR=2000. RM=27.5 BETA=0.

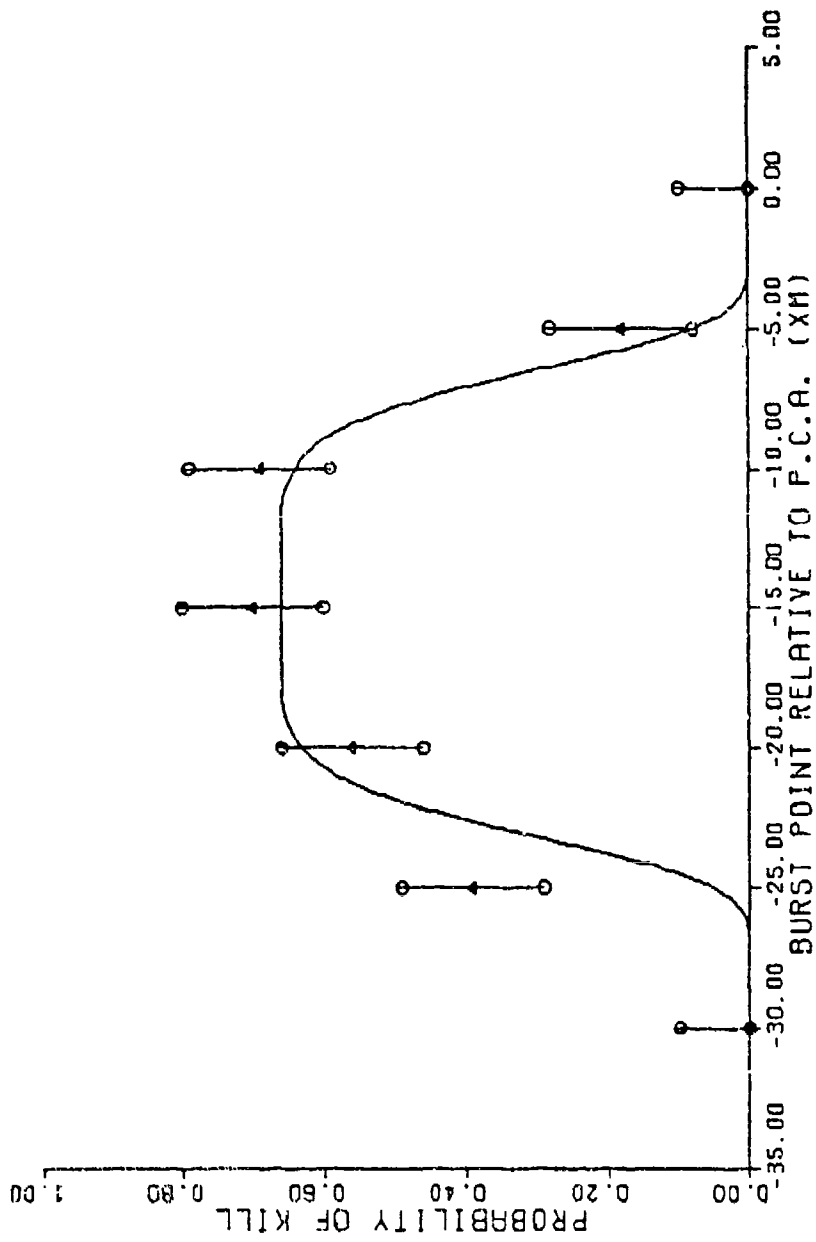


FIG F-44 : PSI=180. THETA=225. VR=2000. RM=40.0 BETA=0.

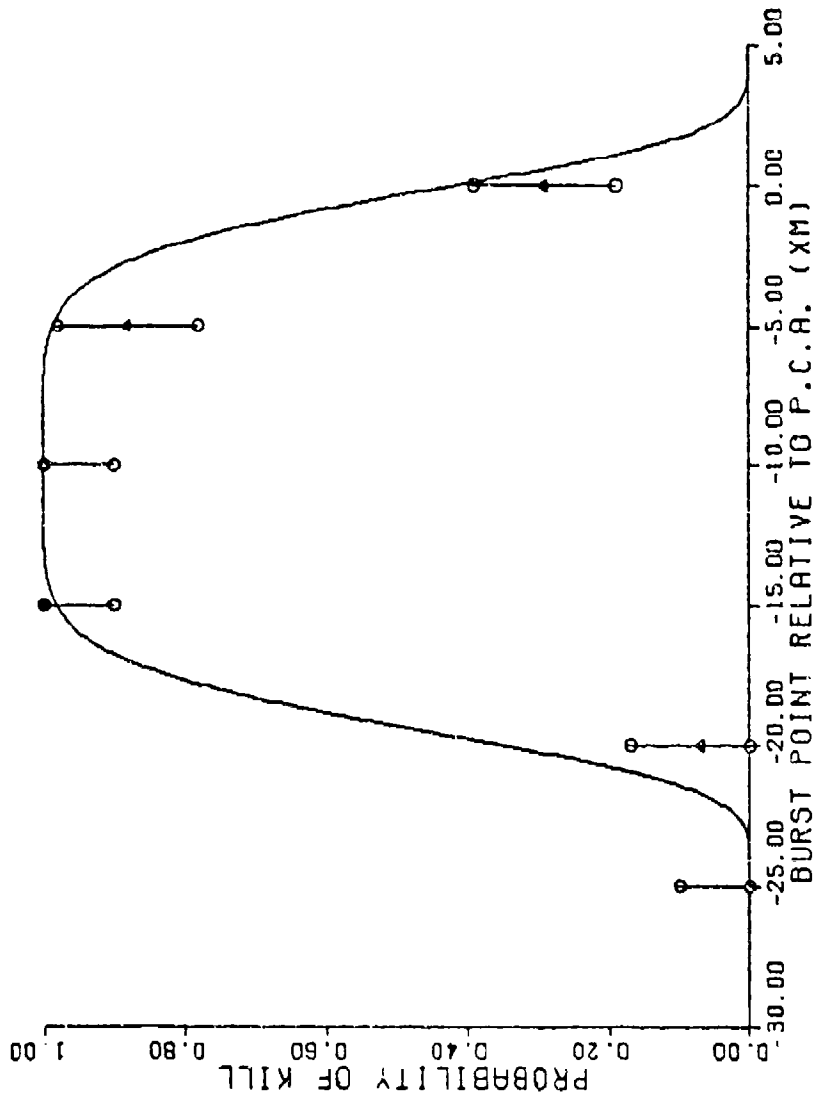


FIG F-45 : PSI=180. THETA=225. VR=3000. RM=15.0 BETA=0.

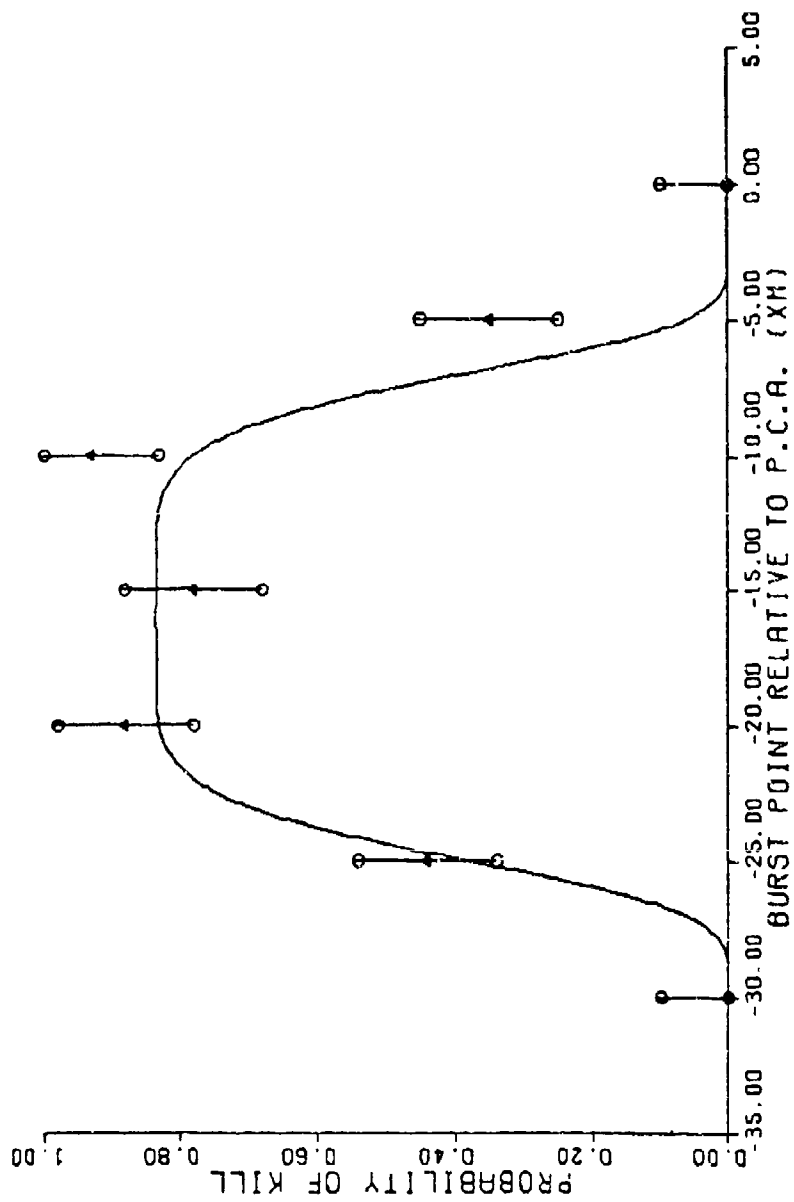


FIG F-46: PSI=180. THETA=225. VR=3000. RM=27.5 BETA=0.

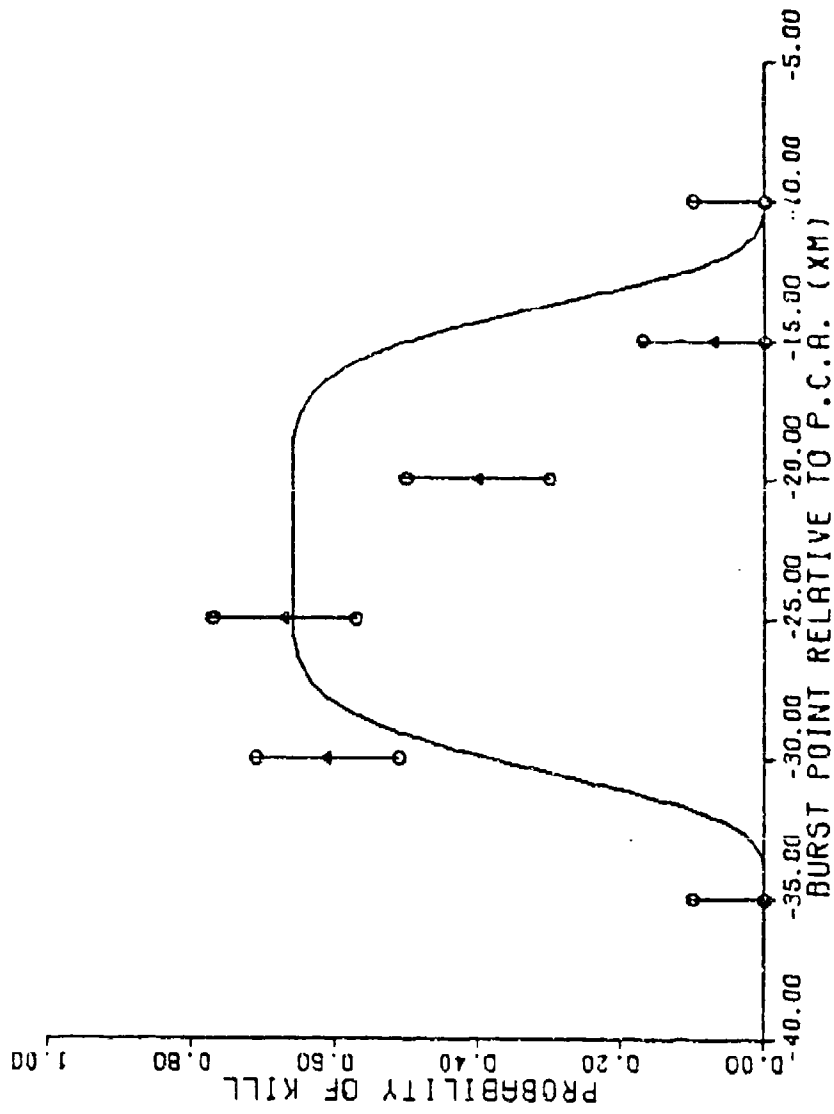


FIG F-47 : PSI=180. THETA=225. VR=3000. RM=40.0 BETA=0.

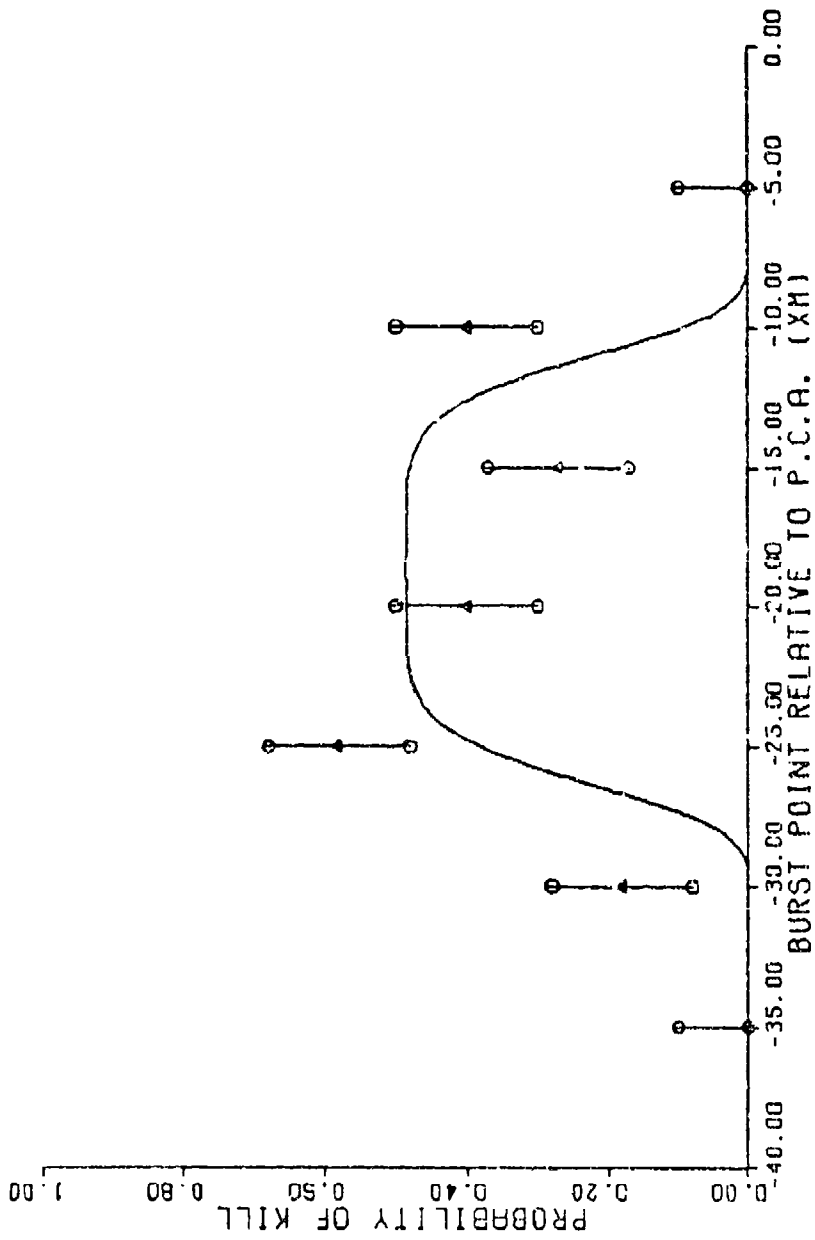


FIG F-49 : PSI=180. THETA=225. VR=2000. RM=52.5 BETA=0.

APPENDIX G

"109 Cell Model" of the Circular

Normal Distribution

The "109 Cell Model of the Circular Normal Distribution consists of a series of rings which are sub-divided into cells as depicted in Figure G-1. The probability of occurrence of each cell in the first seven rings is .01. The cells in the outer ring each have a .0025 probability of occurrence. The point in the center of each cell is the probabilistic "center" of that cell--i.e. the probability, within that cell, of being either closer or farther from the origin is the same and there is also an equal probability of being clockwise or counter-clockwise of this point. The radius of each ring in terms of σ is given below.

Ring	# of Cells in Ring	Total Inside Ring	Ring Radius(σ)	Probabilistic Center Radius (σ)
1	1	1	.1418	0
2	7	8	.4083	.2949
3	13	21	.6867	.5556
4	18	39	.9943	.8433
5	21	60	1.3540	1.1715
6	21	81	1.8226	1.5700
7	16	97	2.648	2.1390
8	12	109	∞	2.9871

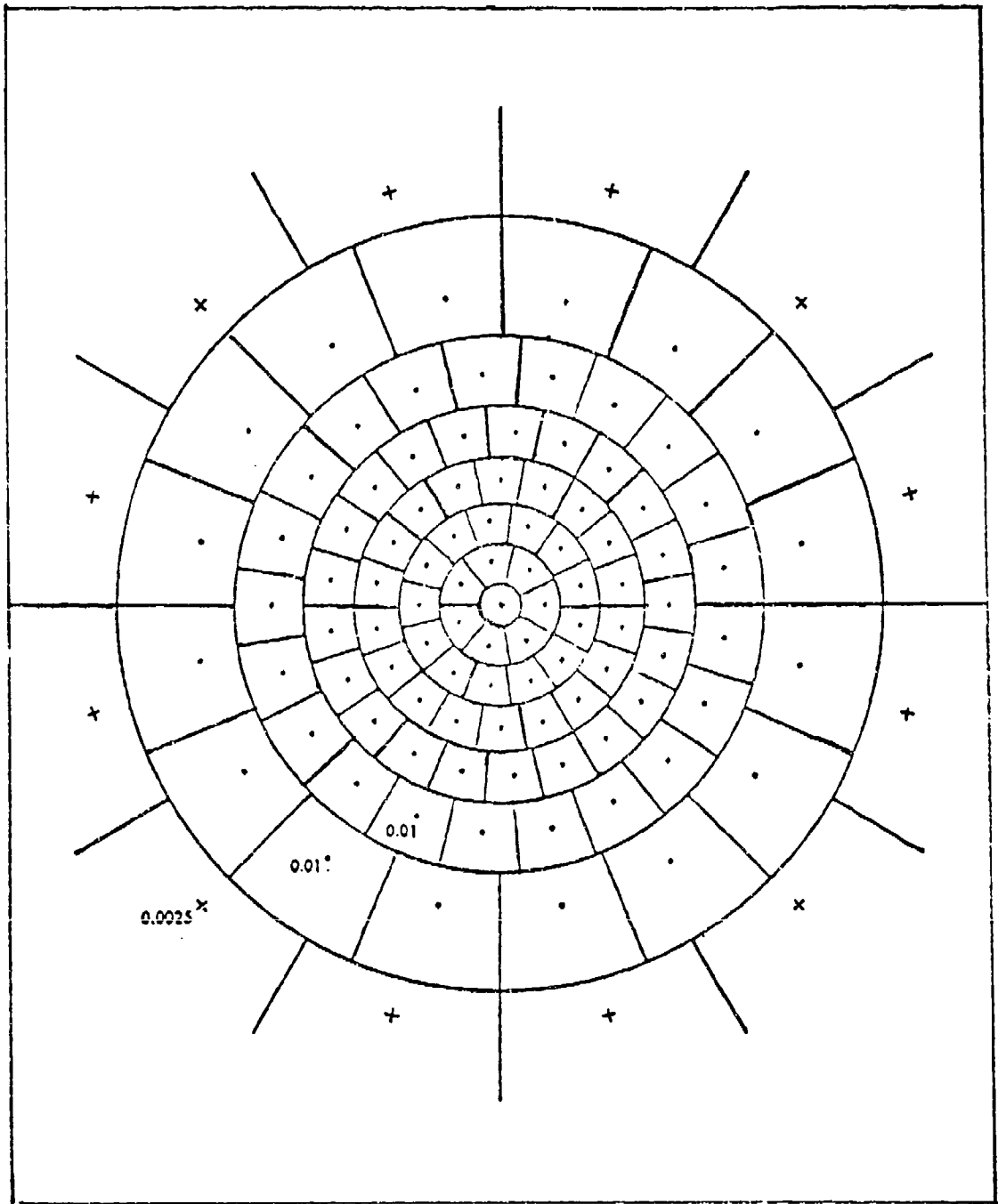


Fig G-1. The 109 Cell Model

APPENDIX H

The First Characterization With Random Miss Distance

The thirteen plots in this appendix are a comparison between data generated by SHAZAM (the points) and the corresponding data (the curves) produced by the first semi-empirical characterization described in Appendix F. For all of these plots, miss distance was treated as a random variable in both SHAZAM and the characterization. Values of ψ , V_R , β , and σ are given on each plot.

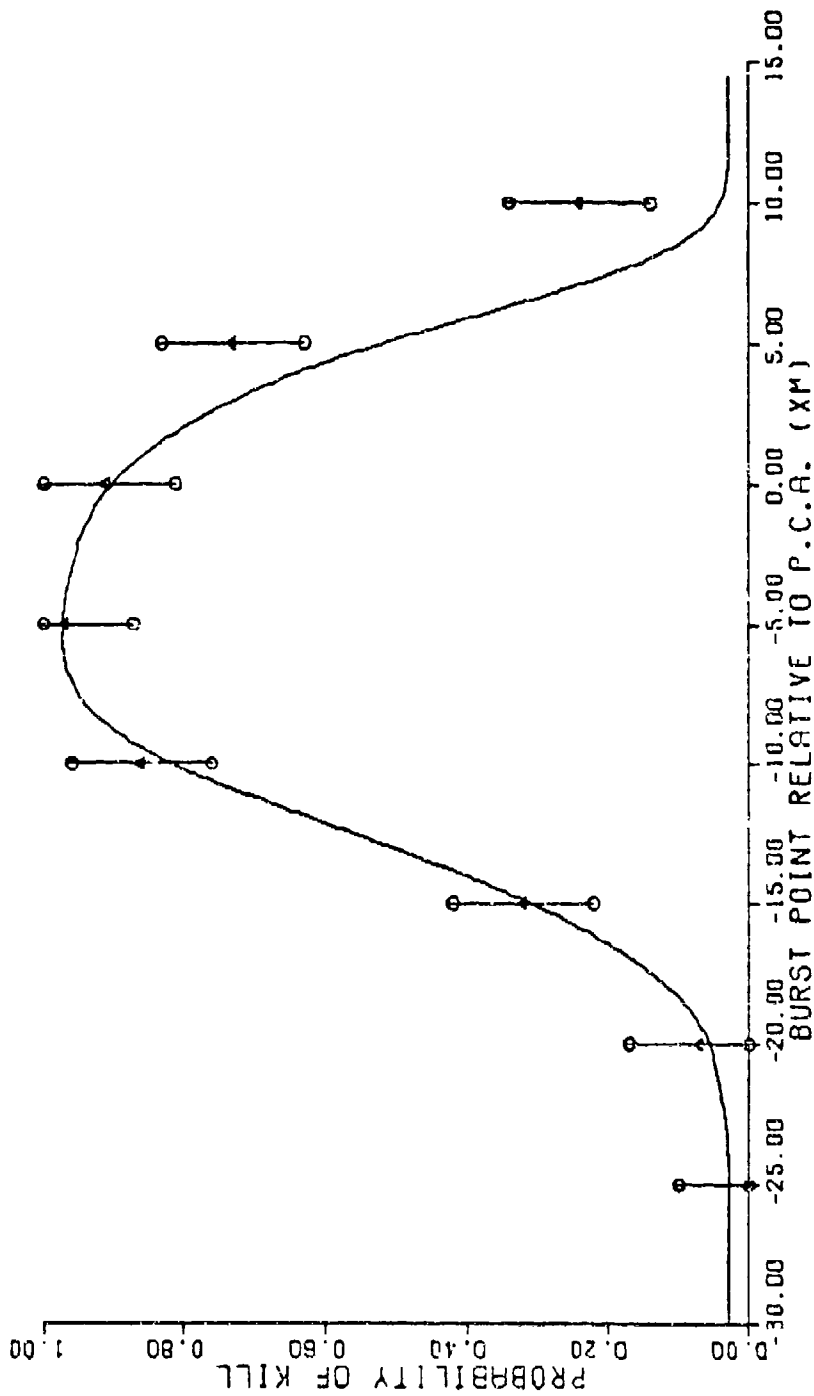


FIG H-1 : PSI=0. VR=2000. BETA=0. SIGMA=10.0

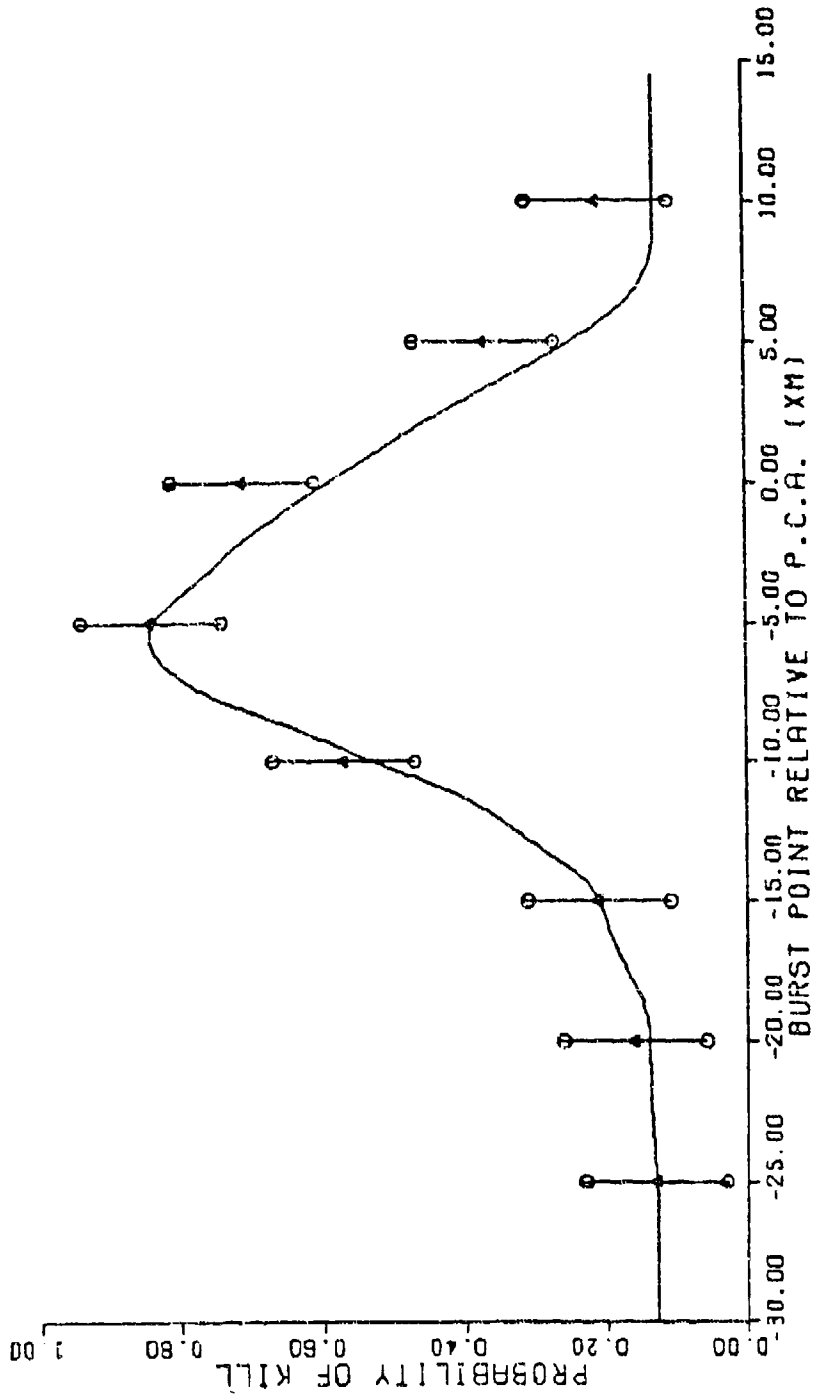


FIG H-2 : PSI=45. VR=2000. BETA=15. SIGMA=10.0

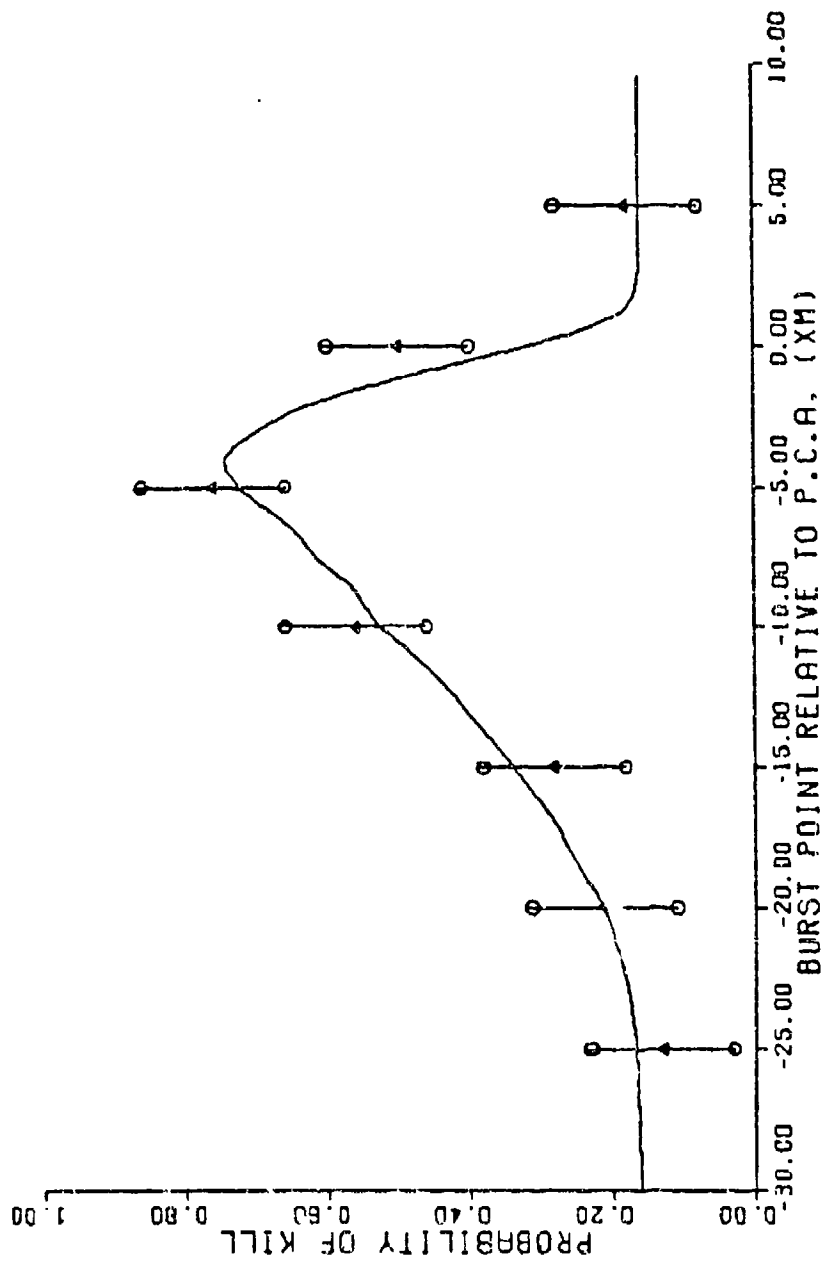


FIG H-3 : PSI=90. VR=2000. BETA=15. SIGMA=10.0

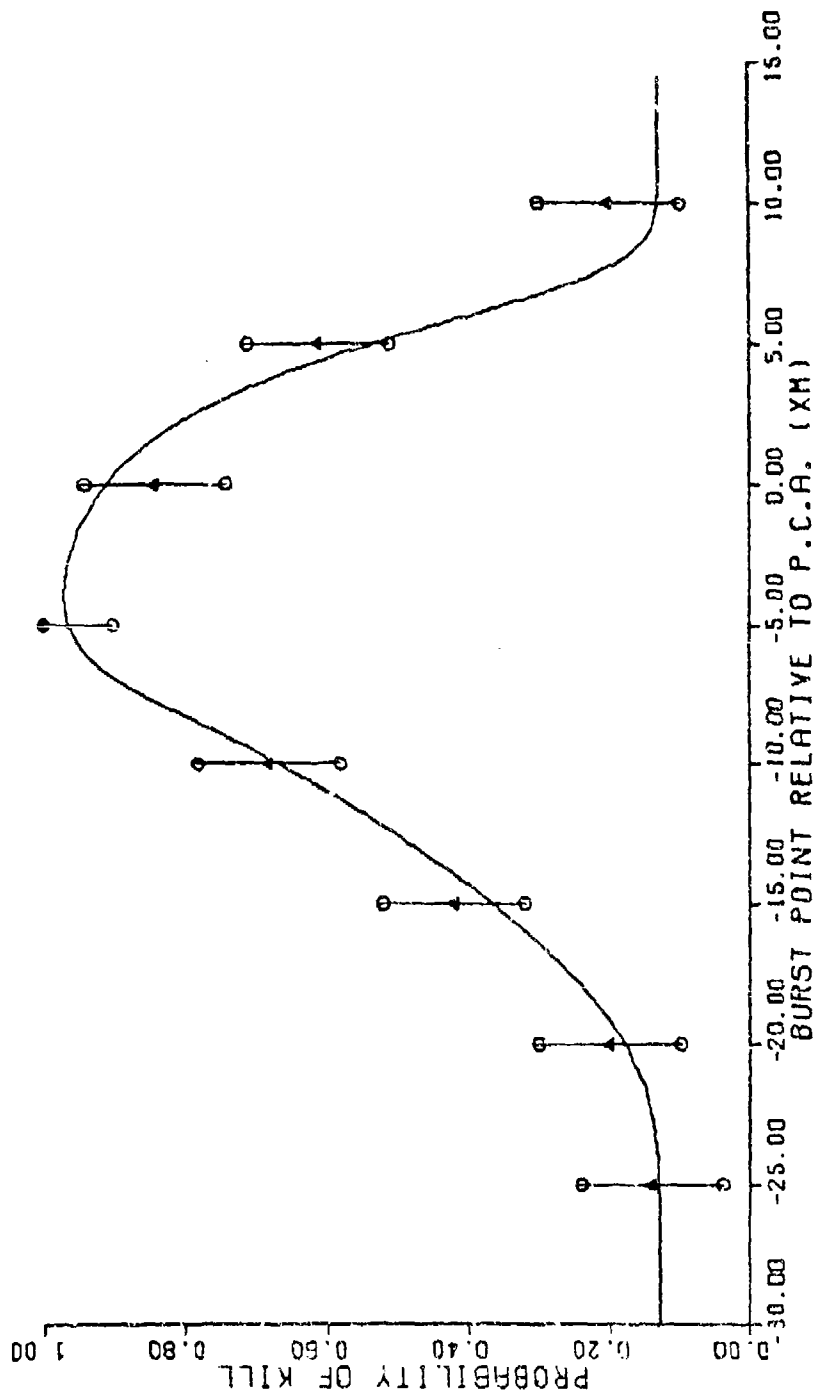


FIG H-4 : PSI=135. VR=1000. BETA=15. SIGMA=10.0

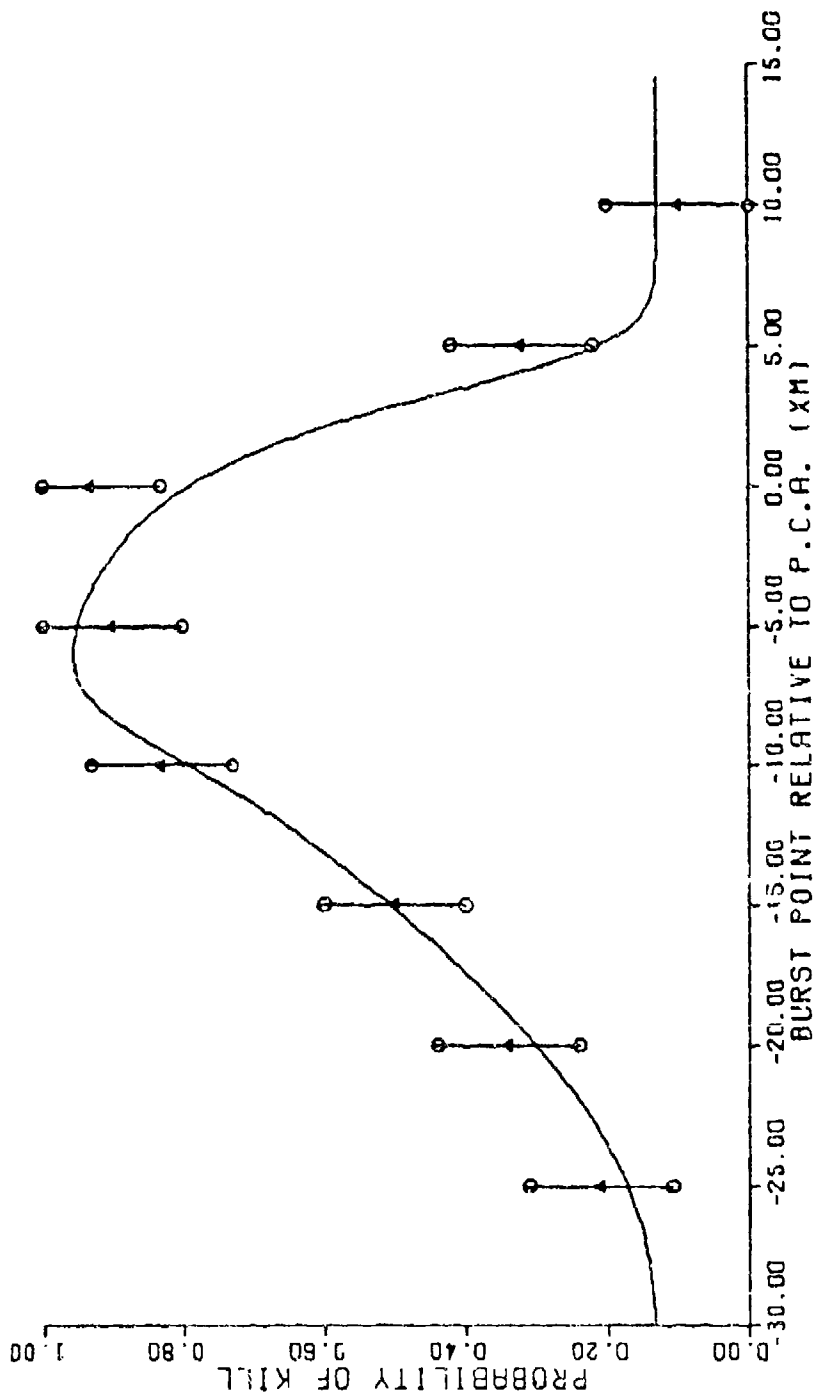


FIG H-5 : PSI=135. VR=2000. BETA=15. SIGMA=10.0

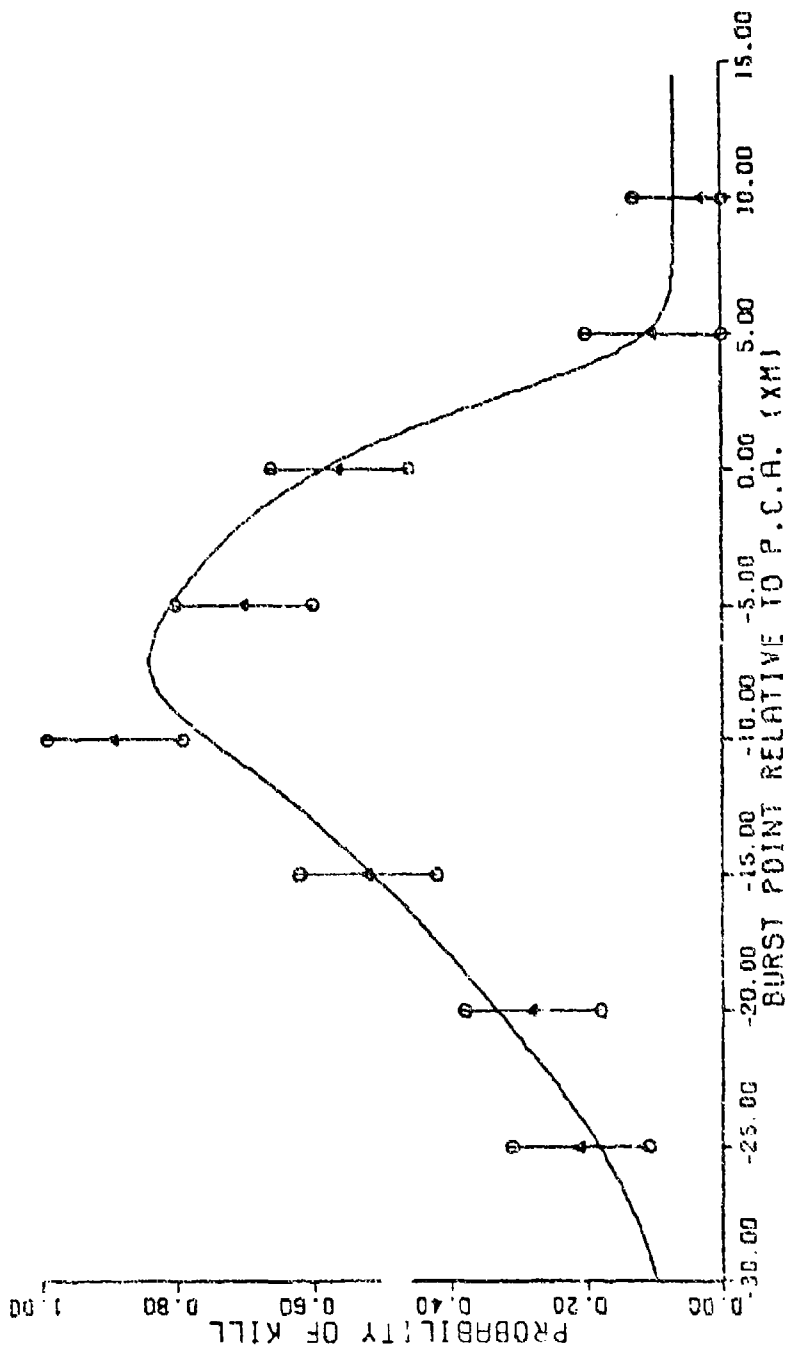


FIG H-6 : PSI=135. VR=2000. BETA=15. SIGMA=15.0

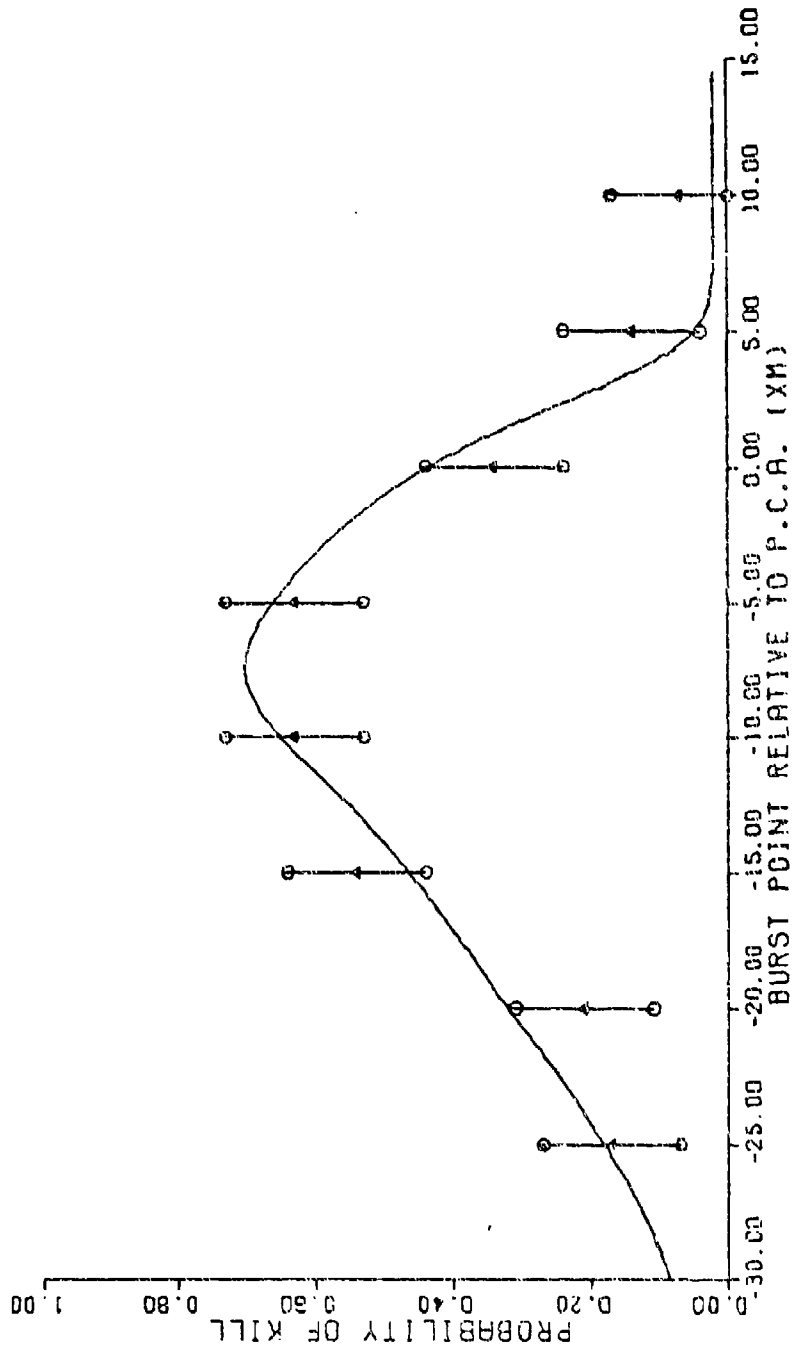


FIG H-7 : PSI=135. VR=2000. BETA=15. SIGMA=20.0

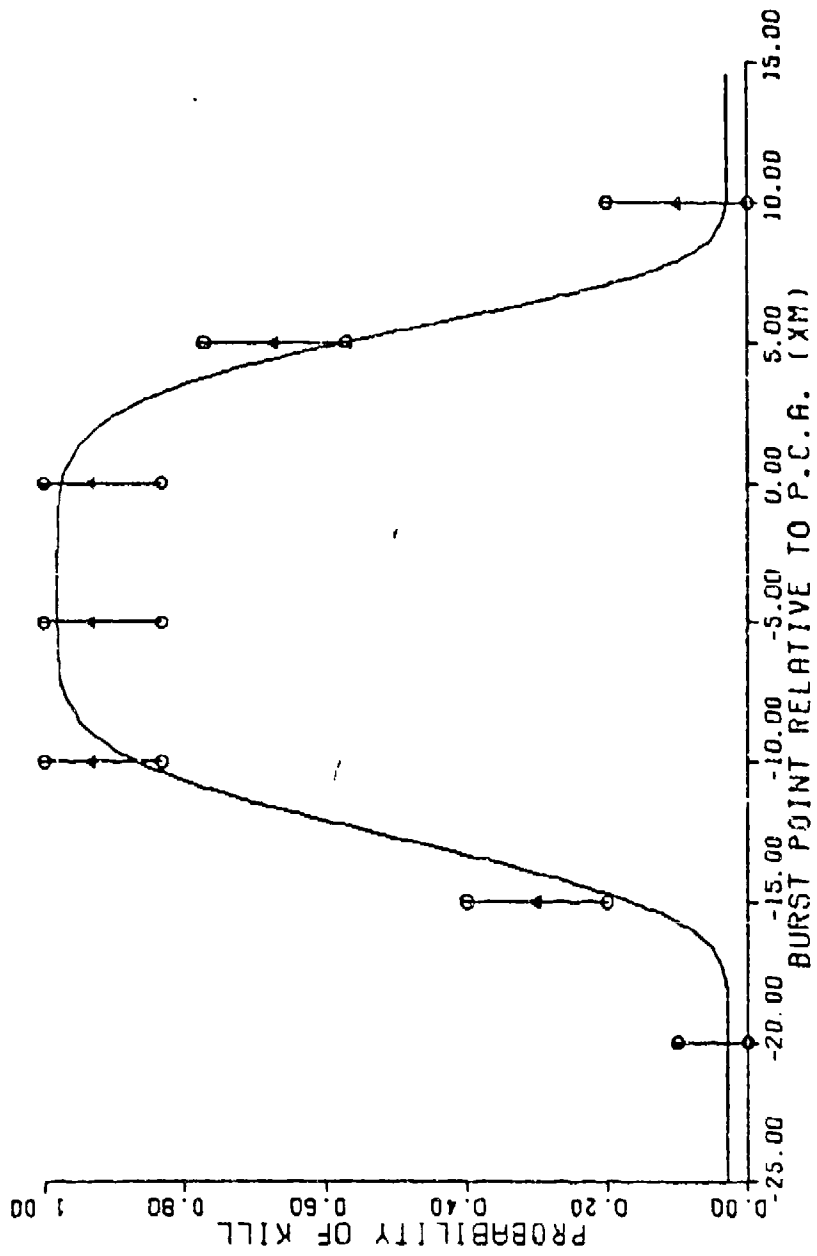


FIG H-8 : PSI=180. VR=1000. BETA=0. SIGMA=10.0

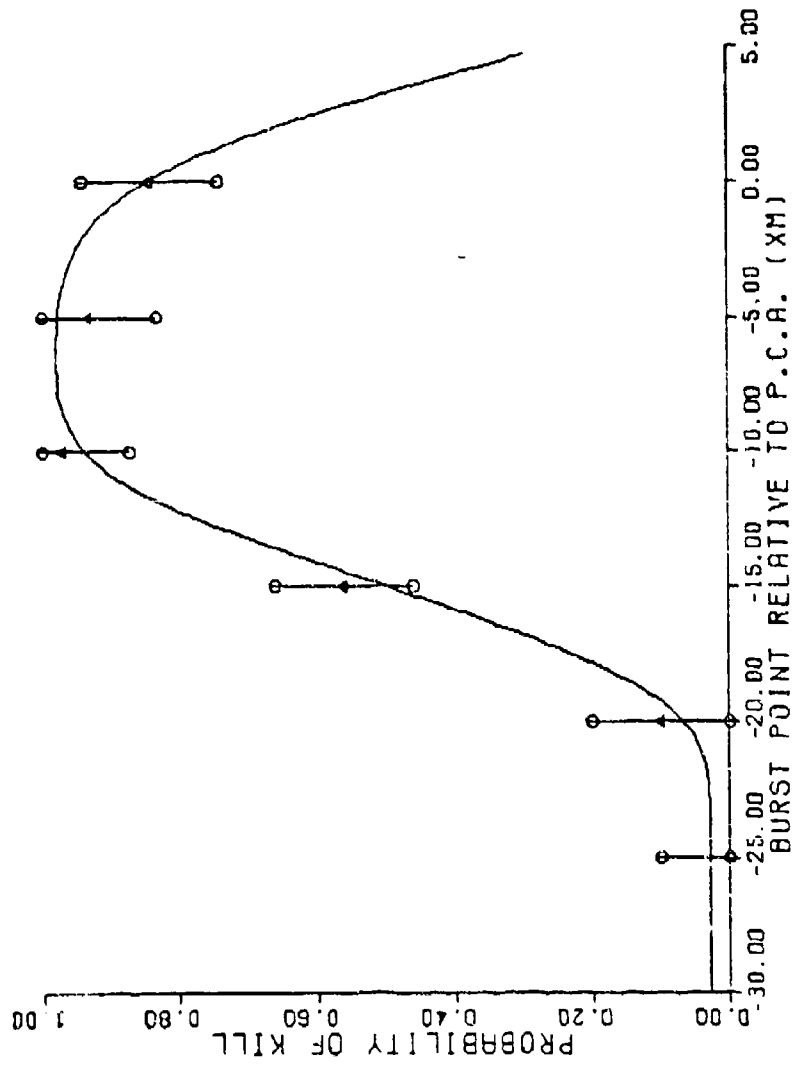


FIG H-9 : PSI=180. VR=2000. BETA=0. SIGMA=10.0

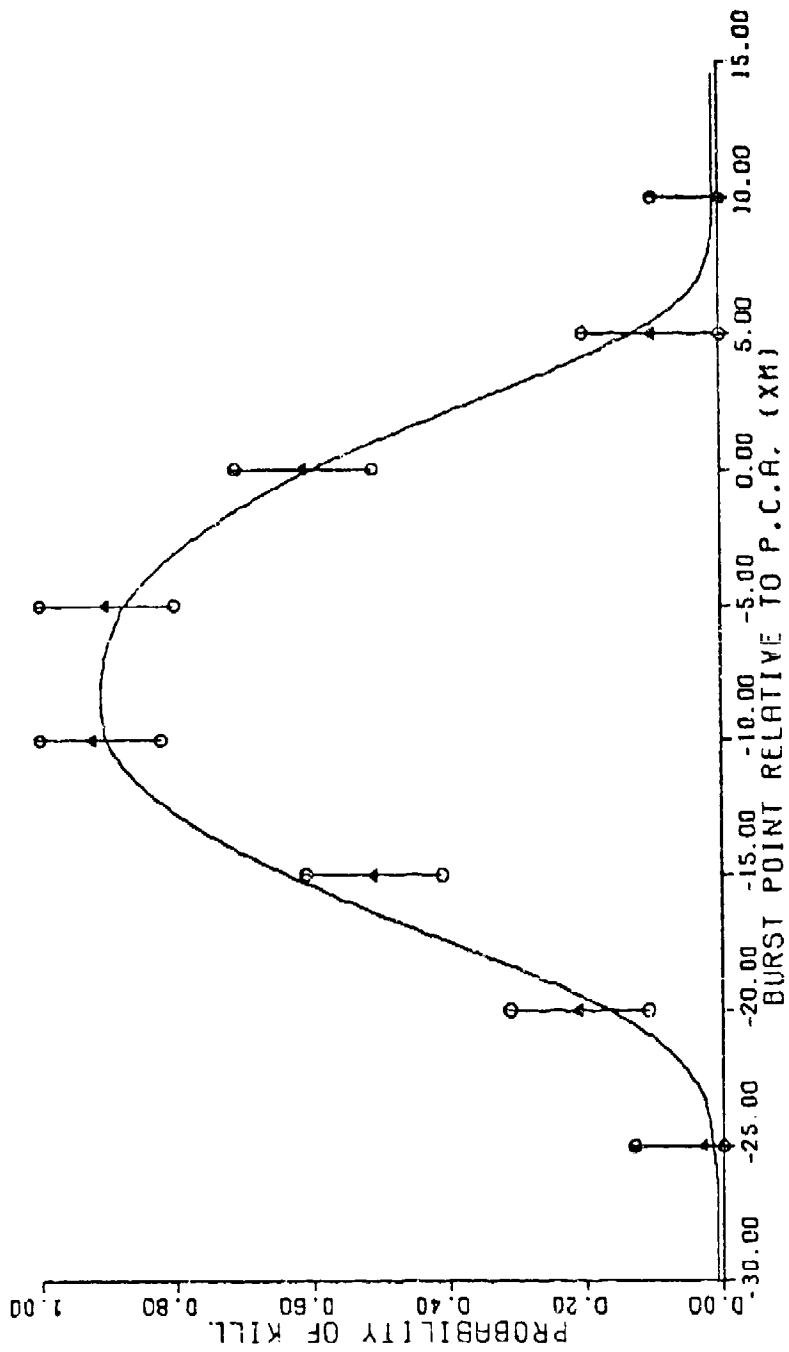


FIG H-10: PSI=180. VR=2000. BETA=0. SIGMA=15.0

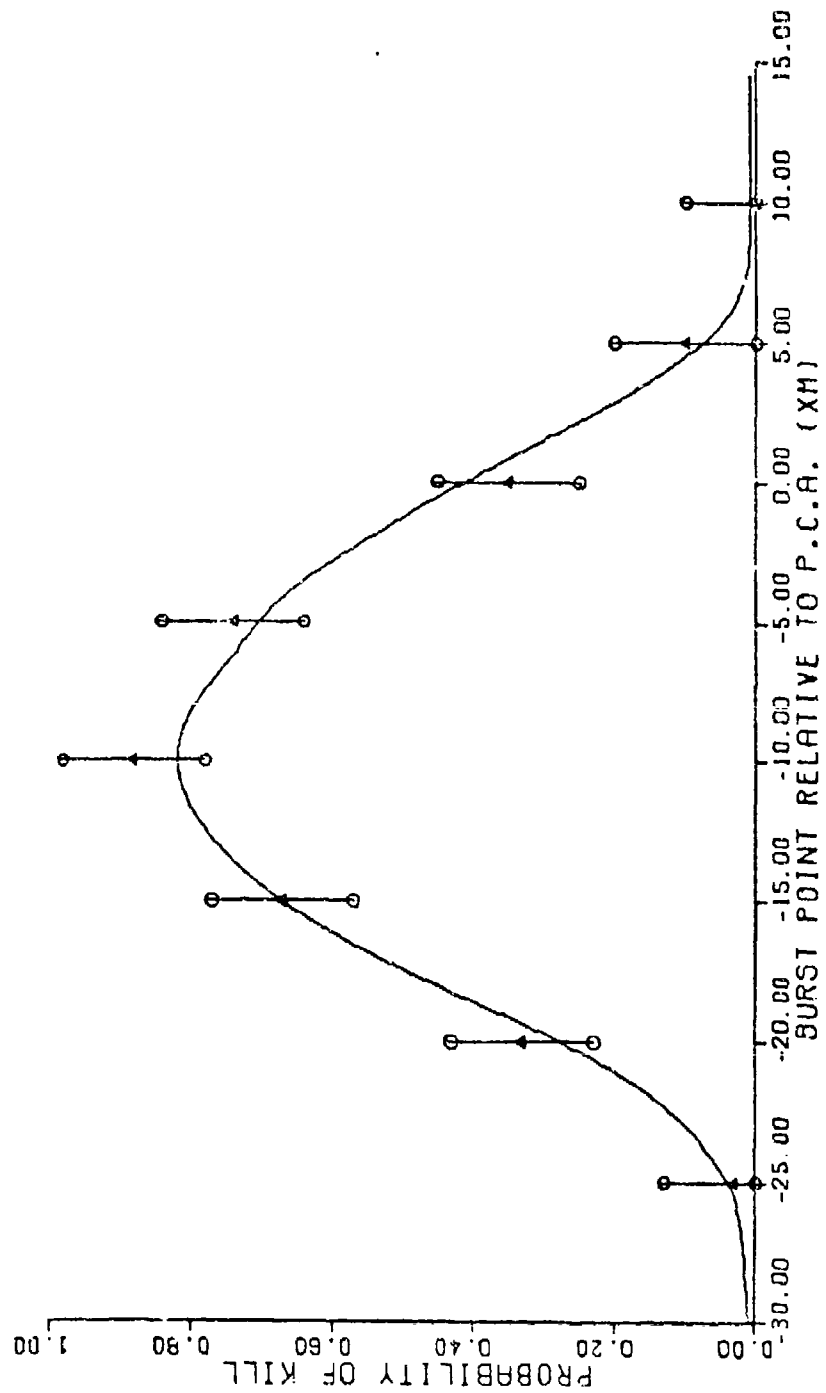


FIG H-11 : PSI=180. VR=2000. BETA=0. SIGMA=20.0

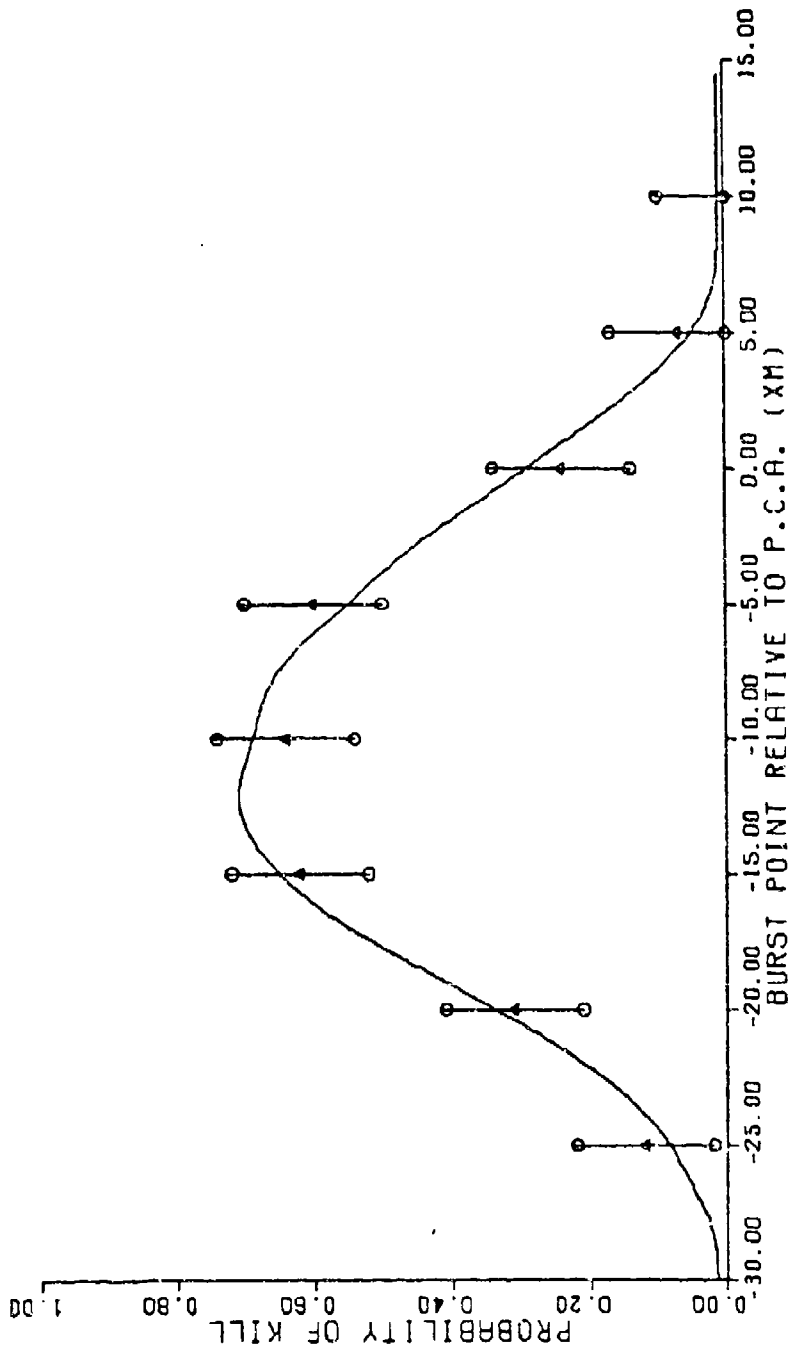


FIG H-12: PSI=180. VR=2000. BETA=0. SIGMA=25.0

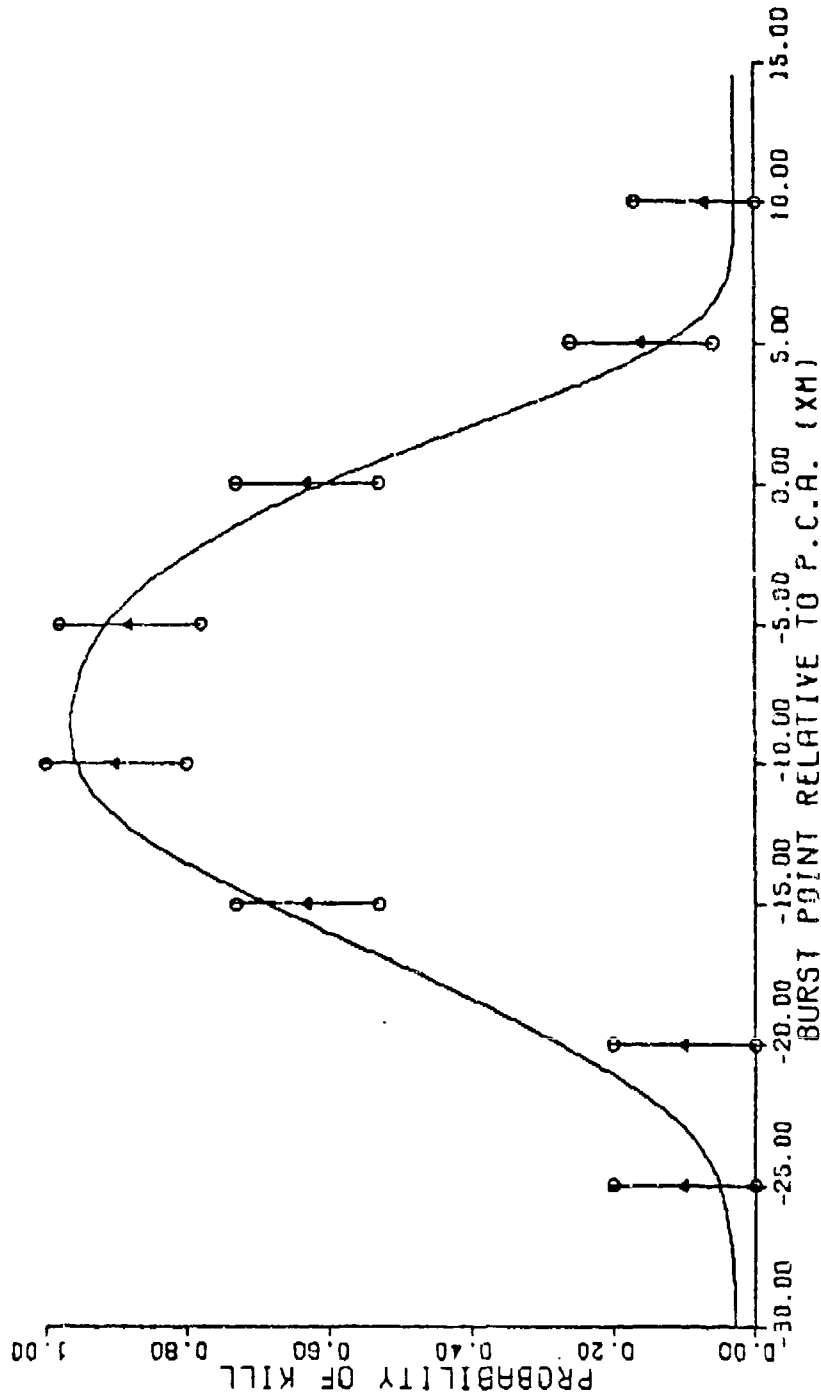


FIG II-13 : PSI=180. VR=3000. BETA=0. SIGMA=10.0

APPENDIX I

Improved Characterization With
Random Miss Distance

The plots in this appendix correspond to those in Appendix H except that the curves were generated with the final characterization.

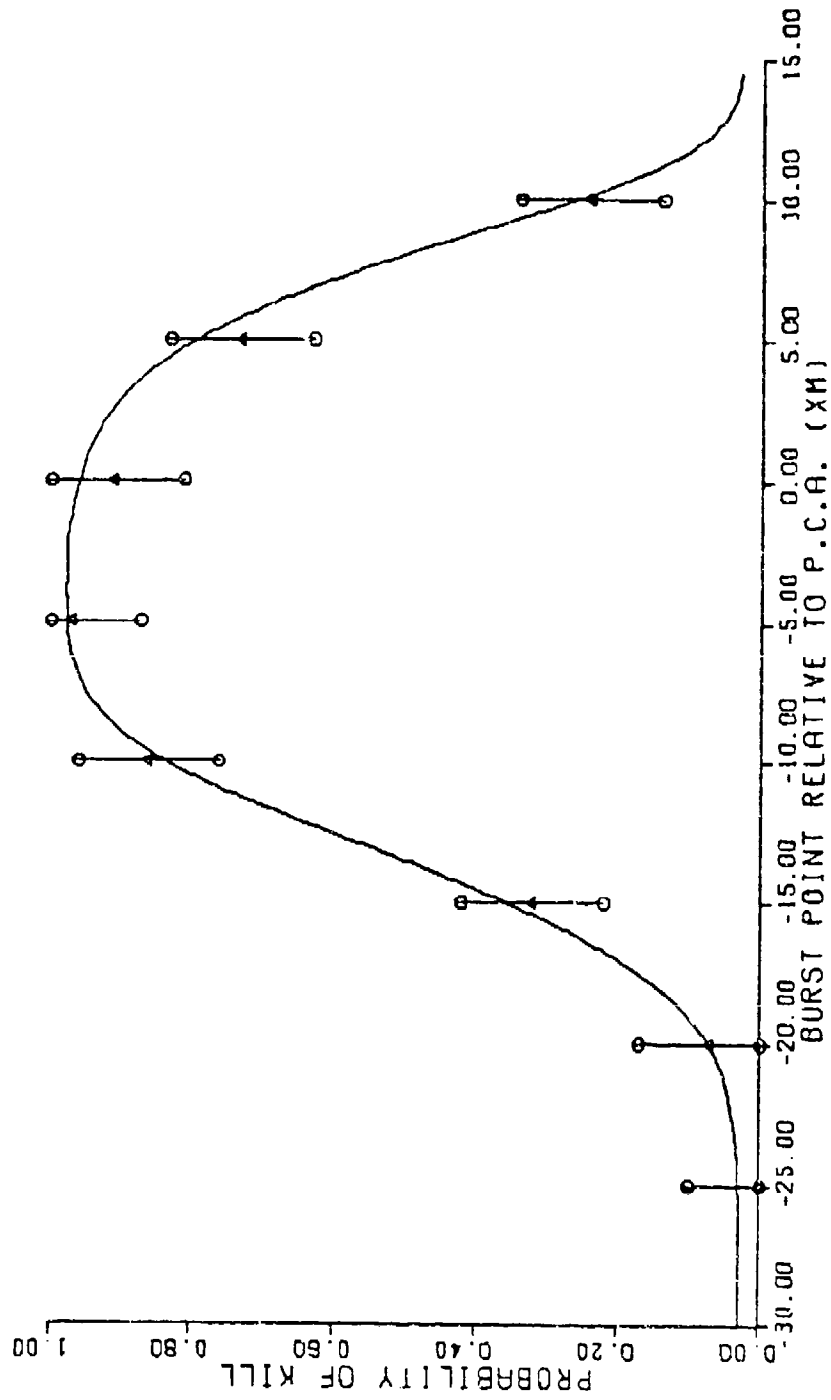


FIG I-1 : PSI=0. VR=2000. BETA=0. SIGMA=10.0

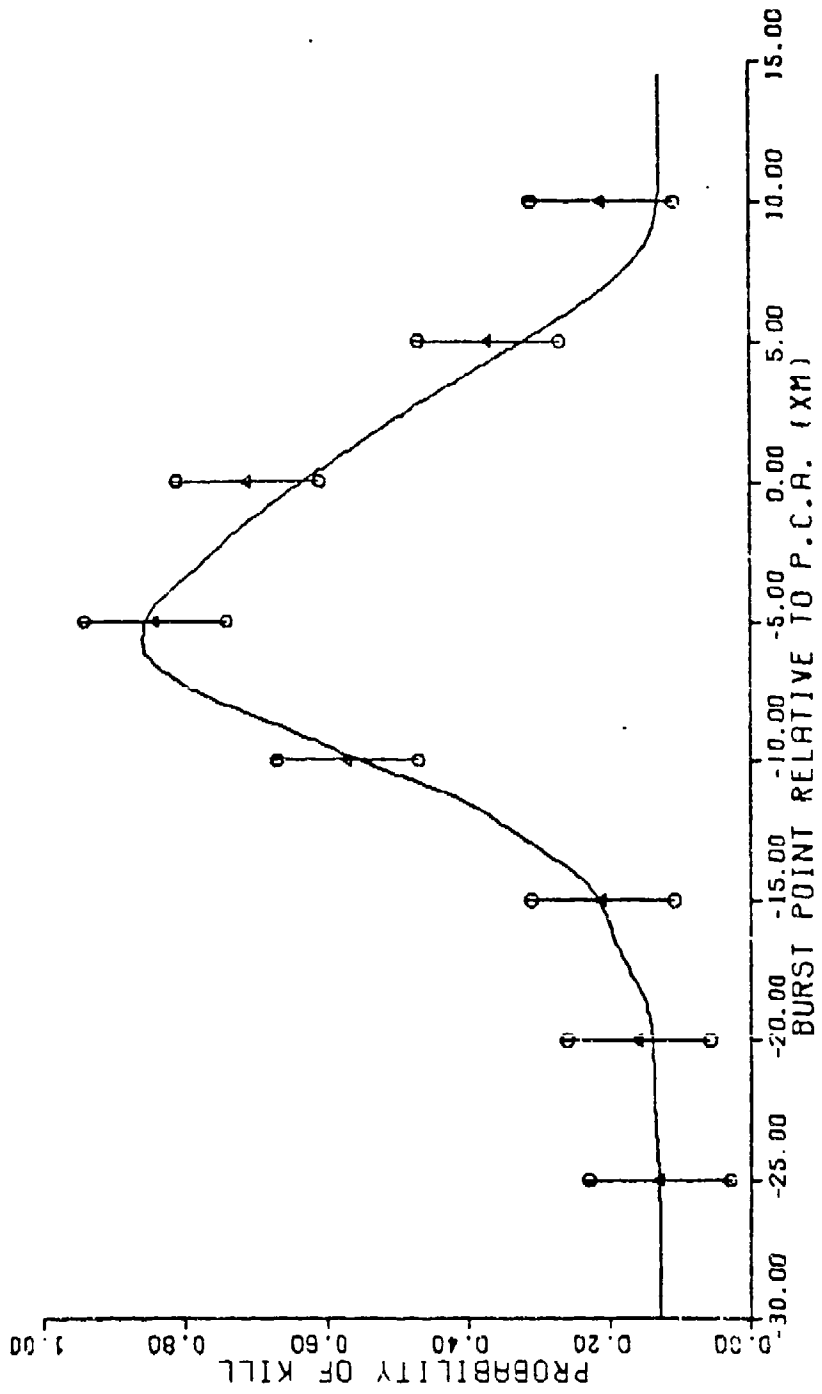


FIG I-2: PSI=45. VR=2000. BETA=15. SIGMA=10.0

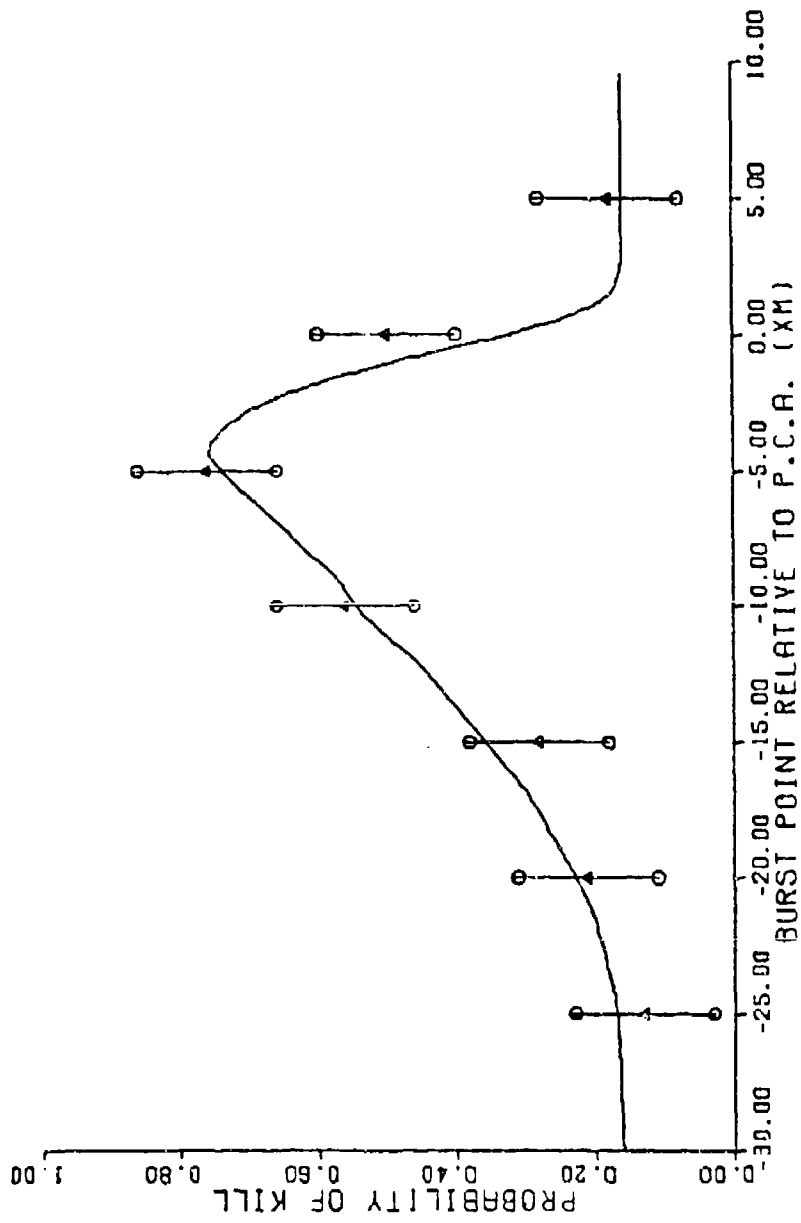


FIG I-3 : PSI=90. VR=2000. BETA=15. SIGMA=10.0

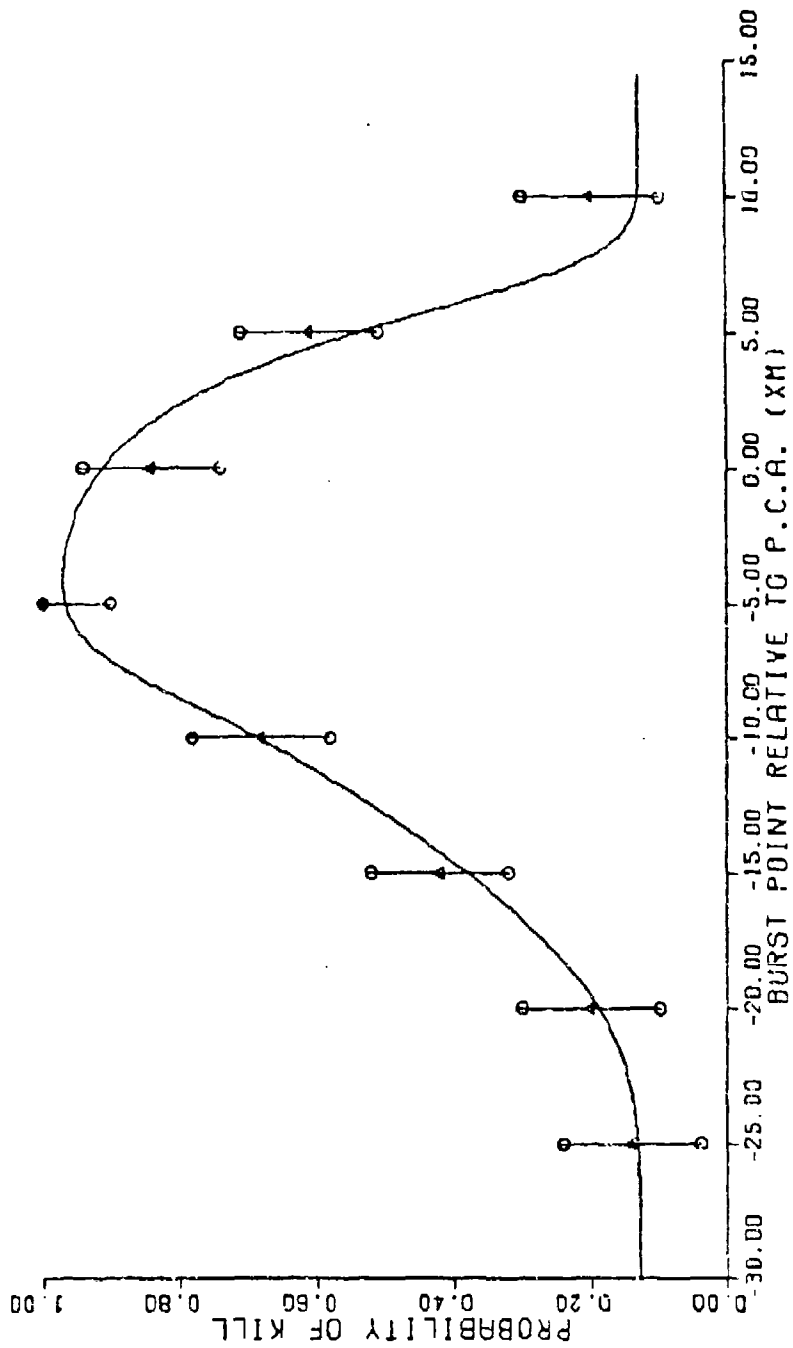


FIG I-4 : PSI=135. VR=1000. BETA=15. SIGMA=10.0

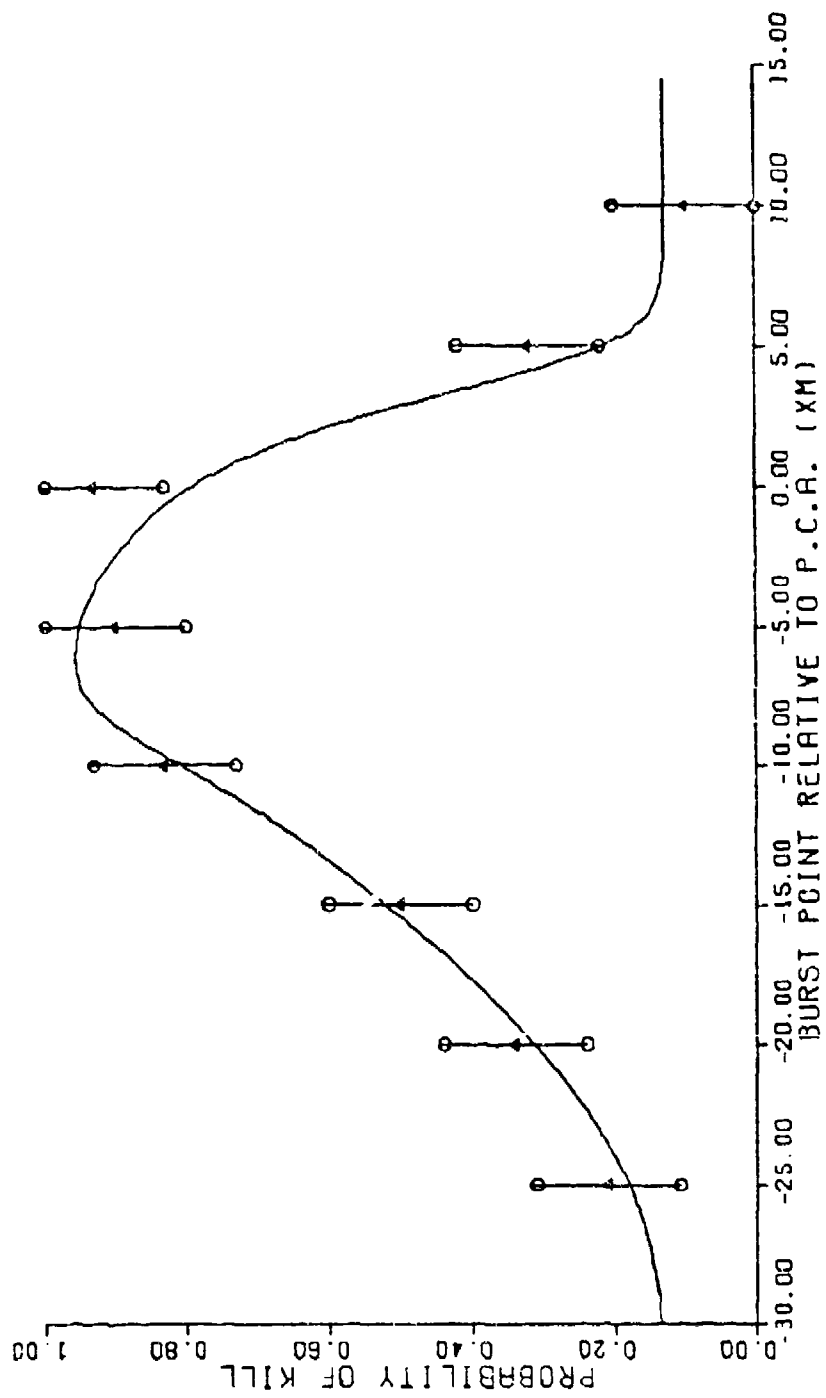


FIG I-5 : PSI=135. VR=2000. BETA=15. SIGMA=10.0

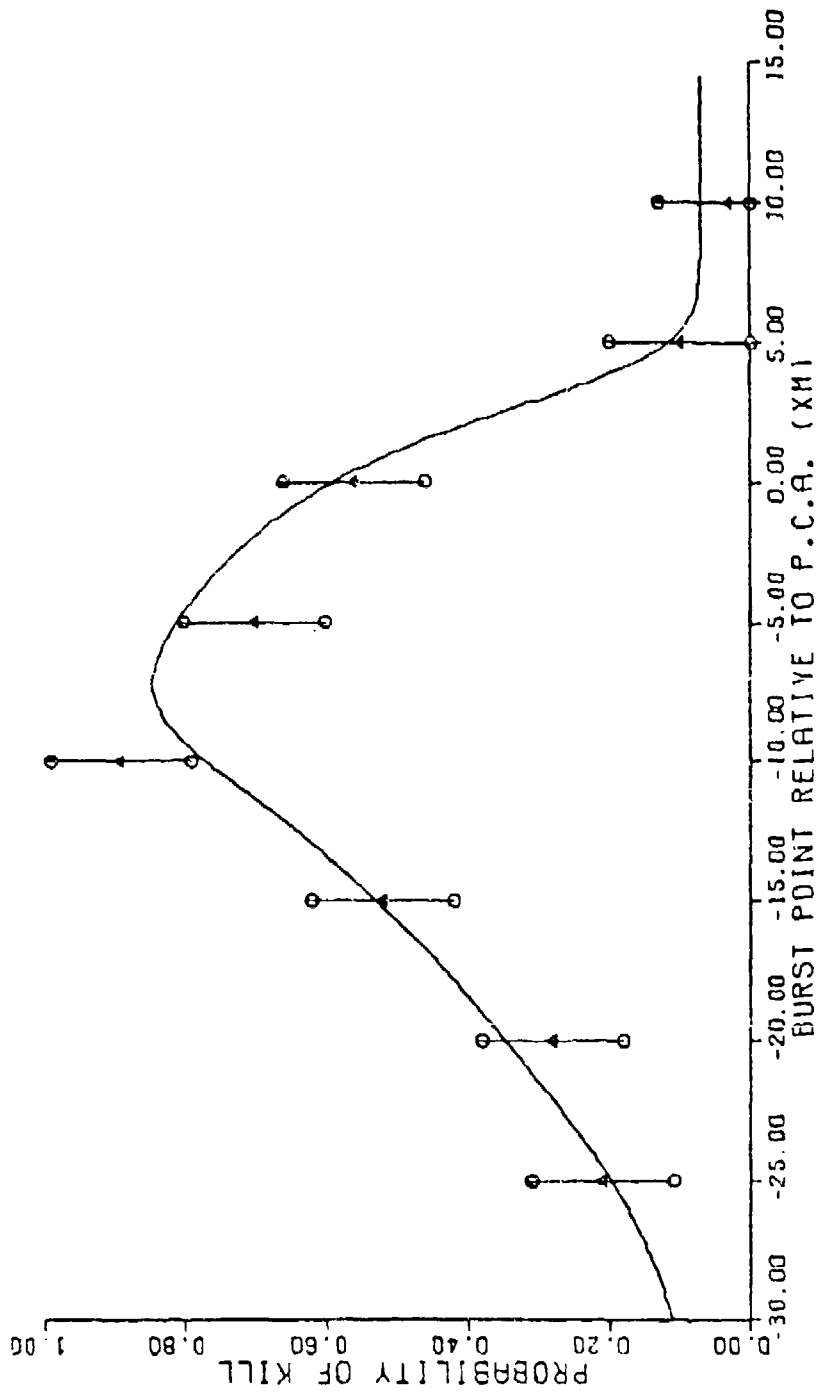


FIG 1-6 : PSI=135. VR=2000. BETA=15. SIGMA=15.0

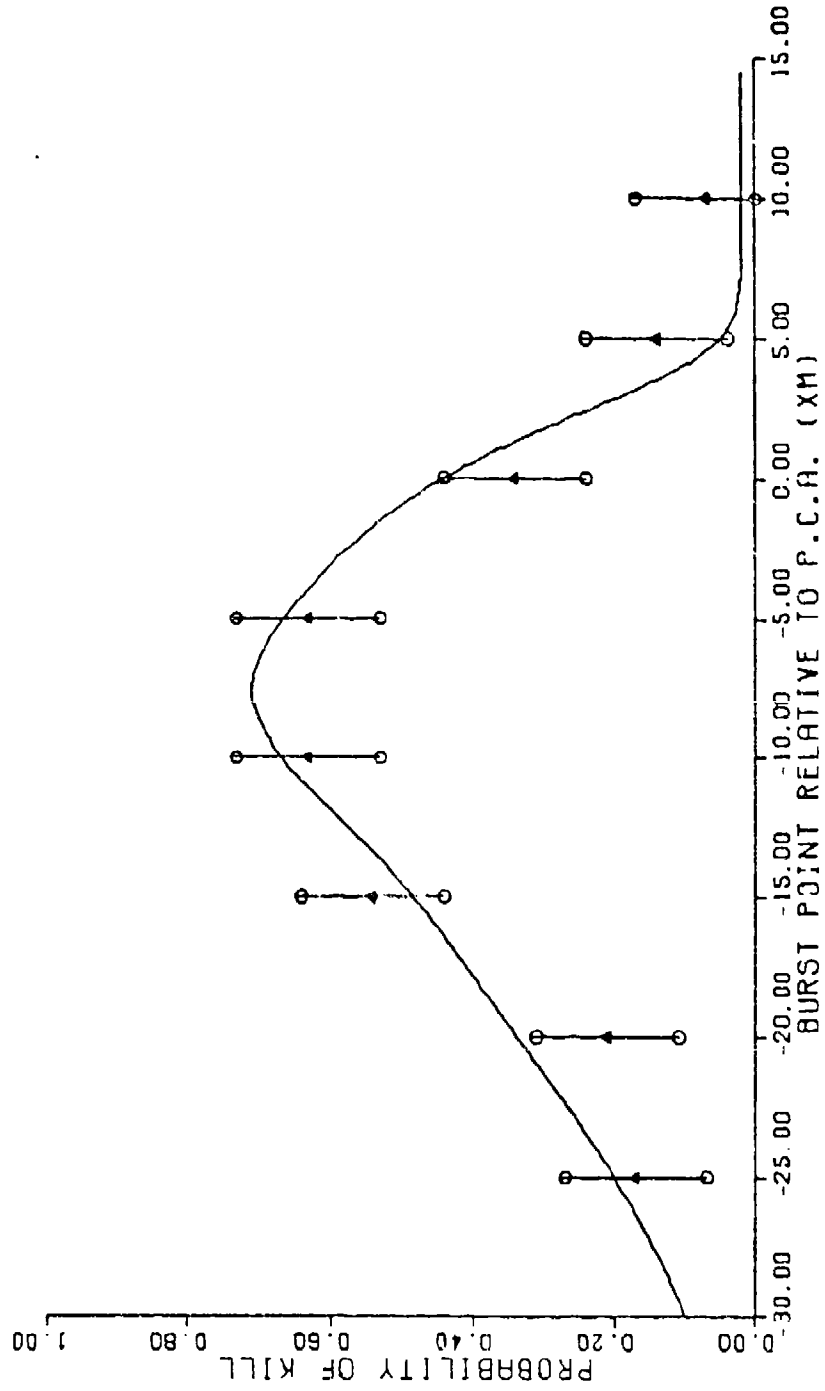


FIG I-7 : PSI=135. VR=2000. BETA=15. SIGMA=20.0

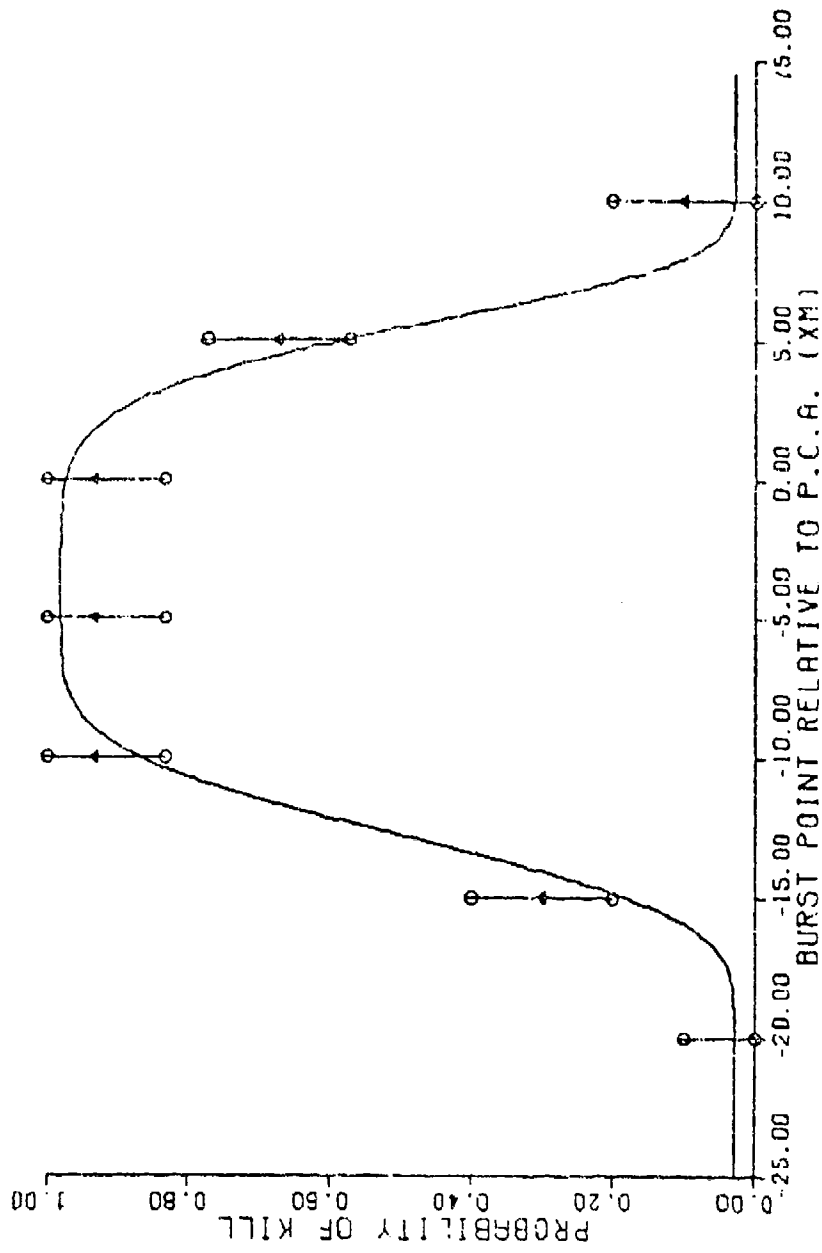


FIG I-8 : PSI=180. VR=1000. BETA=0. SIGMA=10.0

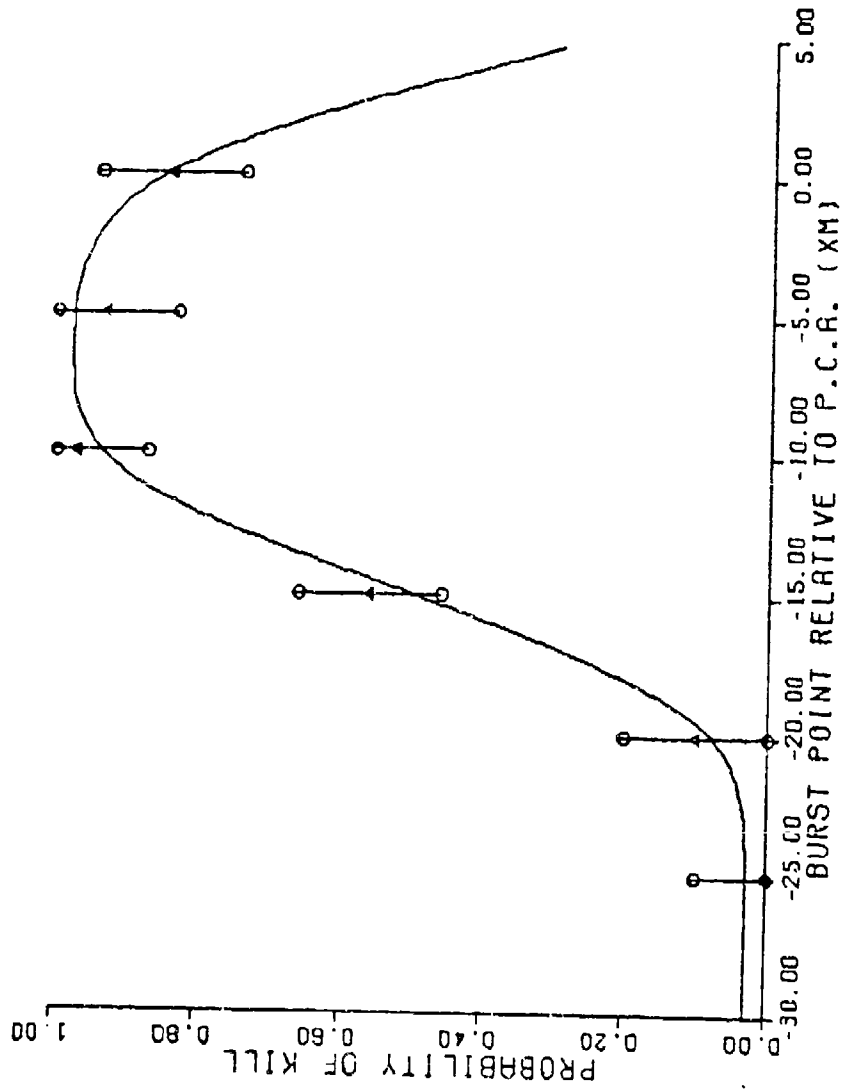


FIG I-9: PSI=180. VR=2000. BETA=0. SIGMA=10.0

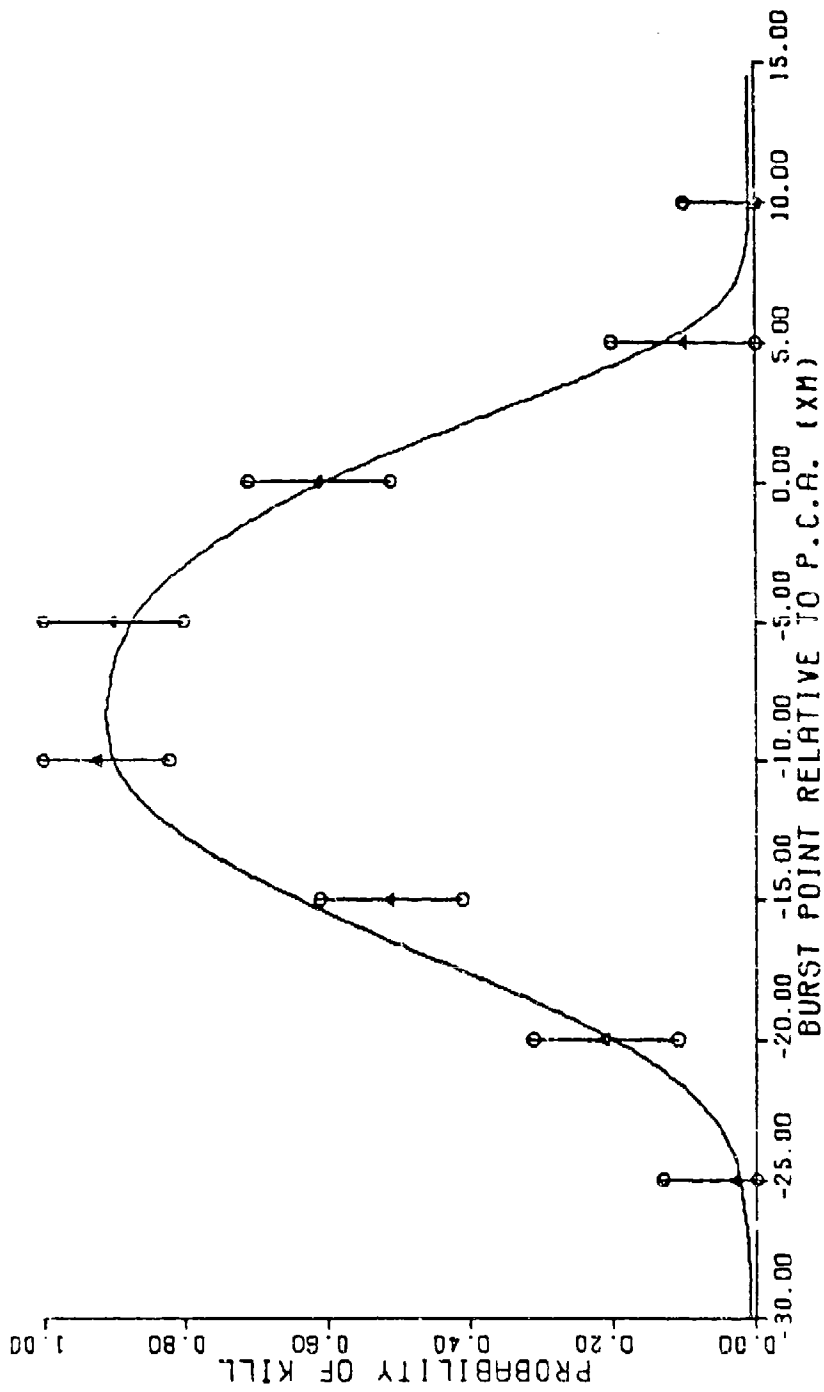


FIG I-10 : PSI=180. VR=2000. BETA=0. SIGMA=15.0

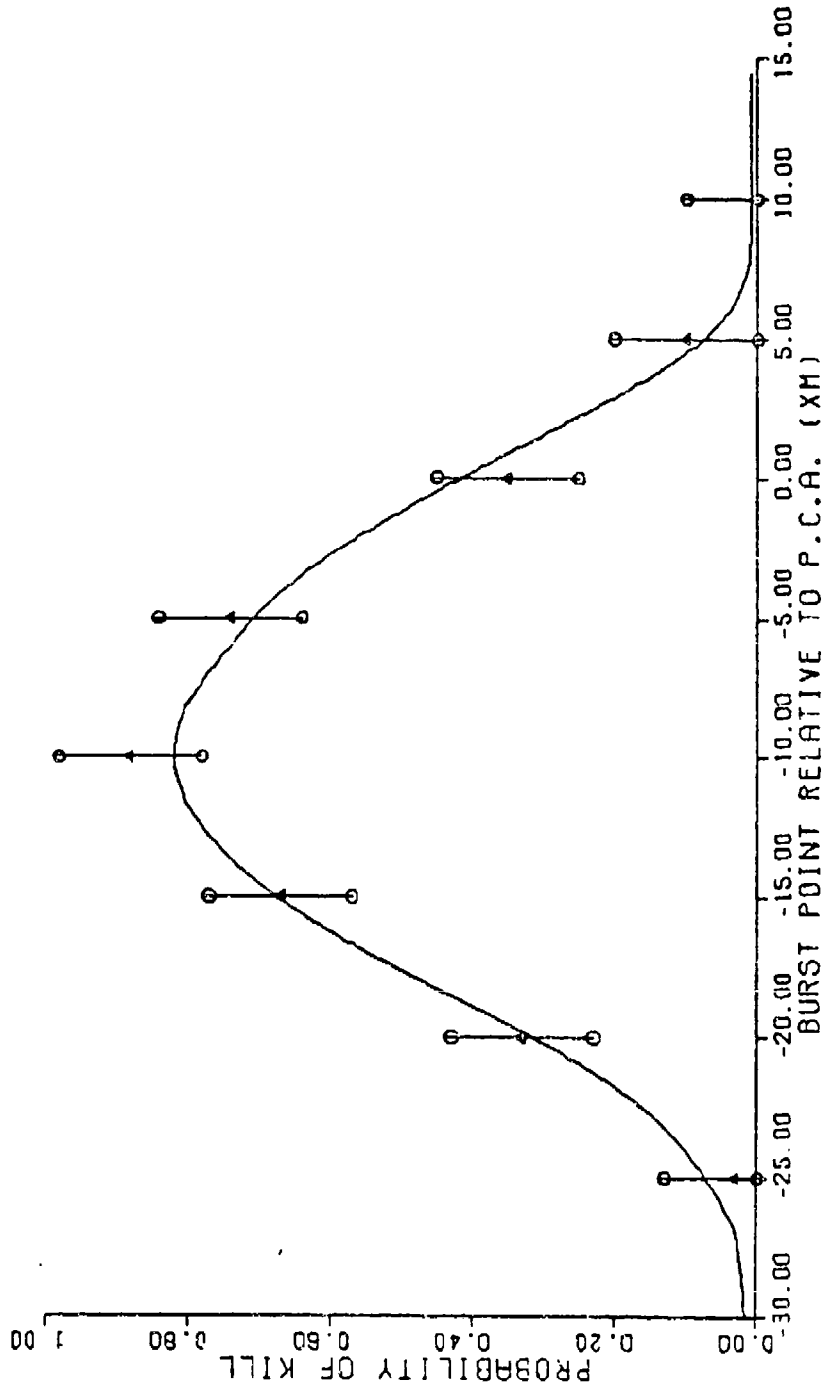


FIG I-11: PSI=180. VR=2000. BETA=0. SIGMA=20.0

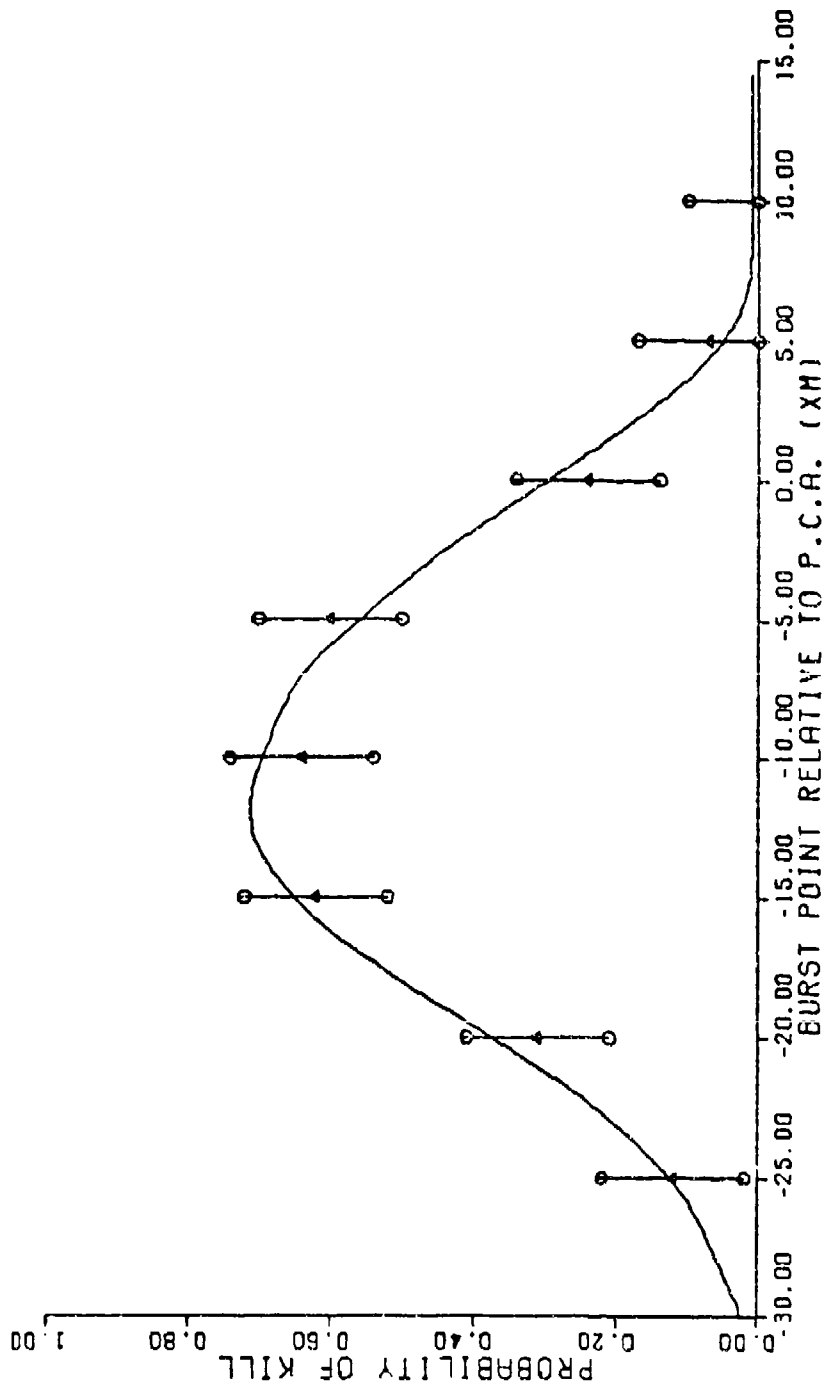


FIG I-12: PSI=180. VR=2000. BETA=0. SIGMA=25.0

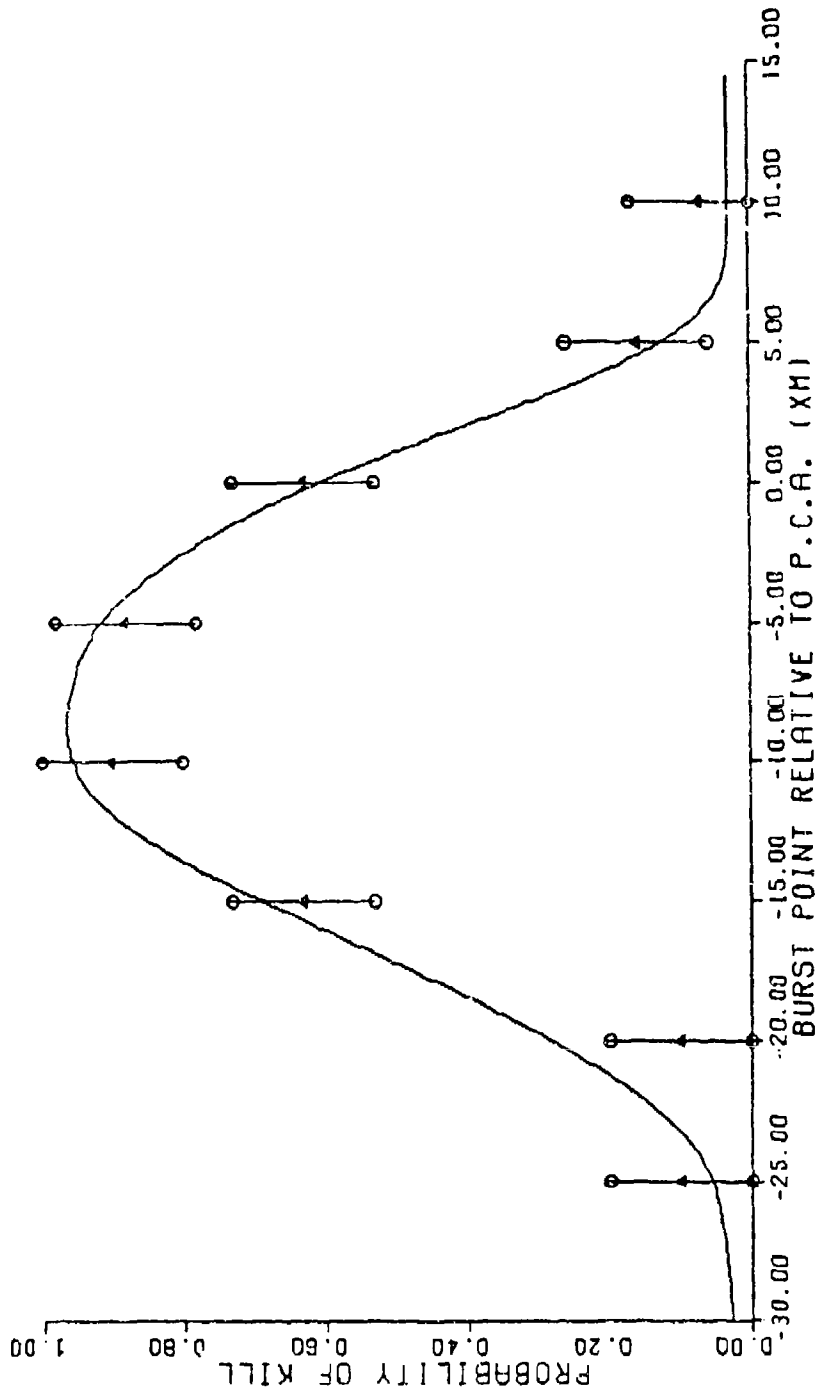


FIG 1-13: PSI=180. VR=3000. BETA=0. SIGMA=10.0

APPENDIX J

Selected Plots of the Improved
Characterization Applied to the
Basic Data

The 10 plots in this appendix are comparisons of the final characterization with selected factor combinations from the basic data. The corresponding plots for the first characterization appear in Appendix F.

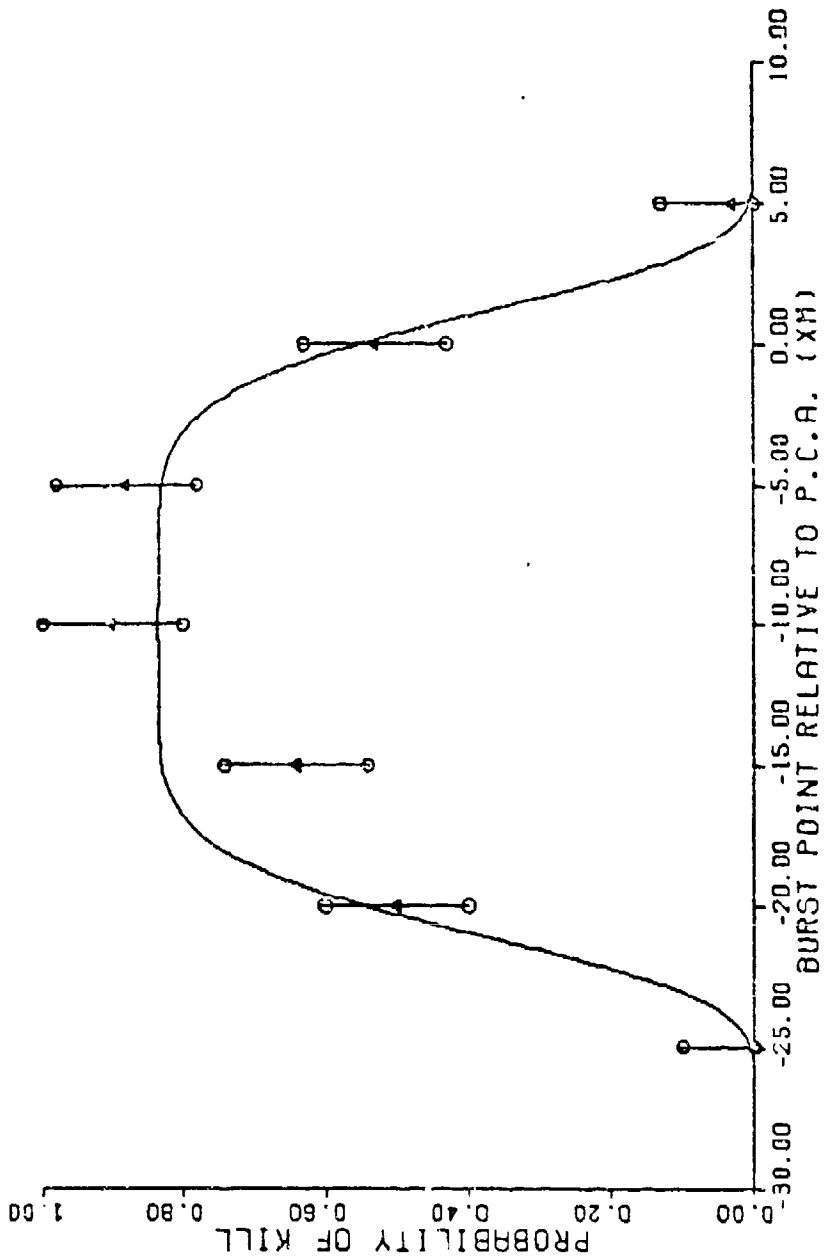


FIG J-1 : PSI=0. THETA=225. VR=2000. RM=27.5 BETA=0.

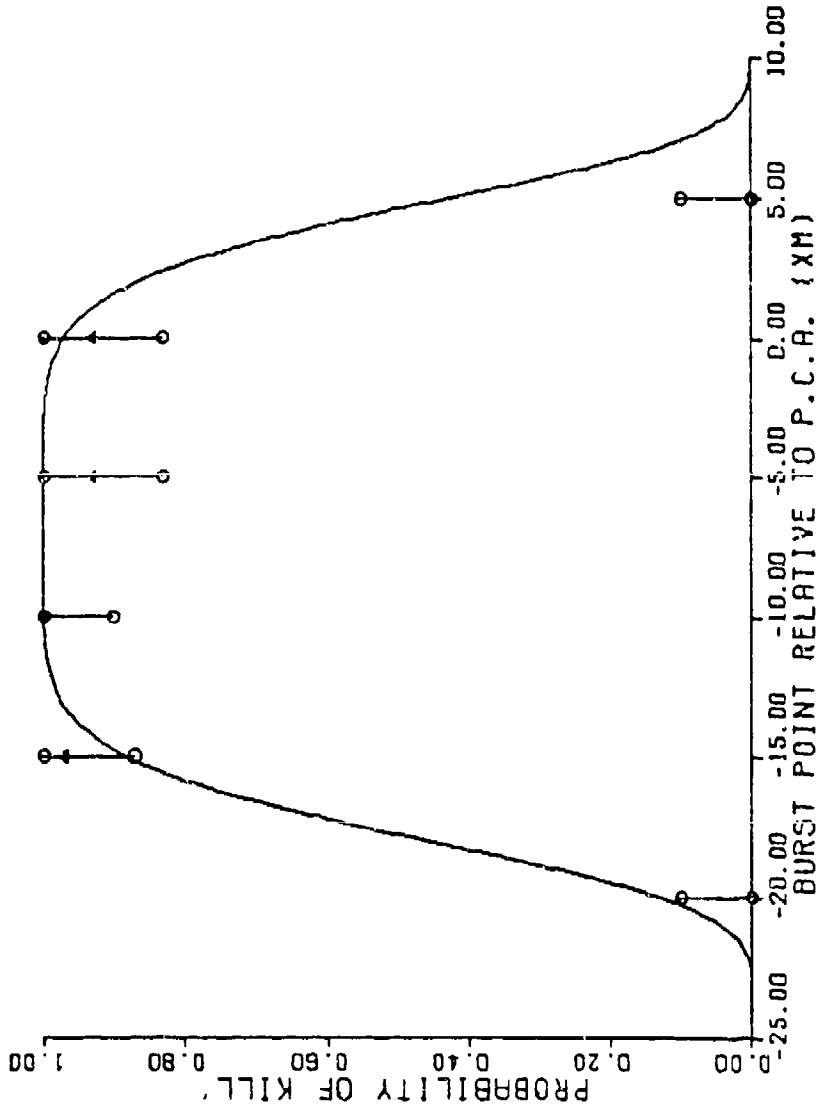


FIG J-2 : PSI=0. THETA=225. VR=3000. RM=15.0 BETA=0.

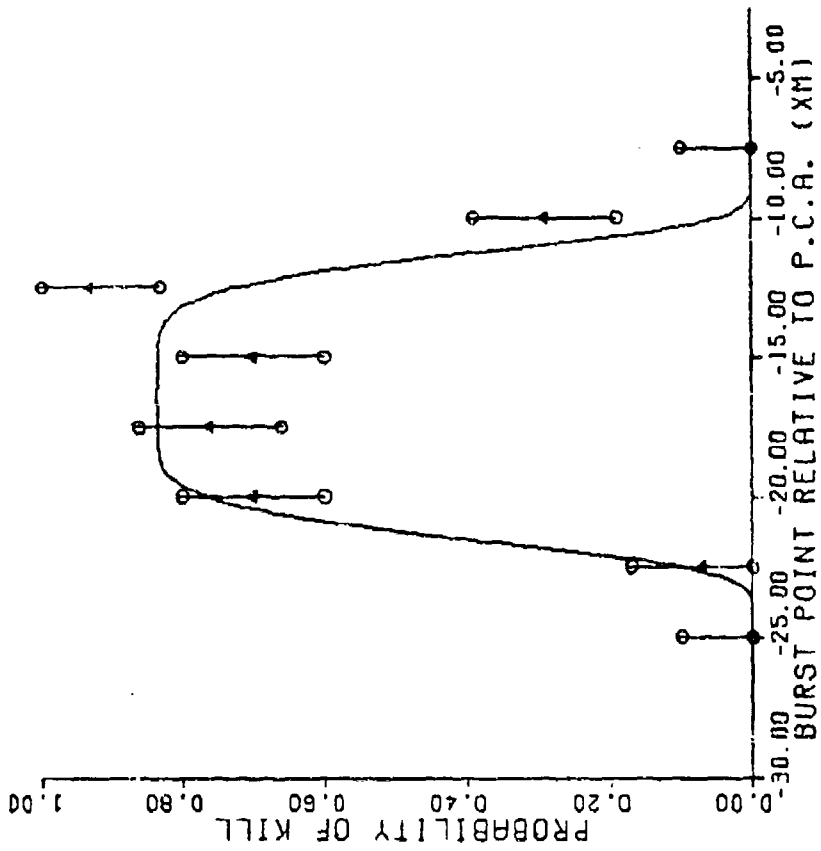


FIG J-3 : PSJ=45. THETA=45. VR=2000. RM=27.5 BETA=15.

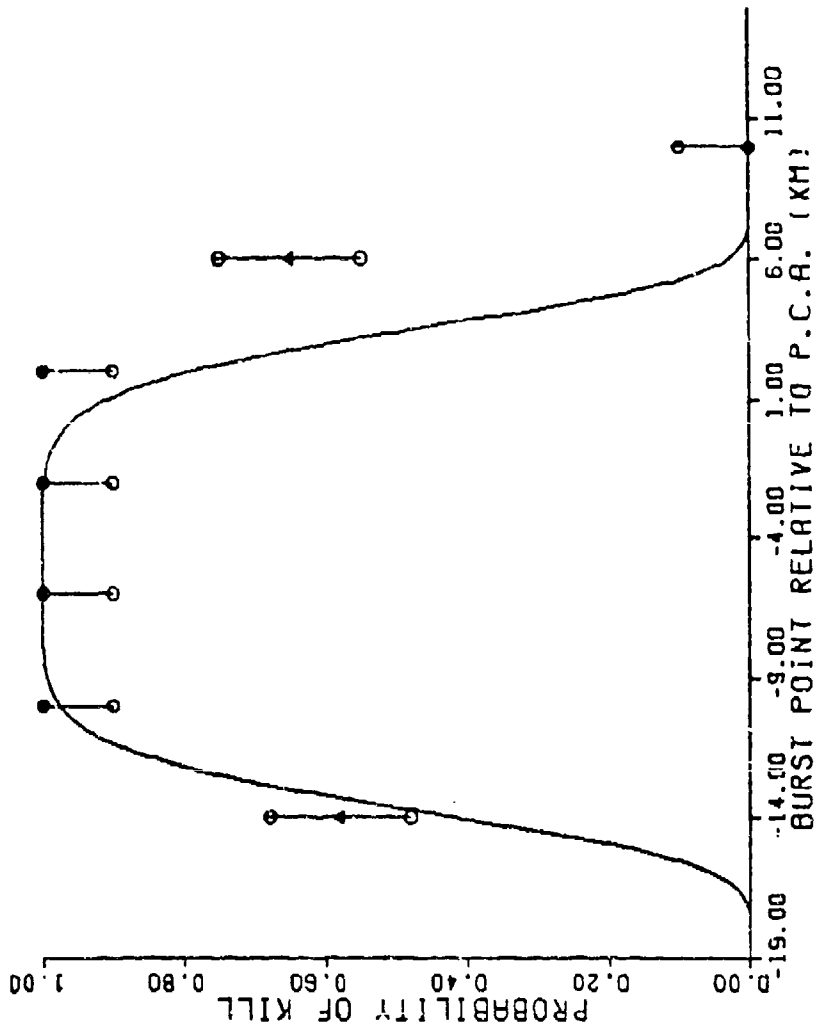


FIG J-4 : PSI=45. THETA=135. VR=3000. RM=15.0 BETA=15.

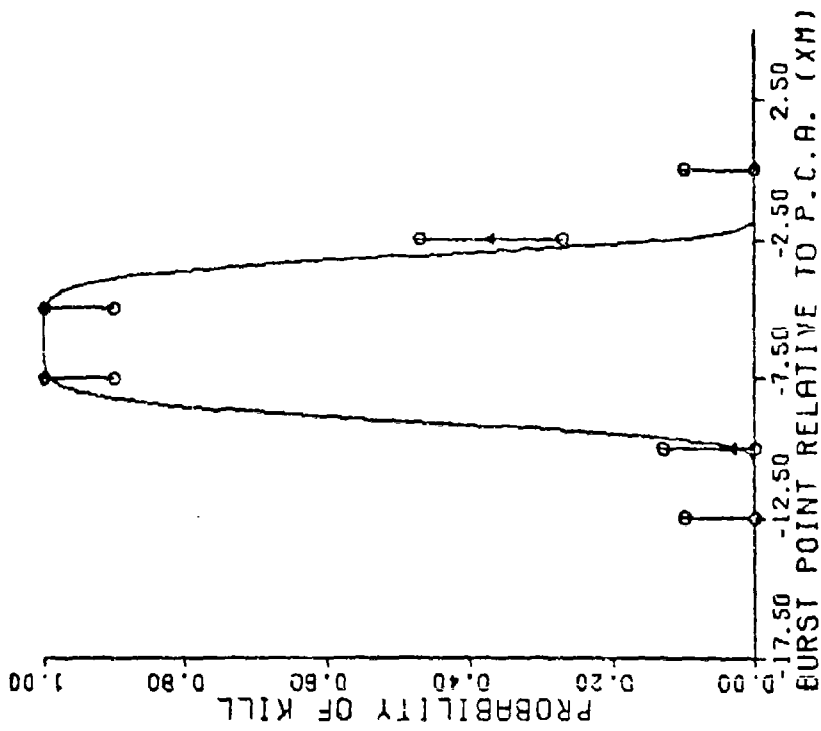


FIG J-5 : PSI=90. THETA=135. VR=3000. RM=15.0 BETA=15

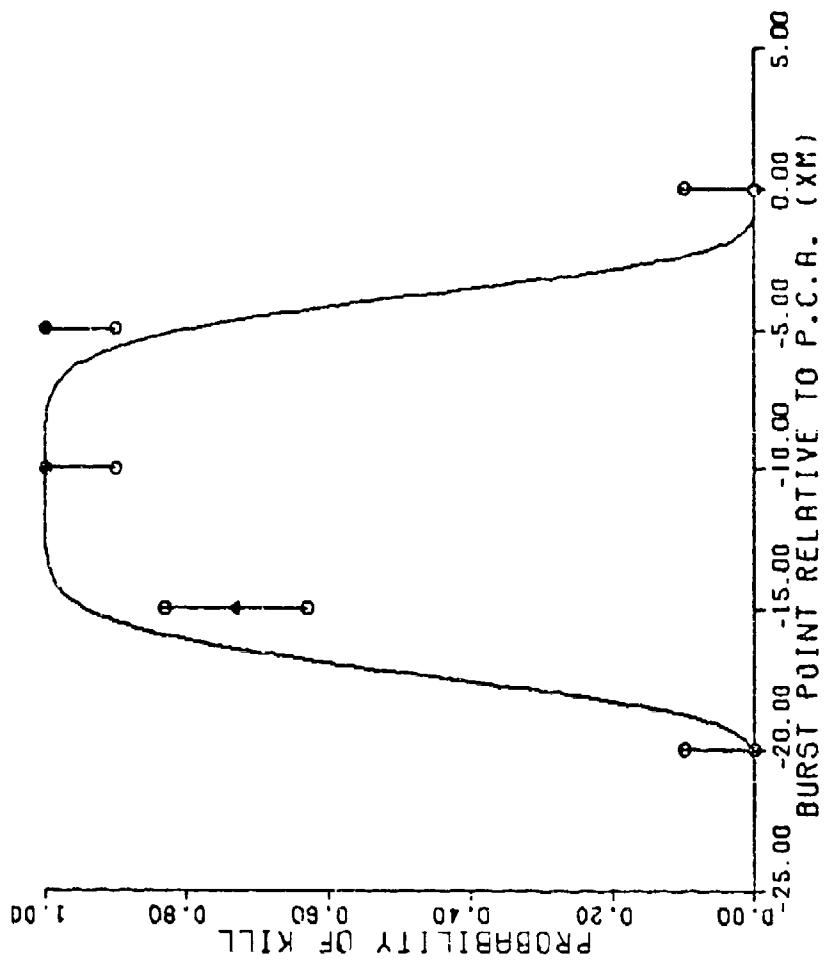


FIG J-6 : PSI=90. THETA=315. VR=2000. RM=15.0 BETA=15.

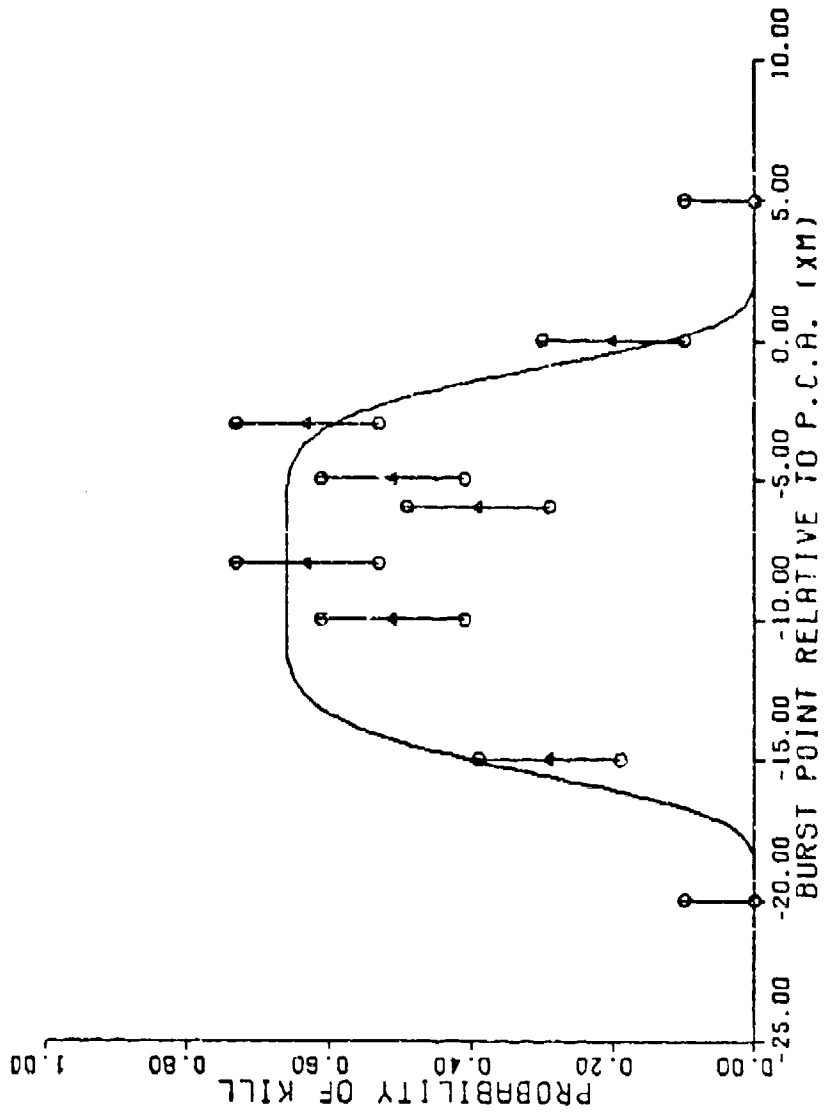


FIG J-7: PSI=135. THETA=135. VR=2000. RM=40.0 BETA=15.

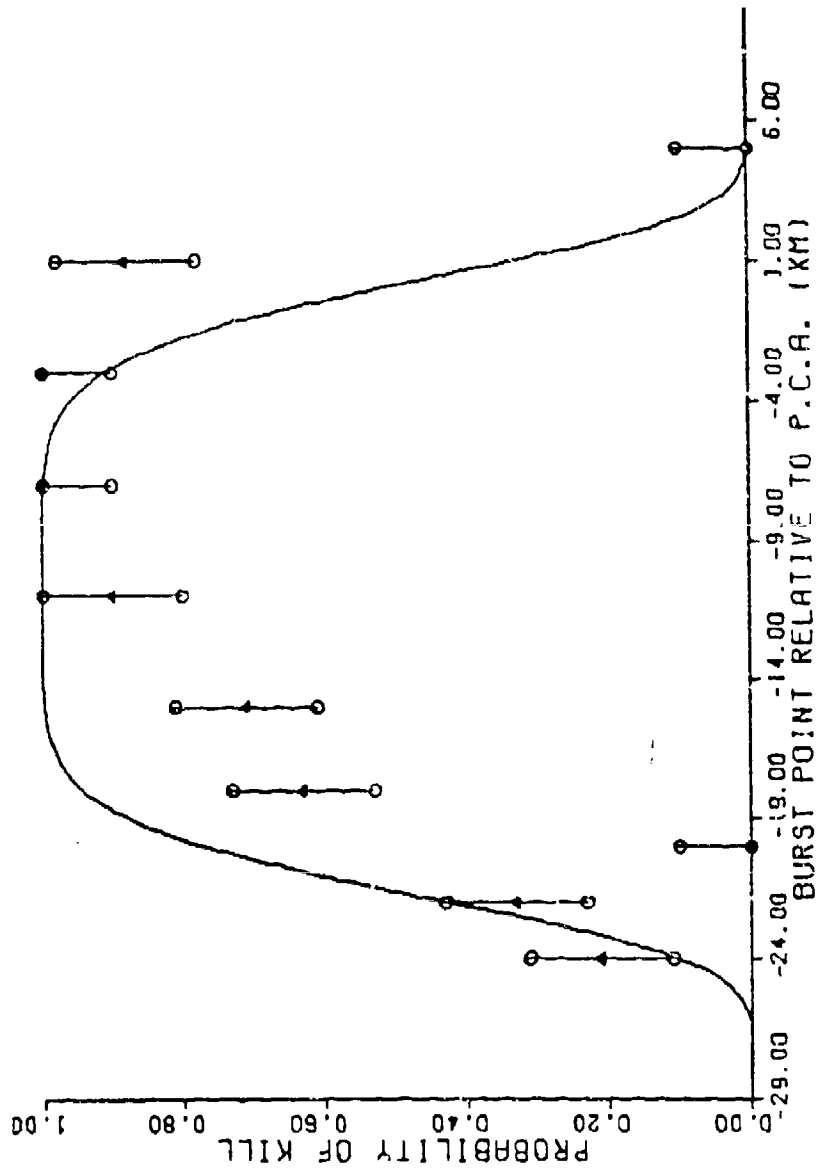


FIG J-8 : PSI=135. THETA=315. VR=2000. RM=15.0 BETA=15.

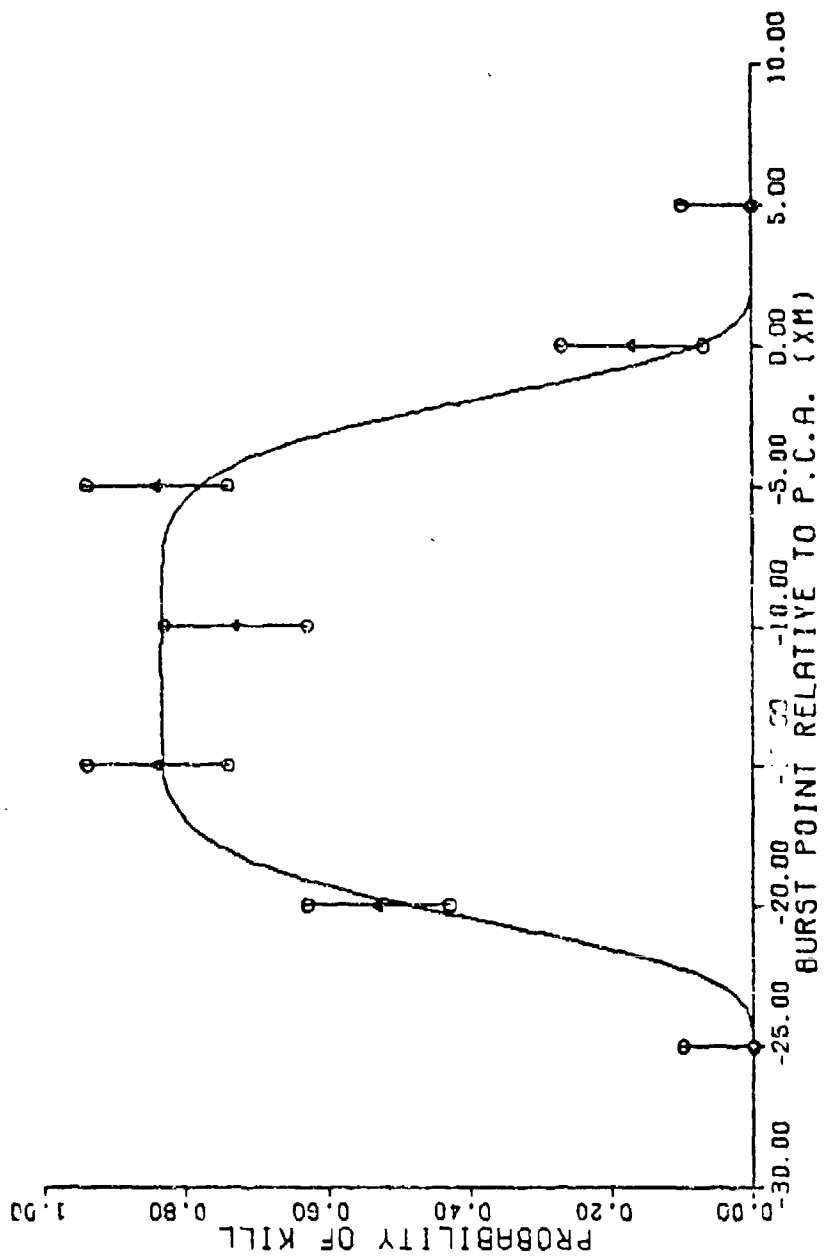


FIG J-9 : PSI=180. THETA=225. VR=2000. RM=27.5 BETA=0.

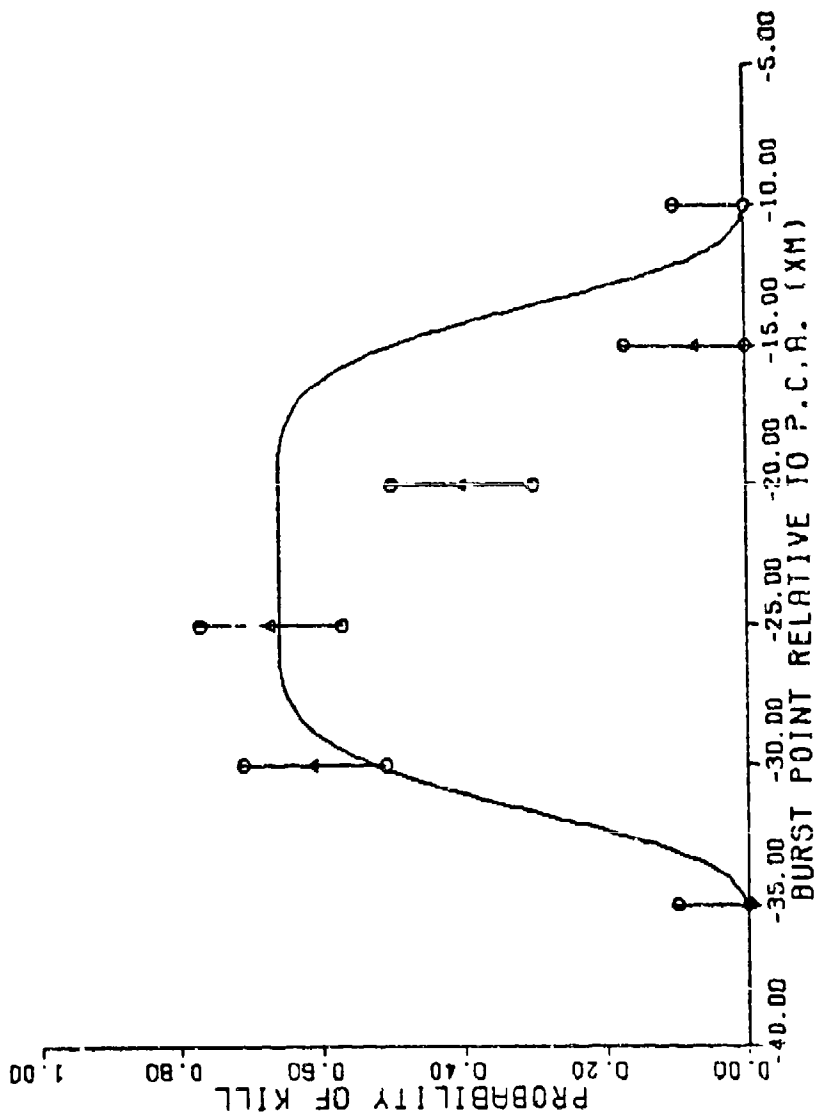


FIG J-10: PSI=180. THETA=225. VR=3000. RM=40.0 BETA=0.

APPENDIX K

Comparison of the Final Characterization to the 10 Selected Random Trajectories

The 11 plots in this appendix show the final characterization versus the data generated by SHAZAM for the ten random trajectories in Table VI. For all of these plots, the error bars on the data points are intended to graphically depict a distance of ± 0.1 from each point. They do not represent confidence intervals in this appendix. The 90% confidence intervals about the SHAZAM P_K 's for these ten random trajectories is ± 0.04 .

Figures K-8 and K-9 are the trajectory with α treated as a random variable. In both plots, the SHAZAM data is the same. The characterization curve in Figure K-8 was generated with the 109 Cell Model while in Figure 9, it was generated with 1000 randomly selected combinations of R_M , θ , and α .

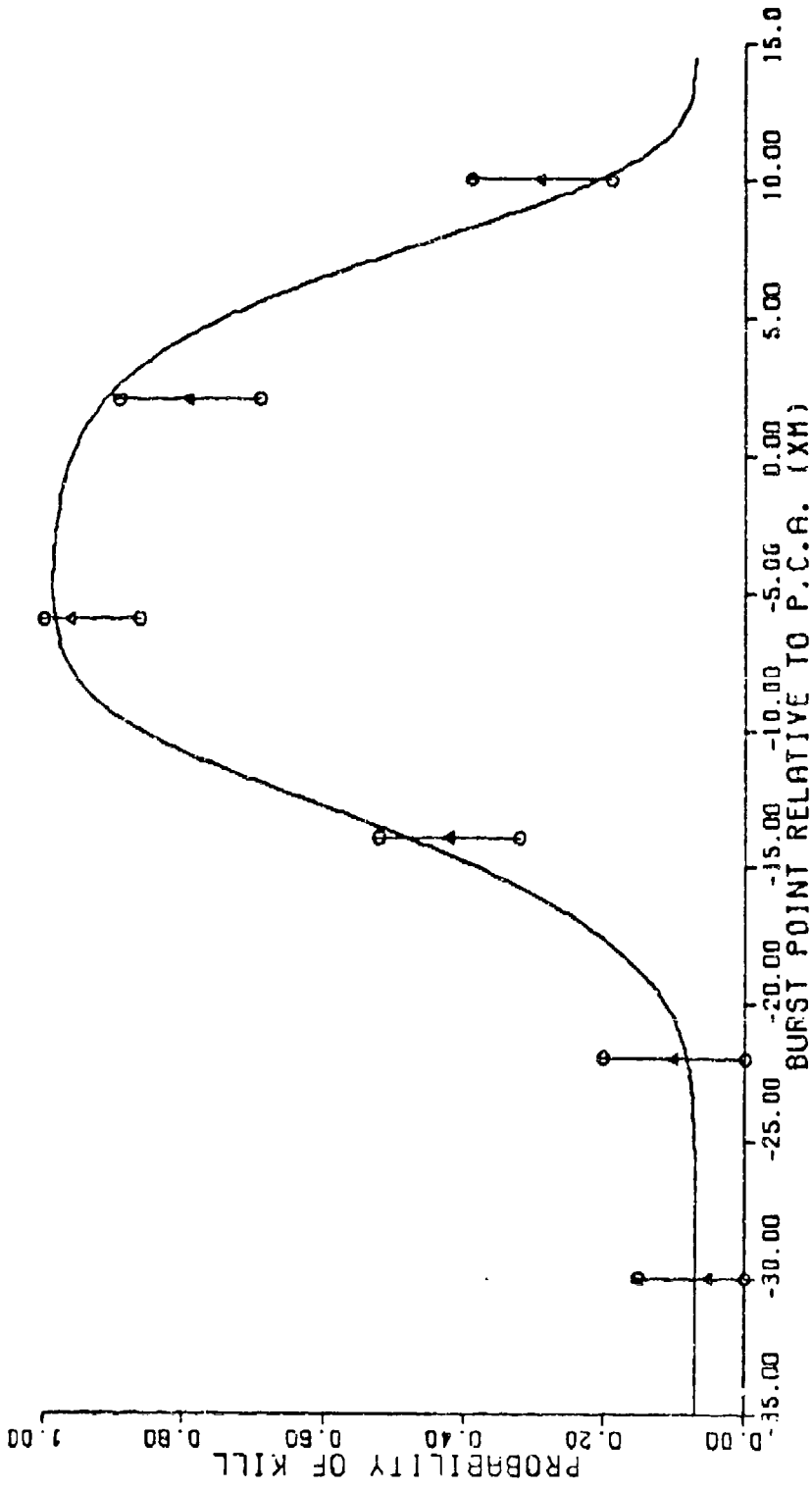


FIG K-1 : PSI=9. VR=2480. BETA=4. SIGMA=8.5

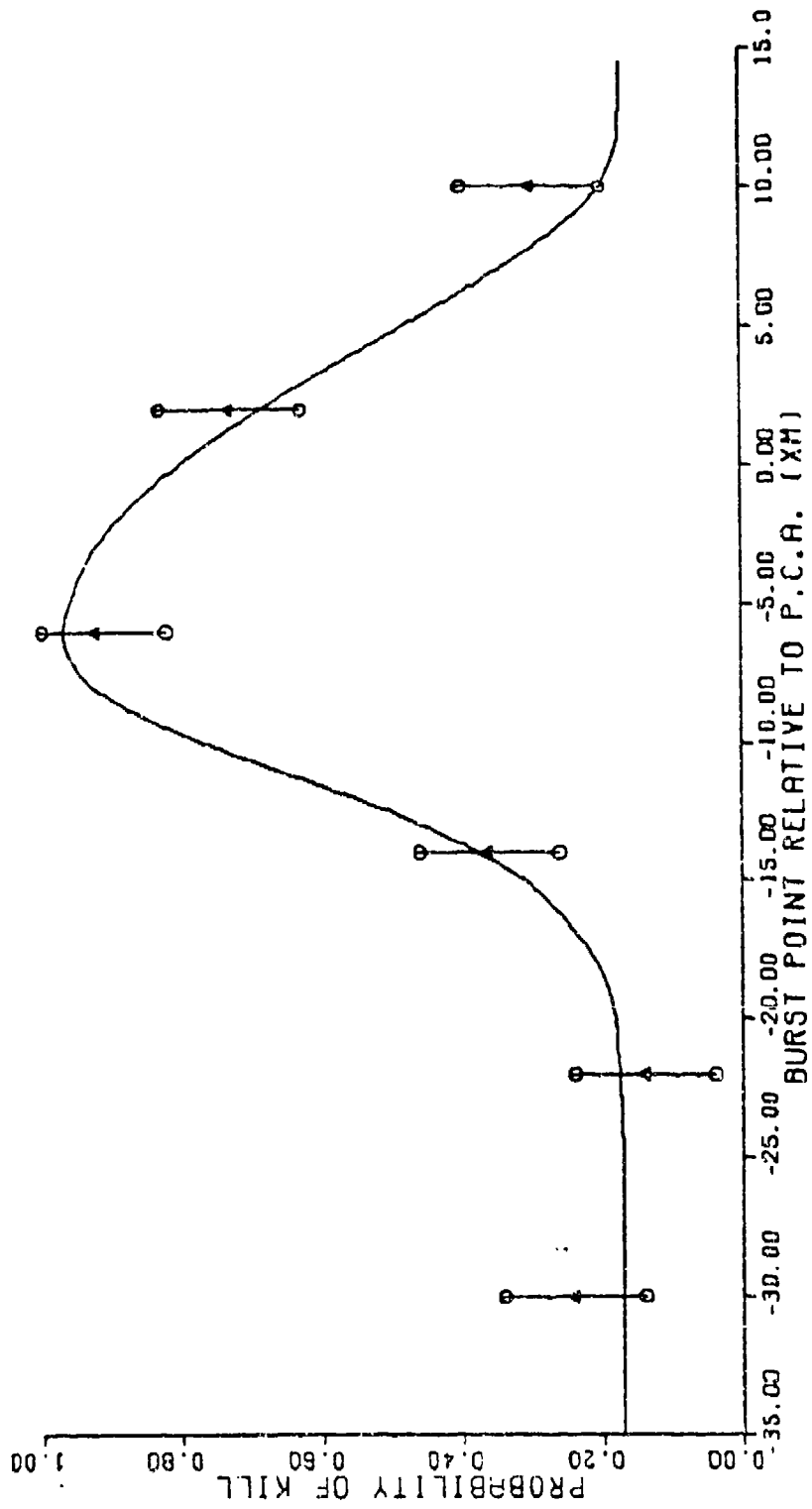


FIG K-2 : PSI=30. VR=2604. BETA=14. SIGMA=7.6

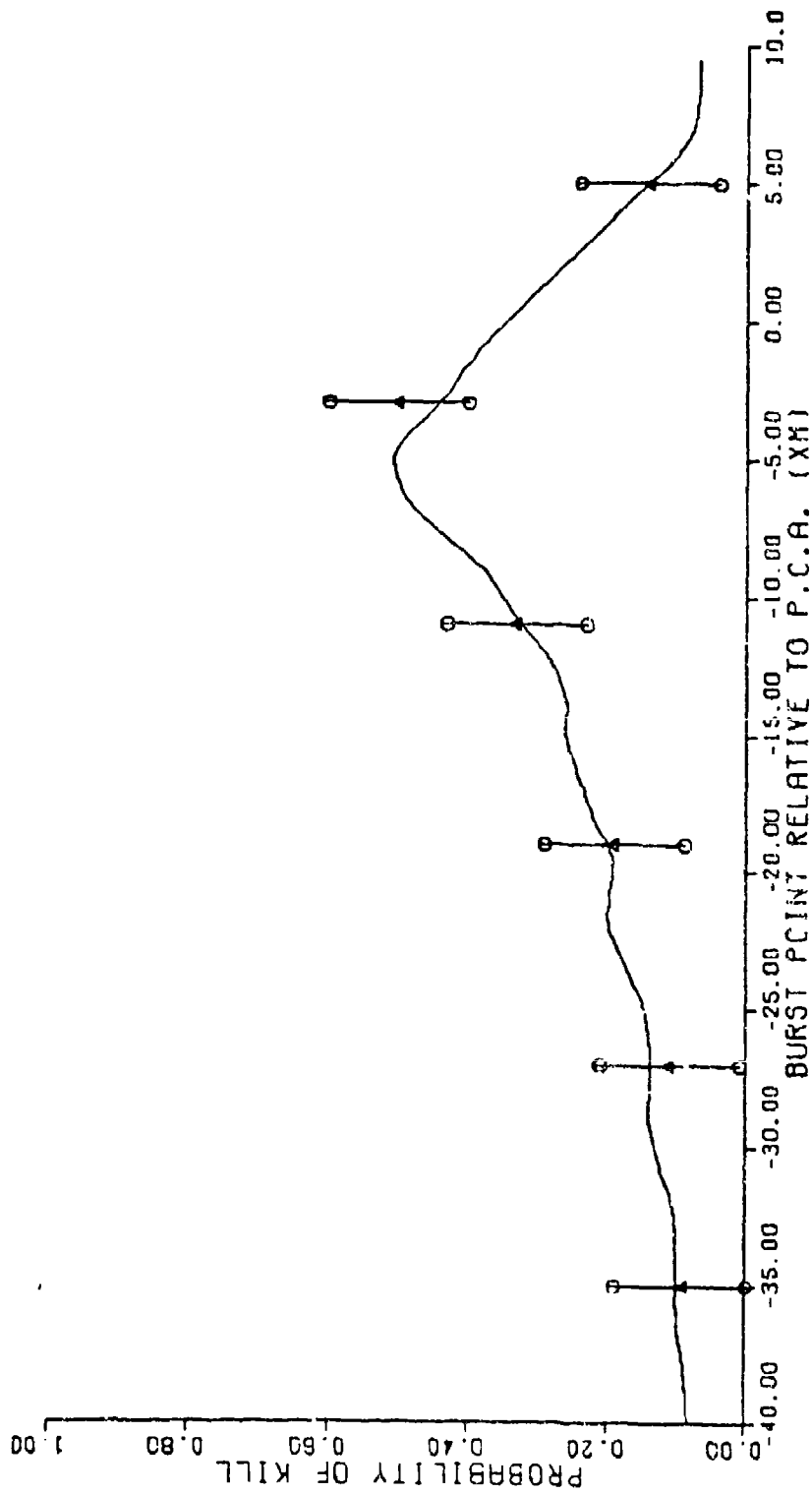


FIG K-3: PSI=55. VR=2447. BETA=24. SIGMA=16.1

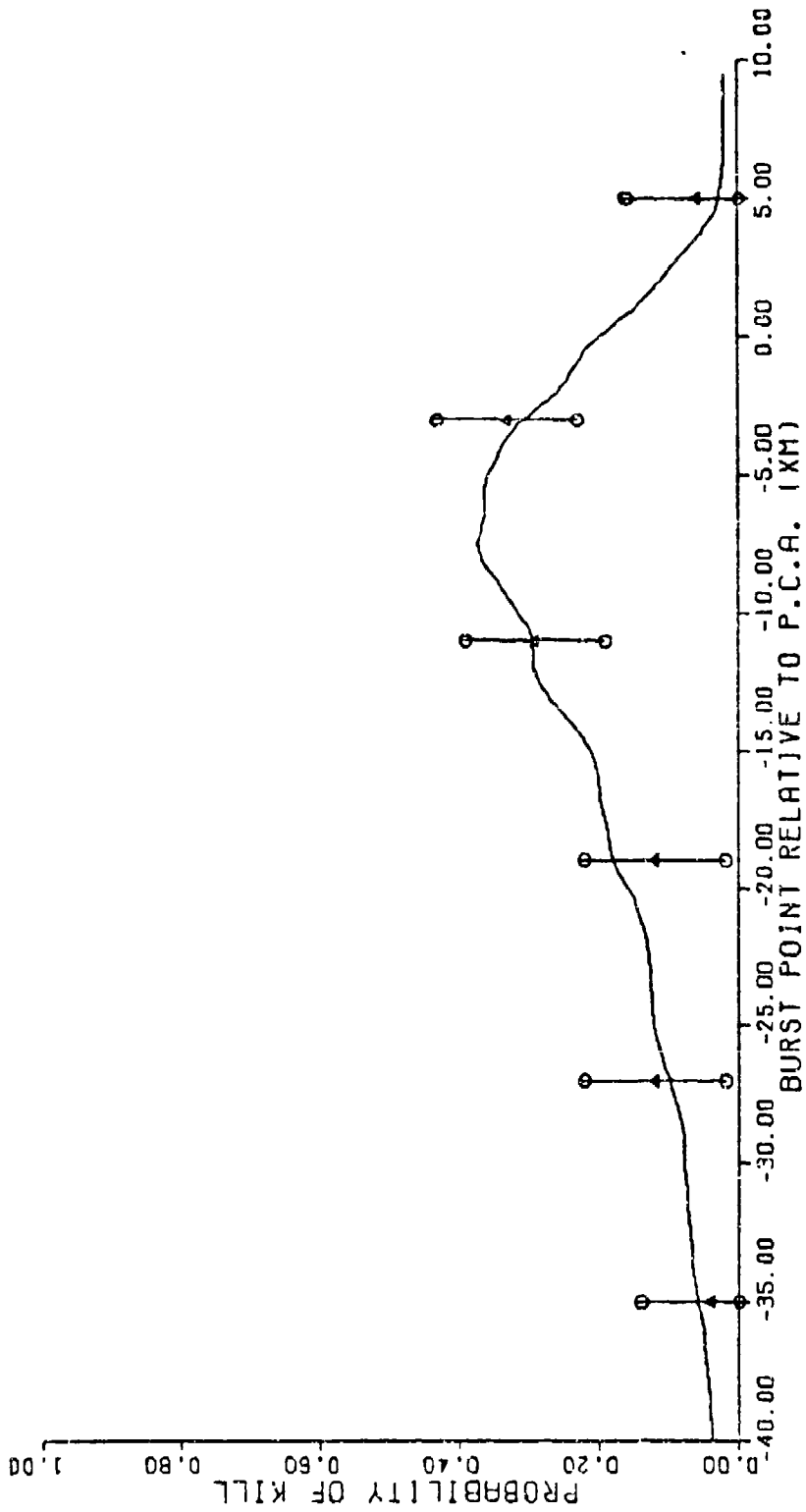


FIG K-4 : PSI=64. VR=2105. BETA=17. SIGMA=24.8

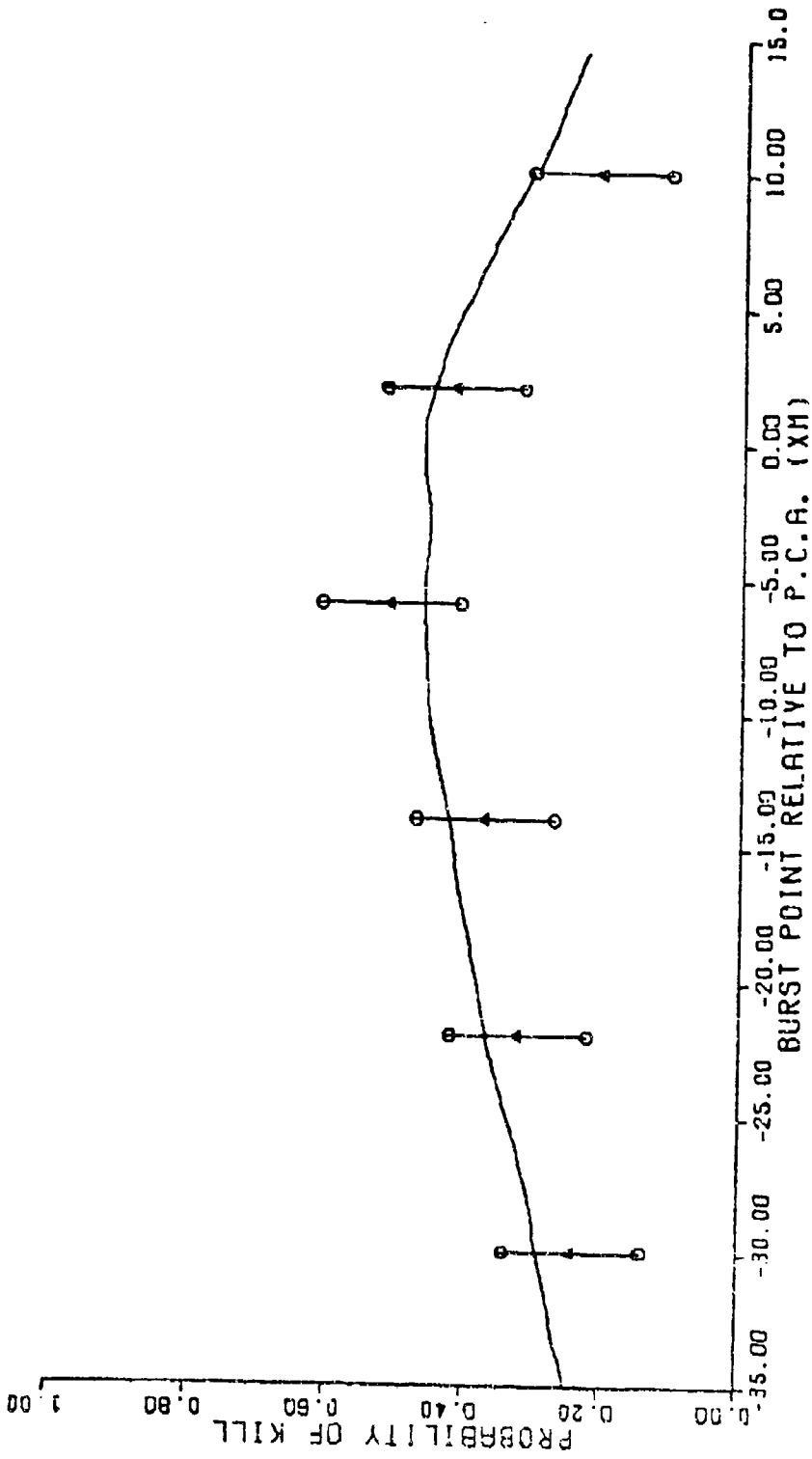


FIG K-5: PSI=89. VR=1152. BETA=41. SIGMA=16.8

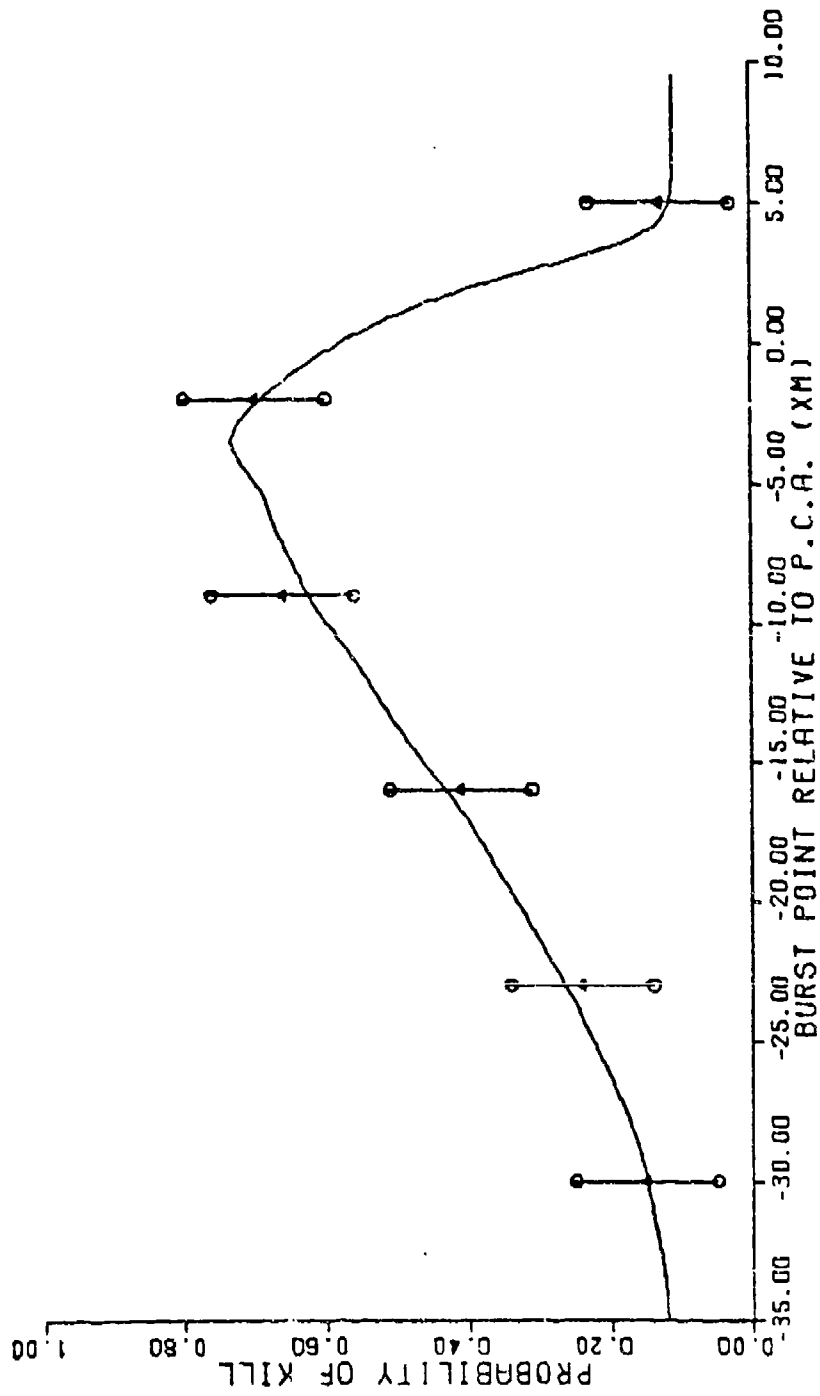


FIG K-6 : PSI=105. VR=1799. BETA=21. SIGMA=13.5

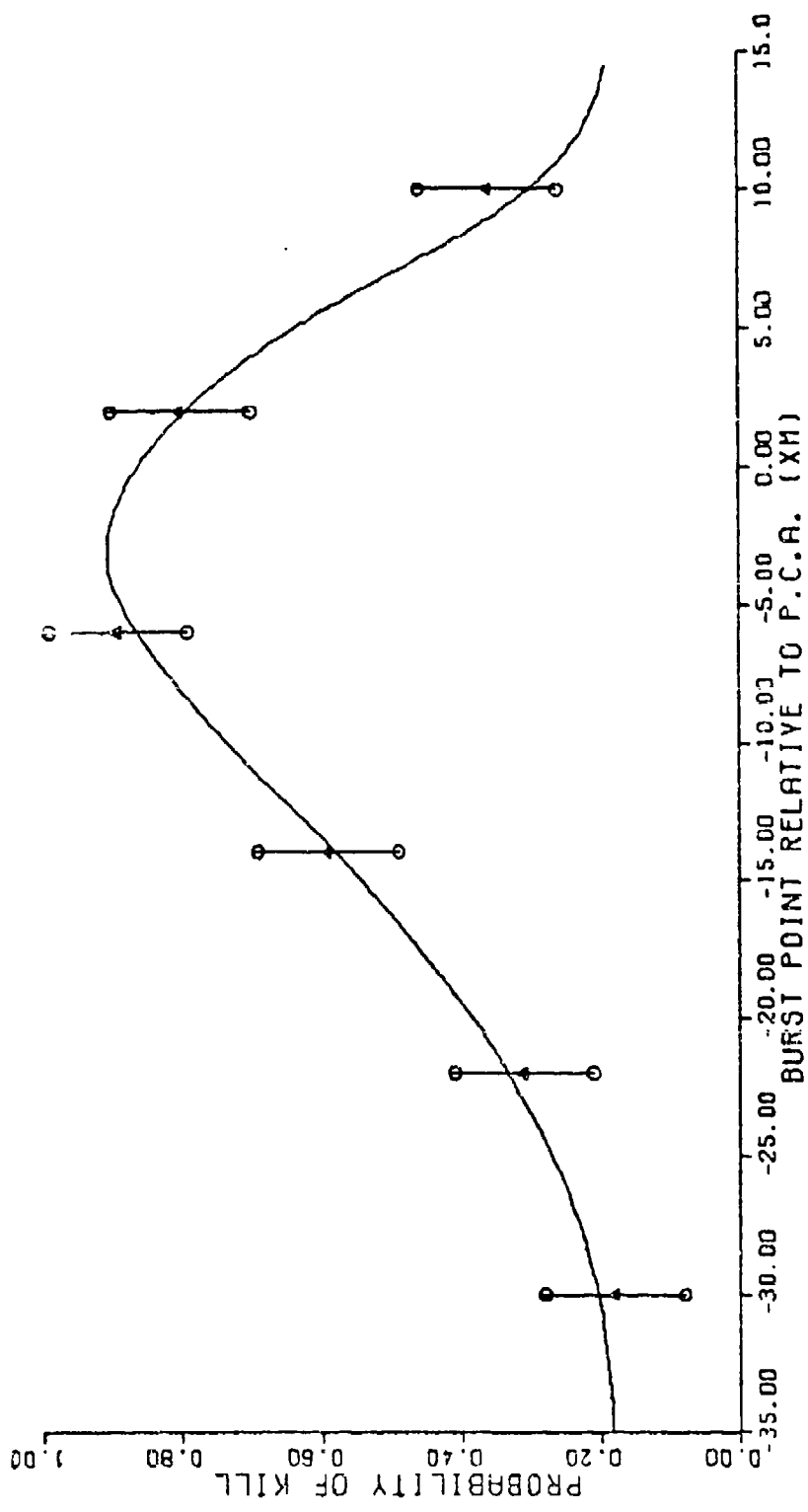


FIG K-7 : PSI=122. VR=1068. BETA=30. SIGMA=9.0

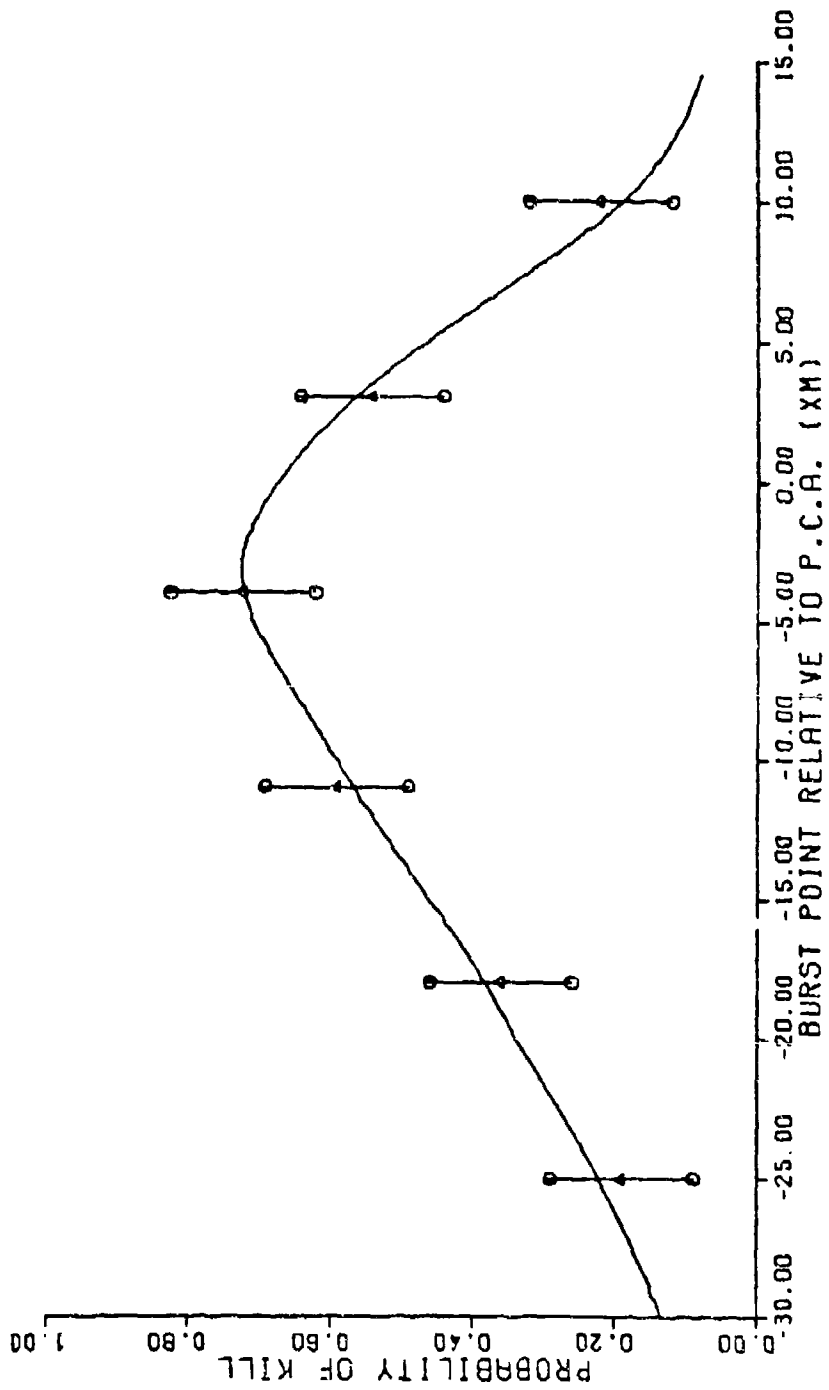


FIG K-8 : PSI=128. VR=1171. BETA=20. SIGMA=15.9

(109 Cell Model)

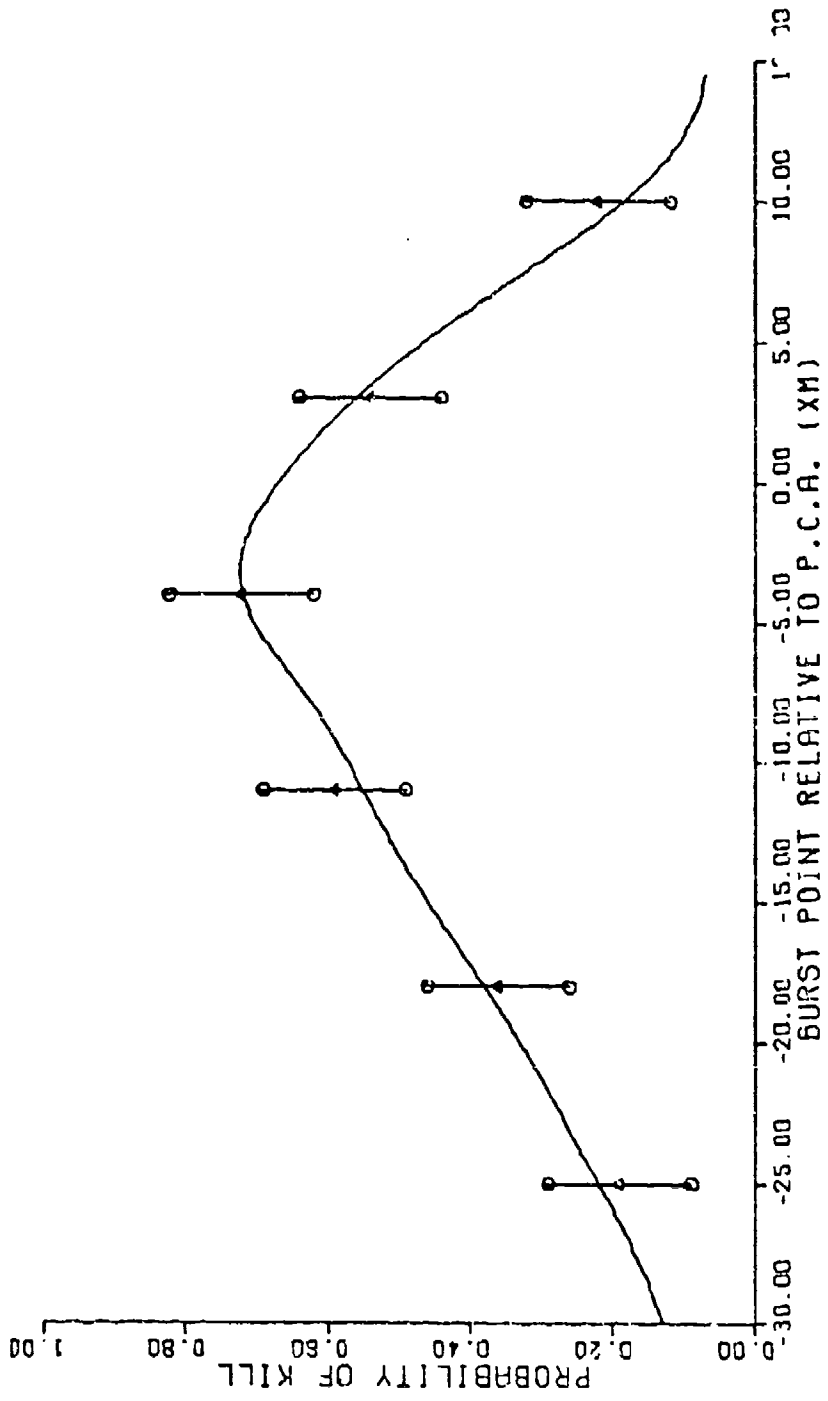


FIG K-9 : PSI=128. VR=1171. BETA=20. SIGMA=15.9

(1000 Samples)

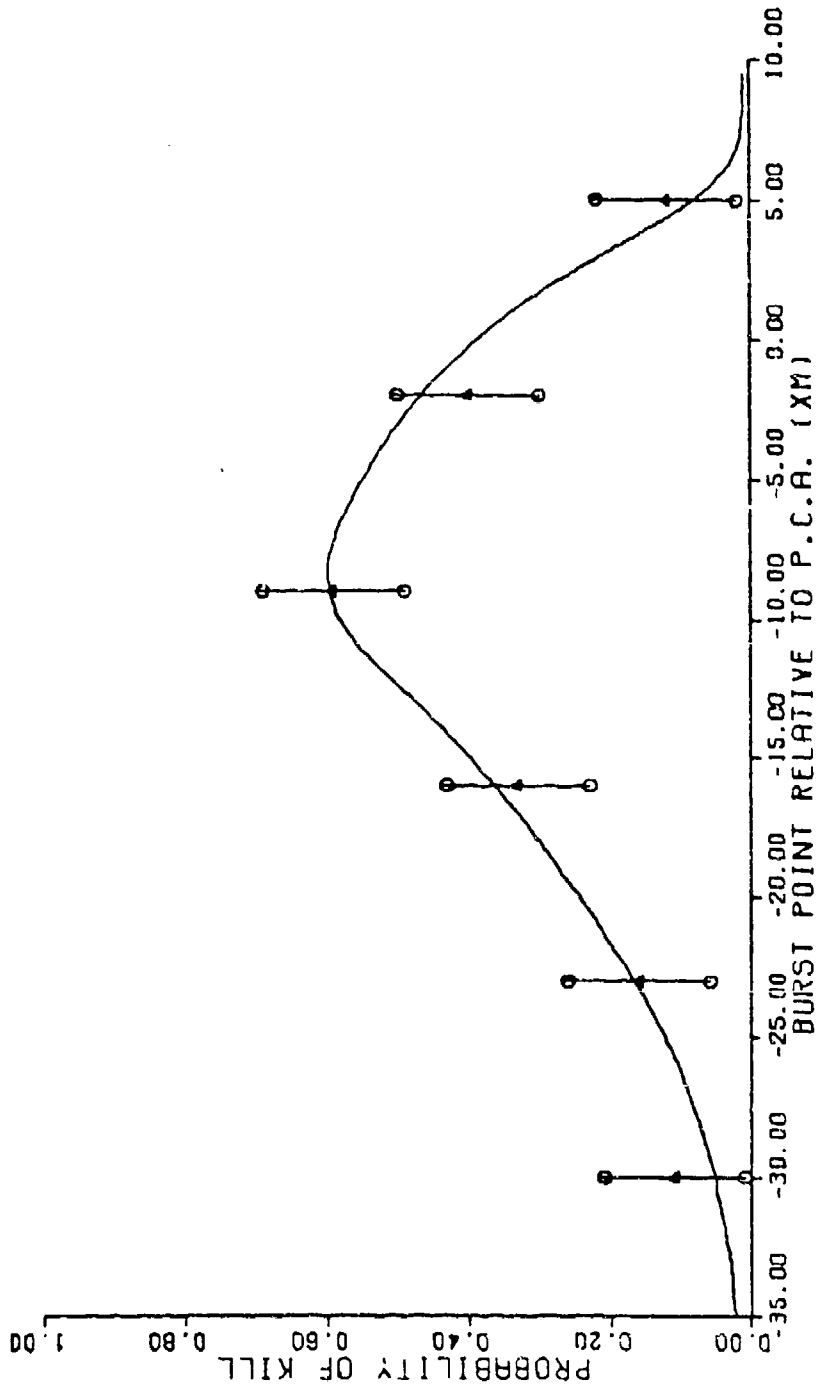


FIG K-10: PSI=146. VR=1467. BETA=11. SIGMA=29.7

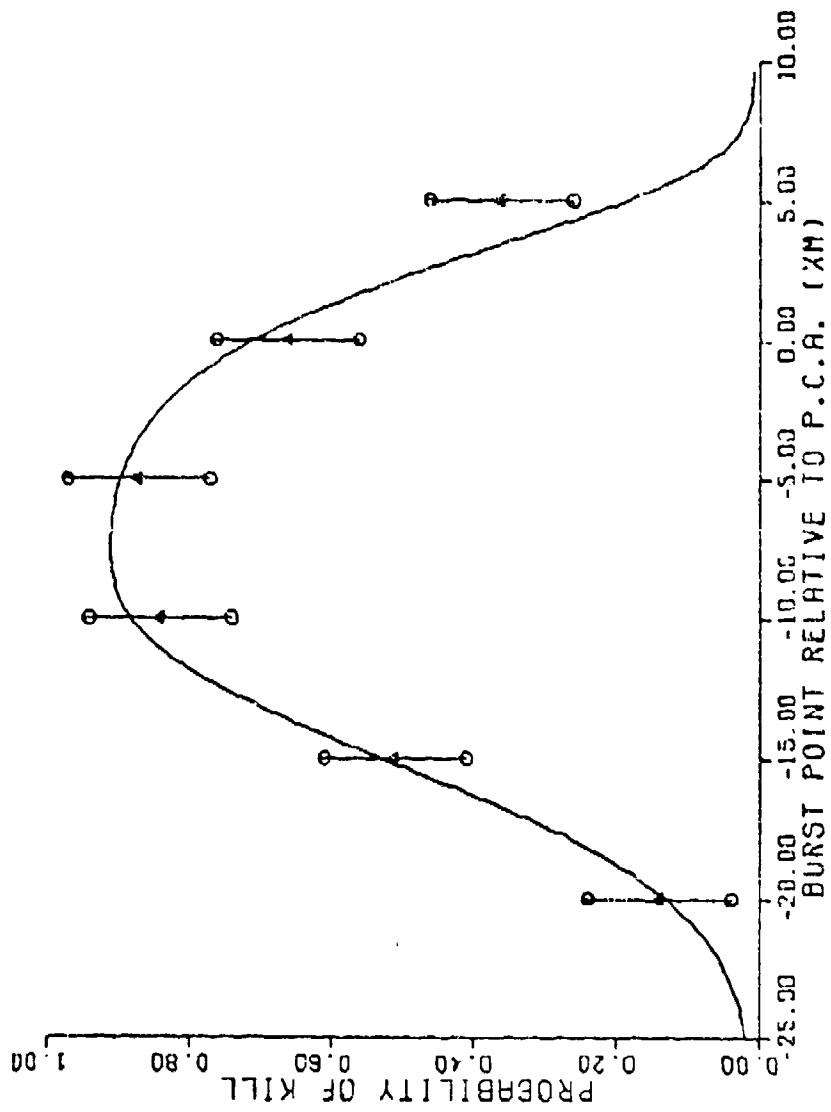


FIG K-11: PSI=168. VR=1646. BETA=5. SIGMA=15.2

Vita

Gregory A. Keethler was born on 16 June 1954 in Munich, Germany. He graduated from high school in 1972 in El Paso, Texas where he then attended the University of Texas at El Paso as a mathematics major. He was awarded the degree of Bachelor of Science in the Sciences in August 1975. Before joining the Air Force, he was employed as a mathematics teacher at El Paso High School. He received his commission from OTS on 11 March 1976 and was assigned to the Air Force Armament Laboratory, Eglin AFB, Florida before entering the School of Engineering, Air Force Institute of Technology in August 1978.

He and his wife, the former Gloria M. Zamora, have two children, Benjamin and Nathan.

Permanent Address: 5119 Cornell Ave.
El Paso, Texas 79924

UNCLASSIFIED

SECURITY CLASSIFICATION OF THIS PAGE (When Data Entered)

REPORT DOCUMENTATION PAGE		READ INSTRUCTIONS BEFORE COMPLETING FORM
1. REPORT NUMBER AFIT/GST/MA/80M-2	2. GOVT ACCESSION NO. AD-A083 517	3. RECIPIENT'S CATALOG NUMBER
4. TITLE (and Subtitle) A METHOD OF CHARACTERIZING AIR-TO-AIR MISSILE ENDGAME MODELS		5. TYPE OF REPORT & PERIOD COVERED Master's Thesis
7. AUTHOR(s) Gregory A. Keethler Captain USAF		6. PERFORMING ORG. REPORT NUMBER
9. PERFORMING ORGANIZATION NAME AND ADDRESS Air Force Institute of Technology (EN) Wright-Patterson AFB, OH 45433		8. CONTRACT OR GRANT NUMBER(s)
11. CONTROLLING OFFICE NAME AND ADDRESS		10. PROGRAM ELEMENT, PROJECT, TASK AREA & WORK UNIT NUMBERS
14. MONITORING AGENCY NAME & ADDRESS (if different from Controlling Office)		12. REPORT DATE March 1980
		13. NUMBER OF PAGES 231
		15. SECURITY CL ASS. (of this report) UNCLASSIFIED
		15a. DECLASSIFICATION/DOWNGRADING SCHEDULE
16. DISTRIBUTION STATEMENT (of this Report) Approved for public release; distribution unlimited		
17. DISTRIBUTION STATEMENT (of the abstract entered in Block 20, if different from Report) APPROVED FOR PUBLIC RELEASE AFR 190-17. JOSEPH D. HIPPS, Major, USAF Director of Public Affairs		
18. SUPPLEMENTARY NOTES		
19. KEY WORDS (Continue on reverse side if necessary and identify by block number) Endgame Model Characterization Air-to-Air Missiles Missile Warhead Lethality		
20. ABSTRACT (Continue on reverse side if necessary and identify by block number) Air-to-air missile endgame programs typically require tens of seconds of computer time to calculate a single estimate of probability of kill (P_k). Thousands of these estimates may be required in any given endgame analysis. The main objective of this research was to develop a method for characterizing an endgame model using only a fraction of the amount of data generated		

DD FORM 1473
1 JAN 73

EDITION OF 1 NOV 65 IS OBSOLETE

UNCLASSIFIED

SECURITY CLASSIFICATION OF THIS PAGE (When Data Entered)

Block 20:

by such analyses. In pursuit of this objective, a second objective of actually accomplishing a characterization of an existing endgame program was established.

The endgame program SHAZAM was used to generate data upon which to base a characterization. A purely empirical approach was first attempted wherein all main and interactive effects of the critical factors were to be assessed strictly by experimentation with and observation of the behavior of SHAZAM. The high order of interactions between the factors precluded completion of this approach.

A semi-empirical approach was then pursued whereby the interactions between the endgame geometry and warhead characteristics were accounted for geometrically. A two-parameter exponential function was used to describe the behavior of P_K as a function of the warhead burst point. Values of the two parameters were calculated based upon the settings of the remaining factors. A "vulnerable length" was used to account for the target's vulnerability. After several iterations of refinement, the characterization was compared to SHAZAM for ten randomly selected trajectories. The characterization's P_K estimates were within 0.1 of SHAZAM's estimates for 97 percent of these random data. A simple computer program implementing the mathematics of the characterization required a maximum of 0.2 seconds of computer time per P_K estimate.

Approximately two hours of computer time were consumed by SHAZAM in generating the necessary data. Thus, with a relatively modest investment of computer time, two orders of magnitude improvement in time required per P_K estimate was achieved.

→ The suggested method for characterizing air-to-air missile endgame programs is based on the semi-empirical approach and its application to SHAZAM. The method is heuristic, rather than algorithmic, due to the subjective nature of the characterization process.